Direct lineage conversion enables the generation of rejuvenated donor cells for neurotransplantation

Dissertation

zur

Erlangung des Doktorgrades (Dr. rer. nat.)

der

Mathematisch-Naturwissenschaftlichen Fakultät

der

Rheinischen Friedrich-Wilhelms-Universität Bonn

vorgelegt von

Lea Jessica Berg, geb. Flitsch

aus

Troisdorf

Bonn April, 2022

Angefertigt mit Genehmigung der Mathematisch-Naturwissenschaftlichen Fakultät

der Rheinischen Friedrich-Wilhelms-Universität Bonn

Gutachter: Prof. Dr. med. Oliver Brüstle

Gutachter: Prof. Dr. rer. nat. Waldemar Kolanus

Tag der Promotion: 14.10.2022

Erscheinungsjahr: 2022

Abstract

With the advent of cell programming, several strategies for disease modeling and cell replacement have become available. While directly converted somatic cell-derived induced neurons largely preserve age-associated traits, induced pluripotent stem cells (iPSCs) and their derivatives represent an embryonic-like stage. Here, we investigated whether age-related cellular properties are also conserved upon direct conversion of adult human peripheral blood cells into induced neural stem cells (iNSCs). Specifically, employing Sendai virus (SeV)-mediated overexpression of the two transcription factors SOX2 and cMYC, we generated a *bona fide* NSC population from erythroid progenitor cells. Despite the lack of a pluripotency transit, we found that even iNSCs converted from >85-year-old donors display a remarkable degree of epigenetic rejuvenation and lack age-associated cellular hallmarks similar to iPSC-derived NSCs. We next characterized the dynamics underlying DNA methylation age changes induced by iNSC conversion in greater detail, revealing that the process of epigenetic rejuvenation is protracted in this conversion paradigm and most likely independent of stem cell proliferation. This could make iNSC conversion a blueprint for somatic cell rejuvenation and a promising alternative for the derivation of neural cells for regenerative applications.

Therefore, we next confirmed that iNSCs survive neurotransplantation in neonatal and adult mice, generating electrophysiologically active neurons as well as glial cells upon engraftment. Most importantly, iNSC-derived neurons exhibit transplantation site-appropriate efferent projection patterns and undergo synaptic integration into the host brain as suggested by human NCAM-based fiber tracking and pseudotyped Rabies virus-based monosynaptic tracing, respectively. Finally, we aimed to explore whether this direct conversion approach could, in principle, be extended to microglia, the immune cells of the central nervous system. Due to the highly restricted access to primary human microglia, we employed iPSC-derived microglia-like cells (iPSdMiG) to address this question. Within two weeks after infection of directly harvested or CD11b-sorted iPSdMiG with temperature-sensitive SeVs, colonies consisting of neuroepithelial-like-shaped cells emerged, and the derived cells expressed characteristic NSC markers. As for blood-derived iNSCs, temporary cultivation at 39 °C yielded transgene-free cell lines, which could be further proliferated for multiple passages and gave rise to functional neurons, astrocytes and oligodendrocytes upon differentiation. Considering their epigenetically rejuvenated state, their amenability to *in vivo* application and the fact that they can be generated from different somatic cell types, directly converted iNSCs provide interesting prospects for disease-related research and neuroregeneration.

Table of Contents

Table of Figures

Table of Tables

Abbreviations List

AAV: Adeno-associated virus; AAVS1: Adeno-associated virus integration site 1; ACSF: Artificial cerebral spinal fluid; AD: Alzheimer's disease; Adgrg6: Adhesion G protein-coupled receptor G6; ADP: Adenosine diphosphate; Aif1: Allograft inflammatory factor 1; Akt (aka PKB): Protein kinase B; Aldh1l1: Aldehyde dehydrogenase 1 family member L1; Ampk: Adenosine monophosphate-activated protein kinase; AP: Action potential; Ap2α: Transcription factor AP-2-alpha; APS: Ammonium persulfate; Ara-C: Cytarabin; Ascl1: Achaete-scute holomog 1; Atg5/7/8/12: Autophagy related 5/7/8/12; Atm: ATM serine/threonine kinase; Atoh1: Protein atonal homolog 1; ATP: Adenosine triphosphate; BAFA: Bafilomycin-A; Bcl-XL: B cell lymphoma-extra large; Bdnf: Brain-derived neurotrophic factor; Becn1: Beclin-1; bHLH: Basic helix-loop-helix; Brn2/4 (aka POU3F2/4): POU domain class 3 transcription factor 2/4; BSA: Bovine serum albumin; CA: Cornu ammonis; Casp3: Caspase 3; CD11b/49d/68/73: Cluster of differentiation 11b/49d/68/73; Cdc42: Cell division cycle 42; cMyc: C-Myelocytomatosis oncogene; CNS: Central nervous system; CNV: Copy number variation; Col3a1: Collagen type III alpha 1 chain; Creb1: Cyclic adenosine monophosphate-responsive element-binding protein 1; CRISPR: Clustered regularly interspaced short palindromic repeats; Crm1 (aka Xpo1): Exportin 1; CSA/B: Cockayne syndrome group A/B protein; Csf1: Colony-stimulating factor 1; Ctip2: Chicken ovalbumin upstream promoter transcription factor-interacting protein 2; DAB: 3,3'-diaminobenzidine; DABCO: 1,4-Diazabicyclo(2,2,2)octane; Dach1: Dachshund homolog 1; DAPI: 4',6-Diamidino-2-phenyl-indol-dihydrochloride; DAPT: Dual antiplatelet therapy; Darpp-32: Dopamine and cyclic adenosine monophosphate-regulated phosphoprotein of apparent molecular weight 32 kDa; Dat: Dopamine transporter; dATP: Deoxyadenosine triphosphate; dbcAMP: Dibutyryl cyclic adenosine monophosphate; dCTP: Deoxycytidine triphosphate; DEG: Differentially expressed gene; dGTP: Deoxyguanosine triphosphate; DIFF: NGN2-overexpressing iNSC differentiation cultures; Dlk1: Delta-like 1 homolog; Dlx1/2: Distal-less homeobox 1/2; DMEM: Dulbecco's modified eagle medium; DMP: Differentially methylated probe; DMR: Differentially methylated region; DMSO: Dimethyl sulfoxide; DNAm: Deoxyribonucleic acid methylation; Dnmt1: Deoxyribonucleic acid-methyltransferase 1; DOX: Doxycycline; DPBS: Dulbecco's phosphate-buffered saline; DSB: Double strand break; dTTP: Deoxythymidine triphosphate; E47: A basic helix-loop-helix transcription factor that is generated via alternative splicing from the transcription factor 3 gene; EB: Embryoid body; Ed1: Ectodysplasin 1; EDTA: Ethylenediaminetetraacetic acid; Egf: Epidermal growth factor; En1/2: Engrailed 1/2; EPC: Erythroid progenitor cell; Ercc2: Excision repair cross-complementing rodent repair deficiency, complementation group 2; ESC: Embryonic stem cell; Etv5: E26 transformation-specific translocation variant 5; Ezh2: Enhancer of zeste homolog 2; FA: Formaldehyde; FACS: Fluorescence-activated cell sorting; FCCP: Trifluoromethoxy carbonyl cyanide phenylhydrazone; FCS: Fetal calf serum; FDR: False discovery rate; Fezf2: Forebrain embryonic zinc finger 2; Fgf2/4: Fibroblast growth factor 2/4; Foxa2: Forkhead box protein 2A; Foxo1/3: Forkhead box protein O1/3; FUDR: 5-Fluoro-2'-deoxyuridine; GABA: Gamma-aminobutyric acid; Gad: Glutamate decarboxylase; Gadd45b: Growth arrest and deoxyribonucleic acid damage-inducible beta; Gdf15: Growth/differentiation factor 15; Gdnf: Glial cell-derived neurotrophic factor; Gfap: Glial fibrillary acidic protein; GFP: Green fluorescent protein (with eGFP indicating endogenous fluorescence); Girk2: Potassium channel 2; Glis1: Gli-similar 1; GLY: Glycerol-treated iNSCs; GM-Csf: Granulocyte-macrophage colony-stimulating factor; GO: Gene ontology; GP130: Glycoprotein 130; Gsk3β: Glycogen synthase kinase 3β; γH2AX: Phosphorylated H2A histone family member X; H2A.Z: Z variant of histone H2A; HAT: Histone acetyltransferase; HBSS: Hank's balanced salt solution; HD: Huntington's disease; HDAC: Histone deacetylase;

Hes1/5: Hairy/enhancer of split 1/5; HGPS: Hutchinson-Gilford progeria syndrome; HIF1α: Hypoxia-inducible factor 1α; hN: Human nuclei; HP1: Heterochromatin protein 1; HRP: Horseradish peroxidase; Iba1: Ionized calcium-binding adapter molecule 1; Id1: Inhibitor of differentiation 1; Ifnγ: Interferon gamma; Igf1: Insulin-like growth factor 1; Igfbp3: Insulin-like growth factor-binding protein 3; Il1/3/6: Interleukin 1/3/6; iNBSC: Induced neural plate border stem cell; iN: Induced neuron; iNSC: Induced neural stem cell; Insm1: Insulinoma-associated 1; iOPC: Induced oligodendrocyte progenitor cell; iPSC: Induced pluripotent stem cell; iPSdMiG: Induced pluripotent stem cell-derived microglia; Itgam: Integrin subunit alpha M; Jak2: Janus kinase 2; Klf4: Krueppel-like factor 4; Ku70/80: Polypeptides encoded by the X-ray repair complementing defective repair in Chinese hamster cells 6/5; LAAP: L-ascorbic acid 2-phosphate; Lamna (aka Lama3): Laminin subunit alpha 3; Lap2α: Lamin-associated polypeptide 2, isoform alpha; LC3: Microtubule-associated protein 1A/1B-light chain 3; LGE: Lateral ganglionic eminence; Lif: Leukemia inhibitory factor; LIFR: Leukemia inhibitory factor receptor subunit alpha; Lin28: Zinc finger CCHC domain-containing protein 1; Lmna: Lamin A; Lmnb: Lamin B; Lmnc: Lamin C; Lmx1a/b: LIM homeobox transcription factor 1 a/b; l-Myc: V-Myelocytomatosis oncogene homolog 1, lung; LSFM: Light sheet fluorescence microscopy; lt-NES: Long-term neuroepithelial stem cell; Map2: Microtubule-associated protein 2; Mbp: Myelin basic protein; Mdm2: Mouse double minute homolog 2; MDS: Multidimensional scaling; MHC: Major histocompatibility complex; miciNSC: Induced pluripotent stem cell-derived microglia-derived induced neural stem cell, miR: Micro-RNA; MN: Motor neuron; MOI: multiplicity of infection; MPTP: 1-Methyl-4-phenyl-1,2,3,6-tetrahydropyridine; MSC: Mesenchymal stromal cell; MSN: Medium spiny neuron; mTOR: Mammalian target of rapamycin; MVP: Most variable position; Myod3: Myoblast determination protein 3; Myt1l: Myelin transcription factor 1-like protein; NAD: Nicotinamide adenine dinucleoride; Nanog: Homeobox protein Nanog; NCAM: Neural cell adhesion molecule; NES: Nestin; NeuN: Neuronal nuclei; Neurod1/2/3/4: Neuronal differentiation 1/2/3/4; NextGenSeq: Next generation sequencing; NF-κB: Nuclear factor kappa-light-chain-enhancer of activated B cells; NG2: Neuron-glial antigen 2; Ngn1/2/3: Neurogenin 1/2/3; NGS: Normal goat serum; NHS: Normal horse serum; Nkx2.2: NK2 homeobox 2; NMDAR: N-methyl-D-aspartate receptor; NPC: Neural precursor cell; Nr0b1: Nuclear receptor subfamily 0 group b member 1; Nrf2: Nuclear factor erythroid 2-related; NSC: Neural stem cell; NT-3: Neurotrophin-3; Nurr1: Nuclear receptor-related 1 protein; O4: Oligodendrocyte marker O4; Oct3/4 (aka POU5F1): Octamer-binding transcription factor 3/4; 6-OHDA: 6-Hydroxydopamine; Olig2: Oligodendrocyte transcription factor; Otx2: Orthodenticle homeobox 2; P: Passage; $p14^{Arf}$ and $p16^{Ink4a}$: Protein isoforms encoded by cyclin-dependent kinase inhibitor 2A (CDKN2A); p21: Protein encoded by cyclin-dependent kinase inhibitor 1A (CDKN1A); p53: Protein encoded by tumor protein P53 (TP53); p62 (aka SQSTM1): Sequestosome-1; Pax6/8: Paired box gene 6/8; PB-iNSC: Peripheral blood-derived induced neural stem cell; PBMC: Peripheral blood mononuclear cell; PCA: Principal component analysis; PD: Parkinson's disease; Pdgf-aa: Platelet-derived growth factor-AA; Pdgfrα: Platelet-derived growth factor receptor alpha; Pdlim3 (aka ALP): Actin-associated LIM protein; PFA: Paraformaldehyde; Pgc1: Proliferator-activated receptor gamma coactivator 1; Pitx3: Paired-like homeodomain 3; PNS: Peripheral nervous system; Polg: DNA polymerase subunit gamma; pRABV: Pseudotyped Rabies virus; PROL: Proliferating iNSCs harvested between D42 and D49 of conversion; PSC: Pluripotent stem cell; Ptbp1: Polypyrimidine tract-binding protein 1; PTF1a: Pancreas transcription factor 1-alpha; PTM: Post-translational modification; PVDF: Polyvinylidene fluoride; QC: Quality control; qPCR: Quantitative polymerase chain reaction; Raf1: Raf-1 proto-oncogene, serine/threonine kinase; Rbfox1: RNA-binding protein, fox-1 homolog; RBPj-κ: Recombinant signal-binding protein for immunoglobulin kappa J region; RecQ: RecQ helicase; RFP: Red fluorescent protein (with

eRFP indicating endogenous fluorescence); RMP: Resting membrane potential; ROS: Reactive oxygen species; Rosa26: Reverse orientation slice acceptor 26; RT-PCR: reverse-transcription polymerase chain reaction; rtTA: Reverse tetracycline transactivator; S100β: S100 calcium-binding protein B; SA-β-gal: Senescence-associated beta-galactosidase; SAG: Smoothened agonist; Sall4: Sal-like protein 4; SASP: Senescence-associated secretory profile; SCF: Stem cell factor; scRNAseq: Single cell RNA sequencing; SDS: Sodium dodecyl sulfate; SEM: Standard error of the mean; SeV: Sendai virus; Shank2: SH3 and multiple ankyrin repeat domains 2; Shh: Sonic hedgehog; Sirt1: Sirtuin 1; Smad3: Mothers against decapentaplegic homolog 3; SOCS: Suppressor of cytokine signaling; Sox2/4: Sex-determining region Y-box 2/4; SP: Spinal cord; sPSC: Spontaneous postsynaptic current; Src kinase: Sarcoma kinase; Stat3: Signal transducer and activator of transcription 3; SV40LT: Simian virus 40 large T antigen; T3: Thyroid hormone; TAE: Tris-acetate-EDTA; TALEN: Transcription activator-like effector nuclease; TEMED: Tetramethylethylene diamine; Tert: Telomerase reverse transcriptase; Tet1/2/3: Ten-eleven translocation methylcytosine dioxygenase 1/2/3; TF: Transcription factor; Tgfβ: Transforming growth factor beta; TH: Tyrosine hydroxylase; THY: Thymidine-treated iNSCs; Tmem119: Transmembrane protein 119; TRA-1-60: Podocalyxin; Tubb3: Class III beta-tubulin; TRE: Tetracycline responsive element; vGat: Vesicular gamma-aminobutyric acid transporter; vGlut1/2: Vesicular glutamate transporter 1/2; Vmat: Vesicular monoamine transporter; Wnt1: Int/Wingless family member 1; Wrn: Werner syndrome protein; Xpd: Xeroderma pigmentosum group D; Xfp1: Xylulose 5-phosphate/fructose 6-phosphate phosphoketolase 1; Xrcc5: X-ray repair complementing defective repair in Chinese hamster cells 5; YFP: Yellow fluorescent protein; Zfp521: Zinc finger protein 521; Zic3: Zinc finger in cerebellum 3.

1. Introduction[1]

1.1. The toolbox of cellular programming

Multicellular organisms are made up of several organs and tissues that are formed by hundreds of distinct cell types with various different functions (*e.g.*, muscle, skin and blood cells, neurons and many more). Astonishingly, during mammalian embryogenesis, this immense cell type diversity arises from a single totipotent cell – the diploid zygote. From this unicellular stage on, organisms develop by a cascade of cell fate shifts and differentiation processes: The fertilized oocyte develops into the blastocyst, whose inner cell mass gives rise to the epiblast containing embryonic stem cells (ESCs; reviewed by White & Plachta, 2020). ESCs are pluripotent stem cells (PSCs), which can either divide symmetrically or further differentiate into the diverse cell types of the three germ layers – the endoderm, mesoderm and ectoderm. Within each germ layer, more restricted multipotent tissue stem cell populations arise, representing self-renewing stem cells whose differentiation capacity is limited to their specific cell lineage (see reviews by Behr *et al.*, 2010 and Tabansky & Stern, 2016). Tripotent neural stem cells (NSCs), for example, are able to give rise to the three neuroectodermal cell types of the central nervous system (CNS), namely neurons, astrocytes and oligodendrocytes, but cannot differentiate into cell types of the endodermal or mesodermal lineage (compare review by Svendsen *et al.*, 1999). During embryonic development, the establishment of cell type identity is achieved by the activation of specific transcriptional networks that shape the individual protein profile within each cell, allowing cells to perform their basic as well as cell type-specific functions. These networks are governed by transcription factors (TFs), which act as molecular switches, and the expression levels of individual TFs within one cell types regulates which gene modules are induced or repressed. Thus, the combinatorial activity of several TFs encodes cellular identity in an orchestrated and collaborative way (reviewed by Wilkinson *et al.*, 2017). Notably though, the expression of individual TFs and, thus, the regulation of complete TF networks is in turn controlled by highly complex mechanisms. On the one hand, epigenetic modifications, which can occur at different levels of chromatin organization ranging from the modification of DNA itself (*e.g.*, DNA methylation (DNAm)) via the modification of histones to the spatial arrangement of chromatin (Figure 1), are highly involved in regulating gene expression and are therefore relevant for embryogenesis (see work by Waddington, 1957; Bernstein *et al.*, 2007 and Yadav *et al.*, 2018). On the other hand, coordinated gene expression is dependent on tightly regulated morphogen concentrations (in detail reviewed by

[1] Components of the introduction and discussion are partially verbatim citations from own publications or text passages generated by the author of this thesis as contributions to co-authored publications. Specifically, entailed phrasings have been published in Flitsch, L.J. & Brüstle, O. (2019) 'Evolving principles underlying neural lineage conversion and their relevance for biomedical translation', *F1000Research*, 8, p. F1000 Faculty Rev-1548 (Flitsch & Brüstle, 2019), Flitsch, L.J., Laupman, K.E. & Brüstle, O. (2020) 'Transcription factor-based fate specification and forward programming for neural regeneration', *Frontiers in Cellular Neuroscience*, 14, p. 121 (Flitsch *et al.*, 2020) and Cenini, G., Hebisch, M., Iefremova, V., Flitsch, L.J., Breitkreuz, Y., Tanzi, R.E., Kim, D.Y., Peitz, M. & Brüstle, O. (2021) 'Dissecting Alzheimer's disease pathogenesis in human 2D and 3D models', *Molecular and Cellular Neuroscience*, 110, p. 103568 (Cenini *et al.*, 2021). The origin of each text passage is indicated by font color. Black font indicates that the respective text has been added in the context of this thesis and is not yet published.

Tao & Zhang, 2016 for the development of the neural system). Therefore, the processes of acquiring as well as maintaining or changing a specific cell fate might represent some of the most intricate and sophisticated building blocks of evolutionary biology.

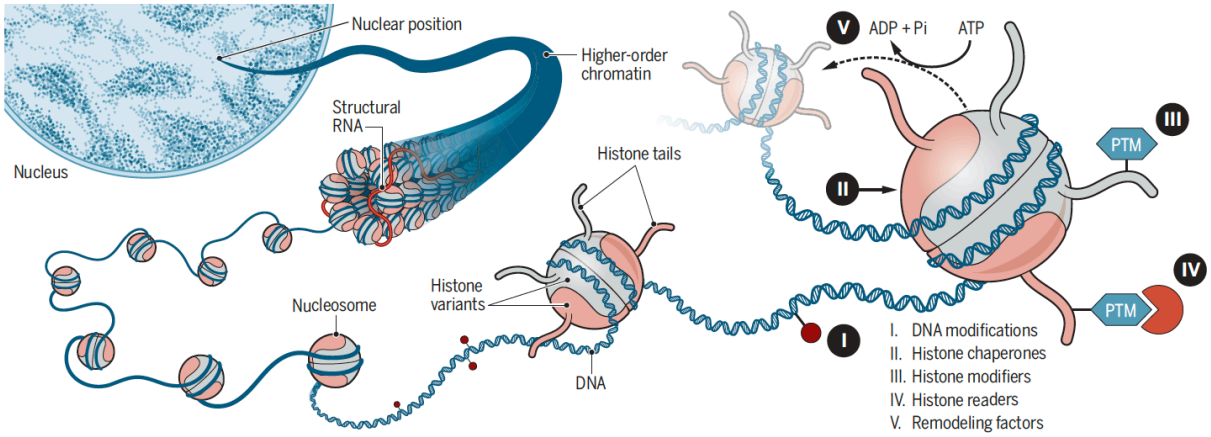

Figure 1: Levels of epigenetic regulation.
Transcription is regulated by epigenetic mechanisms modifying chromatin plasticity at several levels. The figure depicts an interphase nucleus consisting of higher-order chromatin structures and structural RNA, which contributes to local organization. Chromatin is built by several nucleosomes, representing units in which double-stranded DNA is condensed by wrapping around histones. Nucleosomes might vary in the composition of histone variants, posttranslational modifications (PTMs) of histone tails and modifications of the DNA bases themselves, altogether facilitating chromatin plasticity. From Yadav, T., Quivy, J.P. & Almouzni, G. (2018) 'Chromatin plasticity: A versatile landscape that underlies cell fate and identity', Science, 361(6409), pp. 1332–1336 (Yadav et al., 2018). Reprinted with permission from American Association for the Advancement of Science (AAAS).

The term cellular programming describes the manipulation of transcriptional networks underlying cell identity. Research on cell programming has a remarkable history: Dating back to the 1960s, experiments on somatic nuclear transfer were performed, revealing that the transplantation of an adult somatic cell nucleus into an enucleated, unfertilized oocyte results in a pluripotent stage-like cell, which is capable of reconstituting an entire organism upon propagation and differentiation (see review by Zhou & Melton, 2008). These results paved the way for organismal cloning, and inspired further studies on epigenetic reprogramming, for instance, establishing a pluripotent state by fusing an ESC with a terminally differentiated somatic cell (see review by Jaenisch & Young, 2008). First reports describing the principal feasibility of converting one somatic cell type into another were published as early as 1987, when Davis, Weintraub and Lassar derived myoblasts by overexpressing the myoblast TF Myod3 in a mouse fibroblast line (Davis *et al*., 1987). However, at that time, somatic cell-to-cell programming was restricted to the conversion of lineage-related cells of the same germ layer (see review by Graf & Enver, 2009). This changed dramatically when Kazutoshi Takahashi and Shinya Yamanaka revealed that combined overexpression of the four TFs Oct3/4, Sox2, Klf4 and cMyc is sufficient to induce a pluripotent state in mouse (Takahashi & Yamanaka, 2006) and human fibroblasts (Takahashi *et al*., 2007). Their findings mark a turning point in the area of cell programming and ultimately fueled the development of a huge variety of cell fate conversion techniques (Figure 2).

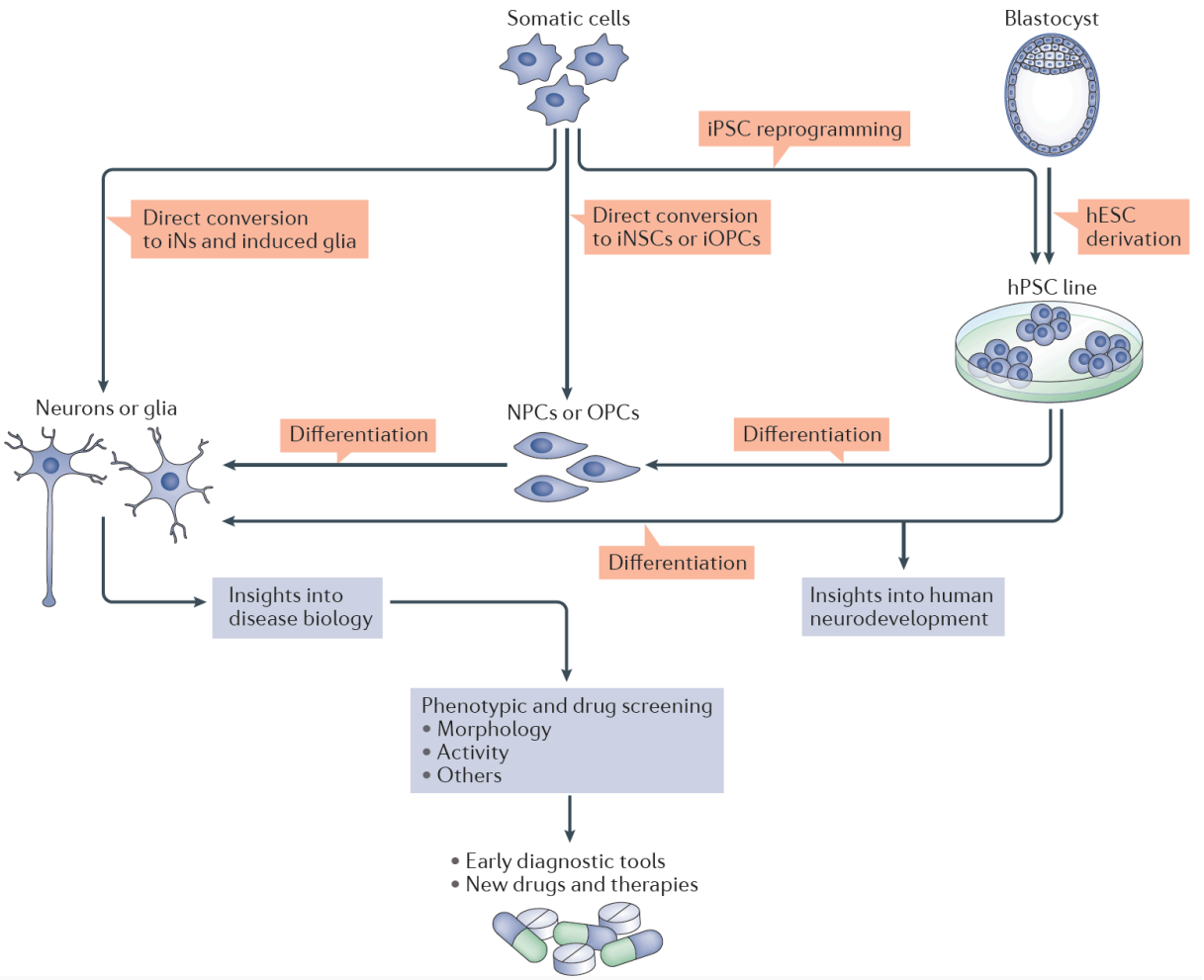

Figure 2: Overview depicting cell programming paradigms available for nervous system-related biomedical research.
Induced pluripotent stem cells (iPSCs) can be reprogrammed from various somatic cell sources, exhibiting cellular properties comparable to blastocyst-derived ESCs. Afterwards, both types of PSCs can be differentiated, for instance, along the neural lineage using extrinsic factors for guiding PSC and subsequently neural precursor cell (NPC) differentiation. Alternatively, the process of differentiating PSCs and/or NPCs into post-mitotic neurons or glia can be sped up by overexpression of cell lineage-specific TFs, *i.e.*, forward programming. In contrast to approaches involving a PSC intermediate, direct cell fate conversion can be used to transdifferentiate somatic cells into induced neural stem cells (iNSCs), induced oligodendrocyte progenitor cells (iOPCs) or terminally differentiated cells, such as induced neurons (iNs). These diverse kinds of cell programming-derived neural cells can finally be used for disease modeling and subsequent drug screening. Reprinted by permission from Springer Nature Customer Service Centre GmbH (license number: 5271341130847): Nature, Nature Reviews Neuroscience, 'Evaluating cell reprogramming, differentiation and conversion technologies in neuroscience', Mertens, J., Marchetto, M.C., Bardy, C. & Gage, F.H., © 2016 (Mertens *et al.*, 2016).

1.1.1 Induced pluripotent stem cell reprogramming

Induced pluripotent stem cells (iPSCs) are somatic cell-derived stem cells possessing many ESC-like properties such as the expression of pluripotency-associated markers as, for instance, TRA-1-60, SALL4 and NANOG, the capacity to divide symmetrically and the capability to differentiate into derivatives of all three germ layers *in vitro* as well as *in vivo* (Takahashi & Yamanaka, 2006; Takahashi *et al.*, 2007). Further characteristics of ESCs comprise their existence in a pre-X-inactivation state, the possession of a bivalent epigenetic state (*i.e.*, carrying activating as well as silencing chromatin modifications in parallel at multiple gene loci) and the ability to preserve their self-renewal capacity as well as genomic integrity even after complete loss of DNAm. These features supposedly enable ESCs to maintain their pluripotent state, thus suppressing alternative cell fates, while at the same time preserving the possibility to activate somatic cell type-specific transcriptional programs upon the induction of differentiation

(reviewed by Silva & Smith, 2008). Although extensive histone modification, X-chromosome reactivation and global DNA demethylation are also integral parts of iPSC reprogramming, there are conflicting reports about the overall epigenetic similarity between ESCs and iPSCs. This debate is especially complicated by the substantial degree of variability that is detectable among individual lines of both cell types. Notably, cell line variability is not only evident when PSC lines are derived from genetically distinct donors, but can also be detected in different clones generated from one single donor (see reviews by Buganim *et al*., 2013 and Hanna *et al*., 2010).

In iPSCs, cellular heterogeneity might be to some extent explained by the fact that the reprogramming process itself seems to be at least partially stochastic: In 2009, a mechanistic study on the generation of clonal iPSC lines from mouse pre-B cells, carrying a doxycycline (DOX)-inducible transgene cassette encoding for Oct4, Sox2, Klf4 and cMyc, revealed that up to 93 % of all starter cells can eventually give rise to fully reprogrammed Nanog-positive iPSC clones. However, the time span required for completing the reprogramming process considerably varies from 2 to 18 weeks of DOX treatment. The authors concluded that according to the mathematical model that best described the data acquired in their study, iPSC reprogramming depends on an early, rate-limiting stochastic event, which can be described as a function of cell division and the cell-intrinsic reprogramming rate per cell division (Hanna *et al*., 2009).

Further studies meanwhile corroborated the notion that iPSC reprogramming consists of at least two phases: A first phase associated with the silencing of the cell of origin's transcriptional program, as well as the upregulation of genes related to proliferation, metabolism and cytoskeleton organization, and a second phase that is governed by the activation of a regulatory core TF network, which is relevant for the stabilization and maintenance of the acquired pluripotent state. Focusing on the originally described iPSC reprogramming TF combination (*i.e*., Oct3/4, Sox2, Klf4 and cMyc), Klf4 was reported to be the only TF within this cocktail playing a significant role during both reprogramming phases, as it predominantly represses somatic genes. Conversely, while cMyc mainly aids the first phase of reprogramming inducing proliferation-associated genes, Oct3/4 and Sox2 are especially relevant for establishing and maintaining the core pluripotent network during the second stage (reviewed by (Buganim *et al*., 2013). In line with this, chromatin immunoprecipitation combined with DNA microarray analysis in human ESCs demonstrated that OCT4, SOX2 and NANOG form an autoregulatory feed-forward loop. Additionally these factors co-occupy a number of shared target genes (Boyer *et al*., 2005), and the affinity of OCT4 and SOX2 to form heterodimers seems to be particularly important in this trinity (reviewed by Li & Izpisua Belmonte, 2018). Next to the circumscribed functions of each individual TF, the whole cocktail is thought to stochastically elicit expression changes in pluripotency-associated genes during the first phase of iPSC reprogramming, which are crucial for the consolidation of stable pluripotency later in phase two (see review by Buganim *et al*., 2013 for further details). For reprogramming mouse embryonic fibroblasts into iPSCs, these changes were shown to include upregulation of the ESC markers *Nr0b1* and *Etv5*, which characterizes the emergence of an intermediate reprogramming-prone progenitor population expressing CD73 and CD49d (Lujan *et al*., 2015). Notably though, the group of Jose Polo convincingly showed that iPSC reprogramming starting from mouse fibroblasts, keratinocytes or neutrophils elicits significantly different transcriptional trajectories, which only fully converge at later stages of the reprogramming process. Importantly, their elegant experimental setup further allowed the retrieval of conserved transcriptional changes (*i.e*., changes that were observed in all three paradigms), comprising the concomitant regulation of genes associated with germ cell development, transcription, cell differentiation and stem cell maintenance (Nefzger *et al*., 2017).

Altogether, these mechanistic studies significantly increased our understanding of pluripotency in general and iPSC generation in particular, facilitating the development of the myriad of protocols nowadays available to derive iPSCs from various species and starting cell types. Some of these even make use of different TFs such as NANOG or LIN28 alone or in conjunction with the classical iPSC reprogramming TF cocktail, microRNAs and/or small molecules in combination with a variety of delivery techniques (for further reading see, for instance, Li *et al*., 2013; Yu *et al*., 2014; Biswas & Jiang, 2016 and Tian *et al*., 2016).

Besides efforts to improve the iPSC reprogramming method as such, a major research focus in recent years has been to establish and optimize *in vitro* differentiation protocols starting from PSCs. Classically, these protocols involve extrinsic factors such as morphogens to guide the differentiation process toward a specific cell fate, thereby mimicking regionalization processes during nervous system development. This approach has led to significant advances, for instance, for the generation of midbrain dopamine neurons for the treatment of Parkinson's disease (PD; Kriks *et al*., 2011; Kirkeby *et al*., 2012). To name one specific example, Malin Parmar's lab reported in 2012 that recapitulating the embryonic development of dopaminergic neurons by modelling their transition through a floor plate-like state *in vitro*, significantly improved the authenticity of PSC-derived midbrain progenitors. Upon transplantation into 6-hydroxydopamine (6-OHDA)-lesioned adult rat brains, these cells performed comparable to human fetal ventral midbrain-derived transplants with regard to overall graft survival, the morphology and marker expression of transplant-derived dopaminergic neurons, as well as their capacity to convey behavioral improvements in this PD model (Kirkeby *et al*., 2012). Despite this impressive success, the generation of many neural subtypes is frequently complicated by long differentiation times and complex multi-step growth factor-regimens, which often yield cultures exhibiting a high degree of heterogeneity (see review by Tao & Zhang, 2016). Thus, many growth factor-based protocols still have to be regarded as insufficiently precise when it comes to fine-tuning the specification of distinct neural subtypes, especially considering future biomedical applications.

1.1.2. Forward programming

Since morphogen-based cell specification finally converges on the modulation of specific transcriptional programs, TF overexpression by itself represents an alternative method to guide cell fate acquisition (in the following also referred to as 'forward programming'). How broadly TF overexpression can impact the differentiation of PSCs is illustrated by studies of Minoru Ko and colleagues. The authors established more than 180 transgenic mouse ESC lines by integrating DOX-inducible expression cassettes, each encoding for a distinct TF, into the genomic safe harbor ROSA26 locus of mouse ESCs, and revealed that differentiation of these various engineered ESC lines by DOX-mediated TF overexpression resulted in the specification of a large variety of different somatic cell lineages (Nishiyama *et al*., 2009; Correa-Cerro *et al*., 2011; Yamamizu *et al*., 2016).

Notably, specifying cell fates by TF overexpression is comparably easy to accomplish within one lineage, especially when starting from cell types which are direct progenitors of the target cell type. Almost 20 years ago, Sun *et al*. already reported about the successful derivation of neurons by retrovirally overexpressing the pro-neural basic helix-loop-helix (bHLH) TF Ngn1 in primary rat cortical neural precursor cells (NPCs; Sun *et al*., 2001). Since then, other TFs belonging to the bHLH family have been shown to be capable of forcing neuronal differentiation from different NPC populations. These TFs include various neurogenins (Ngns) such as Ngn1

(Serre *et al*., 2012; Song *et al*., 2017), Ngn2 (Geoffroy *et al*., 2009; Serre *et al*., 2012; Bolós *et al*., 2014; Ho *et al*., 2016; Li *et al*., 2016) and Ngn3 (Serre *et al*., 2012), Ascl1 (Geoffroy *et al*., 2009; Kim *et al*., 2009; Serre *et al*., 2012; Li *et al*., 2016; Barretto *et al*., 2020) as well as members of the Neurod TF family (Hsieh *et al*., 2004).

Interestingly, also rapid neuronal differentiation of PSCs, which are not yet committed to the neural lineage, was shown to be feasible with bHLH TFs. A milestone in the field of neuronal forward programming was reached in 2011, when the groups of Marius Wernig and Thomas Südhof reported that combined overexpression of the TFs ASCL1, BRN2 and MYT1L efficiently drives neuronal specification from human PSCs (Pang *et al*., 2011). The authors revealed that ASCL1 is most crucial for neural fate acquisition, whereas the TFs BRN2 and MYT1L rather promote downstream neuronal maturation. Using the full TF cocktail, electrophysiologically active neurons can be derived from human PSCs after only 6 days of *in vitro* differentiation (Pang *et al*., 2011). Several other labs subsequently demonstrated that Ascl1 alone can efficiently forward program mouse ESCs (Yamamizu *et al*., 2013; Teratani-Ota *et al*., 2016) and human PSCs (Chanda *et al*., 2014; Robinson *et al*., 2016) toward a neuronal fate, albeit with slower differentiation dynamics than the full ASCL1, BRN2 and MYT1L TF combination. Overexpression of other bHLH TFs, too, induces rapid neuronal differentiation of PSCs. In one of the first *in vitro* studies employing overexpression of Ngn1 in mouse ESCs, transduced cells underwent morphological rearrangements forming neurite-like structures already within the first 72 hours and became electrophysiologically excitable as early as 4 days after transgene induction (Tong *et al*., 2010). After 5 days of Ngn2 overexpression, mouse ESC-derived cells express the mature neuronal marker Map2, display neuronal electrophysiological properties at day 10, and form synapses in co-culture with primary mouse hippocampal neurons 20 days post induction (Thoma *et al*., 2012). The first ground-breaking proof that NGN2 has the same effect in human PSCs was – again – provided by the groups of Marius Wernig and Thomas Südhof in 2013. The authors demonstrated that forward programming human PSCs with NGN2 reproducibly yields neurons with almost 100 % purity within 2 weeks, and as was observed in mouse cells, these neurons do not only acquire neuronal-like electrophysiological properties but are also capable of functionally integrating into synaptic networks with cortical mouse neurons. Notably, the authors further reported that overexpressing the bHLH TF NEUROD1 can instruct neuronal differentiation from human PSCs, too (Zhang *et al*., 2013). Already in 2001, O'Shea had investigated the neurogenic effect of Neurod TFs by overexpressing Neurod1, Neurod2 and Neurod3 in mouse ESCs and found that all three Neurod TFs suffice to induce immature neuronal-like cells within 72 hours (O'Shea, 2001). Lastly, also the bHLH TF ATOH1 was demonstrated to instruct neuronal differentiation within a time frame as short as 4 days, being among the top hits when screening a library comprising more than 1,500 TFs for their differentiation-promoting effect in human iPSCs (Alex H. M. Ng *et al*., 2021).

When thinking of forward programming as a tool to rapidly produce neural cell types for brain repair, it is particularly relevant to thoroughly characterize the exact phenotype of the obtained cells. Already Serre *et al*. noted that the four different bHLH TFs NGN1, NGN2, NGN3 and ASCL1 had slightly varying effects on neuronal subtype specification from human primary cortical NPCs, although cultures generally consisted of a mixed population of GABAergic, cholinergic, serotonergic, adrenergic and motor neurons (MNs; Serre *et al*., 2012). This observation is in line with other reports demonstrating divergent effects for different bHLH TFs on neuronal subtype derivation. Overexpression of ASCL1 induces a GABAergic bias in neuronal cultures differentiating from neurospheres isolated from both human fetal cortex and mesencephalon (Kim *et al*., 2009), whereas NGN2 overexpression in human iPSC-derived NPCs (Ho *et al*., 2016) and PSCs (Zhang *et al*., 2013; Nehme *et al*., 2018;

Meijer *et al*., 2019; Rhee *et al*., 2019; Nickolls *et al*., 2020) leads to the derivation of mostly glutamatergic neurons. Mechanistically, Aydin *et al*. reported that although Ascl1 and Ngn2 do not differ in their capacity to target inaccessible (and accessible) genomic regions, their individual binding patterns are largely non-overlapping. In fact, 90 % of all targeted sites were found to be differentially bound by the two TFs as a consequence of their bHLH domain-mediated specificity to distinct E-box motifs. As Ascl1 and Ngn2 both increase chromatin accessibility at their respective target sites, they recruit shared downstream TFs such as Brn2 to different genomic sites, thereby leading to distinct patterns of transcriptional activity. Thus, albeit equivalently inducing pan-neuronal genes, the divergent binding of Ascl1 and Ngn2 elicits distinct neuronal subtype-specific signatures (Aydin *et al*., 2019). Notably, single cell RNA sequencing (scRNAseq) analysis of neurons differentiated from ape as well as human PSCs via NGN2 overexpression very recently revealed that these neuronal cultures still exhibit a quite high degree of overall heterogeneity, although the vast majority could be classified as glutamatergic sensory neurons, unphysiologically co-expressing central and peripheral nervous system (PNS) markers (Lin *et al*., 2021; Schörnig *et al*., 2021). Besides pursuing the derivation of more homogeneous glutamatergic and GABAergic neurons, the combination of pro-neural TFs with TFs exhibiting, for instance, a region-instructing and/or fate-specifying capacity represents a major research focus. Accordingly, forward programming is increasingly been used to generate clinically relevant neuronal subtypes such as midbrain dopaminergic neurons, striatal medium spiny neurons (MSNs), MNs and sensory neurons, as well as astrocytes and oligodendrocytes (for more details see Flitsch *et al*., 2020).

1.1.3. Direct cell fate conversion

The overall success of the iPSC approach demonstrated that cell programming is not restricted to the conversion of related cell types and fueled attempts to achieve somatic-to-somatic cell conversion across germ layers. One avenue pursued in this direction has been the combination of time-restricted expression of the classical iPSC reprogramming TF cocktails with growth factors and small molecules promoting neural lineage development. An exemplar for such a 'partial' reprogramming is the Oct3/4, Sox2, Klf4 and cMyc-driven derivation of neural stem cells (NSCs) from fibroblasts (Janghwan Kim *et al*., 2011; Matsui *et al*., 2012; Thier *et al*., 2012; Lu *et al*., 2013; Meyer *et al*., 2014) or blood cells (Tongguang Wang *et al*., 2013), where transgene expression was combined with an exposure to FGF2, FGF4 and/or EGF (Janghwan Kim *et al*., 2011; Thier *et al*., 2012; Tongguang Wang *et al*., 2013; Meyer *et al*., 2014), FGF2 and/or EGF in conjunction with LIF (Matsui *et al*., 2012) or LIF in combination with the TGFβ-inhibitor SB431542 and the GSK3β-inhibitor CHIR99021 (Lu *et al*., 2013). It is worth mentioning, though, that in accordance with the transient expression of TFs used for generating iPSCs, partial reprogramming to NSCs may involve a short transit through a pluripotency-like state and can result in mixed cultures of iPSCs and NSCs (Bar-Nur *et al*., 2015; Maza *et al*., 2015). Interestingly, such a pluripotency transit can also occur without forced Oct4 expression. Lineage tracing using an Oct4 reporter revealed that NSCs derived by overexpression of Sox2, Klf4 and cMyc in conjunction with the neural-specific TF Brn4 instead of Oct4 (a protocol originally published by Han *et al*., 2012) originate from Oct4-expressing iPSC-like cells (Bar-Nur *et al*., 2015). Although a mechanistic follow-up study from Dong Wook Han's lab revealed that a transient pluripotent intermediate is only established when Brn4, Sox2, Klf4 and cMyc are delivered as a polycistronic construct, while combined overexpression of these four TFs as single vector-constructs mediates direct conversion of mouse embryonic

fibroblasts to NSCs (Velychko *et al*., 2019), such a pluripotency transit can be used to mechanistically discriminate partial reprogramming from direct cell fate conversion (hereafter also denoted as 'transdifferentiation').

A major break-through concerning transdifferentiation across germ layers was in 2010, when the groups of Marius Wernig and Thomas Südhof succeeded in inducing neurons from mouse fibroblasts by overexpressing the neural lineage-specific TFs Ascl1, Brn2 and Myt1l (Vierbuchen *et al*., 2010) – paralleling their experiments on the forward programming of PSCs. Soon thereafter, conversion of human fibroblasts to induced neurons (iNs) was achieved using exactly this ASCL1, BRN2, MYT1L TF combination (Pfisterer, Kirkeby, *et al*., 2011; Pfisterer, Wood, *et al*., 2011), ASCL1, BRN2 and MYT1L in conjunction with NEUROD1 (Pang *et al*., 2011) or BRN2 and MYT1L together with the neuronal microRNA miR124 (Ambasudhan *et al*., 2011). These first seminal reports on transdifferentiating somatic cells into neurons raised strong interest to make this process more efficient and, in particular, to tailor it toward the generation of distinct neural subpopulations. While the initial TF combinations used for iN generation resulted primarily in excitatory neurons, these cultures also contained inhibitory GABAergic neurons (Ambasudhan *et al*., 2011; Pang *et al*., 2011; Ladewig *et al*., 2012; Xiang Li *et al*., 2015; Matsuda *et al*., 2019). However, some groups reported on iN paradigms that strongly enrich for either glutamatergic (Chanda *et al*., 2014; Hu *et al*., 2015; Miskinyte *et al*., 2017) or GABAergic neurons (Karow *et al*., 2012, 2018; Shi *et al*., 2016; Park *et al*., 2017). In order to derive dopaminergic iNs from human fibroblasts, the classic iN reprogramming cocktail ASCL1, BRN2 and MYT1L can be combined with the dopaminergic fate-specifying TFs LMX1A and FOXA2 (Pfisterer, Wood, *et al*., 2011) or a further enriched combination of LMX1A, LMX1B, FOXA2 and OTX2 (Torper *et al*., 2013; Pereira *et al*., 2014). Alternatively, Ascl1 alone has been shown to be sufficient to induce a dopaminergic fate in fibroblasts when combined with Nurr1 and Lmx1a (Caiazzo *et al*., 2011), Nurr1, Lmx1a, Foxa2, Pitx3 and En1 (Jongpil Kim *et al*., 2011) or Nurr1, Lmx1a and miR124 (Jiang *et al*., 2015). Very recently, it has been shown that in the presence of the neurotrophic factors Bdnf and Gdnf, overexpression of Ascl1 and Myt1l alone in human ESCs as well as mouse embryonic fibroblasts can yield dopaminergic neurons with a peripheral subtype identity – a differentiation path that is facilitated by paracrine stimulation of the Wnt1 pathway (Yi Han Ng *et al*., 2021). Moreover, a protocol achieving the conversion of human fibroblasts into dopaminergic iNs by chemical reprogramming using extrinsic factors that inhibit HDAC, TGFβ, GSK3 and ROCK signaling or induce adenylate cyclase, SHH, FGF and WNT activity was lately published (Qin *et al*., 2020). For the derivation of MSNs, combined overexpression of the CNS-enriched miR9/9* and miR124 with MYT1L and the striatal TFs CTIP2, DLX1 and DLX2 was used to convert human fibroblasts into mainly DARPP32-positive GABAergic neurons (Victor *et al*., 2014). Direct conversion has also been used to generate serotonergic (Vadodaria *et al*., 2016; Xu *et al*., 2016) and noradrenergic neurons (Li *et al*., 2019), as well as peripheral sensory neurons (Blanchard *et al*., 2015; Wainger *et al*., 2015) and MNs (Son *et al*., 2011; Liu *et al*., 2016; Abernathy *et al*., 2017; Ichida *et al*., 2018).

Dissecting the process of fibroblast-to-iN conversion using combined overexpression of Ascl1, Brn2 and Myt1l, Marius Wernig and colleagues demonstrated in 2013 that Ascl1 acts as a neuronal pioneer TF. Pioneer TFs are defined as TFs being able to bind to and open up closed chromatin. Therefore, pioneer TFs can not only induce their own target genes in non-permissive epigenetic states but also enable binding and regulation of secondary TFs (Figure 3). Ascl1, for example, binds almost the same target genes in NSCs and fibroblasts, although these sites are mostly in closed chromatin states in fibroblasts. In contrast to Ascl1, Brn2 and Myt1l preferentially bind to open, accessible chromatin regions. In the context of iN conversion, Ascl1 at least partially mediates the

recruitment of Brn2 and thereby regulates the binding of Brn2 to a proportion of its pro-neural target genes (Wapinski *et al*., 2013). In agreement with this concept, overexpression of Ascl1, Brn2 and Myt1l in mouse embryonic fibroblasts yields transient demethylation of a majority of Ascl1's targets in the early phase of iN conversion, and such demethylated regions are enriched in Brn2 binding sites (Luo *et al*., 2019). In contrast to Brn2, Myt1l's main function is to interact with the Sin3b-HDAC1 complex to repress non-neuronal transcriptional programs. Myt1l-repressed targets include genes promoting proliferation, such as *Hes1*, and genes inducing alternative lineages, including targets relevant for myocyte differentiation (Mall *et al*., 2017).

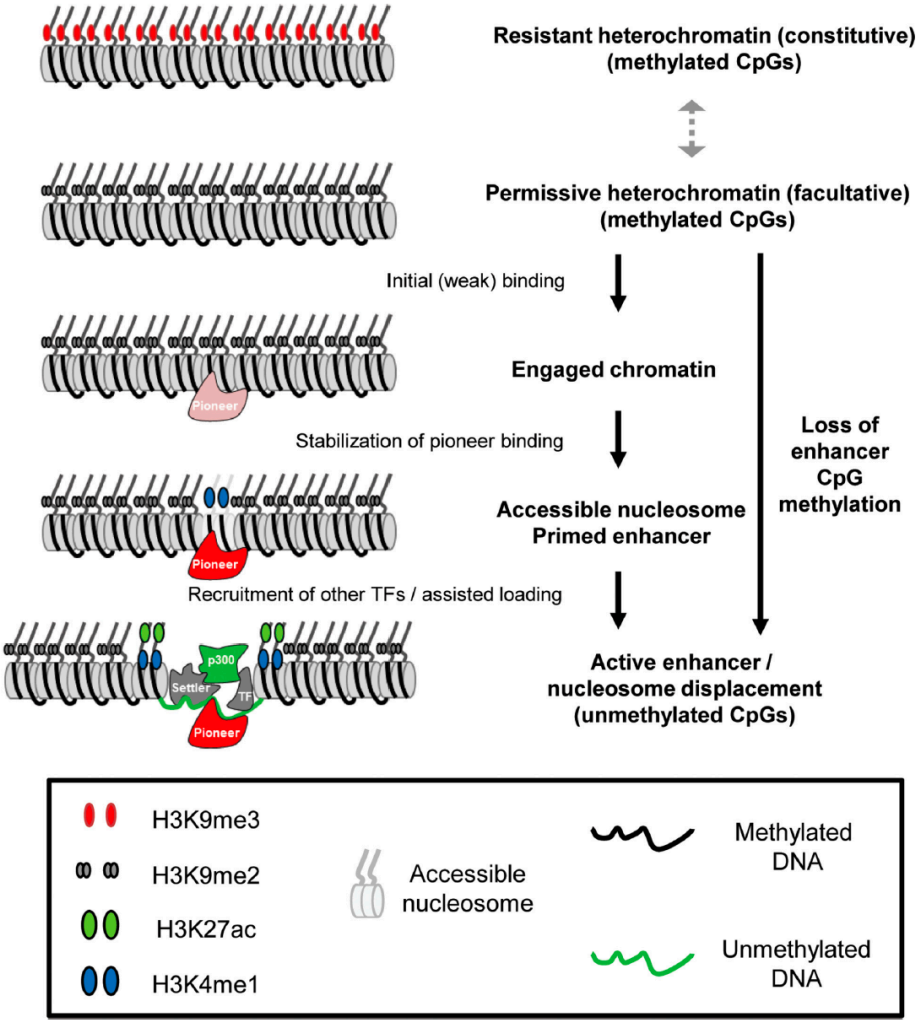

Figure 3: Pioneer TFs can target closed chromatin and enable subsequent binding of secondary TFs.
Pioneer TFs are able to weakly bind to facultative heterochromatin, inducing a chromatin transition that allows the stabilization of pioneer TF binding. Central nucleosomes that become more accessible during this transition can represent the state of primed enhancers. Pioneer TFs subsequently recruit the general coactivator p300 and other TFs to the accessible nucleosome, which is further characterized by bimodal distribution of H3K27ac and H3K4me1, as well as loss of CpG methylation. Figure from Mayran, A. & Drouin, J. (2018) 'Pioneer transcription factors shape the epigenetic landscape', Journal of Biological Chemistry, 293(36), pp. 13795–13804. doi:10.1074/jbc.R117.001232 (Mayran & Drouin, 2018), published under the terms of the Creative Commons CC-BY license.

Although Ascl1 alone is, in principle, sufficient to induce a neuronal state in fibroblasts, transdifferentiation with Ascl1 in conjunction with Brn2, Myt1l is far more efficient and exhibits faster maturation dynamics (Chanda *et al*., 2014). In line with this finding, a scRNAseq study conducted by Barbara Treutlein's group found the continued

expression of Ascl1 as well as co-expression of Brn2 and Myt1l to be essential for stabilization of the neuronal fate and subsequent neuronal maturation, whereas silencing of Ascl1 in the course of the conversion process resulted in the reappearance of fibroblast signatures. Notably, the majority of Ascl1 only-induced cells do not acquire a neuronal identity, even if Ascl1 expression levels are maintained, but activate a myocyte-related transcriptional program (Treutlein *et al*., 2016). In accordance with this, upon mouse fibroblast-to-iN conversion, epigenetic remodeling, especially with regard to neuron-associated non-CG methylation, is much less pronounced in the absence of Brn2 and Myt1l. Non-CG methylation was shown to be highly relevant for gene repression during neuronal conversion, either constitutively or dynamically upon TF induction, significantly contributing to the suppression of fibroblast- and myocyte-related transcriptional signatures (Luo *et al*., 2019).

Similar to ASCL1, NGN2 is – in principle – able to convert human fetal fibroblasts into neurons, although transdifferentiation mediated by overexpression of this TF alone is extremely inefficient. However, this low conversion efficiency is significantly enhanced by the small molecules forskolin and dorsomorphin, which promote chromatin accessibility at pro-neural NGN2 binding sites. More specifically, forskolin and dorsomorphin enhance the enrichment of CREB1 at sites bound by NGN2, thereby inducing the expression of the pro-neural gene *SOX4*. SOX4, in turn, elicits further downstream chromatin remodeling and consequently facilitates the activation of other pro-neural genes such as *NEUROD1* and *NEUROD4* (Smith *et al*., 2016).

Notably, for other somatic cell types, different pioneer factors might be required to promote cell fate conversion. In mouse microglia, for instance, not Ngn2 or Ascl1 but Neurod1 acts as a neuronal pioneer TF, specifically inducing transcription of its bivalently marked pro-neural target genes. Along the same line, oligodendrocytes, which also feature bivalent histone modifications at pro-neural Neurod1 target genes, were successfully reprogrammed into neurons by Neurod1 overexpression (Matsuda *et al*., 2019). Together, these data indicate that, in addition to pioneer factors, secondary fate-specifying or alternative fate-repressing cues (or both) are necessary to ensure proper phenotype stabilization. Consequently, Kristin Baldwin and colleagues recently screened a library of 598 TF pairs for their ability to convert mouse embryonic fibroblasts into functional iNs. As expected, almost all successful combinations included at least one member of the Ascl, Ngn or Neurod families. However, also pairs of pro-neural TFs comprising no pioneer TF yielded functional iNs, demonstrating that pioneer TFs are not an indispensable condition for direct cell fate conversion (Tsunemoto *et al*., 2018). Along similar lines, the group of Lei Qi performed a CRISPR activation screen to identify single TFs and TF combinations that promote differentiation of mouse ESCs and direct conversion of fibroblasts into neurons. In addition to known pro-neural TFs such as Ngns or Brn2, their top hits included also non-pioneer TFs and even non-neural-specific TFs such as the epigenetic regulator Ezh2 (Liu *et al*., 2018).

Taken together, the currently available data support a two-stage architecture of the conversion process. First, target cell type-specific genes need to be made accessible in case they are in an unfavorable chromatin state in the starting cell type. In addition to pioneer TFs, epigenetic modifiers or other factors modulating chromatin accessibility can exert this effect. Overexpression of miR9/9* and miR124, for instance, has been shown to promote gradual remodeling of chromatin accessibility at fibroblast-specific enhancers (change to closed chromatin) and chromatin opening at pan-neuronal gene loci (Abernathy *et al*., 2017). Second, after induction of epigenetic plasticity, acquisition and stabilization of a new cell fate has to take place. Although this process can be initiated and orchestrated by pioneer TFs, too, it mostly involves additional TFs. These can be either co-transduced in the

starting cell along with the pioneer TF (*i.e.*, by overexpressing TF combinations), induced by small molecules used to promote the direct conversion process or they are direct transcriptional targets of the pioneer TF and thus secondarily induced by the pioneer itself. Eventually, pioneer as well as non-pioneer TFs instruct the adoption of a specific cell fate either through active induction of target lineage-specific genes (as was demonstrated for, *e.g.*, Ascl1 (Treutlein *et al.*, 2016) or Neurod1 (Matsuda *et al.*, 2019)) or transcriptional repression of genes instructing alternative cell fates (as shown for, *e.g.*, Myt1l (Mall *et al.*, 2017)). Notably, however, the process of fate acquisition might involve additional intermediate steps, since scRNAseq time course analyses of the iN conversion process indicate the presence of transient, unstable progenitor-like identities before a stable neuronal phenotype is adopted (Treutlein *et al.*, 2016; Karow *et al.*, 2018). As overarching mechanistic principles underlying cell fate conversion become increasingly uncovered, it is important to note that the exact mechanisms of fate switches will always comprise components highly specific to the identity of the interconverted cell types and the individual conversion paradigm.

While direct transdifferentiation into a neuron remains a fascinating concept, the applicability of this approach can be limited by the fact that neurons are post-mitotic. Due to their inability to divide, low conversion efficiencies and cell death accompanying the transdifferentiation procedure are major limiting factors restricting large-scale applications (see also review by Prasad *et al.*, 2017). Several studies addressed this bottle neck, showing that modulation of signaling pathways by small molecules (*e.g.*, inhibition of SMAD, GSK3, Src kinase and HDAC signaling or activation of cAMP and SIRT1 signaling) significantly improves iN conversion (Ladewig *et al.*, 2012; Pfisterer *et al.*, 2016). For example, Herdy *et al.* reported that combining JAK2 inhibition (promoting cell cycle arrest and mesenchymal-to-epithelial transition) with integrin and RAF1 activation (facilitating morphological rearrangements) as well as HIF1α inhibition (fostering the switch from glycolysis to oxidative phosphorylation) efficiently improves human fibroblast-to-neuron conversion (Herdy *et al.*, 2019). Moreover, in inducible viral systems, delivering multiple programming factors by all-in-one, polycistronic vectors (Herdy *et al.*, 2019) and including a recovery phase between viral transduction and transgene activation (Pereira *et al.*, 2014) has been shown to increase conversion efficiency. Lastly, reducing reprogramming barriers in somatic cells, such as inhibiting REST signaling in human fibroblasts (Drouin-Ouellet *et al.*, 2017), overcoming senescence (Sun *et al.*, 2014) or inducing epigenetic remodeling by *TET1* activation (Jiang *et al.*, 2015), have been reported to boost iN generation, too. In addition, however, since not all cells undergo successful transdifferentiation, elimination of partially reprogrammed cells remains an issue. Moreover, each transdifferentiated neuron represents a singular event and thus cannot be subjected to common batch control-based quality-control (QC) regimens, limiting the degree of standardization that can be reached with iN cultures. In light of this, expandable NSCs or NPCs could offer an interesting alternative. Indeed, several groups reported on the successful transdifferentiation of mouse (Lujan *et al.*, 2012; Tian *et al.*, 2012) and human fibroblasts (Ring *et al.*, 2012; Zou *et al.*, 2014; Yu *et al.*, 2015; Shahbazi *et al.*, 2016; Hou *et al.*, 2017; Xiao *et al.*, 2018) into still-proliferative NSCs or NPCs using different NSC-enriched TFs or TF combinations. Other somatic cells, too, were found to be amenable to direct neural conversion. In this context, easily accessible cell populations such as blood-derived (Giorgetti *et al.*, 2012; Castaño *et al.*, 2014; Sheng *et al.*, 2018; Thier *et al.*, 2019) and urine-derived cells (Lihui Wang *et al.*, 2013) are of particular interest for personalized medicine.

1.2. The aging caveat

The rise of cell programming has created the general opportunity to derive neural cells from basically any adult human and thus revealed new avenues for disease modeling and cell replacement strategies. Yet, since significant transcriptomic and epigenetic remodeling plays a pivotal role in the process of cell programming, it seems natural to ask how different programming paradigms affect other cellular signatures relevant to biomedical applications, such as those related to age. This becomes especially relevant considering that aging is itself characterized by massive epigenetic changes, including the remodeling of histone marks (*e.g.*, H3K4me3 activation mark in euchromatin and H3K27me3 repressive modification in eu- as well as heterochromatin), as well as a global loss of DNAm mainly at repetitive regions of the genome associated with constitutive heterochromatin and local hypermethylation especially at promoter CpG dinucleotides (reviewed by (Sen *et al.*, 2016) and (Zhang *et al.*, 2020). Yet, age is a highly multi-faceted and inter-connected phenomenon that affects the whole organism, and is thus hard to assess by simple means (see also reviews by Studer *et al.*, 2015 and Galkin *et al.*, 2019). Therefore, several animal models were implemented over the last decades to study physiological aging and assess the effects of longevity-promoting strategies (for a comprehensive review see Mitchell *et al.*, 2015). In conjunction with cell culture-based basic research, these studies led to the identification of several pathways that are dysregulated upon aging and can be targeted to increase life span. Amongst others, potential targets include contributors to DNA damage, mitochondrial dysfunction, telomere shortening, altered nutrition sensing, impaired proteostasis and autophagy, as well as inducers of abnormalities in nuclear organization and inflammation (Figure 4). Interestingly, many of the identified pathways are also critically involved in the regulation and maintenance of stem cells, which could explain why their exhaustion represents a key feature of organismal aging (reviewed by Chandel *et al.*, 2016).

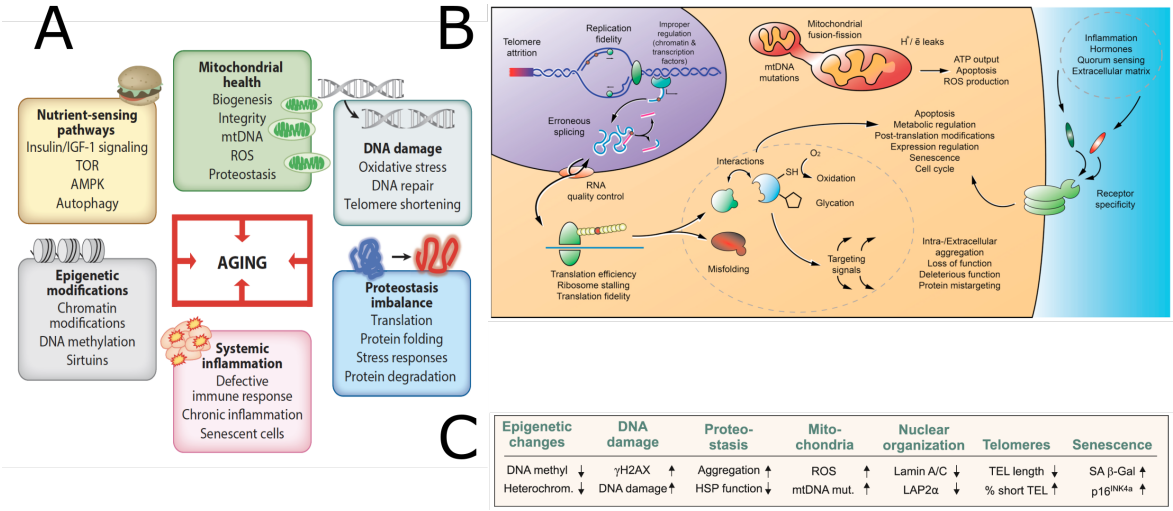

Figure 4: The many facets of aging.
(A) Representation of different pathways associated to organismal aging. Figure panel republished with permission of Annual Reviews, Inc., from 'Signaling networks determining life span', Riera, C.E., Merkwirth, C., De Magalhaes Filho, C.D. & Dillin, A. Annual Review of Biochemistry, 85, pp. 35–64, © 2016 (Riera *et al.*, 2016); permission conveyed through Copyright Clearance Center, Inc. (order license ID: 1200817-1). mtDNA: Mitochondrial DNA, ROS: Reactive oxygen species. **(B)** Simplistic schematic of how diverse age-associated dysfunctions might be interconnected on a cellular level. Figure panel reprinted from Ageing Research Reviews, 49, 'Reversibility of irreversible aging', Galkin, F., Zhang, B., Dmitriev, S.E. & Gladyshev, V.N., pp. 104–114, © 2019 (Galkin *et al.*, 2019), with permission from Elsevier (license number: 5271400452751). **(C)** Table summarizing cellular changes typically observed in aged cells. Figure panel reprinted from Cell Stem Cell, 16(6), 'Programming and reprogramming cellular age in the era of induced pluripotency', Studer, L., Vera, E. & Cornacchia, D., pp. 591–600, © 2015 (Studer *et al.*, 2015), with permission from Elsevier (license number: 5271381408885). HSP: Heat shock protein, TEL: Telomere.

1.2.1. Cellular hallmarks of aging

Cellular aging is associated with a number of biochemical and molecular features that collectively result in increasing functional decline of cells, tissues and eventually the whole organism over time. Although many cause-consequence-relationships are debatable in the aging field, **DNA damage** certainly represents one of the main drivers of organismal aging. Human old donor-derived fibroblasts, for instance, are characterized by an increase of nuclear foci containing core histones H2AX phosphorylated at serine 139 (γH2AX; Scaffidi & Misteli, 2006), a reaction that mainly occurs in response to stochastic or induced DNA double-strand breaks (DSBs). In neurons, γH2AX was shown to accumulate in persistent DNA damage foci consisting of DNA with only slowly repaired or even irreparable DSBs (Mata-Garrido *et al*., 2016). In concordance with this observation, Lodato *et al*. demonstrated in 2017 using single cell whole-genome sequencing that the number of somatic single nucleotide variants in human neurons highly correlates with a donor's chronological age (Lodato *et al*., 2018). On the one hand, accumulation of DNA damage can result from defects in DNA repair mechanism. As such, different mouse models carrying deficiencies in enzymes involved in DNA repair (*e.g*., Ku70, Ku80, Xpf1, Xpd, Xrcc5, Wrn or Ercc2) were reported to be short-lived and exhibit an early aging onset (reviewed by Riera *et al*., 2016). Concordantly, many human pre-mature aging diseases are caused by mutations in relevant components of the DNA repair machinery, applying to the Werner syndrome (caused by mutations in the gene encoding for the RecQ-like DNA helicase WRN), ataxia telangiectasia (related to mutations in the gene encoding for the ATM kinase that is involved in the signaling cascade elicited after DNA DSBs), Xeroderma pigmentosum (associated to mutations in genes involved in nucleotide excision repair) and the Cockayne syndrome (mutations in *CSA* or *CSB*, which are involved in transcription-coupled nucleotide excision repair; reviewed by Mitchell *et al*., 2015).

On the other hand, increased DNA damage can be a consequence of **mitochondrial dysfunctions** that lead to increased oxidative stress. Cells experience oxidative stress when there is a non-physiological excess of reactive oxygen species (ROS), which are molecules derived from molecular oxygen such as superoxide, hydrogen peroxide, hydroxyl radicals or peroxynitrite. Thus, ROS are highly reactive by-products of the energy metabolism via the mitochondrial electron transport chain and can lead to the oxidation of lipids and proteins, as well as the induction of DNA damage (reviewed by Turrens, 2003). In line with the hypothesis that increased ROS levels are implicated in cellular aging, mitochondrial overexpression of human catalase, a ROS-scavenging enzyme, leads to increased life span in mice (Schriner *et al*., 2005). Notably though, mitochondrial dysregulation might contribute to cellular aging via ROS-independent mechanisms, too. For example, mutations in *Polg*, resulting in the generation of an error-prone active mitochondrial DNA polymerase Pol-γ, lead to the accumulation of mitochondrial DNA mutations in mice with increasing age. *Polg*-mutant mice exhibit respiratory chain dysfunctions, but neither increased ROS production nor ROS-induced stress response, as well as symptoms representative of human aging and an overall decreased life span (reviewed by Loeb *et al*., 2005). Furthermore, the NAD-dependent deacetylase Sirt1 is implicated in aging across several species (Mitchell *et al*., 2015). Since Sirt1 activation and the subsequent induction of its downstream target, the transcriptional co-activator Pgc1α, increases mitochondrial biogenesis, metabolism and function (reviewed by Riera *et al*., 2016), mitochondrial health is impaired upon the age-dependent decline of NAD^+ levels (Sen *et al*., 2016). Sirt1 activation can be boosted by physical activity, low caloric diets (which also increase ROS scavenging and can additionally influence DNAm, subsequently regulating p16 expression levels via effects on Tet1, Tet3 and Dnmt1 activity) or the

naturally occurring phytoalexin resveratrol (see reviews by Mitchell *et al*., 2015; Riera *et al*., 2016 and Zhang *et al*., 2020).

Importantly, the Sirt1-Pgc1-axis further represents a linkage point to other pathways dysregulated upon aging, such as oscillatory transcriptomic changes related to the circadian rhythm (Zhang *et al*., 2020) and **telomere shortening**, which was shown to result in activation of p53 signaling that in turn represses Pgc1 isoforms (Sahin *et al*., 2011). Telomeres are repetitive TTAGGG DNA sequences at the end of eukaryotic linear chromosomes that do not encode functionally relevant genetic information. Since the DNA replication machinery is unable to copy the DNA over its entire length, parts at the end of the chromosomes are lost with each cell division. In the absence of telomerase expression and activity, being the enzyme that synthesizes telomeric repeats onto the 3' overhangs of the telomeric region, cell proliferation thus leads to the shortening of this region (also called telomere attrition). If telomeres become critically short, they are recognized as chromosomal breaks, leading to chromosomal instability and finally replicative senescence (see review by Bekaert *et al*., 2005). Although patients diagnosed with dyskeratosis congenita – a disease caused by mutations in genes that are believed to be involved in maintenance of telomeres – are characterized by comparatively mild symptoms of physiological aging (such as varying degrees of nail dystrophy, reticular hypopigmentation, leukoplakia, bone marrow failure, idiopathic lung fibrosis, greying of hair and hair loss), the cellular consequences of telomere shortening and replicative senescence have been manifold associated with aging on a cellular level (Mitchell *et al*., 2015). Although the mechanistic relationship between telomere attrition, replicative senescence and cellular aging remain at least partially elusive to date, p53 might represent a key mediator of this trinity. Next to the well-known role of p53 in carcinogenesis, a case report study utilizing fibroblasts derived from a patient suffering from a segmental progeroid syndrome revealed its mechanistic contribution to cellular aging. Specifically, the study linked the patient's premature aging phenotype to a homozygous antiterminating germline mutation in *MDM2* (c.1492T>C), encoding the E3 ubiquitin-protein ligase that forms an autoregulatory feedback loop with p53. The identified mutation resulted in an MDM2 mutant with compromised capability to oligomerize with and subsequently degrade p53, resulting in constitutive stabilization of p53. As a consequence of the reduced regulatory activity of MDM2, p53 primarily mislocalized to the nucleus and was hyperactivated especially under stress conditions. The cellular consequences resulting from altered p53 signaling included early replicative senescence and loss of LMNB1 expression (see below; Lessel *et al*., 2017).

Furthermore, p53 represents an interesting suspect for mediating aging due to its known diverse interactions with, among others, **nutrient-sensing pathways** such as insulin, IGF1, AMPK and mTOR signaling (see also review by Riera *et al*., 2016). The aging-relevant cross-talk between these diverse pathways is also nicely illustrated, for example, by the various effects of the anti-diabetic drug metformin, which at the same time acts on glucose/insulin signaling, activates AMPK (which has in turn direct consequences for the activity of various epigenetic enzymes such as HATs, HDACs, DNMTs and TETs, see Zhang *et al*., 2020), reduces mitochondrial respiratory chain function and – presumably as a result of the sum of all these effects – mimics the life span-increasing effect of caloric restriction (Sen *et al*., 2016). Notably, while a first clinical trial administering recombinant human growth hormone, dehydroepiandrosterone and metformin to 51- to 65-year-old men resulted in reversal of thymic shrinkage, a decrease in monocytes and increase in naïve CD4 and CD8 T cells being indicative of counteracting immunosenescent trends, as well as a small but significant reduction in epigenetic age (Fahy *et al*., 2019), the mechanisms liking these individual pathways to aging are only partially understood. While IGF1 signaling extends

the life span of mice, nematodes and potentially also birds by increasing the cellular resistance to oxidative stress and compensating DNA damage accumulation, inhibition of the mTOR pathway, for instance by rapamycin, increases the life expectancy of yeast, nematodes, flies and invertebrates presumably via its effects on autophagy (for more details see Mitchell *et al*., 2015 and Riera *et al*., 2016).

While short-lived proteins are mainly subjected to proteasomal degradation, long-lived proteins are typically cleared in lysosomes. To this end, cytosolic proteins are captured in double-membrane vesicles called autophagosomes, which then fuse with lysosomes for degradation – a process called **autophagy**. The conjugate of ATG5, ATG12 and LC3 (mammalian homolog to Atg8) is involved in early autophagosome formation (Mizushima *et al*., 2002), and especially transcriptional downregulation of *ATG5* was previously shown to be associated with physiological aging in humans (Lipinski *et al*., 2010). Accordingly, to investigate the consequences of autophagy activation in mammals, researchers have ubiquitously overexpressed Atg5 in transgenic mice, resulting in a median life span extension of approximately 17 %. Mechanistically, besides increasing autophagy, overexpression of Atg5 enhances insulin sensitivity, glucose tolerance and glucose clearance, as well as elevates mitochondrial oxygen consumption rates, leading to a higher resistance against oxidative stress (Pyo *et al*., 2013). Exogenous application of the naturally occurring polyamine spermidine was also shown to extend the life span of yeast, flies, worms, mice and rejuvenate human peripheral blood mononuclear cells (PBMCs) by various mechanisms, including the induction of histone H3 hypoacetylation at all acetylation sites, the reduction of necrosis and age-related oxidative stress, as well as the increase of alkaline phosphatase activity and thus upregulation of autophagy. Interestingly, attenuating the latter by the knock-out of Atg7 or Becn1 abolishes the life span-prolonging effect of spermidine in yeast, flies and *Caenorhabditis elegans* (Eisenberg *et al*., 2009). Altogether, these studies emphasize the mechanistic connection between autophagy and cellular aging, and a comprehensive study by García-Prat *et al*. illustrated in 2016 that autophagy is additionally related to organismal aging via its impact on stem cells. Specifically, aged murine satellite muscle stem cells were found to exhibit overall increased LC3 and p62 levels, as well as ubiquitin-positive inclusions. Along with the fact that treatment with the autophagic flux inhibitor bafilomycin did not results in further upregulation of LC3-II, as is observed in bafilomycin-treated young muscle stem cells, these findings indicate that old satellite cells are characterized by a significantly impaired autophagic activity. García-Prat *et al*. showed, however, that restoration of basal autophagy by treatment with rapamycin or spermidine can prevent replicative senescence, which is accompanied by decreased $p16^{Ink4a}$, γH2AX and SA-β-gal levels, and restores the dysregulation of mitochondrial membrane potential, ROS levels and mitophagy in aged satellite cells. Atg7 overexpression and treatment with the ROS inhibitor trolox in aged satellite cells, as well as genetic silencing of the $p16^{Ink4a}$ axis in Atg7-deficient young satellite cells, could equally rescue muscle stem cell function, indicating that increased ROS production, resulting from age-associated impairments in autophagy, might lead to replicative senescence via activation of the $p16^{Ink4a}$ axis. The causal link between impaired autophagy and an aged phenotype of muscle stem cells was finally consolidated in human cells, too, in which rapamycin treatment sufficed to normalize p62, ROS and SA-β-gal levels (García-Prat *et al*., 2016).

Besides accumulation of DNA damage, mitochondrial dysregulation, deficient autophagy, and the activation of apoptosis and senescence pathways, **abnormalities of the nuclear envelope** seem to be associated with cellular aging. For instance, the human pre-mature aging disease Hutchinson-Gilford progeria syndrome (HGPS) is predominantly caused by mutations in the *LMNA* gene, leading to the accumulation of a truncated, dominant-negative LMNA form called progerin (Hennekam, 2006). Its expression is associated with various age-associated

hallmarks, including the induction of DNA DSBs, the reduction of proteasome activity and autophagy, as well as epigenetic alterations. Furthermore, progerin was hypothesized to also contribute to defects in the diffusion barrier of the endoplasmic reticulum in NSCs (Moore *et al*., 2015), leading to impairments in maintaining stemness via asymmetrical division and distribution of damaged macromolecules (see review and commentary by Sen *et al*., 2016 and Mendelsohn & Larrick, 2015, respectively). The close relationship between HGPS and aging can also be seen by the various pathways that were demonstrated to be involved in the pathogenesis of HGPS downstream of progerin and/or can be targeted to ameliorate HGPS symptomatology (see review by Guilbert *et al*., 2021). Thus, the pathogenesis underlying HGPS seems to mimic accelerated physiological aging not only on an organismal, but also on a cellular level. In 2006, Paola Scaffidi and Tom Misteli comprehensively characterized age-associated phenotypes in human fibroblasts obtained from young and old donors, as well as HGPS patients. Next to the accumulation of DNA damage, they found loss of HP1, H3K9me3 and LAP2 proteins in physiologically aged fibroblasts. Similar to fibroblast lines obtained from HGPS patients, these defects were shown to aggravate with prolonged *in vitro* cultivation in young as well as old donor-derived cell lines, albeit aged fibroblasts exhibiting an increased speed of defect accumulation. Notably, healthy fibroblasts of both age groups equally expressed progerin, confirming the sporadic use of the *LMNA* cryptic splicing site that is constitutively active in most HGPS patients. In HGPS fibroblasts, the presence of the mutant LMNA form was demonstrated to lead to mislocalization of wild-type LMNA from the nucleoplasm to the nuclear rim, and this phenotype was also observed in old, but not young donor-derived fibroblasts. Blocking aberrant *LMNA* splicing, consequentially reverting nuclear mislocalization of LMNA, in old donor-derived fibroblasts resulted in reduced expression of the p53 target genes *CDKN1a* (encoding for p21), *IGFBP3* and *GADD45B*, and additionally increased proliferation (Scaffidi & Misteli, 2006). Importantly, in contrast to progerin, expression of the Lmna wild-type form was reported to rise with increasing age as well as *in vitro* passage in mouse tail tip fibroblasts on RNA as well as protein level, and low Lmna levels were demonstrated to especially support stemness, as they are associated with a higher proliferative and differentiation capacity of stem cells (Zuo *et al*., 2012).

Another member of the lamin family of proteins with strong implications for aging and senescence is LMNB1. In mammals, LMNB loss is observed in senescent fibroblasts, potentially as a consequence of p53 induction, fibroblasts with shortened telomere lengths or DNA damage accumulation, primary fibroblasts obtained from progeria patients, as well as physiologically aged human skin keratinocytes (see review by Chen *et al*., 2015). In human lung fibroblasts undergoing replicative senescence, transcriptional downregulation of *LMNB1* was suggested to be a consequence of substantial chromatin re-organization (see review by Sen *et al*., 2016), leading to the formation of large-scale domains of H3K4me3 and H3K27me3 over lamin-associated domains (Shah *et al*., 2013). Different from LMNA, LMNB's role in cellular aging is less attributable to its role within the nuclear architecture than to its association with **inflammation**. In *Drosophila melanogaster*, for example, age-related loss of LAM (homolog to mammalian LMNB) reduces H3K9me3 on immune response genes, causing systemic inflammation and finally the disruption of tissue homeostasis. The proposed association between aging, its cellular consequences and inflammation is in accord with various other reports that led to the creation of the term 'inflammaging' in order to describe this profound interaction. Naturally, low-grade systematic inflammation can result from several sources other than LMNB loss. Some of these are distributed throughout the body via the blood stream, and thus presumably account for the health-improving effect of heterochronic parabiosis that has been observed in mice (reviewed by Galkin *et al*., 2019). Next to general age-associated impairments of the adaptive

immune response, circulating inflammaging signals may include metabolic triggers of metainflammation and senescent cells, which release a unique senescence-associated secretory profile (SASP; see also reviews by Riera *et al*., 2016 and Galkin *et al*., 2019). Interestingly, upregulation of SASP genes and the $p16^{INK4a}$/$p14^{ARF}$-encoding *CDKN2a* gene locus in senescent cells can – again – result from epigenetic alterations such as the loss of H3K27me3 (Bracken *et al*., 2007; Shah *et al*., 2013). In this context, it is interesting to note that the group of Hartmut Geiger introduced 4-day-long systemic application of a Cdc42-inhibiting small molecule termed 'CASIN' as an intervention prolonging the lifespan of mice, which were 75 weeks-old at the onset of treatment. In their study, inhibition of Cdc42 activity led to epigenetic rejuvenation of peripheral blood 9 weeks post treatment. Albeit not altering blood cell composition, CASIN treatment rescued the age-related increase in serum concentrations of the pro-inflammatory cytokines Ifnγ, Il1α and Il1β already 7 days after intraperitoneal CASIN injection (Florian *et al*., 2020), providing further evidence for a link between age-associated epigenetic alterations and inflammaging. Finally, it is important to note that non-cell-autonomous age-associated changes such as systemic inflammation can impact the microenvironment of stem cells (also called stem cell niches). Altered niche signaling might, in turn, affect stem cell properties and functions, and thus also indirectly contribute to age-associated stem cell exhaustion (next to the afore-mentioned cell-intrinsic, aging-related changes; see review by Ermolaeva *et al*., 2018).

In sum, aging is a highly complex process that is induced, regulated and modulated at various different levels within a cell as well as by non-cell-autonomous mechanisms. While not all of the discussed cellular aging hallmarks might appear with the same timing and/or within all tissues, the accumulation of functional decline, which is a consequence of the various described age-associated processes, can certainly be expected to shape the aging state of the whole organism, determining its lifespan.

1.2.2. Age preservation upon cell programming

Some aspects of cellular aging, such as compromised nuclear architecture, cannot be easily assessed in a quantitative manner. Others, as for instance senescence and telomere length, might not strictly correlate with biological age, depending on the tissue context (Lowe *et al*., 2016; Baek *et al*., 2019). One alternative way to estimate the biological age of a cell independent of its somatic cell fate is to analyze DNAm signatures and apply algorithms calculating a DNAm age (Horvath, 2013; Horvath *et al*., 2018). When applied to iPSC generation, DNAm ages have been shown to be reset upon induction of pluripotency, which is in line with the fact that iPSC reprogramming resets the starting cell's identity back to an embryonic-like state (Horvath, 2013; Lo Sardo *et al*., 2017). Moreover, iPSCs lose age-related cellular signatures, such as shortened telomeres, nuclear lamina abnormalities, mitochondrial and proteostatic dysfunctions, as well as DNA damage and senescence, in the course of the reprogramming process (Lapasset *et al*., 2011; Prigione *et al*., 2011; Miller *et al*., 2013; further reviewed by Ly, 2011; Studer *et al*., 2015). Thus, somatic-to-iPSC reprogramming represents a tool to derive epigenetically and cellularly rejuvenated cells.

Conversely, in 2015, the groups of Yixuan Wang and Fred Gage demonstrated that aging hallmarks such as age-specific transcriptional signatures and the age-dependent loss of nucleocytoplasmic compartmentalization are preserved in mouse (Yang *et al*., 2015) and human (Mertens *et al*., 2015) iNs, respectively. In the latter study,

three genes – namely the nuclear pore-associated transport receptor gene *RANBP17*, the laminin subunit alpha-3 encoding gene *LAMA3* (alias *LAMNA*) and the p53 target gene and negative regulator of telomerase activity *PCDH10* (Shi *et al*., 2015; Zhou *et al*., 2015) – were identified as potential cell type-independent master regulators of aging, since these genes were concordantly regulated in differentially aged human fibroblasts, *postmortem* cortex samples and fibroblast-derived iNs (Mertens *et al*., 2015). One year after these reports it was demonstrated that the telomere lengths and DNAm ages of iNs are retained, too, and almost perfectly correlate with their donor cells' signatures. Moreover, fourteen microRNAs were identified that are similarly regulated in fibroblasts obtained from donors of varying ages and the iNs derived thereof. Among these microRNAs are miR-10a and miR-497, which were shown to be upregulated in aged striatum and cortex samples, too, and have been linked to age-associated pathways such as senescence and telomerase activity (Huh *et al*., 2016). Over the last few years, several other studies corroborated the notion that age-associated cellular alterations such as senescence, susceptibility to DNA damage, mitochondrial defects, loss of heterochromatin and alterations in nuclear organization are preserved in fibroblast-derived iNs (Tang *et al*., 2017; Yongsung Kim *et al*., 2018). These findings altogether indicate that iNs maintain not only epigenetic but also functional age-related phenotypes of their cells of origin.

Taken together, since the beginning of this century, the cell programming toolbox has expanded rapidly, and despite the many mechanistic similarities underlying the different techniques, some features such as the preservation of age memory seem to be unique for each paradigm.

1.3. Biomedical applications for programmed human cells

Notwithstanding the many fundamental and translational questions that remain to be addressed in the context of cell programming, this field provides fascinating prospects for a number of biomedical applications ranging from disease modeling via drug discovery to cell therapy and endogenous regeneration. While PSC-based models might be valuable for studying diseases with a developmental component, the prospect of age preservation in iNs could render these cells a preferred resource for patient-specific modelling of late-onset neurodegenerative disorders. Both paradigms could, thus, be useful for establishing *in vitro* systems for disease modeling and subsequent compound screening. As for regeneration, somatic cell fate conversion and TF-based forward programming of PSCs could enable intricate approaches for generating neural subtypes faster and with much higher precision than conventional iPSC-based and extrinsic factors-driven cell derivation methods. Finally, *in vivo* transdifferentiation is about to revolutionize our concepts for neuroregeneration and might, for some applications, eventually substitute traditional cell transplantation strategies.

1.3.1. Cell programming-derived neurons for disease modeling and drug screening

Research utilizing animal disease models is undeniably a valuable component for generating knowledge that could eventually help to develop new treatment options for various disorders, which might also affect humans. Often enough, however, it has been demonstrated that the translatability to the human system can be heavily compromised by species-specific aspects of pathogenesis. This especially applies to neurological and

neuropsychiatric disorders, which can be associated with proteins or protein functions that might not be conserved across species, depend on the comparatively long human life span, and/or primarily affect higher-order cognitive functions that are exclusive to more complex brains. Accordingly, simplified *in vitro* models employing human cells for disease modeling and drug screening by now represent an indispensable staging post on the route to the clinics. Owing to the relatively long history of iPSC reprogramming, a huge variety of patient-derived iPSC lines has meanwhile been generated, banked and used to this end. Moreover, initiatives to implement common QC regimens, increasing the robustness and reproducibility of iPSC-based research, have been undertaken (more information on the use of iPSCs for studying brain disorder can be found, for instance, in Csete, 2010; Payne *et al*., 2015 or Brennand *et al*., 2015).

However, the notion whether or not reprogrammed cells preserve age signatures might be especially relevant when it comes to modelling age-related diseases. In particular, successful modelling of neurodegenerative diseases might depend on the preservation of cellular defects naturally accumulating over an organism's life span. Although PSC-based models have been used to study late-onset diseases such as Alzheimer's disease (AD; *e.g.,* Mertens *et al*., 2013, reviewed by us in Cenini *et al*., 2021), PD (*e.g.*, Chung *et al*., 2016, reviewed by us in Weykopf *et al*., 2019), the spinocerebellar ataxia Machado-Joseph disease (*e.g*., Koch *et al*., 2011; Hansen *et al*., 2016; Chuang *et al*., 2019) and Huntington's disease (HD; *e.g*., Szlachcic *et al*., 2015; Yanying Liu *et al*., 2017; Conforti *et al*., 2018), the importance of age preservation for disease modeling was impressively illustrated, for instance by the groups of Andrew Yoo and Fred Gage. Andrew Yoo and colleagues found that aggregation of the HD-causing mutant huntingtin protein can be readily recapitulated in directly converted MSNs but not in iPSC-derived MSNs, a phenomenon the authors attributed to the erasure of age signatures such as the restoration of proteasomal activity in iPSC-derived MSNs. Furthermore, these skin fibroblast-derived iN cultures exhibited age-dependent phenotypes. Whilst iNs from symptomatic HD patients showed oxidative stress-related DNA damage and neurodegeneration, these phenotypes were absent in iNs generated from younger, pre-symptomatic HD patients, despite having similar levels of mutant huntingtin inclusion bodies (Victor *et al*., 2018). Similar findings have very recently been made in the context of AD, showing that disease-associated transcriptomic changes that best accounted for dysregulation of neuronal maturation in glutamatergic iNs converted from fibroblasts of sixteen AD patient were consistently, but not significantly, changed in rejuvenated iPSC-derived neurons (Mertens *et al*., 2021). These findings thus collectively underpin the relevance of age-associated cellular alterations for the development of neurodegenerative pathophenotypes. Unsurprisingly, a number of directly converted neuronal subpopulations have therefore been successfully used for *in vitro* disease modeling (Liu *et al*., 2014, 2016; Wainger *et al*., 2015; Lim, Byung-Ok Choi, *et al*., 2016; Lim, Won Jun Choi, *et al*., 2016; Kim *et al*., 2017; Zhang *et al*., 2017) and drug testing (Liu *et al*., 2016; for a comprehensive review on the use of iNs in disease modeling, see Drouin-Ouellet *et al*., 2017).

Acknowledging that the lack of aging hallmarks in iPSC-derived somatic cells can impede modelling of age-associated pathophenotypes, numerous efforts have been made to bypass this limitation and to induce 'artificial aging' in human iPSC-derived cells. For instance, a variety of cell stress paradigms including antioxidant withdrawal (Byers *et al*., 2011; Reinhardt, Schmid, *et al*., 2013), treatment with hydrogen peroxide (Byers *et al*., 2011; Nguyen *et al*., 2011; Cooper *et al*., 2012), 6-OHDA (Nguyen *et al*., 2011; Cooper *et al*., 2012; Reinhardt, Schmid, *et al*., 2013) or inhibitors of proteasomal function (Nguyen *et al*., 2011; Cooper *et al*., 2012; Liu *et al*., 2012), oxidative phosphorylation (Seibler *et al*., 2011; Cooper *et al*., 2012; Reinhardt, Schmid, *et al*., 2013) or

mitophagy (Cooper *et al*., 2012) have been used to induce alterations that might also be observed with increased age. To what degree these stress paradigms can provoke authentic age-associated cellular states and thus facilitate iPSC-based modelling of late-onset diseases is a matter of debate. More physiological 'aging' strategies include telomere shortening by treating human PSCs with a telomerase inhibitor. Telomerase inhibitor-treated PSC-derived dopamine neurons indeed exhibit increased levels of mitochondrial ROS and DNA damage as well as reduced dendrite numbers (Vera *et al*., 2016). Another strategy to induce aging is overexpression of progerin, the truncated version of the nuclear pore complex protein LMNA, which is causal for the premature aging disease HGPS (Hennekam, 2006). Progerin overexpression in human iPSC-derived fibroblasts has been shown to result in decreased expression of nuclear LAP2α, global loss of heterochromatin markers, increased mitochondrial ROS production, DNA damage, telomere shortening, and senescence. Human iPSC-derived dopamine-like neurons, too, develop aging hallmarks after progerin overexpression, as for instance age-related transcriptional changes, altered nuclear morphology (increased folding and blebbing), accumulation of mitochondrial ROS and DNA damage, as well as progressive neurite degeneration. Notably, progerin overexpression was shown to facilitate the emergence of PD-associated phenotypes in human patient iPSC-derived dopamine neurons. Upon transplantation into 6-OHDA-treated parkinsonian mice, these cells showed pronounced accumulation of neuromelanin with lipofuscin deposits, microtubule breakdown and increased cell death; progerin-overexpressing grafts from one PD patient with homozygous *Parkin* mutation (V324A) even displayed large multilamellar structures resembling Lewy bodies that are α-synuclein-containing inclusions characteristic of PD (Miller *et al*., 2013).

Owing to their age memory, directly converted neurons might not require additional age-promoting treatments for modelling late-onset neurodegenerative diseases. However, it is fair to say that iNs might, *vice versa*, be less suitable for modelling neurodevelopmental disorders. Notably, although occasional reports indicate that iNs are, in principle, able to recapitulate functional deficits characteristic for neuropsychiatric disorder such as autism (Chanda *et al*., 2013), there is a substantial body of literature derived from human PSC-based models that indicates the existence of a neurodevelopmental component in the pathogenesis of such diseases (*e.g*., Yi *et al*., 2016; reviewed by us in the context of autism in Cheffer *et al*., 2020). For this reason, iN-based models of neuropsychiatric diseases might, on their own, not be sufficient to capture all aspects relevant to this group of disorders. Especially diseases impacting brain development at large might be better mimicable using PSC-based models, which are able to capture impairments in intermediate developmental stages such as radial glia-like cells (see Iefremova *et al*., 2017, for an example). Specifically, the capacity of PSCs to assemble and self-organize in 3D organoid structures (reviewed by Lancaster & Knoblich, 2014) might be a crucial asset for studying complex neurodevelopmental disorders that have a spatial dimension, involve the interplay of various cell types and/or are caused by non-cell autonomous mechanisms.

Next to the preservation of cellular aging signatures, the authenticity of cell programming-derived models remains a key challenge in the context of disease modeling and drug screening. Although some diseases affect neurons rather broadly, others are known to target preferentially specific subtypes such as PD, which is associated with a loss of mesencephalic dopaminergic neurons in the substantia nigra. Since cellular pathomechanisms might be cell type-dependent, the authenticity of the transdifferentiated neural subpopulation might thus significantly contribute to the validity and power of cellular disease models. While there is evidence for low levels of residual somatic memory – referring to epigenetic and/or transcriptomic signatures that are aberrantly expressed in the programmed cell type and appear to be inherited from their cell of origin – in low passage iPSCs (Kim *et al*., 2010; Polo *et al*.,

2010; Lo Sardo *et al*., 2017), these signatures appear to vanish after prolonged *in vitro* cultivation (Polo *et al*., 2010). This presents differently in directly converted cells. Kristin Baldwin and coworkers analyzed four fibroblast-derived iN populations reprogrammed by different TF combinations and revealed that although the global transcriptome of iNs is highly similar to endogenous neurons, all iN populations showed residual low-level expression of a subset of fibroblast-specific genes (Tsunemoto *et al*., 2018). Residual somatic signatures were also recently reported for induced NSCs (iNSCs). Thier *et al*. derived iNSCs with neural plate border identity from different populations of human fibroblasts and blood cells. They found that dermal fibroblast-derived but not blood-derived iNSCs still express the fibroblast marker *COL3A1*, although other fibroblast-lineage markers are significantly downregulated upon transdifferentiation (Thier *et al*., 2019). Nevertheless, residual somatic signatures in directly converted cells appear to be insufficient to maintain identity and function of the cell of origin (Marro *et al*., 2011). However, the question whether and to what extent the function of the converted iNs can be compromised by residual somatic signatures of the donor cell certainly merits further investigation, and recent data suggest that authenticity is an issue not restricted to direct cell fate conversion. Kevin Eggan and colleagues compared primary mouse spinal MNs with ESC-derived, iPSC-derived and directly converted MNs and revealed that all *in vitro*-derived MN populations, regardless of the reprogramming paradigm used, expressed only approximately 55 to 86 % of the primary MN transcriptome. These differences were accompanied by even more pronounced discrepancies in the methylation status (Ichida *et al*., 2018). From a biological perspective, such findings point to more general limitations of *in vitro* cell systems in recapitulating *in vivo* scenarios. On the other hand, it remains unclear what degree of somatic authenticity is eventually required to, for example, recapitulate disease-specific phenotypes – an issue which also depends on the specific experimental hypothesis. For other biomedical applications such as replacement of distinct neuronal subpopulations, utmost authenticity will always represent the ultimate goal.

1.3.2. Neuroregeneration by cell replacement

Identifying treatment options for neurological and especially neurodegenerative diseases is one of the most pressing tasks of modern biomedicine. Besides pharmacological treatments aiming at postponing a disease's onset, preventing disease progression or mediating symptomatic relief, approaches striving for the replacement of dysfunctional and/or lost cells have become a major research interest. To this end, efforts to activate endogenous NSCs to proliferate, migrate and differentiate in response to, for instance, a brain insult have been undertaken (Arvidsson *et al*., 2002; Nakatomi *et al*., 2002; Ohori *et al*., 2006; further reviewed by Tian *et al*., 2018). Alternatively, neural cell replacement can be achieved by the transplantation of exogenous donor cells into the lesioned or diseased CNS. Developments in the cell programming field have additionally fueled attempts to compensate neuronal loss by the *in situ* conversion of non-neuronal but brain-resident cell types into neurons. The latter two cell programming-based approaches both pose significant demands to the derived cell product and/or the programming technique used *in vivo*. These key challenges comprise, for example, the mitigation of adverse events such as tumorous-like cell proliferation after transplantation or conversion, the generation of phenotypically stable disease-specific cell populations and the capability of these cells to integrate into the established circuitry of the host brain.

1.3.2.1. Neurotransplantation

Nowadays, neurotransplantation of PSC-derived neural cells has a long-standing history with a vast number of scientific reports reinforcing their potential to survive grafting and subsequently differentiate *in vivo* (*e.g.*, reviewed by Thompson & Björklund, 2015). Even more importantly, it has been convincingly shown by now that grafted PSC-derived cells can integrate into the host neuronal circuitry, representing a major prerequisite for their use in neuroregenerative applications. Pierre Vanderhaeghen's team, for instance, showed that human ESC-derived cortical progenitors sequentially give rise to different cortical neuron populations after transplantation into the frontal cortex of neonatal mice. These graft-derived neuronal populations not only express cortical layer-specific markers, but also exhibit layer-appropriate projection patterns. Next to microscopy-based evidence for the myelination of transplant-derived axons by host oligodendrocytes, electrophysiological recordings demonstrated that transplanted human neurons possess both passive and active neuronal membrane properties, and even engage in cortical microcircuits receiving glutamatergic and GABAergic inputs from murine host neurons (Espuny-Camacho *et al.*, 2013). In order to visualize host-graft neuronal interactions more holistically, our laboratory previously employed a pseudotyped Rabies virus (pRABV)-based monosynaptic, retrograde tracing system in conjunction with tissue clearing and whole-brain light sheet fluorescence microscopy (LSFM) to characterize afferent connections of (i) human ESC-derived long-term neuroepithelial stem cell (lt-NES)- and (ii) human iPSC- and small molecule-derived NPC (smNPC)-derived transplants placed into the striatum or the hippocampal dentate gyrus of adult immunodeficient mice. This approach revealed that human NSC-derived grafts receive orthotopic innervations from the host brain: Mouse neurons being synaptically connected to hippocampal transplants were predominantly detected in the pyramidal cell layer of the cornu ammonis (CA) 1 region, the hippocampal stratum oriens, septal areas and the entorhinal cortex, while projections to striatal transplants mainly descended from cortical neurons (Doerr *et al.*, 2017). Among others, these reports corroborate the wide-spread use of human PSC-derived cell products for neurotransplantation these days.

Notably, the majority of studies reporting about the amenability of PSC-derived cells for neurotransplantation so far utilized extrinsic factor-based differentiation approaches. Tackling this short-coming, Zhang *et al.* demonstrated that 6 weeks after transplanting human forward programmed immature neurons (7 days after infecting ESCs with a lentivirus encoding for NGN2) into the mouse striatum, the grafted cells adopted a neuronal phenotype exhibiting dendritic arborizations, axonal outgrowth and electrophysiological functionality, and received inhibitory synaptic input from host striatal interneurons (Zhang *et al.*, 2013). Likewise, 14-day-old neurons, derived from human PSCs by ASCL1- and DLX2-overexpression, survive transplantation into the subventricular zone and cerebral cortex of neonatal mice and mature into GABAergic neurons within 3 months post transplantation (Yang *et al.*, 2017), and neurons derived from human PSCs by combined ASCL1, DLX2 and LHX6 overexpression mature into GABAergic neurons *in vivo*, too (Sun *et al.*, 2016). Notably, 2 months after grafting, these GABAergic neurons had functionally integrated into cortical layers V and VI, exhibiting repetitive action potential (AP) firing and receiving synaptic input from host neurons (Sun *et al.*, 2016). In an elegant study by the group of Hynek Wichterle, MNs were programmed by overexpressing Ngn2 and Isl1 in combination with either Lhx3 or Phox2a in mouse ESCs, and the resulting cells were grafted into the cervical and brachial tube of chicken embryos 2 days after transgene induction. Already 2 days after transplantation, the grafted cells had spatially segregated and exhibited axonal projections concordant with their MN subclass identity: Like spinal MNs, Ngn2/Isl1/Lhx3-overexpressing cells accumulated in axial and limb nerve branches and exhibited

substantial axonal outgrowth from the ventral root of the spinal cord, whereas Ngn2/Isl1/Phox2a-derived neurons accumulated in the lateral spinal cord and projected axons toward the spinal accessory nerve resembling cranial MNs (Mazzoni *et al*., 2013).

Whilst transplantation into unlesioned healthy recipients can be a highly useful tool to assess the *in vivo* differentiation and function of graft-derived neurons, studies in the context of a disease model can provide information on their regenerative capacity. Since more than 30 years already, clinical trials are being performed placing human fetal tissue-derived allografts into patients suffering from, for example, PD and HD. Although these trials showed highly variable outcomes, occasional reports of good graft survival leading to symptomatic improvements have fueled attempts to optimize graft composition via cell programming, finally aiming at the maximization of clinical efficacy. To this end, approaches to transplant better defined PSC-derived neural cells for exerting neuroregeneration are most advanced and have by now even entered clinical research (see reviews by Grealish *et al*., 2016 and Barker *et al*., 2018). The selection of clinically promising cell products is commonly based on pre-clinical studies in animals, which serve as a basis to estimate the capacity of PSC-derived grafts to promote symptomatic relief, as well as to assess the biodistribution, toxicology and tumorigenicity of the potential cell product (such as in Piao *et al*., 2021). For example, transplantation of human ESC-derived lateral ganglionic eminence (LGE)-like progenitors, giving rise to striatal GABAergic MSNs *in vitro* as well as *in vivo*, restores striatal neuronal circuitry and compensates motor deficits in a mouse model of HD. Notably, these effects are specific to the transplantation of LGE-like progenitors, since GABAergic neurons derived from grafted spinal neuron progenitors neither establish appropriate neuronal projections patterns nor mediate functional recovery (Ma *et al*., 2012). While this finding already highlights the necessity to select region-appropriate progenitors for neuroregenerative approaches, the extent of control over neuronal subtype differentiation that might be required to maximize the efficacy of neural transplants was impressively illustrated in the context of PD. Driven by the finding that transplantation of different batches of human PSC-derived ventral midbrain-patterned dopaminergic neuron progenitors formerly yielded quite variable results with regard to the number and density of TH-positive neurons post grafting, the group of Malin Parmar set out to identify markers expressed in the *in vitro*-derived progenitor population that would be predictive for their *in vivo* performance after transplantation. RNA sequencing analysis revealed that the expression of caudal ventral midbrain markers, such as *EN1* and *PAX8*, was increased in cell batches yielding bigger grafts with an increased dopaminergic content upon transplantation into the striatum of 6-OHDA-lesioned rats (Kirkeby *et al*., 2017). In addition, *DLK1* was identified as a potential marker for human PSC-derived dopaminergic preparations demonstrating improved graft survival and re-establishment of dopaminergic neurotransmission after transplantation into parkinsonian mice (Kirkeby *et al*., 2017) and monkeys (Kikuchi *et al*., 2017). Although this knowledge can be used to further fine-tune small molecule-based protocols to enrich PSC-derived cell products for specialized neural subpopulations, it might likewise be relevant to inform TF-mediated cell programming approaches.

First milestones to use forward programmed neurons for experimental neuroregeneration were already achieved as early as 2002, when Kim *et al*. transplanted Nurr1-overexpressing mouse ESC-derived neurons in the striatum of 6-OHDA-lesioned rats. Four to 8 weeks post transplantation, the majority of transplanted cells expressed the dopaminergic marker TH, and five out of six grafts exhibited spontaneous postsynaptic currents (sPSCs). Most importantly, the authors demonstrated that animals transplanted with Nurr1-overexpressing neurons showed

improved behavioral recovery compared to animals receiving sham injections or grafts of wild-type cells (Kim *et al*., 2002). Martinat *et al*. reported a few years later that Nurr1/Pitx3-induced mouse and human ESC-derived NPCs grafted into the striatum of 6-OHDA-lesioned mice resulted in a significant reduction in apomorphine-induced rotation behavior compared to the transplantation of control vector-transduced cells. However, further immunohistochemical analyses of the grafts revealed that in their setting, neurons retained an immature morphology with only a minority of them expressing TH (Martinat *et al*., 2006). In accordance with this finding, Theka *et al*. showed that 12 days after transplanting immature dopaminergic neurons (8 days post inducing ASCL1, NURR1 and LMX1A in human iPSCs) four out of six grafts survived, and only a fraction of the surviving cells displayed neuronal morphologies and expression of TH (Theka *et al*., 2013). Similar results were reported by Kim *et al*., who demonstrated that although transplantation of rat wild-type midbrain NPCs improves behavior of 6-OHDA-lesioned rats, transplantation of Nurr1-overexpressing midbrain or cortical NPCs does not, presumably because Nurr1-NPC grafts contained fewer TH-positive neurons, which additionally exhibited immature morphologies (Kim *et al*., 2003). Whilst these findings were confirmed by Park *et al*., their study further revealed that 8 weeks after transplanting rat NPCs overexpressing a combination of Nurr1, Ascl1 and Shh or Nurr1, Bcl-XL and Shh, dopaminergic specification and dopamine levels are increased and motor deficits decreased compared to transplantation of NPCs overexpressing Nurr1 alone (Park *et al*., 2006). In a study by Friling *et al*. only 50 % of all grafts survived after transplanting mouse Lmx1a-overexpressing ESC-derived NPCs into 6-OHDA-lesioned rats. In these grafts, the majority of the transplanted cells co-expressed the dopaminergic markers TH, Pitx3, En1/2, Lmx1a and Vmat, and even non-overlapping positivity for Girk2 and calbindin, indicating generation of both, substantia nigra A9 neurons and ventral tegmental area A10 dopaminergic neurons (Friling *et al*., 2009). Lastly, NPCs derived from ESCs via forward programming with Lmx1a differentiate into TH, DAT and GIRK2-expressing dopaminergic neurons *in vivo*, too (Sánchez-Danés *et al*., 2012).

Compared to PSC-based approaches, much less is known about the *in vivo* functionality of directly converted cells. Although iNs have occasionally been grafted (Gao *et al*., 2017; Li *et al*., 2019; Yang *et al*., 2019; Lee *et al*., 2020), transplantation of iNSCs seems more promising, because these cells are less mature and can thus be expected to engraft more efficiently (compare review by Thompson & Björklund, 2015). Yet, while more than 55 paradigms deriving iNSCs from diverse somatic cells of different species were published between 2011 and today, and proof-of-principle transplantation experiments were performed for 34 of them (a selection of these studies applying different conversion paradigms is provided in Table 1), only three publications provided functional data going beyond the survival and differentiation capacity of iNSCs upon grafting. While Hemmer *et al*. reported that iNSCs converted from mouse fibroblasts are able to differentiate into electrophysiologically active neurons receiving synaptic input 6 months after transplantation into the cortex and hippocampus of adult mice (Hemmer *et al*., 2014), Giorgetti *et al*. were able to record APs, but not sPSCs, 3 months after grafting neurons, pre-differentiated from human cord blood-derived iNSCs, into the hippocampus of adult mice (Giorgetti *et al*., 2012). Lastly, Thier *et al*. reported in 2019 about the derivation of induced neural plate border stem cells (iNBSCs) from human blood and fibroblasts via overexpression of the four transcription factors BRN2, KLF4, SOX2 and ZIC3. Repetitive AP firing upon depolarizing current injection was recorded from six cells patched in acute brain slices 8 weeks after grafting pre-differentiated NBSCs into the striatum of adult mice but the cells' capability to synaptically integrate was not assessed in further detail (Thier *et al*., 2019).

Reference	Species/cell of origin	Conversion method	*In vivo* characterization
Han *et al.*, 2012	Mouse fibroblasts	Retroviral **Brn4, Klf4, Sox2, cMyc ± E47**	Subventricular zone of adult mice: Survival and tripotent differentiation after 2 weeks
Hemmer *et al.*, 2014			Cortex and hippocampus of adult mice: Survival and tripotent differentiation after 6 months plus mature electrophysiological activity (APs and sPSCs)
Hong *et al.*, 2014			Contused thoracic spinal cord of rat: Survival and tripotent differentiation after 12 weeks plus reduced lesion and cavity size, axonal regeneration and increased angiogenesis, locomotor functional recovery and restoration of autonomous functions, modulation of host environment (decrease of apoptosis as well as inflammation, and increase of neurotrophic markers)
Giorgetti *et al.*, 2012	Human CD133-positive cord blood cells	Retro- and lentiviral **SOX2 ± cMYC**	Hippocampus of adult mice: Survival and neuronal differentiation after 3 months plus capacity to produce APs but no sPSCs. *Notably, iNSCs were differentiated for 4 weeks in vitro prior to grafting.*
Sheng, Zheng, Wu, Xu, Sang, *et al.*, 2012; Sheng, Zheng, Wu, Xu, Wang, *et al.*, 2012	Mouse Sertoli cells and fibroblasts	Retroviral **Ascl1, Ngn2, Hes1, Id1, Pax6, Brn2, Klf4 and cMyc (± Sox2)**	Hippocampus of adult mice: Survival and neuronal differentiation after 4 weeks
Wu *et al.*, 2015	Mouse Sertoli cells	See above + pNestin-Lmx1a lentivirus	Striatum of 6-OHDA-lesioned mice: Very low survival of engrafted iNSC-derived TH-positive cells after 11 weeks despite improved locomotor function
Lihui Wang *et al.*, 2013	Human urine cells	Episomal vectors OCT4, KLF4, SOX2, SV40LT and miR-302/367	Striatum of newborn rats: Survival and bipotent differentiation (neurons and astrocytes) after 4 weeks
Cheng *et al.*, 2014; Tang *et al.*, 2018	Mouse and human fibroblasts and urine cells	Chemical cocktail	Embryonic day E13.5 mice: Survival and tripotent differentiation after 1 month
Mirakhori *et al.*, 2015	Human fibroblasts	Recombinant TAT-SOX2 protein	Cortex of neonatal rats: Survival and bipotent differentiation (neurons and astrocytes) after 10 days
Tian *et al.*, 2015	Mouse fibroblasts	Retroviral **BRN2, SOX2, FOXA2 ± L-MYC**	Striatum of adult mice: Survival after 6 weeks; 3 weeks after transplantation in MPTP parkinsonian mice, increased density of TH-positive striatal termini and improved locomotor recovery
Lee *et al.*, 2018	Human fibroblasts	Exosomes	Striatum of adult rats: Survival and tripotent differentiation after 4 weeks
Xiao *et al.*, 2018	Mouse and human fibroblasts	Lentiviral PTF1a	Hippocampus of adult healthy mice (both murine and human iNSCs) or two different mouse models of AD (murine iNSCs only): Survival and tripotent differentiation in healthy mice after 1.5 months; in AD mice, spatial memory and learning was improved 1 month after grafting
Thier *et al.*, 2019	Human peripheral blood and dermal as well as pancreatic fibroblasts	Lentiviral BRN2, KLF4, SOX2 and ZIC3	Striatum of adult mice: Survival and tripotent differentiation after 8 weeks plus capacity to produce APs
Kang *et al.*, 2019	Human urine cells	Synthetic mRNA of OCT4, KLF4, SOX2, GLIS1 and recombinant B18R protein	Striatum of mice: Survival and tripotent differentiation after 8 weeks

Table 1: Characterization of iNSCs after neurotransplantation: A selection of published protocols.
If several conversion methods were employed in one publication, bold font indicates which of the protocols tested was used for generating the summarized *in vivo* data.

Notwithstanding that especially the capability of human transdifferentiated neural cells to integrate into host neuronal circuits remains largely elusive to date, first reports indicate that iNSCs might be principally able to contribute to neuroregeneration: The group of Dong Wook Han, for example, demonstrated that transplantation of mouse iNSCs into the contused thoracic spinal cord of rats results in a decreased lesion and cavity size 12 weeks post grafting. Additionally, the authors observed axonal regeneration, including upregulation of myelination, and increased angiogenesis in the area of the spinal cord injury. Most importantly, in this lesion model, transplantation of iNSCs promoted locomotor functional recovery and partially restored autonomous functions such as urination. Interestingly, the authors revealed that besides neuroregeneration, modulation of the host environment significantly contributes to the evoked functional recovery. Specifically, gene expression time course analysis uncovered the downregulation of apoptosis- and inflammation-associated genes, as well as the upregulation of neurotrophic factors. Concordantly, the number of Casp3-positive apoptotic cells as well as Ed1-positive monocytes and macrophages was significantly reduced in the rat spinal cord 4 weeks after iNSC transplantation (Hong *et al.*, 2014). Also in mouse models of PD and AD, transplantation of murine iNSCs mediates behavioral recovery as marked by improvements of locomotor function and spatial memory, respectively (Tian *et al.*, 2015; Wu *et al.*, 2015; Xiao *et al.*, 2018).

1.3.2.2. Cell fate conversion in situ and in vivo

Translation of *in vitro* paradigms of direct cell fate conversion to an *in vivo* scenario remains one of the most fascinating perspectives of regeneration (Figure 5). From a translational point of view, such approaches could eventually replace cell transplantation. Notably, however, a special variant of the *in vivo* conversion concept is the idea to transplant somatic cells that are already engineered to overexpress specific TFs upon an inducing stimulus and can thus be activated to convert *in situ* (Torper *et al.*, 2013). This strategy might be especially relevant for preclinical studies prior to attempting *in vivo* conversion in living humans, addressing the general feasibility to convert cells of human origin *in situ* using the animal brain as a proof-of-principle. From a biological perspective, transdifferentiation of region-specific cells in a native tissue environment – *in situ* or *in vivo* – might represent the ultimate approach to approximate authenticity.

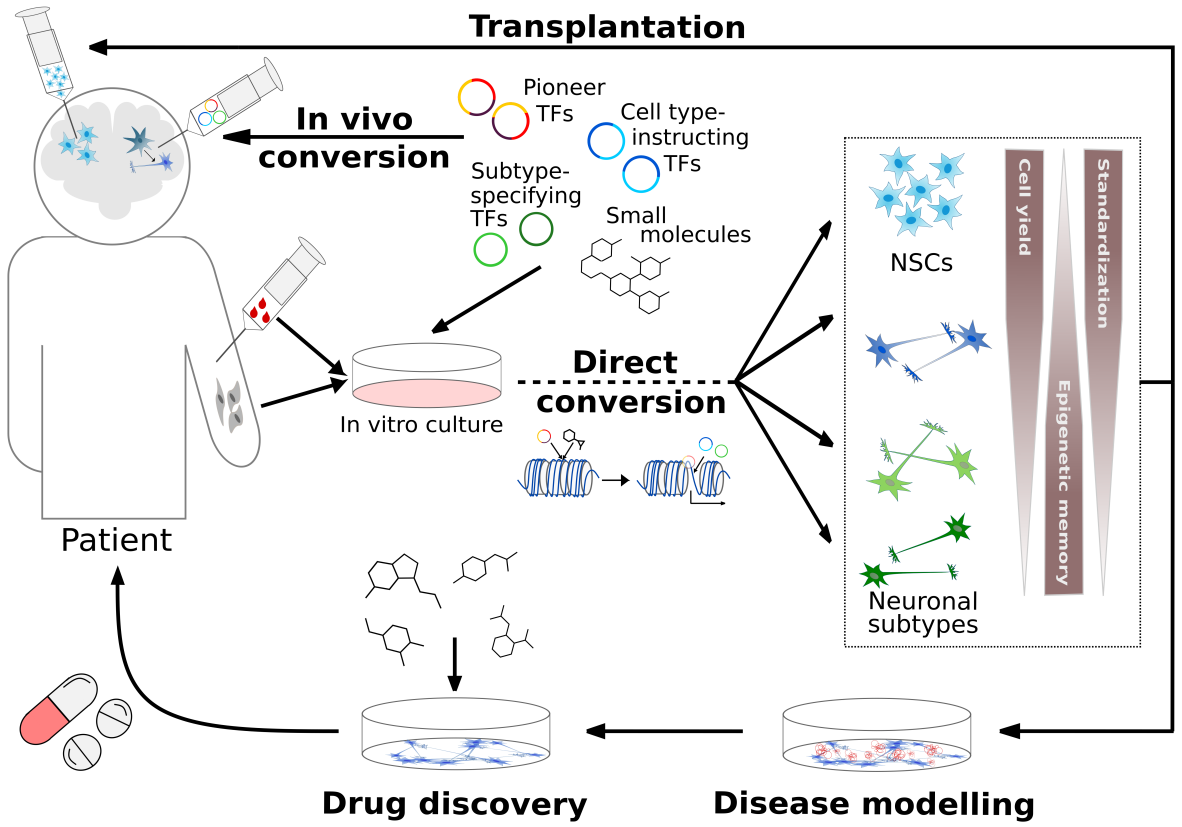

Figure 5: Direct cell fate conversion strategies in the context of biomedical applications.
Depending on the choice of programming factors, direct conversion can be fine-tuned to derive different cell types and even distinct neuronal subtypes, which can serve as platforms for disease modeling and drug discovery or as donor source for neural transplantation. Notably, different cell fate programming paradigms are characterized by varying degrees of scalability (that is, cell yield), retention of epigenetic memory, and standardization (for example, cell culture homogeneity and feasibility to provide quality-controlled batches), which might influence their applicability for biomedical applications. In contrast to transplantation of *in vitro*-derived cells, *in vivo* cell fate conversion might enable restoration of neuronal circuitry from endogenous sources. Figure and associated legend retrieved from Flitsch, L.J. & Brüstle, O. (2019) 'Evolving principles underlying neural lineage conversion and their relevance for biomedical translation', F1000Research, 8, p. F1000 Faculty Rev-1548. doi:10.12688/f1000research.18926.1 (Flitsch & Brüstle, 2019), published under the terms of the Creative Commons CC-BY license.

Accordingly, alongside converting non-CNS-resident cells such as fibroblasts, blood and urine cells, there has been significant progress with the *in vitro* neural conversion of non-neural but CNS-resident cells such as brain pericytes (Karow *et al.*, 2012, 2018) and yolk sac-born microglia (Matsuda *et al.*, 2019), which both represent attractive candidates for *in vivo* reprogramming. In parallel, transdifferentiation of astrocytes – which can be regarded as derivatives of neurogenic radial glia cells at the end of neural development (for further details on the relationship of radial glia cells, NSCs and neurogenesis, see Falk & Götz, 2017) – has been rapidly developing (Buffo *et al.*, 2005; Kronenberg *et al.*, 2010; Sirko *et al.*, 2013) *in vitro* as well as *in vivo*. As for the *in vitro* conversion of astrocytes into neurons, Benedikt Berninger, Magdalena Götz, and colleagues already showed in 2007 that this can be achieved by overexpression of the single neurogenic TF Ngn2 or Ascl1 (Berninger *et al.*, 2007). In 2015, their groups further reported that the overexpression of shared Ngn2 and Ascl1 downstream targets, namely Neurod4 alone or in combination with Insm1, principally suffices to convert mouse and human astrocytes into neurons *in vitro* (Masserdotti *et al.*, 2015). During the last decade, several other conversion paradigms based on TF combinations (Corti *et al.*, 2012), microRNAs (Ghasemi-Kasman *et al.*, 2015) and/or small molecules (Zhang *et al.*, 2015; Gao *et al.*, 2017; Yin *et al.*, 2019) have been reported for astrocyte-to-neuron conversion.

In the CNS, the longest history of *in situ* transdifferentiation has astrocyte-to-neuron conversion, starting with the observation that antagonizing Olig2 or overexpressing Pax6 after traumatic brain injury enables neurogenesis from resident reactive astrocytes (Buffo *et al*., 2005); this phenomenon has also been recapitulated after infliction of mild brain ischemia (Kronenberg *et al*., 2010). Similarly, Neurod1 has been shown to convert reactive astrocytes as well as NG2-positive progenitors into neurons in mouse stab injury and AD models (Guo *et al*., 2014), as well as after cerebral infarction (Chen *et al*., 2019). Heinrich *et al*. demonstrated that retrovirus-mediated overexpression of Sox2 alone or in combination with Ascl1 transdifferentiates NG2 cells into neurons in the acutely injured cortex (Heinrich *et al*., 2014). Astrocyte-to-neuron conversion has also been achieved in the healthy, unlesioned rodent CNS, for example, by the overexpression of the TFs Ascl1 (Faiz *et al*., 2015; Liu *et al*., 2015), Sox2 (Niu *et al*., 2013; Su *et al*., 2014; Wang *et al*., 2016) and Zfp521 (Zarei-Kheirabadi *et al*., 2019) or mediated by miR302/367 (Ghasemi-Kasman *et al*., 2015).

As with *in vitro* conversion, *in vivo* transdifferentiation is being increasingly refined toward the generation of distinct neuronal subpopulations. Pioneering studies by Benedikt Berninger and Magdalena Götz already indicated that overexpression of Ngn2 yields mostly glutamatergic neurons whilst direct conversion of astrocytes with Dlx2 results in neurons biased toward a GABAergic phenotype (Heinrich *et al*., 2010, 2011). Nakafuku and colleagues showed, however, that while Ngn2-mediated conversion of proliferating non-neuronal cells indeed results in the emergence of glutamatergic neurons in the neocortex, it yields GABAergic neurons in the mouse striatum (Grande *et al*., 2013). Likewise, Ngn2 was very recently shown to convert midbrain astrocytes into predominantly glutamatergic neuronal cultures, whereas its overexpression in intact or contused spinal cord yields mixed cultures of glutamatergic and GABAergic neurons (Fei Liu *et al*., 2021). These findings are all in line with work of Magdalena Götz' group, who reported in 2019 that *in vivo* conversion of mouse cortical astrocytes into neurons can preserve region- and even layer-specific identities (Mattugini *et al*., 2019). Following up on this observation, Herrero-Navarro *et al*. could lately show that regional identity in mouse neurons as well as astrocytes is most likely encoded in a cell-autonomous manner. At least within the thalamic nuclei, both cell types seem to inherit their region- and even nucleus-characteristic transcriptomic signatures from shared developmental progenitors. Although these marker genes are typically less expressed in astrocytes than neurons, Ngn2-mediated neuronal conversion is capable of maintaining the regional identity they infer, presumably because of respective epigenetic priming (Herrero-Navarro *et al*., 2021). It is worth noting though, that not all paradigms achieving astrocyte-to-neuron conversion *in vivo* seem to preserve regional identity. Very recently, Dorst *et al*. reported that *in vivo* conversion of striatal astrocytes into neurons by genetic deletion of the Notch effector RBPj-κ in the healthy mouse brain yields majorly VGLUT1-positive glutamatergic neurons. Although these neurons are capable of functionally integrating into striatal host neuronal circuits, they substantially differ from any so far identified striatal neuronal subpopulation in their marker expression as well as morphological and electrophysiological properties (Dorst *et al*., 2021). Moreover, also post-mitotic neurons with defined regional identity still appear to be amenable to TF-based phenotype shifting: The TF Fezf2 was shown to be competent of re-specifying post-mitotic mouse layer II/III callosal projection (Rouaux & Arlotta, 2013) and layer IV spiny neurons (De la Rossa *et al*., 2013) into layer V corticofugal projection neurons. Lastly, recent work by Nakashima and colleagues extended *in vivo* transdifferentiation to mouse microglia, which they converted with Neurod1 into striatal projection neuron-like cells, which were electrophysiologically active and formed excitatory synapses with host neurons (Matsuda *et al*., 2019). Altogether, these studies thus impressively underpin the relevance and potential impact of somatic memory,

arising, for instance, from subspecification within the glial lineage, that seem to be differentially preserved by distinct direct conversion approaches.

With regard to clinically relevant neuronal subtypes, Malin Parmar and colleagues tested the TF combination Ascl1, Nurr1 and Lmx1a, which specifies dopaminergic-like neurons from human PSCs (Theka *et al*., 2013) and fibroblasts (Caiazzo *et al*., 2011) *in vitro*. Notably, although this TF cocktail successfully converted astrocytes and NG2 glia into neurons *in vivo*, these neurons did not adopt a dopaminergic phenotype (Torper *et al*., 2015). Instead, this TF combination was found to promote the generation of interneurons exhibiting a fast-spiking parvalbumin-positive phenotype (Torper *et al*., 2015; Pereira *et al*., 2017), highlighting the necessity to re-assess tools developed *in vitro* for their applicability *in vivo*. The team of Ernest Arenas then showed that supplementation of the TF combination Ascl1 and Lmx1a with Neurod1 and miR218 can successfully instruct the conversion of astrocytes to dopamine neurons, which alleviated gait impairments in a mouse model of PD (Rivetti Di Val Cervo *et al*., 2017). Behavioral recovery was recently also observed in 6-OHDA-lesioned mice following Ptbp1-knock-down-mediated conversion of striatal astrocytes into dopaminergic-like neurons (Zhou *et al*., 2020), emphasizing the relevance of this approach for clinical translation.

The prospects of *in vivo* cell fate conversion for biomedical application were also sophisticatedly demonstrated by the group of Gong Chen in different disease contexts: In 2019, his lab explored Neurod1-mediated conversion of astrocytes into glutamatergic neurons as a therapeutic strategy after ischemic injury. The authors injected an Adeno-associated virus (AAV) expressing Neurod1 specifically in Gfap-positive astrocytes 10 days after eliciting focal stroke in the motor cortex of adult mice. AAV transduction resulted in highly efficient conversion (> 70 %) into electrophysiologically functional neurons, which did not yet deplete the pool of resident astrocytes. Moreover, the authors found that after AAV injection cortical tissue is preserved, as was evident from a significant recovery of the neuronal density within the ischemic area. This recovery was shown to be a consequence of transdifferentiation itself, as well as the protection of stroke-injured primary neurons from undergoing subsequent cell death. By this *in vivo* astrocyte-to-neuron conversion, his lab achieved the re-establishment of long-range axonal projections along pre-existing neuronal bundles, connecting the cortex to the ipsilateral striatum, thalamus and hypothalamus, as well as the contralateral cortex. Finally, neuronal transdifferentiation significantly contributed to the progressive recovery of motor function, which was at least partially attributable to the active engagement of converted neurons in neuronal circuits regulating motor behavior. Moreover, Neurod1-mediated astrocyte-to-neuron conversion was capable of ameliorating cognitive deficits (*i.e*., auditory fear memory) after ischemic injury in the basolateral nucleus of the amygdala (Chen *et al*., 2019). In 2020, his group next set out to investigate whether AAV-mediated overexpression of Neurod1 and Dlx2 *in vivo* could be used to treat HD, too. Specifically, they revealed that the combined expression of these two TFs converts striatal astrocytes into mature GABAergic MSNs with great efficiency within a time frame of roughly 8 weeks in wild-type mice as well as two distinct HD mouse models. Given that striatal astrocytes of R6/2 mice exhibited significantly less mutant huntingtin inclusions than endogenous neurons, also converted neurons thereof expectedly possessed a lower inclusion load compared to their native counterpart. Transdifferentiated neurons further re-innervated the globus pallidus and substantia nigra pars reticulata, representing a neuronal circuit that is severely disrupted upon HD-associated MSN degeneration. Finally, direct astrocyte-to-MSN conversion *in vivo* normalized stride length (a gait change altered in untreated R6/2 mice performing the catwalk test), walking distance (a locomotor symptom of HD mice detected during open field test) and paw clasping (a HD-associated symptom of dystonia and dyskinesia).

Most importantly, AAV-Neurod1-Dlx2-treated mice showed decreased body weight loss and longer survival times (Wu *et al*., 2020).

Although these studies altogether seem to impressively exemplify the diversity of strategies that can be employed for the transdifferentiation of mostly glial cells into neurons, as well as the broad range of neurological dysfunctions that could potentially be treated with *in vivo* cell fate conversion, it has to be noted at this point that this whole approach was very recently challenged by two independently performed studies. First, by a series of experiments utilizing different mouse lines enabling lineage tracing of astrocytes (*i.e*., tamoxifen-inducible Aldh1l1-CreER^{T2} or mGfap-Cre ± R26R-YFP/tdTomato mice), Chun-Li Zhang's group demonstrated that although an increasing number of virus-infected neurons can be detected after AAV-mediated overexpression of Neurod1 ± Dlx2 or knock-down of Ptbp1 in the brain of healthy mice or animals subjected to the controlled cortical impact injury model, these neurons are not of astrocytic origin. Their experiments indicate that, at least when utilizing an AAV5 serotype with human GFAP promoter-driven constructs, several transgenes including Neurod1 can alter the virus' cell type specificity, resulting in the labeling of endogenous neurons, which thus do not represent true astrocyte-to-neuron transdifferentiation events. Although the authors themselves verified that human astrocytoma cells can be converted into neurons by lentiviral NEUROD1 overexpression *in vitro* (Wang *et al*., 2021), their paper questions at least a subset of currently promoted, astrocyte-based *in vivo* conversion strategies. Second, Bo Peng's lab recently reported that Neurod1 overexpression fails to convert primary mouse microglia into neurons, too. More specifically, the authors showed that ectopic Neurod1 expression triggers apoptosis instead of neuronal conversion in different types of mouse microglia *in vitro*, and that overcoming apoptosis in Neurod1-expressing microglia does also not allow neuronal conversion. Moreover, intracranial injection of lentiviruses that were designed to convey microglia-specific overexpression of Neurod1 plus GFP or GFP alone (*e.g*., by the use of lentiviruses driven by presumably cell type-specific promoters such as hCD68 or LoxP-constructed viruses that were injected into the brain of Cx3cr1$^{+/CreER}$ microglia reporter mice) unexpectedly resulted in comparable numbers of GFP-labelled neurons, even in mice in which microglia were ablated by PLX5622 treatment prior to lentivirus injection. Similar to Chun-Li Zhang's group, Bo Peng and his team concluded from these and other experiments that previous reports on successful microglia-to-neuron transdifferentiation *in vivo* might have been confounded by non-specific viral leakage (Rao *et al*., 2021). Together, both studies certainly call for the re-evaluation of currently proposed *in vivo* conversion paradigms using more stringent and elaborate cell fate tracing techniques.

1.4. Aims of the study

Our laboratory's previous work focused on the rapid generation of neural cells from easily accessible human somatic cell sources. In this context, our lab developed a protocol to directly convert adult blood-derived erythroid progenitor cells (EPCs) into *bona fide* iNSCs. These iNSCs represent a developmentally early NSC population, consisting of a mixed population of CNS as well as PNS progenitors, that possesses the capacity to differentiate into diverse neuronal subtypes, astrocytes and oligodendrocytes (Sheng *et al*., 2018). This study aimed at exploring how our previously developed direct conversion protocol and the iNSCs generated thereby could be best employed for biomedical applications, such as disease modeling and neuroregeneration. To this end, we wanted to address three main questions (Figure 6):

First, we set out to investigate the degree of age preservation contained in our direct conversion paradigm, since the suitability of cell programming-derived cells for biomedical applications can be substantially influenced by the biological age of the respective cell product. To this end, we intended to generate and characterize isogenic pairs of iNSCs and iPSC-derived smNPCs from blood of newborns and high-age donors, recapitulating the entire human life span. Besides validating the quality and identity of all generated NSC lines by (i) performing immunocytochemical stainings for established NSC markers, (ii) assessing genomic integrity by single nucleotide polymorphism (SNP) profiling and (iii) validating the tripotent differentiation potential of the derived NSC populations by performing distinct differentiation assays, the performed characterization was devised to comprise age-associated parameters including the calculation of the cells' DNAm ages and the assessment of various cellular aging hallmarks. Employing diverse molecular biology techniques, we specifically aimed to (i) assess telomere lengths, (ii) profile the expression of genes and/or proteins associated to aging overall (*RANBP17*, *LAMNA* and *PCDH10*), autophagy (p62 and LC3), nuclear lamina (LMNA, LMNC, LAP2α and *LMNB*), senescence and apoptosis (*CDKN2a* and *CDKN1a*), as well as to (iii) quantify DNA damage and mitochondrial ROS production. Within this first aim, we finally intended to dissect the blood-to-iNSC conversion process by performing DNAm and RNA sequencing analyses in the time course of transdifferentiation.

Second, we aimed at providing a comprehensive description of the capacity of iNSCs to long-term survive transplantation into the unlesioned striatum and hippocampus of adult mice and to differentiate into distinct derivatives of the neural lineage *in vivo* by performing immunohistochemical analyses of various neural markers. Furthermore, we intended to put a specific emphasis on the functional assessment of grafted iNSCs at different time points after transplantation, performing (i) pRABV-mediated transsynaptic tracing of transplant afferents and (ii) human NCAM-based fiber tracking of graft efferents after transcardial perfusion, as well as (iii) electrophysiological recordings of human iNSC-derived cells within acute brain slices.

Third, we intended to investigate whether our iNSC paradigm can be adopted to the conversion of microglia, since the principal feasibility to transdifferentiate these brain-resident immune cells into tripotent NSCs would hold great promises for future clinical *in situ*/*in vivo* applications. Within this aim, we thus set out to infect iPSC-derived microglia (iPSdMiG) with Sendai-viruses (SeVs) overexpressing the two TFs SOX2 and cMYC, and to subsequently assess successfully transdifferentiated neuroepithelial-like cells for the expression of cell type-specific markers and respective NSC function.

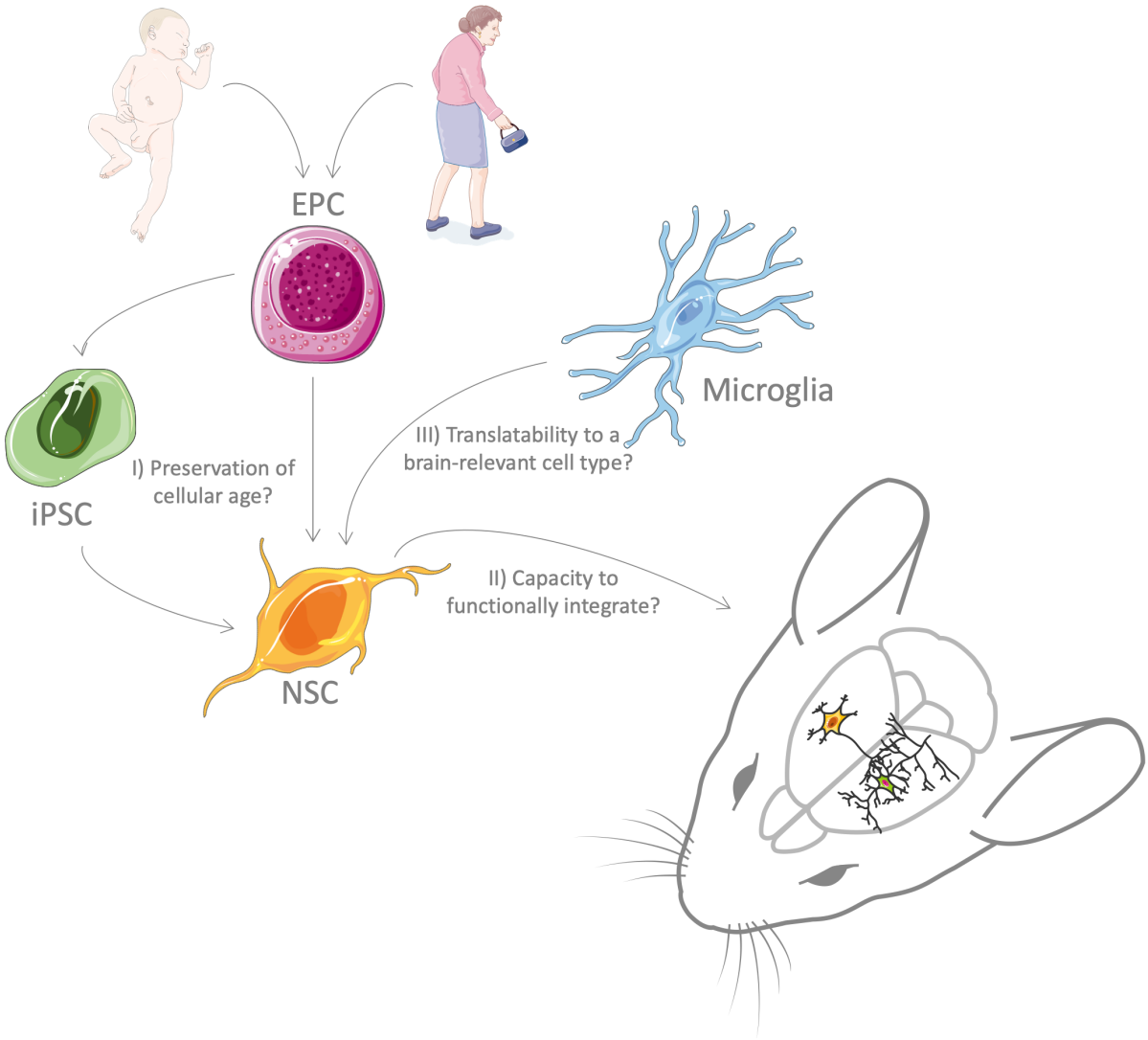

Figure 6: Schematic representation of the study's aims.
The aims of this project were three-fold. First, we set out to analyze isogenic sets of iPSC-derived smNPCs and directly converted iNSCs, generated from blood of newborns as well as aged donors, with regard to their cellular age characteristics. Second, we aimed to assess the capacity of blood-derived iNSCs to undergo functional integration into the adult mouse brain after neurotransplantation. Third, we intended to translate the blood-to-iNSC conversion paradigm established in our laboratory to the transdifferentiation of microglia into NSCs. Figure elements for cell types and humans were retrieved from Servier Medical Art by Servier (SMART; https://smart.servier.com), licensed under a Creative Commons Attribution 3.0 Unported License. Figure element representing mouse head and brain modified from Luigi Petrucco, © 2020, 'Mouse head schema', Zenodo (https://doi.org/10.5281/zenodo.3925903), licensed under a Creative Commons Attribution 4.0 International License.

2. Material and Methods

2.1. Material

2.1.1. Cell culture media

Medium	Components	Concentration	Vendor (Headquarter)
EMII	StemSpan SFEM	1x	Stemcell Technologies (Vancouver, Canada)
	CD Lipid	1 %	Thermo Fisher Scientific (Waltham, United States)
	Epo	2 U/ml	Bio-Techne (Minneapolis, USA)
	SCF	100 ng/ml	Bio-Techne (Minneapolis, USA)
	IGF1	40 ng/ml	Bio-Techne (Minneapolis, USA)
	Dexamethasone	1 µM	Sigma Aldrich (St. Louis, United States)
For EMI, add	IL3	10 ng/ml	Bio-Techne (Minneapolis, USA)
iPSC medium	StemMACS™ iPS-Brew XF	1x	Miltenyi Biotec (Bergisch Gladbach, Germany)
	StemMACS™ iPS-Brew XF Suppl.	1x	Miltenyi Biotec (Bergisch Gladbach, Germany)
1xN2B27	DMEM/F12	0.5x	Thermo Fisher Scientific (Waltham, United States)
+P/S+CPSD	Neurobasal	0.5x	Thermo Fisher Scientific (Waltham, United States)
	Bovine serum albumin (BSA)	0.0025 %	Thermo Fisher Scientific (Waltham, United States)
	N2	0.5x	Thermo Fisher Scientific (Waltham, United States)
	B27 without vitamin A	0.5x	Thermo Fisher Scientific (Waltham, United States)
	L-glutamine	1 mM	Thermo Fisher Scientific (Waltham, United States)
	Penicillin / Streptomycin	100 U/ml / µg/ml	Thermo Fisher Scientific (Waltham, United States)
	CHIR 99021	3 µM	Miltenyi Biotec (Bergisch Gladbach, Germany)
	Purmorphamine	0.5 µM	Miltenyi Biotec (Bergisch Gladbach, Germany)
	SB 431542	10 µM	Axon Biotech (Hengersberg, Germany)
	Dorsomorphine	1 µM	Tocris Bioscience (Bristol, UK)
1xN2B27	DMEM/F12	0.5x	Thermo Fisher Scientific (Waltham, United States)
+CPL	Neurobasal	0.5x	Thermo Fisher Scientific (Waltham, United States)
	BSA	0.0025 %	Thermo Fisher Scientific (Waltham, United States)
	N2	0.5x	Thermo Fisher Scientific (Waltham, United States)
	B27 without vitamin A	0.5x	Thermo Fisher Scientific (Waltham, United States)
	L-glutamine	1 mM	Thermo Fisher Scientific (Waltham, United States)
	CHIR 99021	3 µM	Miltenyi Biotec (Bergisch Gladbach, Germany)
	Purmorphamine	0.5 µM	Miltenyi Biotec (Bergisch Gladbach, Germany)
	LAAP	64 µg/ml	Sigma Aldrich (St. Louis, United States)
For +P/S, add	Penicillin / Streptomycin	100 U/ml / µg/ml	Thermo Fisher Scientific (Waltham, United States)
1xN2B27	DMEM/F12	0.5x	Thermo Fisher Scientific (Waltham, United States)
-AO+CP	Neurobasal	0.5x	Thermo Fisher Scientific (Waltham, United States)
	BSA	0.0025 %	Thermo Fisher Scientific (Waltham, United States)
	N2	0.5x	Thermo Fisher Scientific (Waltham, United States)
	B27 without antioxidants	0.5x	Thermo Fisher Scientific (Waltham, United States)
	L-glutamine	1 mM	Thermo Fisher Scientific (Waltham, United States)
	CHIR 99021	3 µM	Miltenyi Biotec (Bergisch Gladbach, Germany)
	Purmorphamine	0.5 µM	Miltenyi Biotec (Bergisch Gladbach, Germany)
2xN2B27	Advanced DMEM/F12	0.5x	Thermo Fisher Scientific (Waltham, United States)
+CPALLLT	Neurobasal	0.5x	Thermo Fisher Scientific (Waltham, United States)
	BSA	0.0025 %	Thermo Fisher Scientific (Waltham, United States)
	N2	1x	Thermo Fisher Scientific (Waltham, United States)
	B27 without vitamin A	1x	Thermo Fisher Scientific (Waltham, United States)
	L-glutamine	1 mM	Thermo Fisher Scientific (Waltham, United States)
	CHIR 99021	3 µM	Miltenyi Biotec (Bergisch Gladbach, Germany)
	Purmorphamine	1 µM	Miltenyi Biotec (Bergisch Gladbach, Germany)
	A83-01	0.5 µM	Tocris Bioscience (Bristol, UK)
	LIF	10 ng/ml	Novoprotein Scientific Inc. (Summit, USA)
	LAAP	64 µg/ml	Sigma Aldrich (St. Louis, United States)
	Laminin	1 µg/ml	Sigma Aldrich (St. Louis, United States)
	Tranylcypromine	5 µM	Enzo Biochem, Inc. (Farmingdale, USA)
2xN2B27	Advanced DMEM/F12	0.5x	Thermo Fisher Scientific (Waltham, United States)
+CPALL	Neurobasal	0.5x	Thermo Fisher Scientific (Waltham, United States)
	BSA	0.0025 %	Thermo Fisher Scientific (Waltham, United States)
	N2	1x	Thermo Fisher Scientific (Waltham, United States)
	B27 without vitamin A	1x	Thermo Fisher Scientific (Waltham, United States)
	L-glutamine	1 mM	Thermo Fisher Scientific (Waltham, United States)
	CHIR 99021	3 µM	Miltenyi Biotec (Bergisch Gladbach, Germany)
	Purmorphamine	0.5 µM	Miltenyi Biotec (Bergisch Gladbach, Germany)
	A83-01	0.5 µM	Tocris Bioscience (Bristol, UK)
	LIF	10 ng/ml	Novoprotein Scientific Inc. (Summit, USA)
	LAAP	64 µg/ml	Sigma Aldrich (St. Louis, United States)
HEK medium	Advanced DMEM	1x	Thermo Fisher Scientific (Waltham, United States)
	L-glutamine	1 mM	Thermo Fisher Scientific (Waltham, United States)

Table continued on p. 48

NGMC+SponDiff	DMEM/F12	0.5x	Thermo Fisher Scientific (Waltham, United States)
	Neurobasal	0.5x	Thermo Fisher Scientific (Waltham, United States)
	N2	0.5x	Thermo Fisher Scientific (Waltham, United States)
	B27 without vitamin A	0.5x	Thermo Fisher Scientific (Waltham, United States)
	L-glutamine	0.5 mM	Thermo Fisher Scientific (Waltham, United States)
	D(+)glucose	800 µg/ml	Carl Roth (Karlsruhe, Germany)
	Penicillin / Streptomycin	100 U/ml / µg/ml	Thermo Fisher Scientific (Waltham, United States)
	dbcAMP	0.5 mM	Sigma Aldrich (St. Louis, United States)
	BDNF	10 ng/ml	Cell Guidance Systems (Cambridge, UK)
	GDNF	10 ng/ml	Cell Guidance Systems (Cambridge, UK)
	LAAP	64 µg/ml	Sigma Aldrich (St. Louis, United States)
For +DAPT, add	DAPT	5 µM	Axon Biotech (Hengersberg, Germany)
Oligodendrocyte differentiation medium stage I	DMEM/F12	1x	Thermo Fisher Scientific (Waltham, United States)
	N2	1x	Thermo Fisher Scientific (Waltham, United States)
	L-glutamine	1 mM	Thermo Fisher Scientific (Waltham, United States)
	D(+)glucose	1.6 mg/ml	Carl Roth (Karlsruhe, Germany)
	Apo-transferrin	200 µg/ml	Sigma Aldrich (St. Louis, United States)
	Insulin	20 µg/ml	Sigma Aldrich (St. Louis, United States)
	EGF	10 ng/ml	Sigma Aldrich (St. Louis, United States)
	PDGF-AA	10 ng/ml	Bio-Techne (Minneapolis, USA)
	Forskolin	10 µM	Tocris Bioscience (Bristol, UK)
	SAG	1 µM	Merck Millipore (Burlington, USA)
Oligodendrocyte differentiation medium stage II	DMEM/F12	1x	Thermo Fisher Scientific (Waltham, United States)
	N2	1x	Thermo Fisher Scientific (Waltham, United States)
	B27 without vitamin A	1x	Thermo Fisher Scientific (Waltham, United States)
	L-glutamine	1 mM	Thermo Fisher Scientific (Waltham, United States)
	D(+)glucose	1.6 mg/ml	Carl Roth (Karlsruhe, Germany)
	Apotransferrin	200 µg/ml	Sigma Aldrich (St. Louis, United States)
	Insulin	20 µg/ml	Sigma Aldrich (St. Louis, United States)
	PDGF-AA	10 ng/ml	Bio-Techne (Minneapolis, USA)
	T3	30 ng/ml	Sigma Aldrich (St. Louis, United States)
	Noggin	200 ng/ml	Bio-Techne (Minneapolis, USA)
	Ascorbic acid	200 µM	Sigma Aldrich (St. Louis, United States)
Oligodendrocyte differentiation medium stage III	DMEM/F12	1x	Thermo Fisher Scientific (Waltham, United States)
	N2	1x	Thermo Fisher Scientific (Waltham, United States)
	B27 without vitamin A	1x	Thermo Fisher Scientific (Waltham, United States)
	L-glutamine	1 mM	Thermo Fisher Scientific (Waltham, United States)
	D(+)glucose	1.6 mg/ml	Carl Roth (Karlsruhe, Germany)
	Apotransferrin	200 µg/ml	Sigma Aldrich (St. Louis, United States)
	Insulin	20 µg/ml	Sigma Aldrich (St. Louis, United States)
	IGF1	10 ng/ml	Bio-Techne (Minneapolis, USA)
	T3	60 ng/ml	Sigma Aldrich (St. Louis, United States)
	NT-3	10 ng/ml	PeproTech, Inc. (Rocky Hill, USA)
	Ascorbic acid	200 µM	Sigma Aldrich (St. Louis, United States)
	Laminin	1 µg/ml	Sigma Aldrich (St. Louis, United States)
Fibroblast medium	DMEM (high glucose)	1x	Thermo Fisher Scientific (Waltham, United States)
	Tet system-approved fetal bovine serum	10 %	Takara Holdings (Kyoto, Japan)
	Sodium pyruvate	1 mM	Thermo Fisher Scientific (Waltham, United States)
	Non-essential amino acids	1x	Thermo Fisher Scientific (Waltham, United States)
	L-glutamine	1 mM	Thermo Fisher Scientific (Waltham, United States)
	Penicillin / Streptomycin	100 U/ml / µg/ml	Thermo Fisher Scientific (Waltham, United States)

Table 2: Cell culture media

2.1.2. Cell culture reagents

Component	Vendor (Headquarter)
1x DPBS	Thermo Fisher Scientific (Waltham, USA)
10x DPBS	Thermo Fisher Scientific (Waltham, USA)
Fetal calf serum (FCS)	Thermo Fisher Scientific (Waltham, USA)
Dimethyl sulfoxide (DMSO)	Sigma-Aldrich (St. Louis, USA)
Percoll	Sigma-Aldrich (St. Louis, USA)
CytoTune 1.0 SeVs	Thermo Fisher Scientific (Waltham, USA)
CytoTune 2.0 SeVs	Thermo Fisher Scientific (Waltham, USA)
Ethylenediaminetetraacetic acid (EDTA)	Carl Roth (Karlsruhe, Germany)
DOX	Sigma-Aldrich (St. Louis, USA)
Rock inhibitor Y-27632	Cell Guidance Systems (Cambridge, UK)
Accutase	Thermo Fisher Scientific (Waltham, USA)
0.5 % Trypsin-EDTA	Thermo Fisher Scientific (Waltham, USA)
Matrigel	Corning Inc. (Corning, USA)
Vitronectin	Thermo Fisher Scientific (Waltham, USA)
Gelatin	Sigma-Aldrich (St. Louis, USA)
Glycerol	Sigma-Aldrich (St. Louis, USA)
Thymidine	Sigma-Aldrich (St. Louis, USA)
Chloroquine	Sigma-Aldrich (St. Louis, USA)
Lipofectamine 2000	Thermo Fisher Scientific (Waltham, USA)
OptiMEM	Thermo Fisher Scientific (Waltham, USA)
Lenti-X™ concentrator	Clontech Laboratories (Mountain View, USA)
Blasticidin	InvivoGen (San Diego, USA)
Puromycin	PAA Laboratories GmbH (Cölbe, Germany)
G418	InvivoGen (San Diego, USA)
Uridine	Sigma-Aldrich (St. Louis, USA)
5-Fluoro-2'-deoxyuridine (FUDR)	Sigma-Aldrich (St. Louis, USA)
Cytarabin (Ara-C)	Merck Millipore (Burlington, USA)
Collagenase VI	Thermo Fisher Scientific (Waltham, USA)
Cytocon™ buffer II	Evotech Technologies GmbH (Hamburg, Germany)
DNase	Worthington Biochemical Corp. (Lakewood, USA)
Bafilomycin-A (BAFA)	Enzo Biochem, Inc. (Farmingdale, USA)
HBSS	Thermo Fisher Scientific (Waltham, USA)
Trifluoromethoxy carbonyl cyanide phenylhydrazone (FCCP)	Cayman Chemical (Ann Arbor, USA)
MitoSOX Red	Thermo Fisher Scientific (Waltham, USA)

Table 3: Cell culture reagents

2.1.3. Plastic ware

Component	Vendor (Headquarter)
Vacutainer CPT tubes	BD Bioscience (San Jose, USA)
AggreWell™ 800 microwell culture plate	Stemcell Technologies (Vancouver, Canada)
96-well plate for protein concentration determination	Greiner Bio-One (Solingen, Germany)
96-well plate for imaging	ibidi (Gräfelfing, Germany)
4-well plate	Thermo Fisher Scientific (Waltham, USA)
24-well plate	Corning Inc. (Corning, USA)
12-well plate	Corning Inc. (Corning, USA)
6-well plate	Corning Inc. (Corning, USA)
3.5 cm-cell culture dish	Corning Inc. (Corning, USA)
3.5 cm-cell culture dish with staining inserts	Greiner Bio-One (Solingen, Germany)
3.5 cm-petri dish	Corning Inc. (Corning, USA)
6 cm-cell culture dish	Corning Inc. (Corning, USA)
6 cm Petri-dish	Corning Inc. (Corning, USA)
10 cm-cell culture dish	Corning Inc. (Corning, USA)
10 cm Petri-dish	Corning Inc. (Corning, USA)
13 mm-cell culture-treated Nunc coverslip	Thermo Fisher Scientific (Waltham, USA)
1.0 ml-cryo vial	Thermo Fisher Scientific (Waltham, USA)
1.8 ml-cryo vial	Thermo Fisher Scientific (Waltham, USA)
0.5 ml-tube	Eppendorf (Hamburg, Germany)
1.5 ml-tube	Eppendorf (Hamburg, Germany)
2.0 ml-tube	Eppendorf (Hamburg, Germany)
15 ml-tube	Corning Inc. (Corning, USA)
50 ml-tube	Corning Inc. (Corning, USA)
T75-flasks	Greiner AG (Kremsmünster, Austria)
0.45 µm acetate filters	Corning Inc. (Corning, USA)
Cell scraper	Corning Inc. (Corning, USA)
40 µm cell strainer	Corning Inc. (Corning, USA)
8-strips for reverse-transcription polymerase chain reaction (RT-PCR)	Biozym Scientific GmbH (Oldendorf, Germany)
96-well plates and plate seals for quantitative real-time PCR (qPCR)	4titude (Wotton, UK)
Parafilm	Thermo Fisher Scientific (Waltham, USA)
Serological pipettes	Corning Inc. (Corning, USA)
Microliter pipette tips	Nerbe plus GmbH & Co. KG (Winsen, Germany)

Table 4: Plastic ware

2.1.4. Solutions used for animal experiments

Solution	Components	Concentration	Vendor (Headquarter)
Anesthesia used for animal surgery	Fentanyl	0.05 mg/kg body weight	Vifor Pharma (St. Gallen, Switzerland)
	Midazolam (alias Dormicum)	5 mg/kg body weight	B. Braun (Melsungen, Germany)
	Medetomidine (alias Cepetor)	0.5 mg/kg body weight	CP-Pharma (Burgdorf, Germany)
Antidot used for animal surgery	Naloxon	1.2 mg/kg body weight	PUREN Pharma (Munich, Germany)
	Flumazenil (alias Annexate)	0.5 mg/kg body weight	Hikma Pharmaceuticals (London, UK)
	Atipamezol (alias Antisedan)	2.5 mg/kg body weight	Orion Pharma GmbH (Hamburg, Germany)
Anesthesia used for perfusion	NaCl	0.45 %	Fresenius Kabi (Bad Homburg, Germany)
	Ketanest S	10 mg/ml	Pfizer (New York, USA)
	Rompun	0.2 %	Bayer AG (Leverkusen, Germany)

Table 5: Solutions used for animal experiments

2.1.5. Components used for animal experiments

Component	Vendor (Headquarter)
Carprofen (alias Rimadyl)	Pfizer (New York, USA)
Bepanthen	Bayer AG (Leverkusen, Germany)
Isoflurane	Piramal Group (Mumbai, India)
Antiseptic spray	Schülke & Mayr (Norderstedt, Germany)
Betaisodona	Mundipharma (Frankfurt a. M., Germany)
Scalpel	pfm medical AG (Cologne, Germany)
Cotton swabs	Hartmann GmbH Medizintechnik (Hainichen, Germany)
27 G needle	B. Braun (Melsungen, Germany)
Bone wax	Fine Science Tools GmbH (Heidelberg, Germany)
0.9 % NaCl	Fresenius Kabi (Bad Homburg, Germany)
23G butterfly needle	Sarstedt GmbH (Nümbrecht, Germany)
Infusion bag	Fresenius Kabi (Bad Homburg, Germany)
Heparin	B. Braun (Melsungen, Germany)
50 ml-syringe	B. Braun (Melsungen, Germany)
4 % formaldehyde (FA), pH 7.6	VWR International (Radnor, USA)

Table 6: Components used for animal experiments

2.1.6. Molecular biology solutions

Solution	Components	Concentration	Vendor (Headquarter)
BABB (pH 9.4)	Benzyl alcohol	33.33 %	Sigma-Aldrich (St. Louis, USA)
	Benzyl benzoate	66.66 %	Sigma-Aldrich (St. Louis, USA)
RT-PCR master mix	ddH_2O	1x	Fresenius Kabi (Bad Homburg, Germany)
	RT-PCR Green Flex buffer	1x	Promega (Madison, USA)
	$MgCl_2$	4 mM	Promega (Madison, USA)
	dATP	200 µM	Peqlab Biotechnologie GmbH (Erlangen, Germany)
	dGTP	200 µM	Peqlab Biotechnologie GmbH (Erlangen, Germany)
	dCTP	200 µM	Peqlab Biotechnologie GmbH (Erlangen, Germany)
	dTTP	200 µM	Peqlab Biotechnologie GmbH (Erlangen, Germany)
	DMSO	4 %	Sigma-Aldrich (St. Louis, USA)
	Taq-Polymerase	0.625 U	Promega (Madison, USA)
qPCR master mix	ddH_2O	1x	Fresenius Kabi (Bad Homburg, Germany)
	qPCR Rxn buffer	1x	Thermo Fisher Scientific (Waltham, USA)
	$MgCl_2$	3 mM	Thermo Fisher Scientific (Waltham, USA)
	dATP	200 µM	Peqlab Biotechnologie GmbH (Erlangen, Germany)
	dGTP	200 µM	Peqlab Biotechnologie GmbH (Erlangen, Germany)
	dCTP	200 µM	Peqlab Biotechnologie GmbH (Erlangen, Germany)
	dTTP	200 µM	Peqlab Biotechnologie GmbH (Erlangen, Germany)
	SyBr Green	0.75x	Sigma-Aldrich (St. Louis, USA)
	Fluorescin	10 nM	Bio-Rad Laboratories, Inc. (Hercules, USA)
	DMSO	4 %	Sigma-Aldrich (St. Louis, USA)
	Taq-Polymerase	0.6 U	Thermo Fisher Scientific (Waltham, USA)
Telomere qPCR master mix	ddH_2O	1x	Fresenius Kabi (Bad Homburg, Germany)
	Buffer II	1x	Thermo Fisher Scientific (Waltham, USA)
	$MgCl_2$	3 mM	Thermo Fisher Scientific (Waltham, USA)
	dATP	200 µM	Peqlab Biotechnologie GmbH (Erlangen, Germany)
	dGTP	200 µM	Peqlab Biotechnologie GmbH (Erlangen, Germany)
	dCTP	200 µM	Peqlab Biotechnologie GmbH (Erlangen, Germany)
	dTTP	200 µM	Peqlab Biotechnologie GmbH (Erlangen, Germany)
	DL-dithiothreitol	1 mM	Sigma-Aldrich (St. Louis, USA)
	Betaine	1 M	Sigma-Aldrich (St. Louis, USA)
	SyBr Green	0.75x	Sigma-Aldrich (St. Louis, USA)
	Taq-Gold	0.5 U	Thermo Fisher Scientific (Waltham, USA)
1x TAE buffer	Tris-Base	40 mM	Carl Roth (Karlsruhe, Germany)
	EDTA (pH 8.0)	1 mM	Carl Roth (Karlsruhe, Germany)
	Acetic acid	0.11 %	Carl Roth (Karlsruhe, Germany)
10x loading buffer	1x TAE buffer	70 %	See above
	Glycine	30 %	Carl Roth (Karlsruhe, Germany)
	Bromophenol blue	As needed	Sigma-Aldrich (St. Louis, USA)
	Xylene cyanole	As needed	Sigma-Aldrich (St. Louis, USA)

Table continued on p. 52

Radioimmuno-precipitation assay (RIPA) buffer	Tris-HCl (pH 7.6)	25 mM	Carl Roth (Karlsruhe, Germany)
	NaCl	150 mM	Carl Roth (Karlsruhe, Germany)
	Nonoxiol 40	1 %	Thermo Fisher Scientific (Waltham, USA)
	Sodium deoxycholate	1 %	Sigma-Aldrich (St. Louis, USA)
	Sodium dodecyl sulfate (SDS)	0.1 %	Carl Roth (Karlsruhe, Germany)
4x Laemmli buffer	Tris-HCl	20 mM	Carl Roth (Karlsruhe, Germany)
	Acetic acid	10 mM	Carl Roth (Karlsruhe, Germany)
	EDTA	10 mM	Sigma-Aldrich (St. Louis, USA)
	Glycerol	20 %	Sigma-Aldrich (St. Louis, USA)
	SDS	8 %	Carl Roth (Karlsruhe, Germany)
	Bromophenol blue	1 %	Sigma-Aldrich (St. Louis, USA)
4x Tris/HCl-SDS buffer (pH 8.8)	Tris-Base (pH 8.8)	1.5 M	Carl Roth (Karlsruhe, Germany)
	SDS	0.4 %	Carl Roth (Karlsruhe, Germany)
4x Tris/HCl-SDS buffer (pH 6.8)	Tris-Base (pH 6.8)	0.5 M	Carl Roth (Karlsruhe, Germany)
	SDS	0.4 %	Carl Roth (Karlsruhe, Germany)
1x SDS running buffer	Tris-Base (pH 8.3)	25 mM	Carl Roth (Karlsruhe, Germany)
	Glycine	192 mM	Carl Roth (Karlsruhe, Germany)
	SDS	0.1 %	Carl Roth (Karlsruhe, Germany)
1x Western blot transfer buffer	Tris-Base	25 mM	Carl Roth (Karlsruhe, Germany)
	Glycine	192 mM	Carl Roth (Karlsruhe, Germany)
	Methanol	10 %	Carl Roth (Karlsruhe, Germany)
Amido-Black solution	Amido-Black	0.2 %	Carl Roth (Karlsruhe, Germany)
	Acetic acid	10 %	Carl Roth (Karlsruhe, Germany)
	Methanol	40 %	Carl Roth (Karlsruhe, Germany)
1x TBS	Tris-Base (pH 7.4)	25 mM	Carl Roth (Karlsruhe, Germany)
	NaCl	150 mM	Carl Roth (Karlsruhe, Germany)
For TBS-T, add	Tween-20	0.1 %	Sigma-Aldrich (St. Louis, USA)
Mounting medium	Tris-HCl (pH 8.5)	133.33 mM	Carl Roth (Karlsruhe, Germany)
	Mowiol-488	133.33 mg/ml	Carl Roth (Karlsruhe, Germany)
	Glycerin	333.33 mg/ml	Carl Roth (Karlsruhe, Germany)
	DABCO	25 mg/ml	Carl Roth (Karlsruhe, Germany)

Table 7: Molecular biology solutions

2.1.7. Molecular biology reagents and kits

Component	Vendor (Headquarter)
Sucrose	Carl Roth (Karlsruhe, Germany)
TissueTek	Sakura (Alphen aan den Rijn, Netherlands)
Tert-butanol	Sigma-Aldrich (St. Louis, USA)
Triethylamine	Sigma-Aldrich (St. Louis, USA)
RNeasy kit	Qiagen (Hilden, Germany)
2-mercapto ethanol	Sigma-Aldrich (St. Louis, USA)
100 % ethanol	Carl Roth (Karlsruhe, Germany)
qScript kit	Quanta Biosciences (Beverly, USA)
Blood & tissue kit	Qiagen (Hilden, Germany)
Agarose	Peqlab Biotechnologie GmbH (Erlangen, Germany)
Ethidium bromide	Sigma-Aldrich (St. Louis, USA)
100 bp ladder	Peqlab Biotechnologie GmbH (Erlangen, Germany)
100x Protease and phosphatase inhibitor cocktail	Thermo Fisher Scientific (Waltham, USA)
Roti-Quant reagent	Carl Roth (Karlsruhe, Germany)
Page ruler pre-stained protein ladder	Thermo Fisher Scientific (Waltham, USA)
Acryl amide	Carl Roth (Karlsruhe, Germany)
Tetramethylethylene diamine (TEMED)	Sigma-Aldrich (St. Louis, USA)
Ammonium persulfate (APS)	Sigma-Aldrich (St. Louis, USA)
Whatman paper	Thermo Fisher Scientific (Waltham, USA)
0.2 µm polyvinylidene fluoride (PVDF) membrane	Bio-Rad Laboratories, Inc. (Hercules, USA)
Milk powder	Carl Roth (Karlsruhe, Germany)
Classico horseradish peroxidase (HRP) substrate	Merck Millipore (Burlington, USA)
Femto HRP sustrate	Thermo Fisher Scientific (Waltham, USA)
Paraformaldehyde (PFA)	Thermo Fisher Scientific (Waltham, USA)
Triton-X100	Sigma-Aldrich (St. Louis, USA)
4',6-Diamidino-2-phenyl-indol-dihydrochloride (DAPI)	Sigma-Aldrich (St. Louis, USA)
Grease stick	Daido Sangyo Do. Ltd. (Tokyo, Japan)
Hematoxylin	BIOZOL Diagnostica GmbH (Eching, Germany)
37 % HCl	Carl Roth (Karlsruhe, Germany)
Eosin	Carl Roth (Karlsruhe, Germany)
Xylol	Carl Roth (Karlsruhe, Germany)
Isopropanol	Carl Roth (Karlsruhe, Germany)
Cytoseal XYL	Thermo Fisher Scientific (Waltham, USA)
Normal horse serum (NHS)	Thermo Fisher Scientific (Waltham, USA)
Normal goat serum (NGS)	Sigma-Aldrich (St. Louis, USA)
Tween-20	Sigma-Aldrich (St. Louis, USA)
VectaShield	Maravai LifeSciences (San Diego, USA)
30 % hydrogen peroxide	Carl Roth (Karlsruhe, Germany)
Blocking solution	Zytomed Systems GmbH (Bargteheide, Germany)
3,3'-diaminobenzidine (DAB) high contrast kit	Zytomed Systems GmbH (Bargteheide, Germany)

Table 8: Molecular biology reagents and kits

2.1.8. Primers

Target	Sequence Forward Primer (5'-3')	Sequence Reverse Primer (5'-3')	Application
18S	TTCCTTGGACCGGCGCAAG	GCCGCATCGCCGGTCGG	RT-PCR, qPCR
Albumin 'S'	CGGCGGCGGGCGGCGCGGGCTGGG CGGAAATGCTGCACAGAATCCTTG	GCCCGGCCCGCCGCGCCCGTCCCGCCG GAAAAGCATGGTCGCCTGTT	Telomere qPCR
AIF1	GCGCTTATCCCTTCTGCTCT	TCTCTCCTCTCCCACTTCCG	qPCR
CDKN1a	TGACCCTGAAGTGAGCACAG	AAGGTACAGGGGAGCCAAAG	qPCR
CDKN2a-p16-INK4a	GGGTCGGGTAGAGGAGGTG	ACCGTAACTATTCGGTGCGT	qPCR
CDKN2a-p14-ARF	TCTTGGTGACCCTCCGGATT	CGGGATGTGAACCACGAAAAC	qPCR
total cMYC	AAGACTCCAGCGCCTTCTCT	TCTTGTTCCTCCTCAGAGTCG	qPCR
ITGAM	ACACAGCAGCTTCTCTCCAC	AGTGGGCATCTTTATTGGGCA	qPCR
LAMNA	CACCTGGAACTGGACACAGA	AGGGACAGGGATGTGATTGA	qPCR
LAP2α	GCAGGCAGACATTAGTCAAGC	CGACCTACAGTGGCATTTCC	qPCR
LMNA	GCTCTTCTGCCTCCAGTGTC	ACATGATGCTGCAGTTCTGG	qPCR
LMNB	GAGGTTGCTCAAAGAAGTACAGTC	TTACATAATTGCACAGCTTCTATTG	qPCR
LMNC	CTCAGTGACTGTGGTTGAGGA	AGTGCAGGCTCGGCCTC	qPCR
MBP	GAGCCCTCTGCCCTCTCATGCC	TCAGGGACAGTCCTCTCCCCTTTCCC	RT-PCR
NG2	ACTTGCATCCGCGGCTTCCTTCTT	ACAACGTGGCCCAGCCCTCTA	RT-PCR
OLIG2	GCTGGCGCGCAACTACATCC	AAGCCAGCGTGGTGGCCC	RT-PCR
PAX6	AATAACCTGCCTATGCAACCC	AACTTGAACTGGAACTGACACAC	qPCR
PCDH10	ATGCCTTCTTTTGTCCCTTCT	AGTCCATCCAGCTCCTTCC	qPCR
PDGFRα	CTATCCACACTGTCAAACAGGTTG	ACTGCTGGACTGAGAAGTTTCATC	RT-PCR
RANBP17	GGATCCTGGATTGAGACGAA	GTGCTTCCAGGCTCGTTCTA	qPCR
SeV-cMYC	TAACTGACTAGCAGGCTTGTCG	TCCACATACAGTCCTGGATGATGATG	RT-PCR
SeV-SOX2	ACAAGAGAAAAAAACATGTATGG	ATGCGCTGGTTCACGCCCGCGCCCAGG	RT-PCR
endogenous SOX2	GTATCAGGAGTTGTCAAGGCAGAG	TCCTAGTCTTAAAGAGGCAGCAAAC	qPCR
total SOX2	GCCGAGTGGAAACTTTTGTCG	GCAGCGTGTACTTATCCTTCTT	qPCR
Telomeres 'T'	ACACTAAGGTTTGGGTTTGGGTTTG GGTTTGGGTTAGTGT	TGTTAGGTATCCCTATCCCTATCCCTAT CCCTATCCCTAACA	Telomere qPCR

Table 9: Primers

2.1.9. Antibodies

Primary Antibodies	Vendor (Headquarter)	Cat.-Number	Application	Dilution
Chicken polyclonal IgY to MAP2	Bio-Techne (Minneapolis, USA)	NB300-213	IHC	1:1,000
Guinea pig polyclonal to SHANK2	Synaptic Systems GmbH (Göttingen, Germany)	162 204	IHC	1:500
Mouse monoclonal IgG to AP2α	Developmental Studies Hybridoma Bank (Iowa, USA)	3B5-c	ICC	1:50
Mouse monoclonal IgG to GAPDH	Santa Cruz Biotechnology (Dallas, USA)	sc-47724	WB	1:1,000
Mouse monoclonal IgG to γH2AX	Merck Millipore (Burlington, USA)	05-636-1	ICC	1:250
Mouse monoclonal IgG to LC3B	Enzo Biochem, Inc. (Farmingdale, USA)	ALX-803-080	WB	1:200
Mouse monoclonal IgG to LMNA/C	Abcam (Cambridge, UK)	ab40567	ICC	1:200
Mouse monoclonal IgG to human nuclei (hN)	Merck Millipore (Burlington, USA)	MAB4383	IHC	1:100
Mouse monoclonal IgG to human NCAM/CD56 (ERIC 1)	Santa Cruz Biotechnology (Dallas, USA)	sc-106	IHC	1:1,000
Mouse monoclonal IgG to Nestin (NES)	BioLegend (San Diego, USA)	656802	ICC	1:100
Mouse monoclonal IgG to neuronal nuclei (NEUN)	Merck Millipore (Burlington, USA)	MAB377	ICC	1:100
Mouse monoclonal IgG to NKX2.2	Abcam (Cambridge, UK)	ab187375	ICC	1:200
Mouse monoclonal IgM to O4	Bio-Techne (Minneapolis, USA)	MAB1326	ICC	1:500
Mouse monoclonal IgG to p62	Abnova (Taipeh, Taiwan)	H00008878-M01	WB	1:1,000
Mouse monoclonal IgG to S100β	Sigma Aldrich (St. Louis, USA)	S2532	ICC	1:1,000
Mouse monoclonal IgG to SOX2	Bio-Techne (Minneapolis, USA)	MAB2018	ICC	1:100
Mouse monoclonal IgG Stem121®	Takara Holdings (Kyoto, Japan)	Y40410	IHC	1:1,000
Mouse monoclonal IgG Stem123®	Takara Holdings (Kyoto, Japan)	Y40420	IHC	1:1,000
Mouse monoclonal IgG to TUBB3	BioLegend (San Diego, USA)	801201	ICC	1:1,000
Rabbit polyclonal IgG to DACH1	ProteinTech Group Inc. (Rosemont, USA)	10914-1-AP	ICC	1:100
Rabbit polyclonal to GFAP	Merck Millipore (Burlington, USA)	AB5804	ICC, IHC	1:1,000
Rabbit polyclonal to IBA1	FUJIFILM Wako Chemicals Europe GmbH (Neuss, Germany)	019-19741	ICC, IHC	1:500
Rabbit polyclonal IgG to LAP2α	Abcam (Cambridge, UK)	ab5162	ICC	1:250
Rabbit polyclonal to MAP2	Abgent (San Diego, USA)	AP2018E	ICC, IHC	1:100
Rabbit polyclonal IgG to NES	Bio-Techne (Minneapolis, USA)	NB300-265	ICC	1:200
Rabbit polyclonal to NG2	Merck Millipore (Burlington, USA)	AB5320	ICC	1:200
Rabbit polyclonal to OLIG2	Merck Millipore (Burlington, USA)	AB9610	ICC	1:200
Rabbit polyclonal IgG to PAX6	BioLegend (San Diego, USA)	901301	ICC	1:300
Rabbit polyclonal IgG to TUBB3	BioLegend (San Diego, USA)	802001	ICC	1:1,000
Rabbit polyclonal to vGLUT1	Synaptic Systems GmbH (Göttingen, Germany)	135 303	IHC	1:1,000
Rat monoclonal IgG to CD11b, directly conjugated to PE	Miltenyi Biotec (Bergisch Gladbach, Germany)	130-113-797	FACS	1:50

Secondary Antibodies	Vendor (Headquarter)	Cat.-Number	Application	Dilution
Goat anti-guinea pig IgG (H+L), Alexa Fluor 633 conjugate	Thermo Fisher Scientific (Waltham, United States)	A21105	IHC	1:500
Goat anti-chicken IgY (H+L), Alexa Fluor 405 conjugate	Abcam (Cambridge, UK)	ab175674	IHC	1:500
Goat anti-mouse IgG (H+L), Alexa Fluor 488 conjugate	Thermo Fisher Scientific (Waltham, United States)	A11001	ICC/IHC	1:1,000
Goat anti-mouse IgM (H+L), Alexa Fluor 488 conjugate	Thermo Fisher Scientific (Waltham, United States)	A21042	ICC	1:500
Goat anti-mouse IgG (H+L), Alexa Fluor 555 conjugate	Thermo Fisher Scientific (Waltham, United States)	A21424	ICC/IHC	1:1,000
Goat anti-mouse IgG (H+L), Alexa Fluor 647 conjugate	Thermo Fisher Scientific (Waltham, United States)	A21236	IHC	1:500
Goat anti-rabbit IgG (H+L), Alexa Fluor 488 conjugate	Thermo Fisher Scientific (Waltham, United States)	A11008	ICC/IHC	1:1,000

Table continued on p. 56

Goat anti-rabbit IgG (H+L), Alexa Fluor 555 conjugate	Thermo Fisher Scientific (Waltham, United States)	A21429	ICC/IHC	1:1,000
HRP-linked anti-mouse IgG	Cell Signaling Technology (Danvers, United States)	7076S	WB	1:7,500
HRP-polymer anti-mouse	Zytomed Systems GmbH (Bargteheide, Germany)	ZUC050-006	IHC	-

Table 10: Antibodies.
WB: Western blot, FACS: Fluorescence-activated cell sorting, ICC: Immunocytochemistry, IHC: Immunohistochemistry.

2.1.10. Hardware and software

Hardware with according software, if applicable	Vendor (Headquarter)
Medifuge for CPT tubes	Thermo Fisher Scientific (Waltham, USA)
CASY cell counter	Hoffman-La Roche (Basel, Switzerland)
HERAcell 150 incubators for NormOx and LowOx	Thermo Fisher Scientific (Waltham, USA)
HERAcell cell culture cabinet	Thermo Fisher Scientific (Waltham, USA)
Rocker	Ohaus Corporation (Parsippany, USA)
Table top bioreactor	Hamilton Bonaduz AG (Bonaduz, Switzerland)
Shaking incubator for bacteria	Edmund Bühler GmbH (Bodelshausen, Germany)
Megafuge 1.0R cell culture centrifuge for S1 work	Thermo Fisher Scientific (Waltham, USA)
Megafuge 16R cell culture centrifuge for S2 work	Thermo Fisher Scientific (Waltham, USA)
Vacuum sucking pump	Vacuubrand GmbH & Co. KG (Wertheim, Germany)
Water bath	Memmert GmbH & Co.KG (Schwabach, Germany)
Neubauer counting chamber	Paul Marienfeld (Lauda-Königshofen, Germany)
4 °C fridge	Liebherr (Bulle, Switzerland) and Robert Bosch GmbH (Gerlingen, Germany)
-20 °C freezer	Liebherr (Bulle, Switzerland)
-80 °C freezer	Thermo Fisher Scientific (Waltham, USA) and Eppendorf (Hamburg, Germany)
-150 °C freezer	Panasonic Corporation (Kadoma, Japan)
Freezing buckets	Corning Inc. (Corning, USA) and Nalge Nunc International Corporation (Rochester, USA)
Axiovert 25 cell culture microscope	Carl Zeiss (Oberkochen, Germany)
PAULA live cell microscope	Leica Microsystems GmbH (Wetzlar, Germany)
EVOS FL live cell microscope	Thermo Fisher Scientific (Waltham, USA)
Warming pad	Harvard Apparatus (Holliston, USA)
Light source	Fortive (Everett, USA)
Operation microscope	Carl Zeiss (Oberkochen, Germany)
Cunning stereotaxic frame with mask	Stoelting (Wood Dale, USA)
Fluovac O_2/isoflurane system	Harvard Apparatus (Holliston, USA)
Surgical instruments	Fine Science Tools GmbH (Heidelberg, Germany)
Instrument-sterilizing heating bath	Fine Science Tools GmbH (Heidelberg, Germany)
Latex beads for sterilizing heating bath	Sigma Aldrich (St. Louis, USA)
Digital instrument to monitor stereotaxic coordinates	Stoelting (Wood Dale, USA)
Ideal Micro Drill	Stoelting (Wood Dale, USA)
0.7 mm drill burr	Fine Science Tools GmbH (Heidelberg, Germany)
Transplantation capillaries	Fine Science Tools GmbH (Heidelberg, Germany)
Needle puller PC-10	Narishige International Limited (London, UK)
Microforge	Narishige International Limited (London, UK)
Microliter pipette for stereotaxic transplantation	Hamilton Company (Reno, USA)
Wound clip system	Fine Science Tools GmbH (Heidelberg, Germany)
Suture material	B. Braun (Melsungen, Germany)
Heater Fuse warming cabinet	Scanbur A/S (Karlslunde, Denmark)
Microm HM 560 cryostat	Thermo Fisher Scientific (Waltham, USA)
54115 R centrifuge with cooling unit for RNA extraction	Eppendorf (Hamburg, Germany)
5415 D centrifuge without cooling unit for DNA extraction	Eppendorf (Hamburg, Germany)

Table continued on p. 57

MICRO STAR 17R centrifuge with cooling unit for protein extraction	VWR International (Radnor, USA)
Megafuge 40R centrifuge for falcons in molecular biology	Thermo Fisher Scientific (Waltham, USA)
1.5 ml-tube minifuge	Carl Roth (Karlsruhe, Germany)
8-strip minifuge	neoLab Migge GmbH (Heidelberg, Germany)
Scales	VWR International (Radnor, USA) and Sartorius (Göttingen, Germany)
Vortexer 2x[3]	VELP Scientifica Srl (Usmate Velate MB, Italy)
Heating block Thermomixer compact	Eppendorf (Hamburg, Germany)
Magnetic stirrer	VELP Scientifica Srl (Usmate Velate MB, Italy)
SevenEasy pH-meter	Mettler-Toledo (Columbus, USA)
Microliter pipettes, several sizes (0.2-1,000 µl)	Eppendorf (Hamburg, Germany)
Pipette boy	Brand GmbH & Co. KG (Wertheim, Germany)
Nanodrop 2000c	Thermo Fisher Scientific (Waltham, USA)
Infinite M Plex plate reader	Tecan Group Ltd. (Männedorf, Switzerland)
T3000 thermocycler	Biometra GmbH (Göttingen, Germany)
Mastercycler **ep***gradient S* realplex[4]	Eppendorf (Hamburg, Germany)
ViiA™7 real-time PCR system	Applied Biosystems (Foster City, USA)
Gel electrophoresis system	Biometra GmbH (Göttingen, Germany)
GelDoc XR+	Bio-Rad Laboratories, Inc. (Hercules, USA)
Western blot modules	Bio-Rad Laboratories, Inc. (Hercules, USA)
ChemiDoc XRS+	Bio-Rad Laboratories, Inc. (Hercules, USA)
FACSCalibur flow cytometer	BD Bioscience (San Jose, USA)
Accuri C6 Plus flow cytometer	BD Bioscience (San Jose, USA)
Table top ventilator	Ako-ismet Elektrogeräte (Nidderau, Germany)
AxioImager with Apotome	Carl Zeiss (Oberkochen, Germany)
AxioObserver with Apotome	Carl Zeiss (Oberkochen, Germany)
DMI6000B live cell fluorescent microscope	Leica Microsystems GmbH (Wetzlar, Germany)
IN Cell Analyzer 2200	GE Healthcare Bio-Sciences Corp (Piscataway, USA)
Light sheet fluorescence microscope	Self-built by the Biophysical Chemistry Workgroup of Ulrich Kubitscheck (University of Bonn, Germany)

Hardware-independent software	**Vendor (Headquarter)**
Salmon	© R. Patro, G. Duggal, M. Love, R. Irizarry & C. Kingsford
R Version 3.5.1 GUI 1.70 El Capitan build (7543)	© R Foundation for Statistical Computing, 2016
Cytoscape Version 3.8.1	© Cytoscape Consortium, 2001-2018
Microsoft Office Version 16.16.27	Microsoft (Redmond, USA)
Imaris x64 Version 8.3.1	Oxford Instruments (Abingdon, UK)
ImageJ Version 1.52a Java 1.8.0_181 (64-bit)	© National Institutes of Health (Bethesda, USA)
CellProfiler Version 2.2.0	© Broad Institute (Cambridge, USA)
Inkscape Version 0.92.2	© Free Software Foundation, Inc. (Boston, USA)

Table 11: Hardware and software

2.2. Methods

2.2.1. Cell culture techniques

2.2.1.1. Institutional approval

The collection of human somatic material (*i.e.*, blood or fibroblasts) for cell programming was approved by the ethics committee of the University of Bonn Medical Centre (approval number 275/08). All subjects gave written informed consent. The donated material was pseudonymized before being processed.

2.2.1.2. Derivation of erythroid progenitor cells

PBMCs were isolated from fresh blood draws, which were kindly obtained and provided by Ullrich Wüllner (Clinic and Polyclinic for Neurology, University Hospital Bonn), Anja Schneider (Clinic for Neurodegenerative Diseases and Gerontopsychiatry, University Hospital Bonn) and Waltraut Merz (Department of Obstetrics and Prenatal Medicine, University Hospital Bonn). For PBMC isolation, peripheral blood was collected in vacutainer CPT tubes, which were centrifuged for 30 minutes at 1,800 rcf in a Medifuge. After centrifugation, whitish layers containing mononuclear cells were transferred to 15 ml-tubes. Cells were diluted with 1x DPBS to a total volume of 15 ml, which was mixed by inverting the tubes. Afterwards, tubes were centrifuged for 15 minutes at 1,200 rpm. The supernatants were discarded and cells were resuspended in 10 ml 1x DPBS. Again, tubes were inverted to mix cell suspensions. The number of living PBMCs was quantified using a CASY cell counter. Afterwards, aliquots of 3-5x10^6 cells were prepared and centrifuged for 5 minutes at 1,200 rpm. The supernatant was discarded and PBMCs were either frozen in 90 % FCS plus 10 % DMSO or directly resuspended in EMI (Table 2) for subsequent EPC genesis (equals to day 0 of EPC enrichment). For cryo-preservation, cells were first kept at -80 °C for 2 to 7 days before being transferred to -150 °C for long-term storage.

For enriching EPCs, a protocol adapted from van den Akker *et al*., 2010 was applied. In short, cells were cultured in uncoated 6-well cell culture plates at 21 % O_2 and 37 °C. From days 1 to 6 of EPC genesis, 1 ml EMI was added freshly per day and well. At day 7, EPCs were enriched by applying a Percoll density gradient. In short, a Percoll gradient with a density of 1.075 ρ was prepared by diluting 20.8 ml Percoll stock solution, consisting of 45 ml Percoll supplemented with 5 ml 10x DPBS, with 19.2 ml DMEM/F12. Per sample, 4 ml Percoll gradient were added to a 15 ml-tube. Afterwards, 7 ml PBMC suspension were collected from each 6-well and slowly pipetted on top of the Percoll gradient, allowing phase separation. Tubes were centrifuged at 1,000 rcf for 20 minutes without brake in order to prevent fast deceleration. After centrifugation, the interphase rings containing EPCs were collected and transferred to new 15 ml-tubes. In order to remove any remaining Percoll traces, two washing steps were performed. For each washing step, tubes were filled with DMEM/F12, centrifuged at 1,000 rpm for 5 minutes and supernatants were discarded. The number of living EPCs was quantified using a CASY cell counter before the first washing. After the second washing, EPCs were resuspended in EMII (Table 2) and plated in uncoated 6-well cell culture-plates at a density of 1-1.5x10^6 cells/6-well for further maturation. Enriched EPCs were expanded up until day 9 of EPC genesis, performing medium addition on day 8. On day 9, EPC-containing cell suspensions were collected in 15 ml-tubes, filled up to a total volume of 10 ml with DMEM/F12, and counted using a CASY cell counter. After counting, aliquots of 1-2x10^6 cells were prepared and centrifuged for 5 minutes at 1,000 rpm. Supernatants were discarded and cells were frozen in 90 % EMII plus 10 % DMSO. During freezing, a fraction of each cell suspension was sampled for DNA extraction (see Section 2.2.4.1. DNA extraction) and subsequently analyzed for DNAm (see Section 2.2.4.3. DNA methylation analysis) as well as SNPs (see Section 2.2.4.2. Single nucleotide polymorphism analysis).

PBMC isolation and EPC enrichment were self-performed for three high-age donors, namely iLB-286bf, iLB-287bf and iLB-288bm. EPCs from iLB-224bm, iLB-225bm, iLB-229bm, iLB-MJD-190bm, iLB-216bm and iLB-218bm were kindly generated and provided by Melanie Bloschies and Cornelia Thiele (both Institute of Reconstructive Neurobiology, University of Bonn). Table 12 provides an overview about all cell types and stable cell lines generated and/or used for experiments in the course of this study.

Donor (years of age)	Cell type(s) generated/used	Generated/provided by	Used for
iLB-224bm (0y)	PBMCs & EPCs iPSCs & smNPCs iNSCs	MB/CT LF LF	Age investigation (DNAm, telomeres and cellular)
iLB-225bm (0y)	PBMCs & EPCs iPSCs & smNPCs iNSCs	MB/CT LF LF	Age investigation (DNAm, telomeres and cellular)
iLB-229bm (0y)	PBMCs & EPCs iPSCs & smNPCs iNSCs	MB/CT LF LF	Age investigation (DNAm and telomeres)
iLB-MJD-190bm (50y)	PBMCs & EPCs iPSCs & smNPCs iNSCs	MB/CT LF LF	Age investigation (DNAm and telomeres)
iLB-216bm (87y)	PBMCs & EPCs iPSCs & smNPCs iNSCs fibroblasts	MB/CT LF LF CT	Age investigation (DNAm, telomeres and cellular)
iLB-218bm (101y)	PBMCs & EPCs iPSCs & smNPCs iNSCs	MB/CT LF LF	Age investigation (DNAm, telomeres and cellular)
iLB-286bf (86y)	PBMCs & EPCs iNSCs	LF LF	Age investigation (DNAm dynamics)
iLB-287bf (81y)	PBMCs & EPCs iNSCs	LF LF	Age investigation (DNAm dynamics)
iLB-288bm (81y)	PBMCs & EPCs iNSCs	LF LF	Age investigation (DNAm dynamics)
iLB-82bf (34y)	iNSCs	CS	Positive control, Transplantation
iLB-107bm (35y)	iNSCs & smNPCs	CS & CT	Age investigation (DNAm and cellular)
iLB-MJD-33bf (49y)	iNSC & smNPCs	CS & CT	Age investigation (DNAm and cellular)
iLB-MJD-96bm (33y)	iNSCs & smNPCs	CS & CT	Age investigation (DNAm and cellular)
iLB-14m (48y)	iPSdMiG	MM	iNSC conversion
iLB-133bm (54y)	iPSdMiG	MM	iNSC conversion
Bioni-c010 (15-19y)	iPSdMiG	MM	iNSC conversion

Table 12: Cell populations and stable cell lines generated and used for experiments in the course of this study.
LF: Lea Flitsch, MB: Melanie Bloschies, CT: Cornelia Thiele, CS: Chao Sheng, MM: Mona Mathews.

2.2.1.3. Reprogramming of erythroid progenitor cells into induced pluripotent stem cells

In order to reprogram EPCs to pluripotency, EPCs were thawed in DMEM/F12. For all cell types cultured in the course of this study, thawing was performed by keeping cryo-vials containing cell suspensions in a 37 °C water bath until approximately 50 % of the frozen cell suspension was melted. Afterwards, cell suspensions were transferred to 15 ml-tubes and diluted in the 10-fold volume of DMEM/F12. Cells were centrifuged for 3-5 minutes at 1,000-1,500 rpm. Supernatants were discarded, cell pellets resuspended in cell type-specific media and plated in appropriate cell culture formats.

After 1-hour incubation at 21 % O_2 and 37 °C, $3x10^5$ EPCs were aliquoted in 15 ml-tubes and centrifuged for 5 minutes at 1,500 rpm. After removing the supernatants, cell pellets were resuspended in 250 μl EMII containing the CytoTune 2.0 SeVs – *i.e.*, a polycistronic vector for KLF4-OCT3/4-SOX2 overexpression, as well as single vectors encoding for cMYC and KLF4 – diluted to a multiplicity of infection (MOI) of 5:5:1. SeV infection marked day 0 of iPSC reprogramming. From this step on, cells were cultured at S2 safety level. Solutions containing cells and viruses, were then transferred to uncoated 4-wells and incubated for approximately 24 hours at 21 % O_2 and 37 °C. The next day, infected cells were collected in 15 ml-tubes and centrifuged for 5 minutes at 1,500 rpm. The supernatants were discarded, cell pellets resuspended in 500 μl EMII and plated in uncoated 4-wells. From this step on, cells were cultured at S1 safety level again at 5 % O_2 and 37 °C. On day 3 of iPSC reprogramming, cells were collected in 15 ml-tubes and centrifuged 5 minutes at 1,300 rpm. Supernatants were discarded and cells were

replated in EMII medium on 10 cm cell culture-dishes coated with Matrigel (1:60 dilution in DMEM/F12). Medium was gradually changed to iPSC medium (Table 2) from days 5 to 11 of iPSC reprogramming by performing partial medium changes with increasing concentrations of iPSC medium. Around day 20 of iPSC reprogramming, up to 24 cell colonies were manually picked under microscopic control and plated in iPSC medium supplemented with 10 μM Rock-inhibitor Y-27632 onto Matrigel-coated 24-well plates (1:60 dilution in DMEM/F12; one colony/24-well). More specifically, iPSC colonies were manually dislodged using a 100 μl-pipette under visual control using an EVOS FL microscope, which was placed in a sterile cell culture bench. This procedure was repeated every week until five single colony picking cycles were completed. After the fifth picking cycle, cells were allowed to grow confluent. Once confluency was reached, cells were dissociated with 0.5 mM EDTA. In short, iPSCs were washed once with 1x DPBS. Afterwards, EDTA was incubated for 3 minutes at room temperature. After removing the EDTA, cells were detached by pipetting using iPSC medium and replated in cell culture formats appropriate for the number of cells detached. Once sufficiently expanded, all single colony-derived iPSC lines were sampled for cell lysis and subsequent RNA extraction (see Section 2.2.4.4. RNA extraction and cDNA synthesis). The harvested RNA was used to perform RT-PCR against SeV sequences (see Section 2.2.4.5. Reverse-transcription polymerase chain reaction). Transgene-free iPSC lines were further expanded before being frozen in 90 % iPSC medium plus 10 % DMSO for cryo-preservation. During freezing, a fraction of each cell suspension was sampled for DNA extraction and subsequently analyzed for genomic integrity via SNP profiling. One transgene-free and genomically intact single colony-derived iPSC line was chosen per genotype, thawed according to the described procedure and subjected to further differentiation into smNPCs (see Section 2.2.1.4. Small molecule-based generation of induced pluripotent stem cell-derived neural precursor cells). IPSC lines of iLB-224bm, iLB-225bm, iLB-229bm, iLB-MJD-190bm, iLB-216bm, and iLB-218bm were reprogramed self-handedly with advisory help from Cornelia Thiele.

For routine iPSC expansion (*e.g.*, to yield sufficient cell numbers to start smNPC generation or in the context of genome editing), cells were cultured in iPSC medium on vitronectin-coated cell culture plates or dishes. For coating, vitronectin was diluted 1:100-1:200 in 1x DPBS. IPSCs were replated once confluency reached around 90 % with EDTA according to the described procedure. Whenever indicated, iPSCs were cryo-preserved as described. All running cell cultures (including blood cells, iPSCs, smNPCs and iNSCs) were microscopically inspected for potential contaminations before every handling. RT-PCRs to detect contamination with mycoplasma were performed every other week by Rachel Konang (Institute of Reconstructive Neurobiology, University of Bonn).

2.2.1.4. Small molecule-based generation of induced pluripotent stem cell-derived neural precursor cells

In order to generate stable NPC populations from iPSCs, a protocol adapted after Reinhardt, Glatza, et al., 2013 was applied. First, iPSCs were singularized by treatment with Accutase. In short, cells were incubated with pre-warmed Accutase for 5-15 minutes at 37 °C. Afterwards, cells were detached by pipetting, diluted in DMEM/F12 and collected in 15 ml-tubes. Manual cell counting was performed using a Neubauer counting chamber. After resuspending $2x10^6$ iPSCs in 1xN2B27+P/S+CPSD (Table 2) supplemented with 10 μM Rock-inhibitor Y-27632, cell suspensions were transferred to AggreWell™ 800 microwell culture plates, which were prepared according to

the manufacturer's instructions. Afterwards, plates were centrifuged for 3 minutes at 300 rpm. The next day, a half medium change with 1xN2B27+P/S+CPSD was performed. Approximately 48 hours after aggregating iPSCs to embryoid bodies (EBs), these were carefully dislodged from the AggreWells and transferred to uncoated 6 cm Petri-dishes. One day later, medium was changed to 1xN2B27+P/S+CPL (Table 2). After another medium change on day 4 of smNPC generation, EBs were triturated in small pieces on day 5 using a 1 ml-pipette. Triturated EBs from one AggreWell were distributed to a full Matrigel-coated (1:60 dilution in DMEM/F12) 6-well cell culture-plate and seeded in 1xN2B27+P/S+CPL supplemented with 10 μM Rock-inhibitor. From this day onwards, smNPCs were routinely cultivated on Matrigel-coated cell culture formats (1:60 dilution in DMEM/F12) in 1xN2B27+CPL (Table 2). Medium was changed every 1 to 2 days, and cells were passaged when reaching confluency using Accutase. Splitting ratios typically ranged from 1:4-1:12. Up until passage 5 (P5), 10 μM Rock-inhibitor was added for replating. Generated smNPC lines were subjected to QC and DNAm analysis at low (P5-P6) and high passages (P20-P21). QC of established smNPC as well as iNSC lines comprised the assessment of (i) genetic integrity via SNP analysis, (ii) NSC marker expression on RNA and protein level using qPCR (see Section 2.2.4.6. Quantitative real-time polymerase chain reaction) and immunocytochemistry (see Section 2.2.4.11.1 Immunocytochemistry), respectively, and (iii) neural differentiation potential (see Sections 2.2.1.7.1. Undirected differentiation of neural stem cells and 2.2.1.7.3. Differentiation of neural stem cells into oligodendrocytes).

2.2.1.5. Direct conversion of erythroid progenitor cells into induced neural stem cells

EPCs were converted into iNSCs according to the procedure published in Sheng *et al*., 2018. On day 0 of iNSC conversion, $1.5x10^5$ EPCs were thawed per genotype as described and spin-infected in EMII containing SeV-SOX2 and SeV-cMYC (each at MOI 5, both single vector-SeVs included in the CytoTune 1.0 kit) for 30 minutes at 1,500 rcf and 32 °C. Cell pellets were resuspended in their same virus-containing supernatant after centrifugation and plated into uncoated 4-wells. Cells were kept in a humidified incubator for approximately 24 hours at 37 °C and 21 % O_2 at S2 safety level. The next day, suspension cells were transferred into 15 ml-tubes, pelleted by 5-minute-long centrifugation at 1,500 rpm, resuspended in 75 % 2xN2B27+CPALLLT (Table 2) plus 25 % EMII and plated onto Matrigel-coated cell culture formats (1:60 dilution in DMEM/F12) at a density of about $1.3x10^4$ cells/cm^2. From this day onwards, converting cells were cultured at S1 safety level, 37 °C and 5 % O_2. On day 3 of conversion, medium consisting of 75 % 2xN2B27+CPALLLT plus 25 % EMII was added. From day 5 onwards, emerging adherent iNSCs were cultured in 100 % 2xN2B27+CPALLLT, performing full medium changes every other day. Starting from day 10 to 11, iNSCs were cultivated in 2xN2B27+CPALL (Table 2). On days 11 and/or 14 of iNSC conversion, up to 24 colonies consisting of neuroepithelial-like shaped cells were picked per genotype under microscopic control as described. Each colony was transferred to one well of a Matrigel-coated 24-well plate (1:60 dilution in DMEM/F12). Medium was supplemented with 10 μM Rock-inhibitor to support the survival of picked colonies. In order to generate polyclonal cell lines, the source plates remained in culture after picking up until day 21 of conversion, when cells were dissociated with Accutase as described and plated in Matrigel-coated cell culture formats (1:60 dilution in DMEM/F12) at a density of approximately $1x10^5$ cells/cm^2. Medium of polyclonal as well as single colony-derived iNSC lines was changed every 1 to 2 days. Lines were passaged at least once a week, ideally when cells had reached a confluency of 100-200 %, using Accutase. Typical splitting

ratios ranged from 1:3-1:9. From day 35 of conversion onwards, iNSCs were cultured under normoxic conditions (21 % O_2) at 37 °C. Generated iNSC lines were characterized at low (P5-P6) and high passages (P20-P21) as described. In-between, starting from P7, iNSC lines that passed low passage QC were cultivated at 39 °C in order to inhibit SeV replication and thus eliminate SeV expression. During this period of cultivation at elevated temperature, SeV-mediated transgene expression was monitored weekly by RT-PCR. Once expression of both SeVs was below the detection level of the RT-PCR, cells were transferred back to 37 °C. One week thereafter, another SeV RT-PCR was performed in order to confirm the persistent absence of SeVs.

For manipulating proliferation speed during EPC-to-iNSC conversion, cells were treated with either 2 % (v/v) glycerol or 2 mM thymidine starting from day 14 of conversion. During this time, iNSCs were replated once a week and cell numbers were estimated at each replating step in order to calculate population doublings. Glycerol was added to the medium with every medium change but was omitted on days when splitting was performed. Thymidine treatment always started the day after splitting and was discontinued after 48 hours and 24 hours for weeks 2 to 5 and 6 to 7 of conversion, respectively. Glycerol- and thymidine-treated cultures as well as untreated controls were harvested at day 49 of conversion for DNAm analysis.

IPSdMiG (details on the derivation of iPSdMiG provided in Section 2.2.1.7.4. Differentiation of induced pluripotent stem cells into microglial cells) were received from Mona Mathews-Ajendra (LIFE & BRAIN GmbH, Bonn) and converted into iNSCs with minor modifications to the described procedure: (i) In order to monitor whether emerging neuroepithelial-like colonies derived from SeV-dependent conversion events, a no virus-control was cultured in parallel at least until day 14 of conversion. (ii) To further exclude that colonies were formed by NSCs or converting neural cells, which might have emerged in the neural-microglial differentiation co-culture and potentially contaminated the iPSdMiG harvests, SeV infection was performed twice for two out of three genotypes, once on directly harvested iPSdMiG and once on iPSdMiG sorted for the microglial surface marker CD11b prior to SeV infection (see Section 2.2.4.10. Flow cytometry and fluorescence-activated cell sorting). (iii) For SeV-mediated conversion, iPSdMiG were spin-infected and cultured in 100 % 2xN2B27+CPALLLT from day 0 of conversion onwards. On day 1 of conversion, cells were replated at a density of about $2.6x10^4$ cells/cm^2. For replating, cells had to be detached using a cell scraper before centrifugation, since iPSdMiG became adherent overnight. Since some microglia-derived iNSC lines formed neurosphere-like structures around day 13 of conversion, these were harvested by medium collection and replated for subsequent adherent culture as neurosphere-derived cell lines, in addition to establishing single colony-derived and polyclonal cell lines on day 14 and 21 of conversion, respectively.

2.2.1.6. Generation of transgenic induced neural stem cells

Transgenic iNSCs were generated in order to prepare cells for pRABV-based monosynaptic tracing (see Section 2.2.2.3. Intracerebral transplantation and pRABV injection). To this end, adherent iNSCs were subsequently infected with pLenti-EF1α-mRFP1 and pLVX-SYN-HTB lentiviruses. These viruses were beforehand produced in HEK cells via lipofection. In short, HEK cells were cultured in HEK medium (Table 2) containing 2 % FCS and 25 μM chloroquine. Per reaction, 60 μl Lipofectamine 2000 was diluted in 440 μl OptiMEM and incubated with 10 μg of the respective target constructs as well as 5 μg of each of the two packaging plasmids psPAX2 and

pMD2G, dissolved in a total volume of 500 µl OptiMEM, for 5 minutes at room temperature. All plasmids were provided by Anke Leinhaas (formerly Institute of Reconstructive Neurobiology, University of Bonn). Afterwards, lipofection mixes were added to the HEK cells. Six hours after lipofection, medium was changed to HEK medium containing 5 % FCS. The next day, FCS concentration was increased to 10 %. Two and 3 days after lipofection, supernatants were collected during medium changes. These supernatants were pooled and centrifuged for 5 minutes at 300 rcf. Afterwards, the supernatants were filtered through 0.45 µm acetate filters. After filtration, ¼ volume of Lenti-X concentrator was added and incubated overnight at 4 °C. Viruses were then concentrated by centrifuging the solutions for 45 minutes at 1,500 rpm and 4 °C before discarding the supernatants. Pellets of virus concentrate were resuspended in Neurobasal. Virus concentrates of pLenti-EF1α-mRFP1 and pLVX-SYN-HTB were diluted 1:80 and 1:50 in 2xN2B27+CPALL for iNSC infection, respectively. After each infection, cells were selected with the respective antibiotics for which plasmids contained resistance genes. Specifically, 20 µg/ml blasticidin were applied for selection after lentiviral infection with pLenti-EF1α-mRFP1 and 0.5 µg/ml puromycin were used to select for cells, which had successfully integrated the pLVX-SYN-HTB transgene. Treatments with selection agents were discontinued once uninfected control cultures treated in parallel underwent cell death.

2.2.1.7. Differentiation paradigms

2.2.1.7.1. Undirected differentiation of neural stem cells

In order to differentiate NSCs spontaneously, cells were plated on Matrigel-coated cell culture formats (1:30-1:45 dilution in DMEM/F12) at a density of $3x10^4$ cells/cm^2 for electrophysiological assessment and $8.3x10^4$ cells/cm^2 for cultures to be assessed for cellular composition by immunocytochemistry. For performing electrophysiological recordings (see Section 2.2.3.1. Electrophysiological assessment of induced neural stem cell-derived neurons *in vitro*), iNSCs were differentiated on primary mouse astrocytes ($3x10^4$ cells/cm^2; provided by Tamara Krutenko, Institute of Reconstructive Neurobiology, University of Bonn), which were inactivated by treatment with 1 mM uridine and 0.4 mM FUDR before seeding iNSCs on top. The day after iNSC plating, medium was changed to NGMC+SponDiff±DAPT (Table 2). To differentiations that were not assessed for electrophysiological functionality, DAPT was added up until days 10 to 14 of differentiation in order to promote cell cycle exit. DAPT-free medium was supplemented with 0.5 % FCS for differentiation cultures containing primary mouse astrocytes. Stainings for neuronal and glial markers were performed after 6 weeks of undirected differentiation. Electrophysiological measurements were performed at weeks 6 and 10 of differentiation.

2.2.1.7.2. Transcription factor-mediated differentiation of induced neural stem cells

A TF-mediated forward programming approach was implemented for rapidly differentiating iNSCs into post-mitotic neurons early in the conversion process. To this end, at day 7 of conversion, iNSCs were infected with two lentiviruses (1:50-1:80 dilution), encoding for a reverse tetracycline-controlled transactivator (rtTA) and a tetracycline-responsive promoter element (TRE)-regulated NGN2 expression cassette. Both lentiviruses were produced according to the previously described procedure. Plasmids were kindly provided by Laura Stappert (formerly Institute of Reconstructive Neurobiology, University of Bonn). Transgenic iNSCs, which were kept in proliferation as negative control for this experiment, were selected by 3-day-long, subsequent treatments with 0.5

μg/ml puromycin and 200 μg/ml G418, selecting for integration of the NGN2 transgene and enriching for iNSCs with incorporated rtTA, respectively. On day 21 of conversion, iNSCs were plated at a density of $8.3x10^4$ cells/cm^2. The day after, forward programming was induced by changing medium to NGMC+SponDiff+DAPT supplemented with 1 μg/ml DOX, and iNSC differentiation was proceeded under normoxic conditions. From day 5 to 7 of differentiation, 5 μM Ara-C was added to the differentiation medium in order to kill remaining mitotically active cells. Differentiated cultures, as well as proliferating transgenic NGN2-iNSC lines, were harvested at day 42 of conversion (equaling to day 20 of differentiation for induced cultures) for DNAm and immunocytochemistry.

2.2.1.7.3. Differentiation of neural stem cells into oligodendrocytes

To generate oligodendrocytes from smNPCs and iNSCs, a multi-stage differentiation paradigm published by Gorris *et al*., 2015 was adapted. In short, cells were plated at a density of $8.9x10^4$ cells/cm^2 onto Matrigel-coated cell culture-dishes (1:60 dilution in DMEM/F12). The day after, medium was changed to oligodendrocyte differentiation medium stage I (Table 2). On day 7 of oligodendrocyte differentiation, cultures were replated onto Matrigel-coated cell culture-dishes (1:30 dilution in DMEM/F12) at a density of $0.9\text{-}1x10^4$ cells/cm^2. On day 14 of differentiation, cells were lysed for RNA extraction and fixed for immunocytochemistry. Remaining cultures were switched to oligodendrocyte differentiation medium stage II (Table 2). One week later (*i.e*., day 21 of differentiation), stage II was harvested and medium was changed to oligodendrocyte differentiation medium stage III (Table 2). The final harvest of stage III oligodendrocyte cultures was performed after 4 more weeks of maturation (*i.e*., day 49 of differentiation).

2.2.1.7.4. Differentiation of induced pluripotent stem cells into microglial cells

Lastly, iPSCs were differentiated in iPSdMiG by Mona Mathews-Ajendra after a recently established protocol (Mathews *et al*., in revision): In short, to induce differentiation, EBs were generated by detaching intact iPSC colonies using 1 mg/ml collagenase in DMEM/F12. Detached colonies were cultured in suspension for 4 days before being seeded on poly-L-ornithine- and fibronectin-coated cell culture plates. EB suspension culture was carried out either under conventional static or dynamic culture conditions using a table top bioreactor. The following terminal differentiation into iPSdMiG was performed according to a proprietary protocol of the LIFE & BRAIN GmbH (patent application number EP20162230). Briefly summarized, EBs were manually inoculated on macrocarriers, which were incubated for up to 48 hours under static culture conditions, facilitating adherence and progenitor outgrowth across the surface of the macrocarriers. Once firmly attached, inoculated macrocarriers were transferred into suspension culture formats such as non-tissue culture-coated T75 flasks, and placed in a rocker incubator for the rest of the differentiation process. Media conditions allowed the emergence of both neuroepithelial and hemogenic endothelial precursors, which were further differentiated into neural and immature microglial cells within the same culture paradigm, respectively. After approximately 6 weeks of differentiation, mature iPSdMiG were released into the supernatant of this mixed differentiation culture, from which they could be repeatedly harvested for up to 14 weeks.

2.2.1.8. Fibroblast cultivation

One high-age donor was re-recruited in order to obtain primary human dermal fibroblasts by invasive skin biopsy. From this biopsy sample, fibroblasts were isolated by Cornelia Thiele. In short, the epidermis and dermis of the skin punch were separated and the dermis was then digested in fibroblast medium (Table 2) plus 10 mg/ml collagenase overnight at 37 °C. Afterwards, isolated fibroblasts were cultivated on gelatin-coated cell culture formats (c = 0.1 %) in fibroblast medium by the author of this thesis. Fibroblasts were commonly replated once a week in a 1:2-1:3 ratio using 0.05 % Trypsin-EDTA. In short, confluent fibroblast cultures were once washed with 1x DBPS before being incubated for 5 minutes at 37 °C with Trypsin-EDTA. Afterwards, cells were detached by pipetting. Trypsin-EDTA was diluted by addition of fibroblast medium and cell suspensions were transferred to 15 ml-tubes. After centrifuging 3 minutes at 800 rpm, supernatants were discarded and cell pellets resuspended in appropriate volumes of fibroblast medium for replating.

2.2.2. Animal experiments

2.2.2.1. Institutional approval

Animal experiments were performed according to the applicable European and German laws (Animal Welfare Act and European legislative Directive 86/609/EEC), and approved by the Agency for Nature, Environment and Consumer Protection of the state North Rhine Westphalia (LANUV; approval numbers 84-02.04.2013.A368, 84-02.04.2016.A179 and 81.02.04.2019.A054).

2.2.2.2. Animals

Colonies of $Rag2^{tm1.1Flv}Il2rg^{tm1.1Flv}$ mice (*i.e.*, Rag2 Il2rg double knock-out mice) were bred in the animal facility of the University of Bonn, serving as immunodeficient host animals for transplantation experiments. All mice were homed in specific-pathogen-free barrier keeping. Mice were kept in single-ventilated cages at 22 °C, 50 % humidity, 15-fold air exchange and 12 hours hell/dark cycle. Water and food were provided *ad libitum*.

2.2.2.3. Intracerebral transplantation and pRABV injection

To prepare wild-type iNSCs, mRFP-expressing iNSCs equipped with relevant components for pRABV-based monosynaptic tracing or GFP-expressing iNSCs (cell line generated by Chao Sheng, formerly Institute of Reconstructive Neurobiology, University of Bonn) for transplantation, cells were detached and singularized by Accutase treatment as described. After detachment, cells were pelleted and resuspended at a concentration of $5x10^4$ cells/μl in Cytocon™ buffer II supplemented with 1 mg/ml DNase. Cell suspensions were kept on ice until transplantation.

In the operation theater for small animals of the University of Bonn's animal facility, adult mice at 8 to 12 weeks of age were prepared for surgery by applying 5 mg/kg body weight Carprofen by subcutaneous injection. Thirty minutes after analgesia, 10 ml/kg body weight anesthesia (Table 5) were applied intraperitoneally. Once animals

were in deep anesthesia (*i.e.*, no reflexes were elicited after pinching between toes), eyes were protected from drying out by application of Bepanthen and heads were shaved. Afterwards, animals were transferred to a warming pad and fixated in a stereotaxic frame by anchoring teeth and ears. In order to prevent dyspnea after fixation inside the stereotaxic frame, tongues were pulled out and O_2 was exogenously applied via a nose mask at a flow rate of 1 l/m. This nose mask was also used to apply isoflurane as additional anesthetic, in case this was needed in the course of the surgical procedure. After head fixation, the shaved skin was disinfected with antiseptic spray and additionally wiped with Betaisodona before the scalp was incised using a scalpel and scissor. The underlying skull was cleaned from the fascia and any remaining pericranium with help of dry, sterilized cotton swabs. Afterwards, the Bregma was identified and used to null x-, y- and z-coordinates. For unilateral, right-sided striatal and hippocampal transplantations, a hole was drilled into the skull at 0.8 mm anterior/1.8 mm lateral and 2.4 mm posterior/1.5 mm lateral (relative to the Bregma), respectively, using 0.7 mm drill burrs. A 27 G needle was utilized to widen the hole, if necessary, and incise the dura. Once the transplantation site was successfully opened, a glass capillary with a 50-100 μm opening, which was connected via a polyethylene tube to a Hamilton microliter pipette filled with 1x DPBS, was filled with 1 μl cell suspension. Glass capillaries were self-handedly prepared prior to transplantation using a needle puller and a Narishige microforge. The transplantation needle was then lowered into the brain parenchyma and cells were released at 2.6 mm and 1.3 mm ventral for striatal and hippocampal grafts, respectively. Five to 10 minutes after releasing the 1 μl cell suspension, the transplantation needle was carefully retracted and the skull was closed with bone wax. Head wounds were either closed with wound clips or absorbable surgical sutures, and finally soaked with Betaisodona solution. Afterwards, 10 ml/kg body weight NaCl and 10 ml/kg body weight antidot (Table 5) were applied by subcutaneous and intraperitoneal injection, respectively. Animals were kept at 28 °C overnight, and 5 mg/kg body weight Carprofen were subcutaneously applied approximately 24 hours after transplantation for post-operative analgesia.

For assessing the neural connectivity and functionality of transplanted iNSCs, grafts were either infected with pRABV 10-, 12-, 16- or 24-weeks post transplantation or transplanted animals were transferred to Jeong Seop Rhee's group at the Max-Planck Institute for Experimental Medicine in Göttingen for electrophysiological assessment of acute slices (see Section 2.2.3.2. Electrophysiological assessment of grafted induced neural stem cells in acute brain slices). For the former approach, surgical procedures were performed as described with minor modifications: For pRABV infection of hippocampal grafts, virus was released at two injection sites with 0.5 μl virus per site. The first injection was performed at the site of transplantation, whilst the second injection was positioned +0.6 mm posterior, +0.5 mm lateral and +0.1 mm ventral to it. Intracerebral transplantations and virus injections were partially performed by Anke Leinhaas.

In addition to the latter experiment addressing the electrophysiological functionality of iNSC grafts in adult mice, four new-born animals were grafted postnatally by non-stereotaxic, cerebral injection of $5x10^4$ iNSCs. Neonatal transplantations were all performed by Anke Leinhaas, and mice were sacrificed and processed by Heinz Beck's group (Institute of Experimental Epileptology and Cognition Research, University of Bonn; see Section 2.2.3.2. Electrophysiological assessment of grafted induced neural stem cells in acute brain slices).

2.2.2.4. Transcardial perfusion and brain tissue processing

Ten days after infecting iNSC transplants with pRABV, animals were sacrificed by transcardial perfusion. To this end, a lethal dose of perfusion anesthesia (Table 5) was applied by intraperitoneal injection. Once mice fell into deep anesthesia, they were fixed onto an operation table. The abdomen was first opened up to the forelimbs. Then, the liver was pulled down by dragging the sternal bone. Afterwards, the diaphragm was cut without damaging lungs or heart. The heart was then secured with forceps and a 23 G butterfly needle, which was connected to an infusion bag filled with 1x DPBS supplemented with 1,000 U/ml heparin, was pricked into the lower tip of the left chamber of the mouse heart. Thereafter, the right atrium was incised and the infusion started. Once approximately 50 ml 1x DPBS plus heparin had passed through the mouse body, the butterfly was disconnected from the infusion bag and plugged to a 50 ml-syringe filled with ice-cold 4 % FA, which was manually pushed through the body at very low speed to ensure proper fixation. Mice perfusions were partially conducted by Anke Leinhaas.

After transcardial perfusion, brains were dissected and post-fixed in 4 % FA at least overnight at 4 °C. Brains were then either prepared for histological and immunohistochemical stainings (see Sections 2.2.4.11.2. Histology and 2.2.4.11.3. Immunohistochemistry) and subsequent imaging, or whole-brain LSFM (Section 2.2.4.12. Microscopy). For the former, brains were first washed in 1x DPBS before being soaked with increasing concentrations of sucrose (*i.e.*, 15 % and 30 % sucrose in 1x DPBS). Afterwards, whole brains were mounted in TissueTek and frozen at -80 °C. Frozen brains were sectioned into 20 μm thick coronal slices using a Cryostat. Sectioning of a subset of the brains processed in this project was supported by Hendrik Wiethoff (formerly Institute of Reconstructive Neurobiology, University of Bonn), Rachel Konang and Anke Leinhaas. Brain slices were stored at -80 °C. Alternatively, tissue dehydration and clearing were performed prior to LSFM. In short, brains were washed three times for 1 hour each in 1x DPBS. Afterwards, brains were subjected to an ascending alcohol series. To this end, brains were first incubated in 30 % (pH 9.9) and then 50 % tert-butanol (pH 9.7), each for 24 hours at room temperature. Thereafter, brains were consecutively subjected to 70 % (pH 9.5), 80 % (pH 9.6), 96 % (pH 9.5) and 100 % tert-butanol (pH 9.4), which were each incubated for 24-48 hours at 30 °C. Two steps of BABB (pH 9.4; Table 7) incubation, each for 24 hours at 30 °C, were performed in order to clear the tissue for LSFM. All solutions, including BABB, were pH-adjusted by the addition of triethylamine. Cleared brains were stored in BABB at 4 °C. After LSFM, a selection of brains was re-hydrated. In essence, the dehydration and clearing procedures were performed in reverse sequence before brains were prepared for immunohistochemistry as described.

2.2.3. Electrophysiology

2.2.3.1. Electrophysiological assessment of induced neural stem cell-derived neurons *in vitro*

Electrophysiological recordings of *in vitro*-cultivated neurons were all performed by Pascal Röderer (Institute of Reconstructive Neurobiology, University of Bonn): Shortly summarized, whole cell current-clamp recordings were performed in a bath solution containing 140 mM NaCl, 3 mM KCl, 2 mM $CaCl_2$, 1 mM $MgCl_2$, 25 mM glucose and 10 mM HEPES (pH 7.4). For recording membrane potential or current, the patch pipette was filled with 140 mM K-gluconate, 5 mM HEPES, 0.16 mM EGTA, 5 mM $MgCl_2$, 5 mM phosphocreatine (pH 7.3). APs

were induced by 500 ms square current injections (-150 pA, -100 pA, -50 pA, 10 pA, 20 pA, 30 pA, 40 pA, 50 pA, 60 pA, 70 pA, 80 pA, 90 pA, 100 pA, 125 pA, 150 pA, 175 pA, 200 pA, 250 pA, 300 pA, 350 pA, 400 pA, 450 pA, 500 pA). The first AP evoked by the square pulse protocol was used to calculate AP properties. Finally, spontaneous neuronal activity was monitored for 2 minutes in a gap-free configuration.

2.2.3.2. Electrophysiological assessment of grafted induced neural stem cells in acute brain slices

Patch clamp recordings of acute slices from animals transplanted neonatally were performed by Pedro Royero (Institute of Experimental Epileptology and Cognition Research, University of Bonn): In short, mice were anesthetized with isoflurane and sacrificed by decapitation. Afterwards, brains were dissected and sliced in 250 μm thick sections, which were incubated for 25 minutes in high sucrose solution at 37 °C, followed by 1-hour-incubation in artificial cerebral spinal fluid (ACSF) at room temperature. Slices were then transferred to recording chambers, and continuously perfused with oxygenated ACSF at 33 °C. Whole cell patch clamp recordings were performed using ACSF as extracellular solution, which was composed of 125 mM NaCl, 3.5 mM KCl, 1.25 mM NaH_2PO_4, 26 mM $NaHCO_3$, 2 mM $CaCl_2$, 2 mM $MgCl_2$ and 15 mM glucose, and a potassium-based intracellular solution composed of 14 mM K-gluconate, 0.5 mM $MgCl_2$, 10 mM HEPES-acid, 0.16 mM EGTA, 5 mM phosphocreatine and 15 mM glucose. During some recordings, 8 mM biocytin was added to the intracellular solution for post-hoc reconstruction of patched cells using a confocal microscope. APs were induced by 250 ms square current injections (-200 pA, -100 pA, -50 pA, -25 pA, 10 pA, 20 pA, 30 pA, 40 pA, 50 pA, 60 pA, 70 pA, 80 pA, 100 pA, 125 pA, 150 pA, 175 pA, 200 pA, 250 pA, 300 pA, 350 pA, 400 pA, 450 pA, 500 pA). Additionally, 100 ms voltage steps from -100 to +60 mV (in steps of 20 mV) were used to assess the activation of voltage-gated sodium channels. Finally, gap-free recordings were performed to measure excitatory and inhibitory sPSCs.

Acute slice culture recordings of animals receiving iNSC grafts at an adult age were performed by Jeong Seop Rhee and his group members Ali Shaib and Chungku Lee (Max-Planck Institute for Experimental Medicine, Göttingen): In essence, mice were anesthetized with isoflurane and decapitated. The skull was opened and the whole brain was immediately transferred to 4 °C-cold sucrose-based slicing solution (230 mM sucrose, 26 mM $NaHCO_3$, 1 mM KH_2PO_4, 2 mM KCl, 2 mM $MgCl_2x6H_2O$, 10 mM glucose, 0.5 mM $CaCl_2$) with application of carbogen gas. The brain was cut transversally at 300 μm thickness using a Leica VT1200S vibrotome. Brain sections were kept in a chamber with carbogen-supplied ACSF (120 mM NaCl, 26 mM $NaHCO_3$, 1 mM KH_2PO_4, 2 mM KCl, 2 mM $MgCl_2x6H_2O$, 10 mM glucose, 2 mM $CaCl_2$; 304 mOsm) at 37 °C for 20 minutes for recovery. Afterwards, the sections in the chamber with carbogen-saturated ACSF were kept at room temperature. Individual brain slices were then placed in a recording chamber at room temperature, supplemented with carbogen gas. For whole-cell recordings, the somata of neurons in hippocampal and striatal regions were voltage clamped at -70 mV by a recording electrode (3.5-4.5 MΩ) containing an internal solution composed of 100 mM KCl, 50 mM K-gluconate, 10 mM HEPES, 4 mM ATP-Mg, 0.3 mM GTP-Na, 0.1 mM EGTA and 0.4 % biocytin (pH 7.4, 300 mOsm). The external solution was carbogen-saturated ACSF. Miniature excitatory and inhibitory sPSCs were recorded in the presence of 1 μM TTX, mixed with 10 μM bicucculine methiodide to block $GABA_A$ receptors for measuring miniature excitatory sPSCs or with 10 μM NBQX to block AMPA receptors for measuring miniature inhibitory sPSCs. An EPC-10 amplifier with Patchmaster v2X80 software was used for data acquisition. In order

to measure the ratio of miniature inhibitory to excitatory sPSCs in the same cells, slices were washed using a flow of ACSF with 1 μM TTX for at least 15 minutes between miniature excitatory and inhibitory sPSC measurements. Data were analyzed using Axograph X software.

2.2.4. Molecular biology techniques

2.2.4.1. DNA extraction

DNA extraction was performed with Qiagen's Blood & Tissue kit according to the manufacturer's instructions. Cell pellets were resuspended in 200 μl 1xDPBS, transferred to 1.5 ml-tubes, and mixed with 200 μl AL buffer as well as 20 μl proteinase K. After vortexing, samples were digested for at least 10 minutes at 56 °C and 1,400 rpm on a heated agitator. After digestion, 200 μl 100 % ethanol were added to each sample, being properly vortexed thereafter. The lysates were then transferred to DNA mini columns, which were placed in 2 ml-collection tubes. Columns were centrifuged for 1 minute at 8,000 rcf. The collection tubes were discarded and 500 μl AW1 buffer were added to the columns. Again, columns were centrifuged for 1 minute at 8,000 rcf and the collection tubes were discarded thereafter. 500 μl AW2 buffer were added to each column before columns were centrifuged for 3 minutes at 16,100 rcf. Afterwards, columns were placed in 1.5 ml-elution tubes and collections tubes were discarded. 100 μl AE buffer were added to each column and incubated for 1 minute before centrifuging 1 minute at 10,000 rcf. The concentration and purity of each extracted DNA sample were determined using a Nanodrop 2000c. DNA samples were stored at -80 °C.

2.2.4.2. Single nucleotide polymorphism analysis

For SNP analyses, DNA samples were diluted to a concentration of around 55 ng/μl with AE buffer and provided to the Next Generation Sequencing (NextGenSeq) Core Facility of the University of Bonn, where samples were further processed by whole-genome amplification, fragmentation and subsequent DNA-oligomer-hybridization and SNP genotyping on Illumina's Infinium Global Screening Array platform versions 1-3 (San Diego, USA). Raw data provided by the NextGenSeq Core Facility were next assessed using the associated GenomeStudio software using chip version-specific parameters. Samples with a call rate below 0.9 were excluded from further analysis. All chromosomes, except the gender-specific X- and Y-chromosomes, were assessed for copy number variations (CNVs). All established cell lines were compared to their cell line of origin (*i.e.*, iPSCs and iNSCs were compared to their respective EPCs of origin, whereas smNPCs were compared to the respective iPSCs of origin and lentivirally infected iNSCs were compared to the respective iNSC line of origin) in order to identify CNVs, which were introduced by the according intervention (*e.g.*, cell programming). Cell lines were considered genomically intact if all newly introduced CNVs were estimated with a confidence score lower than 200 as provided by GenomeStudio and/or were smaller than 500 kb.

2.2.4.3. DNA methylation analysis

Extracted DNAs were diluted to a concentration of 55 ng/µl with AE buffer and provided to the NextGenSeq Core Facility for DNAm analysis. At the NextGenSeq Core Facility, DNA samples were bisulfite-converted before being profiled on Infinium MethylationEPIC chips (850k; Illumina, San Diego, USA). Provided raw data were processed by Julia Franzen (AG Wolfgang Wagner, Helmholtz-Institute for Biomedical Engineering, RWTH Aachen University Medical School) using the minfi package (Aryee *et al*., 2014) in R before the samples' epigenetic age (also called DNAm age) were estimated using a predictor algorithm based on (Horvath *et al*., 2018). In addition, DNAm data were assessed for differentially methylated probes and regions (DMPs and DMRs, respectively) in R using ChAMP (Morris *et al*., 2014; Tian *et al*., 2017). ChAMP's gene set enrichment analysis was followed up with rrvgo (Sayols, 2020), and Venn diagrams were plotted using an online tool provided by the Ghent university (http://bioinformatics.psb.ugent.be/webtools/Venn/).

2.2.4.4. RNA extraction and cDNA synthesis

RNA extraction was performed with Qiagen's RNeasy kit according to the manufacturer's instructions. Shortly summarized, 350 µl RLT buffer supplemented with 1 % 2-mercapto ethanol were used to lyse cells. Lysates were mixed with an equal volume of 70 % ethanol and then transferred to RNA mini columns, which were placed in 2 ml-collection tubes. Columns were centrifuged for 15 seconds at 8,000 rcf. The flow-throughs were discarded. 700 µl RW1 buffer were added to each column and centrifuged for 15 seconds at 8,000 rcf. Two washing steps with RPE buffer followed discarding the flow-through. For each washing step, 500 µl RPE buffer were added to each RNA mini column, which was then centrifuged for 15 seconds and 2 minutes at 8,000 rcf during the first and second washing step, respectively. The flow-through was discarded after the first washing step. After the second washing step, columns were placed into new 2 ml-collection tubes. RNA mini columns were then centrifuged again for 1 minute at 8,000 rcf to remove remaining traces of wash buffers. Thereafter, RNA mini columns were placed into 1.5 ml-elution tubes. 30 µl RNA-free water were added to the RNA mini columns and incubated for 1 minute before centrifugation was performed for 1 minute at 8,000 rcf. All centrifugation steps were performed at 4 °C. The concentration and purity of the extracted RNA samples were analyzed with a Nanodrop 2000c. RNA samples were stored at -80 °C.

Single-stranded cDNA was synthesized using Quanta Biosciences' qScript kit. In short, 1 µg RNA was diluted in a total volume of 15 µl with RNA-free water. 1 µl reverse transcriptase and 4 µl according buffer were added to the diluted RNA samples, and incubated for 5 minutes at 22 °C, followed by 30 minutes at 42 °C and 5 minutes at 85 °C. The concentration and purity of the synthesized cDNA samples were analyzed with a Nanodrop 2000c. cDNA samples were stored at -20 °C.

2.2.4.5. Reverse-transcription polymerase chain reaction

For SeV RT-PCR, cDNAs were diluted to a concentration of 400 ng/µl. Afterwards, 79.2 µl RT-PCR master mix (Table 7) were aliquoted per sample and 1 µl diluted cDNA was added. After aliquoting 22.5 µl of each sample mix, 2.5 µl 5 µM primer mix were added per reaction. All primers used in the course of this project were either

obtained from Thermo Fisher Scientific (Waltham, USA) or IDT (Coralville, USA), and sequences are provided in Table 9. In order to assess the expression of a broad range of oligodendrocyte lineage-associated genes, RT-PCR was performed by diluting 300 ng cDNA in 17.5 μl RT-PCR master mix per reaction and sample. Next, 2.5 μl 5 μM primer mix were added per reaction. Both RT-PCRs, for detecting SeV transgenes and assessing oligodendrocyte lineage marker expression, were conducted in a Thermocycler according to the following program: 3 minutes at 94 °C; 25 or 35 cycles of 30 seconds at 94 °C, 30 seconds at 60 °C and 1 minute at 72 °C; and 5 minutes at 72 °C before cooling down to 4 °C. Amplification of *18S* was performed using 25 cycles, whilst all other genes of interest were amplified using 35 PCR cycles. All PCR products were size-separated on 1.5 % agarose gels containing ethidium bromide (1:10,000), by loading 20 μl sample or 7 μl 100 bp ladder and running gel electrophoresis in 1x TAE buffer (Table 7) at 100 V for a minimum of 30 minutes before documentation using a GelDoc XR+.

2.2.4.6. Quantitative real-time polymerase chain reaction

QPCRs were performed on an Eppendorf Mastercycler in 96-well-format. Per reaction, 300 ng cDNA were diluted in a total volume of 19 μl qPCR master mix (Table 7) and supplemented with 1 μl primer mix consisting of 5 μM forward and reverse primers. All primers used for qPCR were quality-controlled before use by assessing their specificity and linear amplification across a dilution series of a suited positive control cDNA. QPCRs were run in technical duplicates or triplicates for genes of interest and the ribosomal housekeeping gene *18S*. Cycling conditions were as follows: 3 minutes at 95 °C; 40 cycles of 15 seconds at 95 °C, 20 seconds at 60 °C and 30 seconds at 72 °C; 1 minute at 95 °C and 15 seconds at 55 °C, followed by a temperature gradient to 95 °C in the course of 20 minutes and finally 15 seconds at 95 °C before cooling down to 4 °C. Ct values of the genes of interest were normalized to the house-keeping gene *18S* and transformed to mean fold changes using the equation $2^{-\Delta\Delta Ct}$ (according to Livak & Schmittgen, 2001). QPCR products were size-validated by gel electrophoresis as described.

Telomere quantification was performed in 96-well-format on a ViiA™7 real-time PCR system according to a slightly modified protocol based on Cawthon, 2009. Per reaction, 20 ng DNA of each sample of interest were diluted in a total volume of 19 μl telomere qPCR master mix (Table 7). In addition to sample DNA, a concentration series of a DNA standard, which was prepared by pooling 1 μl of each diluted sample DNA, containing 150 ng/μl, 50 ng/μl, 16.7 ng/μl, 5.55 ng/μl and 1.85 ng/μl as well as a no template control, was analyzed in triplicates using a 900 nM primer mix combining primer pairs for both albumin and telomeres. Multiplexing with two different measurement points was performed as follows: 15 minutes at 95 °C; 2 cycles of 15 seconds at 94 °C followed by 15 seconds at 49 °C; 32 cycles of 15 seconds at 94 °C, 10 seconds at 62 °C, 15 seconds at 74 °C (measurement 1), 10 seconds at 84 °C and 15 seconds at 88 °C (measurement 2); 30 seconds at 95 °C, followed by a temperature gradient from 60 °C to 95 °C with 0.05 °C per second before cooling down to 4 °C. Raw data were processed by determining each sample's copy numbers of single-copy gene albumin ('S') and the telomere template ('T') according to the DNA standard concentration series, and subsequently calculating the ratio of T/S.

2.2.4.7. Bulk RNA sequencing analysis

Extracted RNAs used for bulk RNA sequencing were diluted to a concentration of around 50 ng/μl with RNA-free H_2O and provided to the NextGenSeq Core Facility. At the NextGenSeq Core Facility, samples were subjected to QuantSeq 3'mRNA-Seq library preparation (Lexogen GmbH, Vienna, Austria) before being sequenced on a HiSeq 2500 V4 (Illumina, San Diego, USA) in high output mode. Raw data provided by the NextGenSeq Core Facility were quantified and indexed according to the GRCh38 human genome version 96 obtained from ENSEMBL using Salmon (Patro *et al*., 2017). Gene level read counts were then further analyzed in R using tximport (Soneson *et al*., 2016) and DESeq2 (Love *et al*., 2014). Prior to further analysis, genes with less than a total read count of 10 across all samples were removed. All data were normalized based on standard size factor estimates, and differential expression analysis was performed using a Negative Binomial generalized linear and the corresponding Wald test. Resulting *p*-values were corrected for multiple testing using Benjamin–Hochberg correction. Only genes with an adjusted *p*-value < 0.05 and minimum |log2 fold change| > 1 were considered to be differentially expressed between conditions. Gene ontology (GO) enrichment of differentially expressed genes (DEGs) was performed using topGO with Fisher's exact test and the 'elim' algorithm (Alexa *et al*., 2006). GO enrichment was followed up in R using the Bioconductor package rrvgo (Sayols, 2020). Venn diagrams were again plotted using the Ghent university's online tool (http://bioinformatics.psb.ugent.be/webtools/Venn/). Finally, Cytoscape (Shannon *et al*., 2003) was used to visualize gene interaction networks. To this end, the top twenty SOX2 interaction partners with a confidence score of 0.4 or greater were retrieved from STRING protein query and plotted as network. Differential expression analysis results ($p < 0.05$ and |log2 fold change| > 2) were visualized on networks as node filling.

2.2.4.8. Protein extraction

In order to assess autophagic flux, cells were first stimulated with 40 nM BAFA for 4 hours at 37 °C. Afterwards, cells were washed once with 1x DPBS before being mechanically detached with a cell scraper and transferred to 1.5 ml-tubes in 1 ml ice-cold 1x DPBS. Samples were centrifuged for 5 minutes at 500 rcf and 4 °C. Supernatants were discarded and cell pellets were either directly processed or frozen in liquid nitrogen and stored at -80 °C. For protein extraction, cell pellets were lysed in 45 μl RIPA buffer (Table 7), supplemented with 1x protease and phosphatase inhibitor cocktail. RIPA buffer was incubated for 20-30 minutes on ice, with regular vortexing steps every 5 minutes. Afterwards, tubes were centrifuged for 30 minutes at 16,100 rcf and 4 °C. Finally, lysates were transferred into new 1.5 ml-tubes without disturbing the pelleted debris.

Protein concentrations were determined with Roti-Quant reagent. In short, 2 μl of each sample as well as BSA standards containing no protein, 0.3125 mg/ml, 0.625 mg/ml, 1.25 mg/ml, 2.5 mg/ml or 5 mg/ml protein were diluted in 198 μl ddH_2O. 50 μl Roti-Quant were added to each sample and determined for absorbance at 595 nm (10 nm bandwidth, 25 flashes) in duplicates using a Tecan plate reader. A standard curve was fitted to the data points of the BSA standards and used to calculate the protein concentration of all other samples.

2.2.4.9. Western blotting

Extracted protein samples were diluted to a defined protein concentration of 1 μg/μl with ddH_2O. 5 μl 4x Laemmli buffer (Table 7) supplemented with 10 % 2-mercapto ethanol were added to 20 μl of each sample and mixtures were heated at 95 °C for 5 minutes. The total samples' volume or 10 μl page ruler protein ladder was loaded onto home-made 15 % acryl amide SDS-Tris gels. These gels comprised a bottom layer of stacking gel consisting of 1x Tris/HCl-SDS buffer (pH 8.8; Table 7) supplemented with 15 % acryl amide, 0.06 % TEMED and 0.11 % APS and an upper stacking gel layer consisting of 1x Tris/HCl-SDS buffer (pH 6.8; Table 7) supplemented with 4 % acryl amide, 0.06 % TEMED and 0.11 % APS, in which 15 pocket-combs with 1.5 mm spacer were placed. Gels were run at 80-120 V (80 V until buffer front reached the boundary between stacking and resolving gel, 100-120 V thereafter) in 1x SDS running buffer (Table 7) till the loading buffer front reached the end of the gels. Afterwards, blotting chambers were built as follows: Sponge, 3 Whatman papers, gel, methanol-activated PVDF membrane with 0.2 μm pore size, 3 Whatman papers, sponge. The Western blot chamber was cooled during blotting, which was conducted at 80-100 V for 1.5 hours in 1x Western blot transfer buffer (Table 7).

After blotting, membranes were washed once with 1x TBS-T (Table 7) before being stained with Amido-Black solution (Table 7) in order to visualize protein loading. After removing the Amido-Black stain with 2 % SDS, membranes were cut at the height of the 25 kDa marker. The cut parts were separately incubated with 10 % milk powder in 1x TBS-T for 10 and 30 minutes for the low and high molecular weight parts, respectively, before primary antibodies (Table 10) diluted in 5 % milk powder in 1x TBS-T were incubated overnight at 4 °C. The next day, membranes were washed three times for 5 minutes with 1x TBS-T, before incubation with secondary antibodies diluted in 5 % milk powder in 1x TBS-T was performed for 1 hour at room temperature. Three washing steps with 1x TBS-T and one final washing step with 1x TBS, each conducted for 5 minutes, followed secondary antibody incubation. Finally, membranes were subsequently developed using Classico and Femto HRP substrates before documentation using a ChemiDoc XRS+.

2.2.4.10. Flow cytometry and fluorescence-activated cell sorting

Flow cytometry was performed in order to quantify production of ROS using MitoSOX staining. In short, smNPCs and iNSCs were seeded at a density of $5x10^4$ cells/cm^2. The next day, medium was changed to antioxidant-free 1xN2B27-AO+CP (Table 2). After 2 days in antioxidant-free medium, the supernatant was discarded and cells were incubated with HBSS ± 5 µM MitoSOX for 10 minutes at 37 °C. 30-minutes-long treatment with 10 μM FCCP at 37 °C, prior to MitoSOX staining, was used as experimental positive control. Afterwards, cells were washed once with 1x DPBS before being detached using ice-cold 0.5 mM EDTA. Cell suspensions were transferred to 1.5 ml-tubes and measured for fluorescence in FL2 using a FACSCalibur or an Accuri C6 Plus flow cytometer. Gating was performed according to unstained negative control. The percentage of MitoSOX-positive cells as well as relative fluorescence intensities were estimated using the flow cytometers' respective softwares.

In order to purify iPSdMiG before SeV-mediated iNSC conversion, iPSdMiG harvests were subjected to fluorescence-activated cell sorting (FACS) for the microglial marker CD11b. To this end, $1x10^6$ iPSdMiG were harvested from the differentiation's supernatant and transferred to 15 ml-tubes. After centrifuging 5 minutes at 1,500 rpm, supernatants were discarded and cell pellets resuspended in 100 μl 1x DPBS containing CD11b-PE

antibody. The cell-antibody solutions were then passed through 40 μm cell strainers, protected from light and incubated on ice for 1 hour. Afterwards, the 15 ml-tubes were filled up with 1x DPBS in order to dilute the antibody. After another centrifugation for 5 minutes at 1,500 rpm, supernatants were discarded and cell pellets resuspended in 1 ml 1x DPBS containing 0.1 % BSA and 50 μg/ml DNase. FACS was performed by the Flow Cytometry Core Facility of the University of Bonn.

2.2.4.11. Immunocytochemistry, histology and immunohistochemistry

2.2.4.11.1 Immunocytochemistry

For immunocytochemistry, cells were fixed with 4 % PFA for 10 minutes at room temperature before being washed with 1x DPBS once. If not directly processed further, cells were stored in 1x DPBS at 4 °C to prevent drying. Next, cells were incubated with 10 % FCS in 1x DPBS for 2 hours at room temperature in order to eliminate unspecific antibody binding. If the markers stained for were not membrane-bound, blocking solutions were supplemented with 0.5 % Triton-X100 for cell permeabilization. After blocking, cells were incubated overnight at 4 °C with primary antibodies (Table 10) diluted in 1x DPBS containing 5 % FCS ± 0.3 % Triton-X100. The next day, cells were washed three times with 1x DPBS ± 0.3 % Triton-X100 before secondary antibodies, diluted in 1x DPBS containing ± 0.3 % Triton-X100, were incubated for 2 hours at room temperature. After three additional washing steps with 1x DPBS ± 0.3 % Triton-X100, 2 μg/ml DAPI was incubated for 5 minutes at room temperature to counterstain nuclei. Cells were finally washed once with 1x DPBS before mounting (composition mounting medium provided in Table 7). Mounted specimens were dried at least overnight at 4 °C before imaging.

2.2.4.11.2. Histology

Histological stainings were performed by Rachel Konang or Anke Leinhaas. As a first step, transplants were located in cryo-sections using hematoxylin-eosin histological stainings. In short, cryo-sections were thawed under ventilation and subsequently surrounded using a grease stick. Afterwards, sections were washed for 2 minutes in ddH_2O. Hematoxylin was incubated for 30 seconds before being washed off with ddH_2O. Bluing was performed by washing with tab water for 3-5 minutes. After a 30-second-long incubation with 75 % ethanol containing 0.22 % HCl, sections were washed with tab water again, before being incubated in a 0.01 % eosin solution for 45 seconds. Finally, sections were dehydrated by performing two washing steps with 100 % ethanol, one washing step with 100 % isopropanol and two incubation steps each 3-5 minutes with 100 % xylol. Sections were mounted with Cytoseal XYL.

Cryo-sections of brains rehydrated post LSFM-imaging were further used for histological stainings against human NCAM, which were mainly performed by Anke Leinhaas and Rachel Konang. In short, after sections were thawed and washed, endogenous peroxidase was blocked by incubating 1 % hydrogen peroxide for 15 minutes. After washing three times in 1x DPBS, endogenous biotins were blocked by applying Zytomed's blocking solution for 5 minutes. After two additional washing steps using 1x DPBS, primary mouse anti-human NCAM antibody (diluted in 0.1 % Triton-X100) was incubated for 1 hour at room temperature. Again, sections were washed three times in 1x DPBS before secondary HRP-polymer anti-mouse was applied for 30 minutes at room temperature.

Following three more washing steps, signal was developed using Zytomed's DAB high contrast kit. According to the manufacturer's instructions, 500 µl DAB substrate buffer were mixed with 1 drop DAB chromogen solution. Afterwards, each section was incubated with 1 drop of this working dilution until a good signal-to-noise ratio was achieved, which took approximately 1-3 minutes. DAB reaction was stopped by mounting sections in water. Finally, brain slices were dehydrated and sealed with Cytoseal XYL as described.

2.2.4.11.3. Immunohistochemistry

For further transplant characterization, immunofluorescent stainings on cryo-sections were performed. To this end, sections were equilibrated in 1x DPBS for 10 minutes after being thawed under ventilation and surrounded using a grease stick. Unspecific epitopes were blocked by incubation with 1x DPBS supplemented with 10 % NHS, 3 % NGS, 0.1 % Tween and 0.1 % Triton-X100 for 1 hour at room temperature. Sections were then washed two times with 1x DPBS before primary antibodies, diluted in 1x DPBS with 10 % NHS, 3 % NGS, 0.1 % Tween and 0.1 % Triton-X100, were incubated overnight at 4 °C. The next day, sections were washed three times each 5 minutes in 1x DPBS. Secondary antibodies, diluted in 1x DPBS with 10 % NHS, 3 % NGS, 0.1 % Tween and 0.1 % Triton-X100, were incubated for 2 hours at room temperature before sections were washed once for 5 minutes in 1x DPBS and subsequently counterstained with 2 µg/ml DAPI for 45 seconds. Finally, overnight washing at 4 °C with 1x DPBS supplemented with 0.05 % Tween was performed. The next day, Tween was washed-off by 10-minute-long incubation with pure 1x DPBS before sections were mounted with VectaShield. Immunohistochemical stainings were partially performed by Rachel Konang and Anke Leinhaas.

Brain sections that were rehydrated post LSFM were processed as described with minor modifications: Blocking was performed with 1x DPBS supplemented with 10 % NHS, 3 % NGS and 0.5 % Triton-X100. This solution was additionally used to dilute primary and secondary antibodies. Furthermore, sections were washed three times in 1xDPBS after secondary antibody incubation, before being counterstained with 2 µg/ml DAPI for 2 minutes at room temperature, subsequently washed three times each 10 minutes in 1x DPBS and then immediately sealed with VectaShield.

2.2.4.12. Microscopy

Live cell imaging of *in vitro* cultivated cells was performed on a daily basis with an Axiovert microscope. If indicated, live cell images were additionally captured using EVOS or PAULA microscopes. Histological stainings were imaged with an AxioObserver microscope. Image acquisition of immunofluorescent stainings was either performed manually using Leica's DMI6000B live cell or Zeiss' AxioImager and AxioObserver microscopes, or automated utilizing the IN Cell Analyzer. Whole mouse brains were imaged using a LSFM platform, which was previously built by the Biophysical Chemistry Workgroup of Ulrich Kubitscheck (University of Bonn, Germany). A fraction of all LSFM data sets was acquired with help of Anke Leinhaas.

2.2.5. Data processing and statistical analysis

2.2.5.1. Data processing

For qualitative image presentation, color brightness and contrast were either adjusted right after image acquisition with the software associated to the utilized microscope or retrospectively using ImageJ and Imaris for 2D and 3D images, respectively. For 3D images, acquired LSFM raw data were stitched using an ImageJ plugin programmed by the Biophysical Chemistry Workgroup of Ulrich Kubitscheck prior to processing data in Imaris. All performed image manipulations were in accordance with common guidelines for good scientific practice. Quantification of immunofluorescent stainings was performed on unmodified raw data using CellProfiler (Kamentsky *et al*., 2011) pipelines, which automatically and equally applied algorithms for primary object identification and subsequent pixel intensity quantification within identified primary objects to all evaluated pictures according to pre-defined parameters. After image quantification, CellProfiler pipelines were further used to automatically and equally apply background subtraction and color brightness adjustment to all pictures for respective qualitative display.

Numerical raw data were processed as described in the respective sections with Microsoft Excel. For graphical representation of numerical data, means and standard errors of the mean (SEM) were calculated and plotted using Microsoft Excel. If indicated, statistical analyses were performed as described in Section 2.2.5.2. Statistical analysis. Finally, figures were assembled using Microsoft PowerPoint and Inkscape.

2.2.5.2. Statistical analysis

All statistical analyses were conducted in R. First, to determine whether variables met the assumptions of linear models, Kolmogorov-Smirnov's or Shapiro Wilk's and Levene's test or F-test for normal distribution and homogeneity of variance were performed, respectively. If the variables analyzed were normally distributed, student's two-tailed t-test and independent one-way ANOVA were conducted in order to compare two and more than two groups, respectively. ANOVA was followed-up by pairwise comparisons using the Tukey-honest significant difference test, provided variances could be considered homogenous. In case analyzed variables were not normally distributed, the non-parametric equivalents, namely the Wilcoxon signed-rank and Kruskal Wallis tests, were calculated and followed-up by multiple comparisons using the Wilcoxon rank sum test or the Tukey and Kramer (Nemenyi) test with Tukey-Dist approximation for independent samples, as indicated. Correlation was assessed using the non-parametric Kendall's τ. In addition to the correlation analysis performed, a simple linear regression model was estimated and assessed for its goodness of fit. Significance level was set at $p < 0.05$ and adjusted by default when multiple comparisons were performed. Significance levels are indicated in figures as follows: *: $p < 0.05$; **: $p < 0.01$, ***: $p < 0.001$, ****: $p < 0.0001$.

3. Results

3.1. Direct conversion of blood from high-age donors yields rejuvenated NSCs.

3.1.1. Tripotent iNSCs can be derived from blood cells of young and old donors by overexpression of the TFs SOX2 and cMYC.

In the present study, we first set out to investigate how cellular aging signatures are preserved whilst converting blood into NSCs using an iNSC conversion paradigm that was previously established in our laboratory (Sheng *et al*., 2018). To this end, we recruited peripheral blood from newborns (N = 3) and aged donors (N = 6, from 50-101 years of age), and subjected isolated PBMCs to EPC enrichment. In order to deeply characterize cell lines from donors covering the whole human lifespan, EPCs from three young and three old individuals were chosen to generate isogenic pairs of directly converted iNSCs and iPSC-derived smNPCs (Figure 7 A). Specifically, EPCs were converted into iNSCs by SeV-mediated overexpression of the two TFs SOX2 and cMYC. For iPSC reprogramming, the transcription factors OCT4 and KLF4 were overexpressed in addition to SOX2 and cMYC. SeVs were eliminated from iNSC and iPSC lines by intermediate cultivation at elevated temperature and repeated subcloning, respectively. IPSCs were further differentiated into stably proliferating smNPCs, in order to yield iPSC-derived NSCs closely resembling iNSCs with regard to their cell type characteristics (Reinhardt, Glatza, *et al*., 2013; Sheng *et al*., 2018). All lines were cultured for at least 20 passages, equaling to up to 6 months of continuous *in vitro* culture, after which transgene-free iNSCs and smNPCs still homogenously expressed the NSC markers SOX2 and NES (Figure 7 B and C). Furthermore, SNP analysis revealed that iNSC and smNPC lines remained genomically intact after cell programming and subsequent *in vitro* expansion (Figure 7 D).

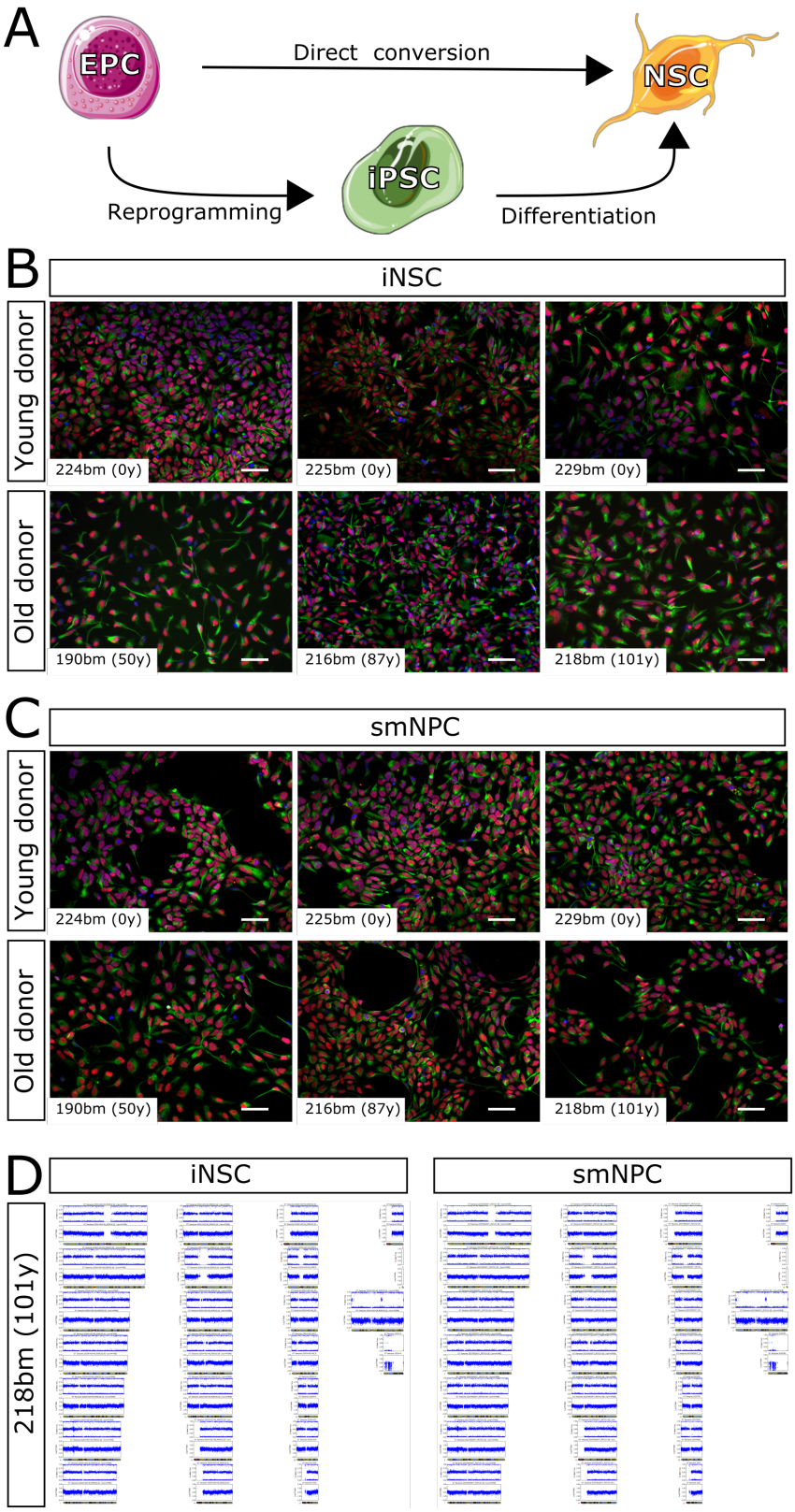

Figure 7: NSC marker expression and genomic integrity in isogenic sets of iNSCs and smNPCs derived from the blood of young and old donors.
(A) Schematic representing the derivation of isogenic pairs of NSCs via direct conversion, on the one hand, and iPSC reprogramming and subsequent neural differentiation, on the other hand. Figure elements were retrieved from Servier Medical Art by Servier (SMART; https://smart.servier.com), licensed under a Creative Commons Attribution 3.0 Unported License. **(B-C)** Blood-derived iNSCs (B) and iPSC-derived smNPCs (C) generated from three newborn (0 years of age) and three old donors (50, 87 and 101 years of age) expressed the NSC markers SOX2 (red) and NES (green) at high passages. Nuclei were counterstained with DAPI (blue). Scale bars = 50 μm. **(D)** Representative SNP profiles of one isogenic set of old donor-derived iNSCs and smNPCs after cell programming and extensive *in vitro* cultivation. Each plot depicts the profiles of the two transformed analysis parameters B allele frequency and Log_2 R ratio for all SNPs on the Illumina array across the entirety of all chromosomes.

In order to next demonstrate their NSC-like differentiation capacity, all generated high passage iNSC and smNPC lines were subjected to spontaneous differentiation yielding TUBB3- and MAP2-positive neurons as well as S100β- and GFAP-positive astrocytes (Figure 8 A). In addition, two isogenic sets of old donor-derived iNSCs and smNPCs were exemplarily subjected to a multistep differentiation paradigm supporting oligodendrogenesis. This successfully yielded mature O4-positive oligodendrocytes from both iNSCs and smNPCs (Figure 8 B).

Together, these data demonstrate the successful derivation of isogenic sets of directly converted and iPSC-derived NSCs from young and old donors, equally exhibiting stable self-renewal and tripotent differentiation capacities.

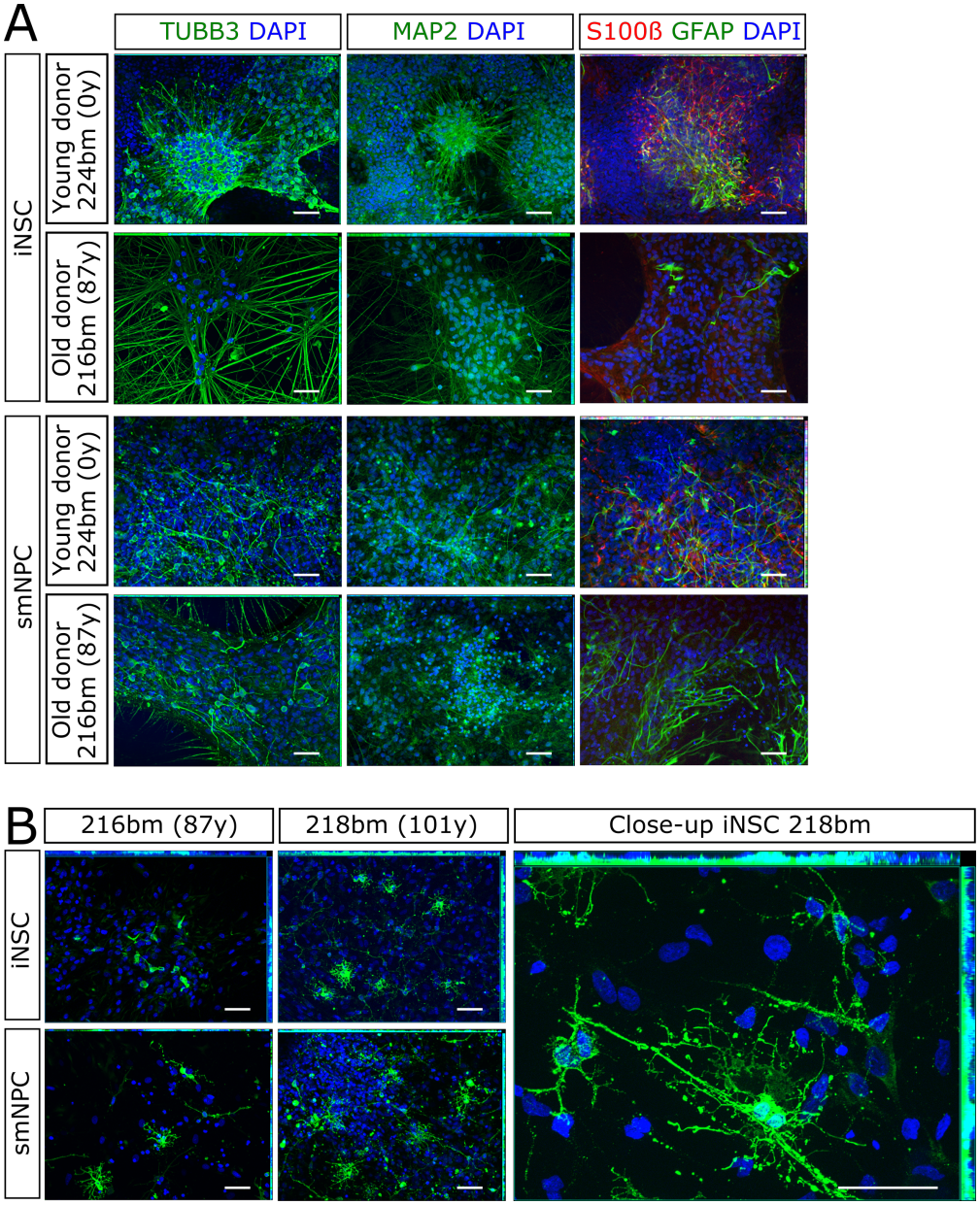

Figure 8: Differentiation of young and old donor-derived iNSCs and smNPCs into neurons, astrocytes and oligodendrocytes.
(A) Directly converted high passage iNSCs as well as iPSC-derived smNPCs generated from young and old donors were subjected to an undirected differentiation paradigm and stained for the neuronal markers TUBB3 and MAP2, as well as the astrocytic markers S100β and GFAP after fixation. Representative pictures are shown for one isogenic pair of NSCs from each donor age class. Scale bars = 50 μm. **(B)** Isogenic sets of transgene-free NSCs, derived from two different high-age donors, were differentiated according to a published multi-stage oligodendrocyte differentiation paradigm. Resulting cultures comprised O4-positive oligodendrocyte-like cells (green, DAPI in blue). Scale bars = 50 μm.

3.1.2. Cellular aging hallmarks are reset after blood-to-NSC transdifferentiation.

Next, we set out to explore how diverse cellular aging hallmarks were represented in young and old donor-derived iNSCs as compared to their isogenic smNPC controls. To this end, we first subjected all cell lines generated in the course of this project, as well as three isogenic sets of iNSCs and smNPCs previously derived from mid-age donors (Sheng *et al*., 2018), to DNAm profiling, and subsequently calculated the epigenetic age of each sample using the DNAm age prediction algorithm published by Horvath (Horvath *et al*., 2018; Figure 9 A). As expected, the DNAm age of EPCs highly correlated with the chronological age of the respective donors, demonstrating the accuracy of the age predictor algorithm. Furthermore, in concordance with published data, all iPSC-derived smNPC lines exhibited an embryonic-like epigenetic age, irrespective of their original donor age. Interestingly, iNSCs also exhibited a substantial degree of epigenetic rejuvenation across donor ages, maintaining around 13 % of the original donor ages at low passages. Notably, the DNAm age of old donor-derived iNSC lines seemed to further decrease upon passaging, as high passage iNSCs only preserved approximately 4 % of the donors' chronological ages.

We further assessed telomere lengths of the generated cell lines via a qPCR-based method, yielding T/S ratios that provide a relative measure of telomere length (normalized to the single-copy gene albumin) and were shown to correlate with absolute telomere lengths (Cawthon, 2009). After implementation of the method, analogous samples to those subjected to telomere length measurement during previous experiments, using Life Length's (Madrid, Spain) proprietary quantitative fluorescence *in situ* hybridization-based telomere analysis technique (Sheng *et al*., 2018), were analyzed using the established qPCR-based system. Indeed, also for our own samples, T/S ratios seemed to correlate with the known median telomere lengths (data not shown), emphasizing the applicability of this technique. Subsequently calculating T/S ratios for our sample set revealed that while telomere lengths of iNSCs neither differed from the telomere lengths measured in the source blood cells nor from iPSC-derived smNPCs, telomeres were overall significantly elongated in smNPCs as compared to EPCs (Figure 9 B). Notably, although old donor-derived samples overall tended to exhibit shorter telomeres than young donor-derived samples, this trend did not reach statistical significance for any of the cell types tested.

In line with the observed DNAm age reset in iNSCs, there were no differences between young and old donor-derived iNSCs and smNPCs with regard to the expression levels of the nuclear pore-associated transport receptor gene *RANBP17*, the laminin subunit *LAMNA* and the negative regulator of telomerase activity *PCDH10* (Figure 9 C), which are the only concordantly regulated DEGs across age in human fibroblasts, fibroblast-derived iNs and human postmortem cortical samples (Mertens *et al*., 2015).

Additionally, old donor-derived iNSCs did not exhibit increased abundance of the autophagy adaptor protein p62 (Figure 9 D), indicating no age-associated impairments in autophagy (Komatsu & Ichimura, 2010). This was further substantiated by the finding that the autophagic flux of iNSCs – as assessed by the conversion of LC3II to LC3I under autophagosome-lysosome fusion-inhibiting conditions (Mizushima & Yoshimori, 2007) – was overall even higher than in isogenic smNPCs.

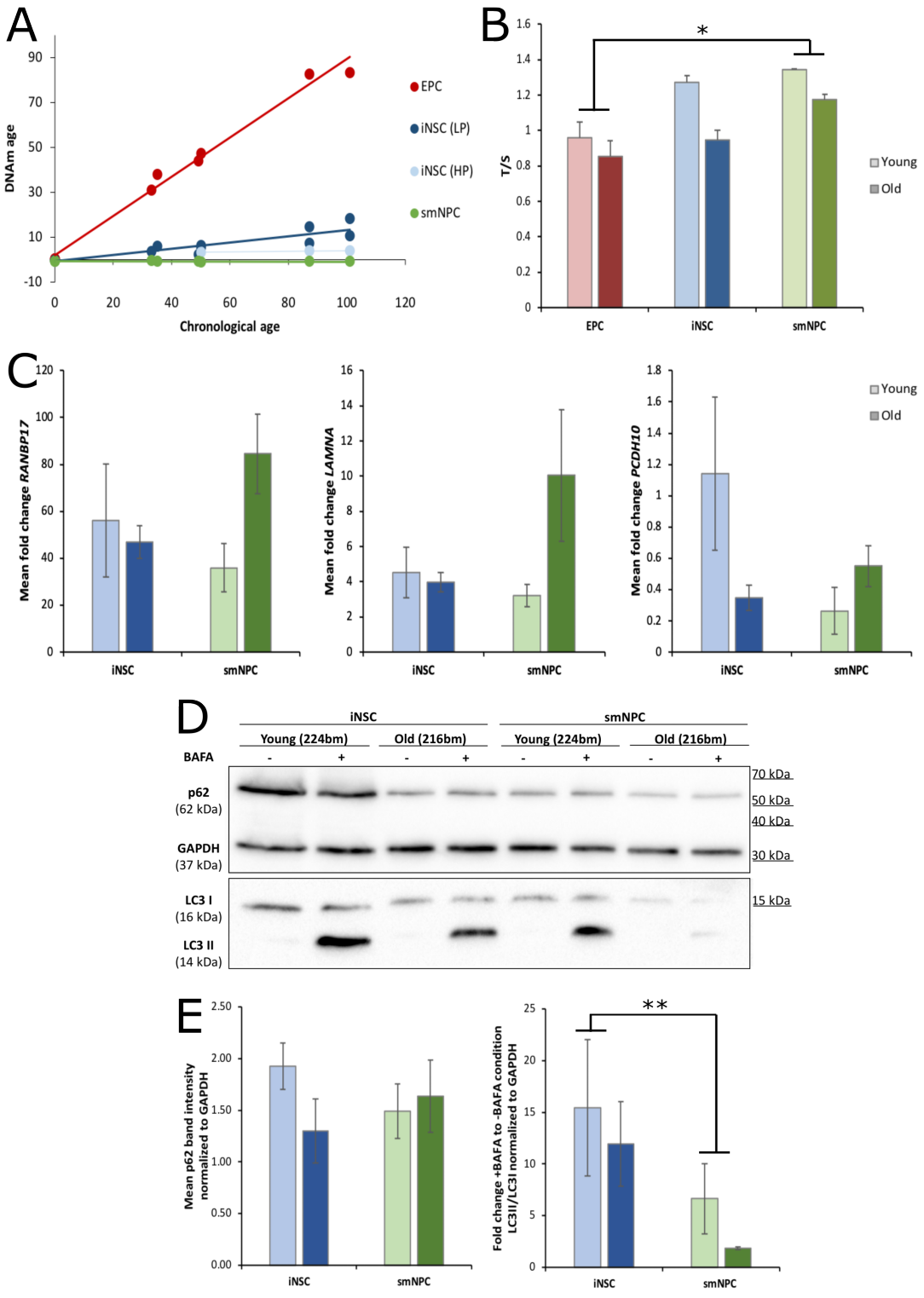

Figure 9: DNAm age, telomere lengths, expression of three pan-tissue, age-related genes and autophagy in iNSCs and smNPCs.
(A) DNAm age predictions based on Horvath's algorithm for EPCs, blood-derived iNSCs and iPSC-derived smNPCs of differentially aged donors. LP: low passage (P5-P6), HP: high passage (P20-P21). Results of Kendall's τ correlation analyses: EPCs: N = 9, $\tau = 0.957$, $p = 0.0005$; Adj. $R^2 = 0.985$, $p = 7.29 \times 10^{-8}$; smNPCs: (N = 9, $\tau = -0.203$, $p = 0.456$; Adj. $R^2 = -0.138$, $p = 0.869$; LP-iNSCs: N = 12, $\tau = 0.826$, $p = 0.0003$; Adj. $R^2 = 0.777$, $p = 9.29 \times 10^{-5}$; HP-iNSCs: N = 3, $\tau = 1$, $p = 0.333$; Adj. $R^2 = 0.896$, $p = 0.147$. **(B)** QPCR-based determination of T/S ratios, being representative of relative telomere lengths. N = 3 per age group and cell type. Result of the Nemenyi Kruskal Wallis post-hoc test: EPCs vs. smNPCs: $p = 0.012$. **(C)** Expression levels of the three age-associated genes *RANBP17*, *LAMNA* and *PCDH10* as measured by qPCR. N = 6 with three independent replicates of two genotypes per age group. **(D)** Representative Western blot detecting p62, the LC3 isoforms I and II as well as the house-keeping protein GAPDH in iNSCs and smNPCs under ± BAFA treatment conditions. Due to the number of samples, each biological replicate was run on two separate gels, with one genotype of each age group per gel. **(E)** Results of Western blot quantification. N = 6 with three independent replicates of two genotypes per age group. Result of the Wilcoxon rank sum Kruskal Wallis post-hoc test: iNSCs vs. smNPCs: $p = 0.002$.

Furthermore, expression levels of the nuclear lamina matrix proteins LMNA and LMNC, as well as their associated protein LAP2α, were assessed in the isogenic sets of young and old donor-derived iNSCs and smNPCs on RNA (Figure 10 A) and protein level (Figure 10 B). For both age groups, *LMNA* expression was significantly increased in iNSCs as compared to their isogenic smNPCs. *LMNC* expression was significantly higher in young donor-derived iNSCs as compared to young donor-derived smNPCs, too. In addition, iNSCs generated from young donors exhibited significantly increased *LMNC* levels than iNSCs generated from old donors (Figure 10 A). Quantification of nuclear LMNA and LMNC (subsequently also called LMNA/C) immunofluorescence recapitulated the same trends observed on RNA levels: For both cell types, young donor-derived cells exhibited increased expression as compared to old donor-derived NSCs, and for both age groups, iNSCs expressed LMNA/C higher than isogenic smNPCs (Figure 10 B). Different from LMNA/C expression, *LAP2α* as well as the nuclear lamin *LMNB* were similarly expressed across all groups on RNA level (Figure 10 A). On protein level, LAP2α was slightly but significantly increased in young as compared to old donor-derived iNSCs, and old donor-derived smNPCs exhibited slightly higher expression levels than isogenic iNSCs (Figure 10 B).

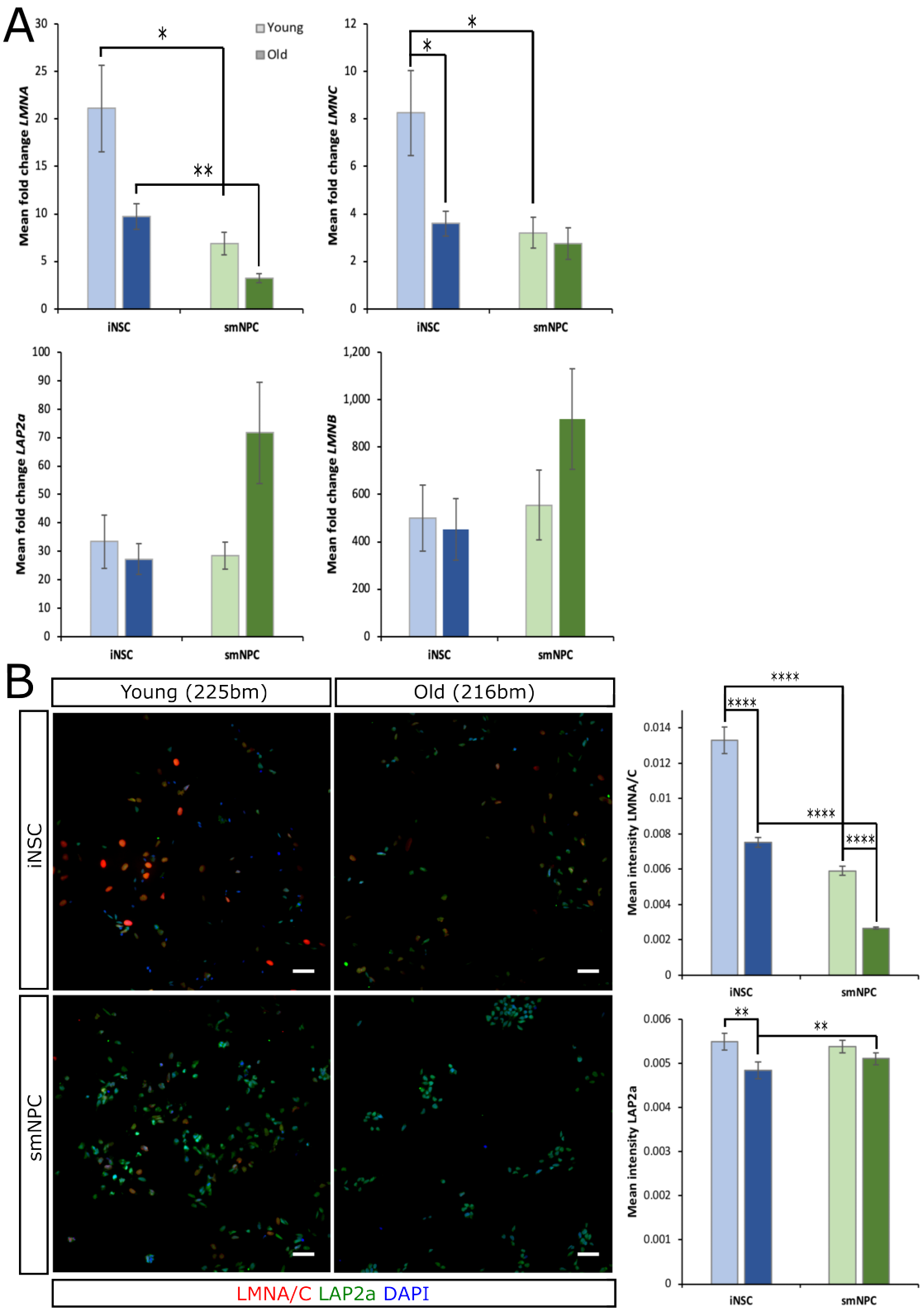

Figure 10: Expression of nuclear lamina-associated genes and proteins in young and old donor-derived iNSCs and smNPCs.
(A) QPCR-based profiling of *LMNA*, *LMNC*, *LAP2α* and *LMNB* expression. N = 6 with three independent replicates of two genotypes per age group. Results of the Wilcoxon rank sum Kruskal Wallis post-hoc test: *LMNA* young donor-derived iNSCs vs. smNPCs: $p = 0.03$; *LMNA* old donor-derived iNSCs vs. smNPCs: $p = 0.007$; *LMNC* young donor-derived iNSCs vs. smNPCs: $p = 0.03$; *LMNC* young vs. old donor-derived iNSCs: $p = 0.03$. **(B)** Left: Representative stainings for LMNA/C and LAP2a of iNSCs and smNPCs of one genotype per age group. Scale bars = 50 μm. Right: CellProfiler-based quantification of nuclear LMNA/C and LAP2a immunofluorescence intensity. N = 12 with two technical per three independent replicates of two genotypes per age group. Results of the Wilcoxon rank sum Kruskal Wallis post-hoc test: LMNA/C young vs. old donor-derived iNSCs: $p = 3.7 \times 10^{-8}$; LMNA/C young vs. old donor-derived smNPCs: $p < 2 \times 10^{-16}$; LMNA/C young donor-derived iNSCs vs. smNPCs: $p = 2.2 \times 10^{-12}$, LMNA/C old donor-derived iNSCs vs. smNPCs: $p < 2 \times 10^{-16}$; LAP2α young vs. old donor-derived iNSCs: $p = 0.007$; LAP2α old donor-derived iNSCs vs. smNPCs: $p = 0.008$.

Lastly, we analyzed the expression of senescence-associated genes and quantified DNA damage as well as mitochondrial ROS production (Figure 11). Specifically, qPCR-based profiling of two *CDKN2a* isoforms encoding for the senescence mediators $p16^{INK4A}$ and $p14^{ARF}$, as well as *CDKN1a* expression, encoding for p21, did not reveal differences between groups (Figure 11 A). DNA damage was visualized by staining for the DNA DSB marker γH2AX (Figure 11 B). Although quantification of immunofluorescence images revealed slight but statistically significant differences between groups, indicating that young donor-derived iNSCs possessed highest levels of DNA damage, these differences seemed biologically neglectable compared to the magnitude of difference elicited by treatment with etoposide, which binds topoisomerase II and thus prevents re-ligation of broken DNA strands (Montecucco *et al*., 2015). Finally, mitochondrial ROS production was assessed by MitoSOX staining and subsequent flow cytometry analysis, demonstrating no differences across groups (Figure 11 C).

Altogether, our data indicate that even old donor-derived iNSCs are epigenetically and cellularly rejuvenated after direct conversion, highly resembling iPSC-derived, embryonic stage-like smNPCs. This conclusion is further supported by data that were independently generated using a different collection of mid-age donors (N = 2-3; 32-49 years of age), for which the characterization of isogenic pairs of iNSCs and smNPCs yielded highly overlapping results. Specifically, within this donor collection, iNSCs and smNPCs only displayed significantly divergent expression levels of the three genes *LMNA*, *LMNC* and *PCDH10* (Supplementary Figure 1). Yet, within this set of cell lines, ROS levels were increased in iNSCs as compared to isogenic smNPCs (Supplementary Figure 2). Nevertheless, none of the other cellular aging assays performed yielded statistically significant differences between directly converted and iPSC-derived NSCs (Supplementary Figure 1 and Supplementary Figure 2). These data were partially published in Sheng, C., Jungverdorben, J., Wiethoff, H., Lin, Q., Flitsch, L.J., Eckert, D., Hebisch, M., Fischer, J., Kesavan, J., Weykopf, B., Schneider, L.; Holtkamp, D.; Beck, H.; Till, A.; Wüllner, U.; Ziller, M.J.; Wagner, W.; Peitz, M. & Brüstle, O. (2018) 'A stably self-renewing adult blood-derived induced neural stem cell exhibiting patternability and epigenetic rejuvenation', *Nature Communications*, 9(1), p. 4047 (Sheng *et al*., 2018), and corroborate the notion that both cell types seem to reset cellular aging signatures in the course of cell programming.

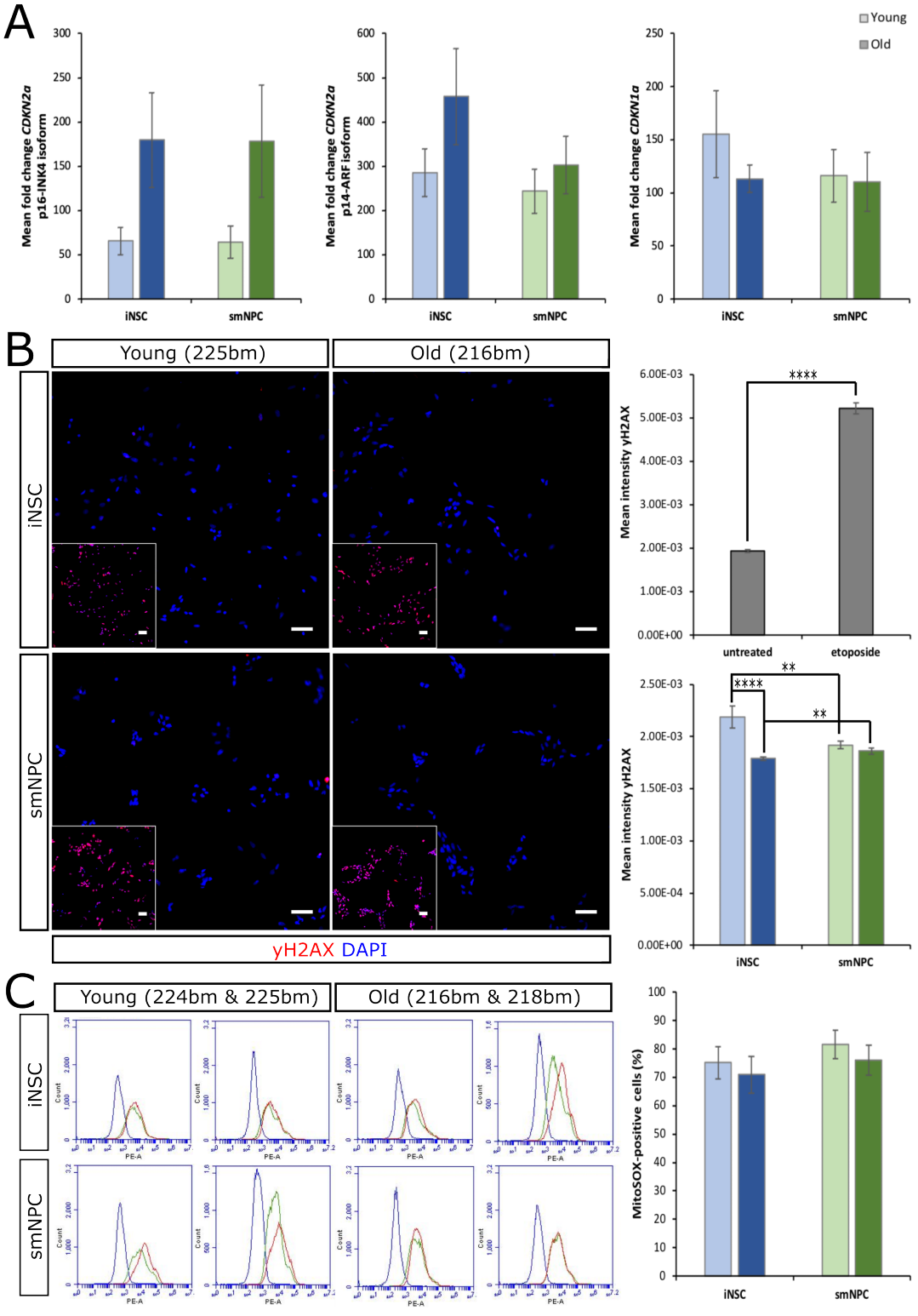

Figure 11: Expression of apoptosis- and senescence-associated genes, DNA damage and mitochondrial ROS production in directly converted and iPSC-derived NSCs of young and old donors.
(A) QPCR-based profiling of two *CDKN2a* isoforms encoding for $p16^{INK4A}$ and $p14^{ARF}$ as well as *CDKN1a* encoding for p21. N = 6 with three independent replicates of two genotypes per age group. **(B)** Left: Representative stainings for γH2AX of iNSCs and smNPCs of one genotype per age group. Inserts on the lower left show the etoposide-treated positive control of each condition. Right: CellProfiler-based quantification of nuclear γH2AX immunofluorescence intensity. Scale bars = 50 μm. N = 6 with three independent replicates of two genotypes per age group and treatment condition. Result of the Wilcoxon signed-rank test with continuity correction for treatment condition: $p < 2.2 \times 10^{-16}$. Results of the Wilcoxon rank sum Kruskal Wallis post-hoc test for differences across groups: Young vs. old donor-derived iNSCs: $p < 8.8 \times 10^{-7}$; young donor-derived iNSCs vs. smNPCs: $p = 0.006$; old donor-derived iNSCs vs. smNPCs: $p = 0.0099$. **(C)** Flow cytometry analysis after MitoSOX staining. Left: Representative flow cytometry raw data (acquired using Accuri C6 Plus flow cytometer) depicting unstained control (blue), MitoSOX-stained sample (green) and FCCP-treated positive control (red) after gating out cell debris. Right: Quantification depicting the percentage of MitoSOX-positive cells.

3.1.3. Continuous proliferation does not represent a main driver of the protracted epigenetic rejuvenation elicited by blood-to-NSC conversion.

In order to investigate the dynamic of epigenetic rejuvenation upon SeV-SOX2 and SeV-cMYC expression, we next collected DNA samples at early time points of the conversion process, namely days 0, 14 and 26 of conversion, as well as at the QC time points at low and high passages (equaling around 45 and 125 days of conversion), and subsequently predicted the DNAm ages of all samples (Figure 12 A). Our analysis revealed that the dynamic of rejuvenation was best fit using an exponential model, although the slope of DNAm age loss slightly varied between individuals. Interestingly, in contrast to iPSC reprogramming in which the induced epigenetic age reset occurs within a time span of approximately 20 days (Olova *et al*., 2019), our data indicated that it took about 50 days of iNSC conversion until the majority of age-related epigenetic signatures were remodeled. This prolonged time window seemed practically suitable for system manipulations aiming at modifying and/or inhibiting the processes driving the observed DNAm age reset, prompting us to investigate potential mechanisms within our cell conversion paradigm.

Considering that epigenetic rejuvenation is induced upon reprogramming of somatic cells into self-renewing iPSCs (Lo Sardo *et al*., 2017) and direct conversion into proliferating iNSCs (Figure 9 A) but not transdifferentiation into post-mitotic neurons (Huh *et al*., 2016), we hypothesized that this phenomenon might be driven by the persistent mitotic activity of stem cells. To address this theory and yield a sufficient difference in epigenetic ages to decipher potential effects of proliferation on the slope of epigenetic rejuvenation, manipulation experiments were performed using EPCs derived from three aged donors (81-86 years of age). First, we infected EPC-derived iNSCs at day 7 of conversion with lentiviruses encoding for rtTA and a TRE-regulated NGN2 expression cassette (Figure 12 B). After 14 additional days of expansion, which were necessary to yield a sufficient number of cells to serve all experimental read-outs, a fraction of the infected cells was kept in proliferation, while others were subjected to DOX induction under differentiation-promoting conditions. Although NGN2 overexpression alone already represents a forceful driver of neurogenesis, Ara-C treatment was performed at day 5 of differentiation in order to ensure that cells still being proliferating at this time point were eliminated from the differentiating culture. At day 42 of conversion (*i.e*., after 3 weeks of differentiation), immunocytochemical analysis confirmed that cultures forced to differentiate by NGN2 overexpression indeed consisted of mostly TUBB3-positive neurons and only few GFAP-positive astrocytes (Figure 12 C). Despite this high enrichment for post-mitotic neurons, the DNAm ages of NGN2-overexpressing, differentiated cultures did not significantly differ from iNSCs that were classically expanded as proliferating cultures until day 42 of conversion (Figure 12 D).

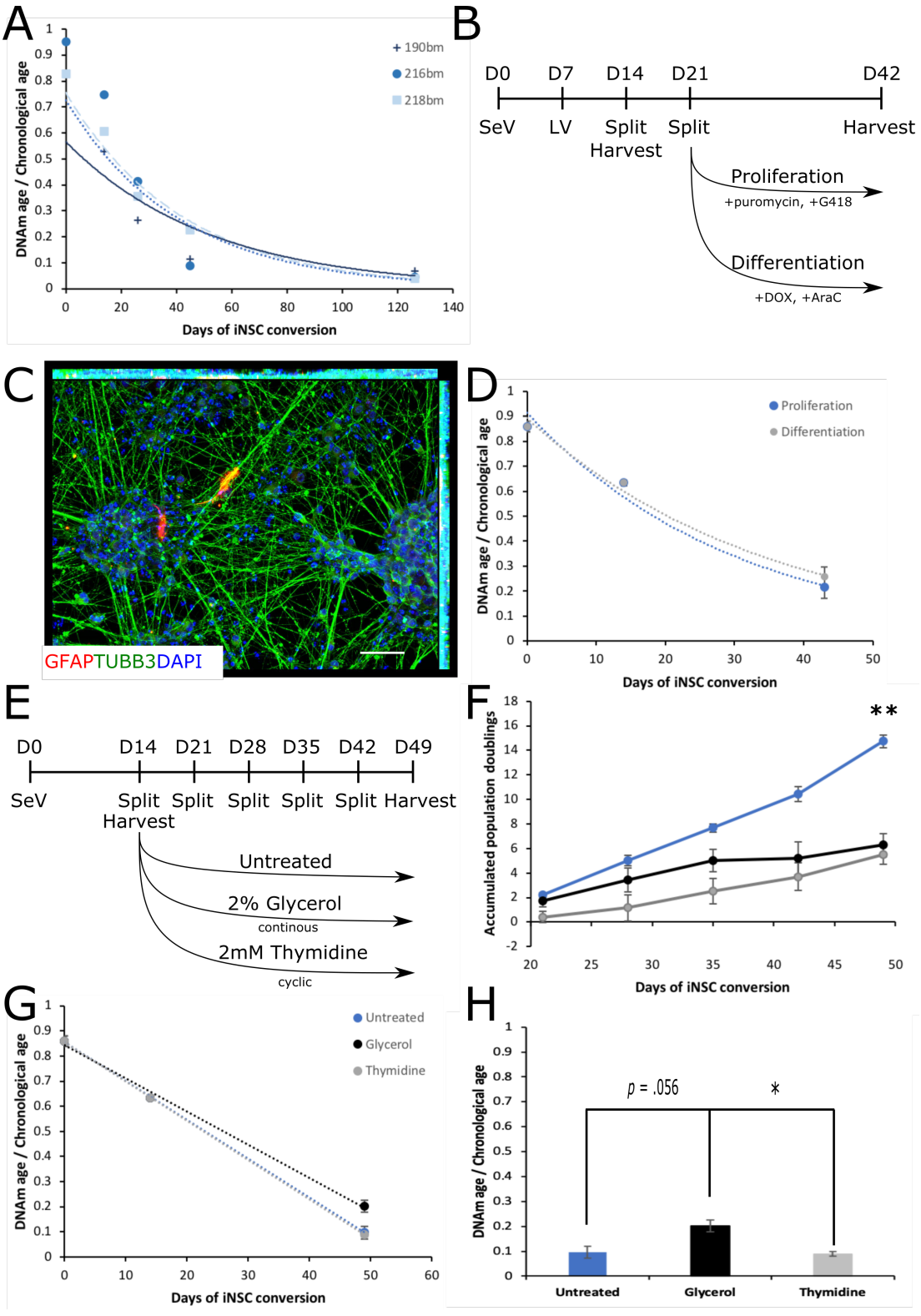

Figure 12: Effects of stem cell proliferation on DNAm age dynamics in the early phase of iNSC conversion.
(A) Time course analysis of DNAm ages upon blood-to-iNSC conversion using three genetically distinct old donor-derived cell preparations. 190bm: $R^2 = 0.78$; 216bm: $R^2 = 0.81$; 218bm: $R^2 = 0.99$. **(B)** Schematic representing the experimental setup of inducing cell cycle exit by forcing neurogenic differentiation during the early phase of iNSC conversion. **(C)** Representative image showing that differentiation cultures mostly consisted of TUBB3-positive neurons and few GFAP-positive astrocytes. N = 3 donors. Scale bar = 50 μm. **(D)** Graph showing predicted DNAm ages, normalized to the chronological age of the respective donor, after three-week-long NGN2-driven differentiation and proliferating control cultures of early stage iNSCs. N = 3 donors. **(E)** Schematic representing the experimental setup of inhibiting proliferation by glycerol or thymidine treatment during the early phase of iNSC conversion. **(F)** Graph plotting accumulated populations doublings over the 5-week-long period of proliferation inhibitor treatment. N = 3 donors. Results of the Tukey ANOVA post-hoc test: Untreated vs. glycerol: $p = 0.002$; glycerol vs. thymidine: $p = 0.001$. **(G)** Graph depicting DNAm ages, normalized to the chronological age of the respective donor, for untreated, glycerol-treated and thymidine-treated iNSCs. N = 3 donors. **(H)** Bar graph representation of the DNAm ages measured at day 49 of iNSC conversion. N = 3 donors. Results of the Tukey ANOVA post-hoc test: Untreated vs. glycerol: $p = 0.056$; glycerol vs. thymidine: $p = 0.044$.

Appreciating that the experimental method of NGN2 overexpression did not only abrogate proliferation, but also induced another cell fate shift from proliferating iNSCs to post-mitotic neurons, we performed another set of experiments aiming at slowing down proliferation while maintaining an NSC phenotype. To this end, we treated iNSCs with glycerol or thymidine starting from day 14 of conversion. More specifically, glycerol – which is known to reduce proliferation of various cell types (Wiebe & Dinsdale, 1991) but at the same time can also affect cytoskeleton dynamics and cell adhesion (Dinsdale *et al*., 1992) – was applied daily except for days when cell lines were replated. Thymidine – which is commonly used as a cell cycle-synchronizing agent, since it arrests cells in the G1/S phase of the cell cycle (Yiangou *et al*., 2019) – was applied cyclically once a week for 24 to 48 hours. Population doublings were quantified weekly for untreated, glycerol- and thymidine-treated iNSC cultures up until day 49 of conversion, when cells were harvested for DNAm age prediction (Figure 12 E). Despite their different modes of action, both treatments resulted in significantly reduced accumulated population doublings at day 49 of conversion (Figure 12 F), while only glycerol treatment seemed to slightly but statistically significantly affect epigenetic rejuvenation (Figure 12 G, H).

Attempting to gain mechanistic insight into the process of epigenetic rejuvenation, we next performed global DMP and DMR analysis, comparing our DNAm data in the time course of conversion as well as in the presence and absence of cell cycle-manipulating conditions. After raw data filtering, in total 725,633 probes were compared between the thirty-six samples of seven distinct groups. Comparing DNAm of the original EPC starter cells with iNSCs at days 14 of conversion, 131,829 most variable positions (MVPs) and 479 DMRs were detected. Samples collected at days 14 and 26 of conversion displayed 73,913 MVPs and 481 DMRs. DNAm in iNSCs at day 26 and in normally cultivated iNSCs collected between days 42 and 49 of conversion (summarized under the term 'proliferating iNSCs') differed in 11,804 positions and 480 regions. Interestingly, yet in line with our observation with mostly unaltered DNAm ages upon manipulation of proliferation, all other comparisons only yielded comparably few, if any MVPs: (i) Proliferating iNSCs versus NGN2-overexpressing, differentiating iNSCs: 1,405 MVPs; (ii) Proliferating iNSCs versus glycerin-treated iNSCs: 27 MVPs; (iii) Proliferating iNSCs versus thymidine-treated iNSCs: 1 MVP; (iv) Glycerin-treated iNSCs versus thymidine-treated iNSCs: No MVP. Accordingly, while EPCs and day 14 iNSCs form very distinct clusters in the heatmap and the multidimensional scaling (MDS) plot provided in Figure 13 A and B, respectively, day 26 iNSCs and iNSC differentiation cultures as well as later-stage untreated, glycerin- and thymidine-treated, proliferating iNSCs intermingle.

Subsequent gene set enrichment analysis identified 543 and 639 GO terms with a false discovery rate (FDR) < 0.05 for EPCs versus day 14 and day 14 versus day 26 iNSCs, respectively. While the comparison of proliferating and differentiating iNSCs still yielded 6 significant GOs, which were associated to the acquisition of a new cell fate, as they contained terms such as negative regulation of cell differentiation and negative regulation of developmental process (data not shown), all other contrasts did not entail enriched GOs. Assuming that epigenetic changes occurring from EPC stage to day 14 and continuing from day 14 to day 26 of iNSC conversion could potentially contribute to the observed protracted epigenetic rejuvenation, we finally focused on the 427 GOs shared by both contrasts (Figure 13 C). Different from our hypothesis, the treemap plot provided in Figure 13 D indicates that these common GOs seemed to be governed by terms attributable to molecular and cellular changes occurring in the process of cell fate conversion rather than showing any obvious enrichment for age-associated processes.

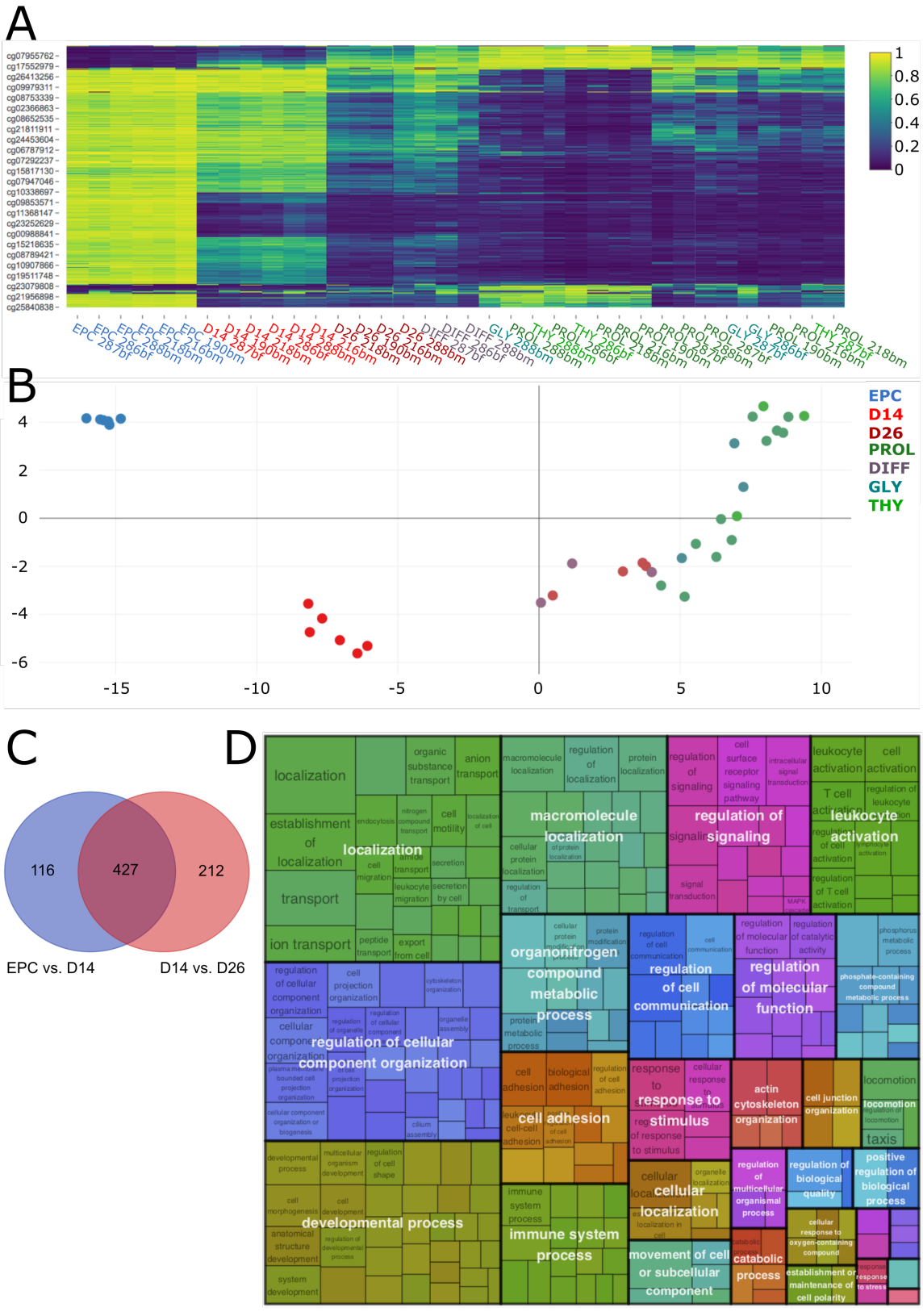

Figure 13: Analysis of global DNAm changes in the process of iNSC conversion.
(A) Heatmap showing the relative methylation values at the 1,000 most variable CpGs across all conditions. PROL: Proliferating iNSCs; DIFF: NGN2-overexpressing iNSC differentiation cultures; GLY: Glycerol-treated iNSCs; THY: Thymidine-treated iNSCs. **(B)** MDS plot visualizing the similarity between samples of distinct groups based on the 1,000 MVPs selected from a singular value decomposition of the data. PROL: Proliferating iNSCs; DIFF: NGN2-overexpressing iNSC differentiation cultures; GLY: Glycerol-treated iNSCs; THY: Thymidine-treated iNSCs. **(C)** Venn diagram representing the number of unique and shared GOs between the contrasts EPC versus D14 and D14 versus D26 iNSCs. **(D)** Treemap visualization of hierarchical clusters. Terms are grouped and colored based on their parent and the terms' space sizes are proportional to their minus log10-transformed FDR.

Since DNAm age in old donor-derived cells eroded with continued time of iNSC conversion and cultivation (see Figure 9 A and Figure 12 A), we finally performed bulk RNA sequencing analysis to profile transcriptomic changes that occurred after blood-derived cells morphologically adopted an NSC-like identity. Specifically, we compared old-donor derived iNSCs at day 14 of conversion with iNSCs at low passage, as well as low passage with high passage iNSCs. Moreover, considering that epigenetic rejuvenation is relevant in the context of old but not young donor EPC-to-iNSC conversion, we performed contrasts between these two entities at day 14 of conversion and low passage (compare Figure 9 A). Following this line of thought, we further included the comparison of old donor-derived iNSCs and isogenic iPSC-derived smNPCs at low passage in our analysis. Interestingly, principal component analysis (PCA) demonstrated that the included samples neither clustered per genotype, nor clearly separated according to their group assignment (Figure 14 A), thus, appearing transcriptionally overall more similar than what was expected based on our DNAm data. Nevertheless, we continued to compare gene expression between groups showing differences in epigenetic age. Therefore, we identified DEGs for the five comparisons described, finding that not a single DEG was shared between all contrasts (Figure 14 B). Thus, we subsequently concentrated on the two comparisons entailing the biggest difference in DNAm age, namely old donor-derived iNSCs at day 14 of conversion versus low passage (148 DEGs) and day 14 samples of old versus young donor-derived iNSCs (619 DEGs). Although these two comparisons also only shared as little as 5 common DEGs (namely uncharacterized *LOC114841035*, *PDLIM3*, *RBFOX1, HES5* and *STAT3*; Figure 14 B), plotting log-transformed gene counts of all samples for the top fifty DEGs of each comparison did not yield cleanly segregated sample clusters (Figure 14 C).

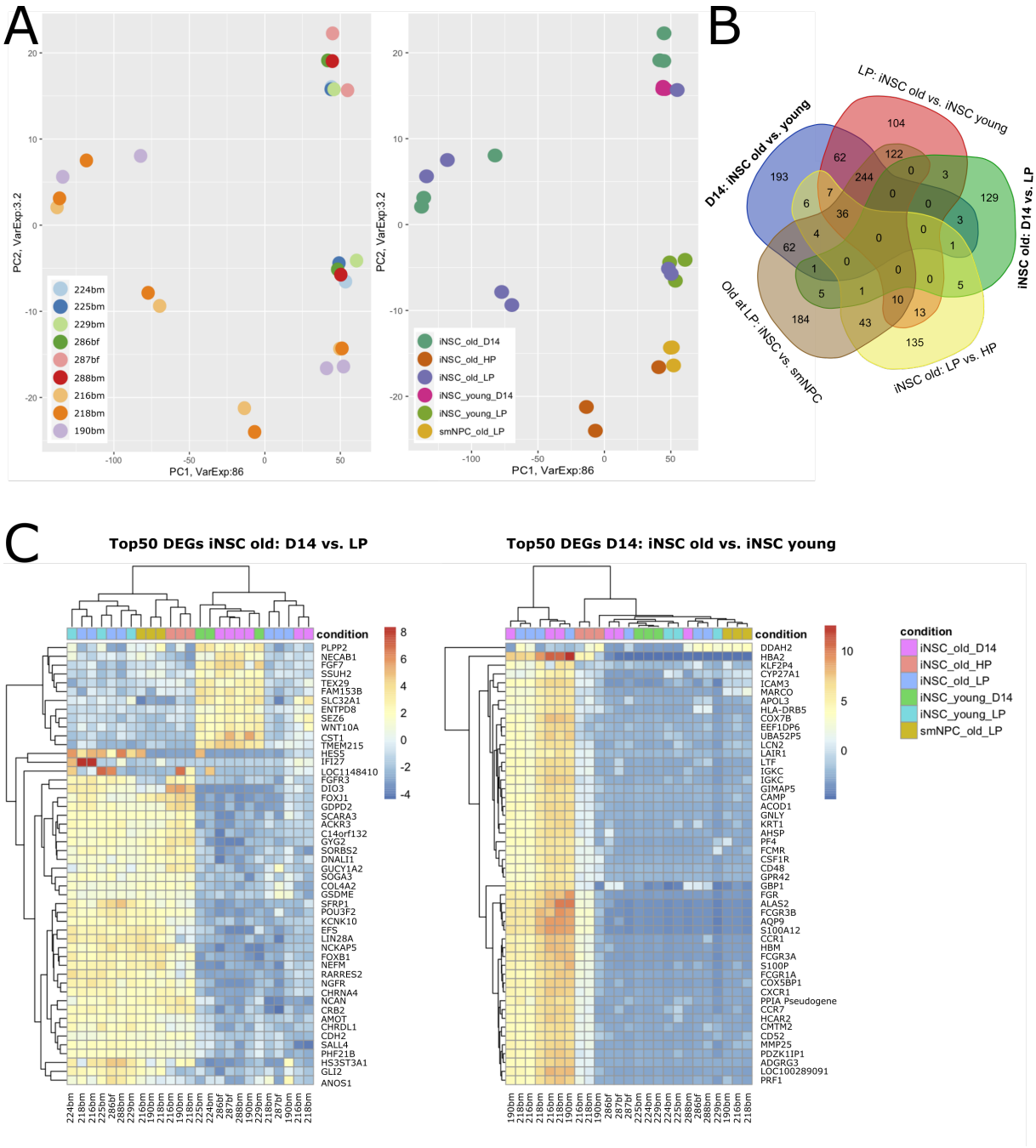

Figure 14: RNA sequencing of iNSCs derived from differentially aged donors.
(A) Transcriptomic data of iNSCs at distinct stages of conversion were compared with each other, as well as to low passage, old donor-derived smNPCs. PCA plot coding samples per genotype (left) or group (right). LP: Low passage (P5-P6); HP: High passage (P20-P21). **(B)** Venn diagram representing the number of DEGs unique for and shared between all performed contrasts. **(C)** Heat maps depicting log-transformed gene counts of all samples for the top 50 DEGs between old donor-derived iNSCs at D14 and low passage (left) as well as D14 samples of old and young donor-derived iNSCs (right). Gene abbreviations are not included in the abbreviations list.

Congruent with the little overlap in differential expression that was observed between old donor-derived iNSCs at different stages of iNSC conversion (*i.e.*, day 14 versus low passage) and old versus young donor-derived iNSCs early in the conversion process (*i.e.*, at day 14 of conversion), identified DEGs were enriched in very different GOs (Figure 15 A). While – in line with our results on DNAm changes upon iNSC conversion – transcriptomic differences between day 14 and low passage old donor-derived iNSCs were enriched in terms that seemed to be predominantly associated with cell fate transitioning and the progressive acquisition of an NSC identity (Figure

15 A left), iNSCs converted from old or young donor EPCs most pronouncedly differed in immune-related terms 14 days after SeV-mediated overexpression of the TFs SOX2 and cMYC (Figure 15 A right). Concentrating on the few similarities of these two contrasts, it is interesting to note that one of the five common DEGs was *STAT3*, representing a TF that is a central part of the protein interaction network around the transdifferentiation-mediating TFs (Figure 15 B). Moreover, JAK-STAT signaling is induced by LIF (see review by Onishi & Zandstra, 2015), a key component of our iNSC conversion and expansion medium. Although variable, *STAT3* normalized gene counts were overall elevated in old donor-derived iNSCs at day 14 of conversion only (Figure 15 C).

In sum, the experiments we performed in order to shed light on the mechanisms governing rejuvenation during iNSC conversion demonstrate that continuous NSC proliferation *per se* does not seem to be a relevant driver of the loss of DNAm age within our paradigm. Although our data do not yet allow us to identify which differentially regulated pathways might account for the observed age reset, they reveal that SOX2 and cMYC overexpression in EPCs results in substantial epigenetic changes associated to the acquisition of a new cell fate even beyond day 14 of iNSC transdifferentiation. Transcriptomic changes emerging after day 14 of conversion seemed comparably mild though. In addition, these changes were mostly non-overlapping with presumably age-associated differences in gene expression, which were identified by comparing transcriptomes of old and young-donor derived iNSCs at day 14 of conversion, when the epigenetic reset of aging signatures is still fully in process. Yet, within these comparisons, we identified the SOX2/cMYC interaction partner *STAT3* as one of the few shared DEGs, that might be an interesting candidate for future mechanistic studies.

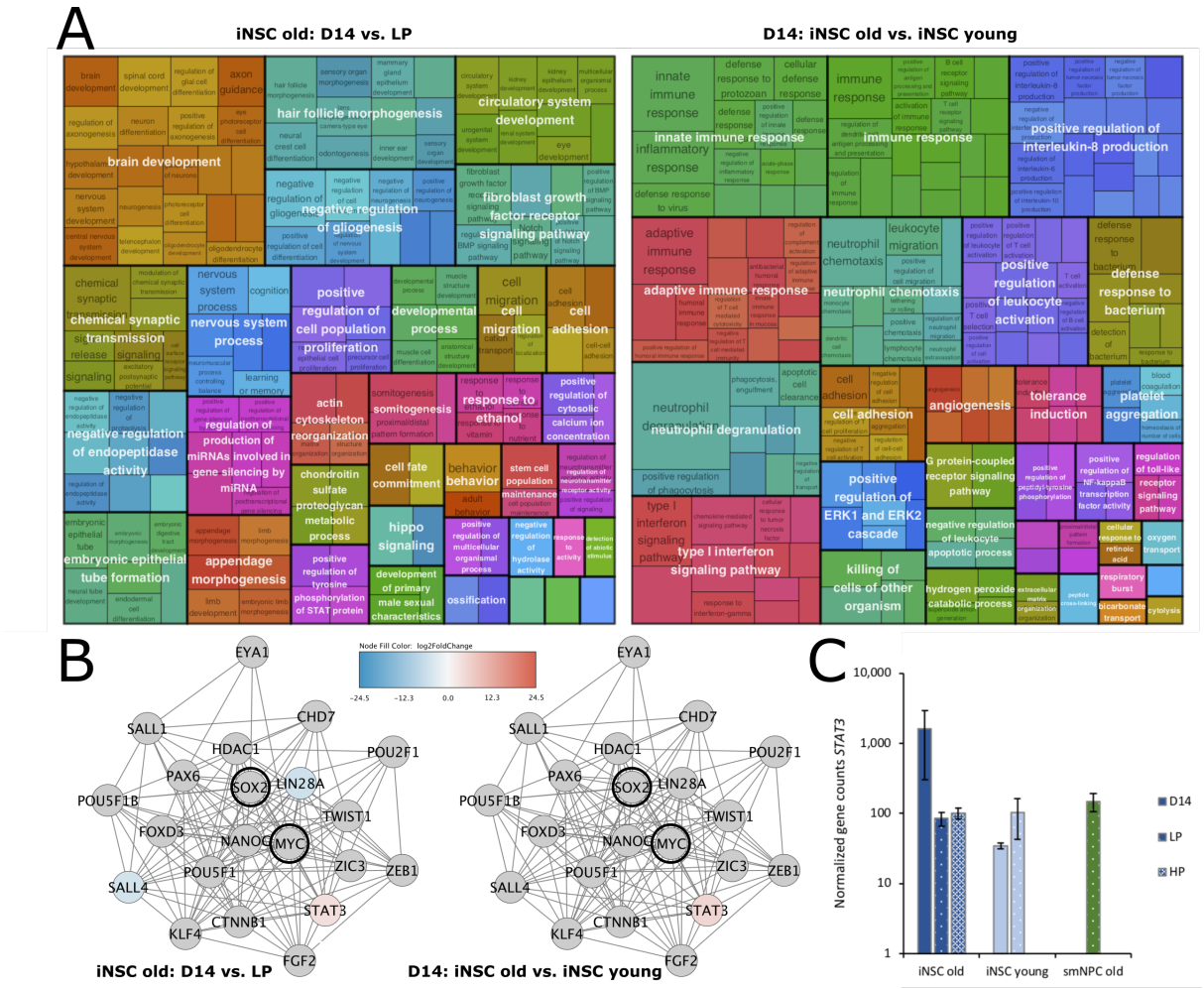

Figure 15: GO enrichment analysis and the assessment of DEGs in the context of SOX2's STRING interaction network.
(A) Treemap visualization of hierarchical clusters for GOs enriched in DEGs in old donor-derived iNSCs at D14 versus low passage (P5-P6; left) and D14 samples of old versus young donor-derived iNSCs (right). Terms are grouped and colored based on their parent and the terms' space sizes are proportional to their minus log10-transformed FDR. **(B)** Network visualization of the twenty strongest SOX2 interaction partners. Node filling encode log2 fold changes of the performed differential expression analyses. Grey node color indicates that the respective gene was not included in the list of DEGs. Black circles highlight the conversion-mediating TFs SOX2 and MYC. Gene abbreviations are not included in the abbreviations list. **(C)** Bar graph depicting normalized *STAT3* gene counts for all conditions subjected to RNA sequencing analysis. LP: Low passage (P5-P6); HP: High passage (P20-P21).

Finally, trying to address the role of the TFs SOX2 and cMYC in a system that could allow us to uncouple the effect of these two TFs on DNAm age from their effect on cell fate, we next conducted a preliminary experiment (N = 1) overexpressing these TFs alone or in combination in proliferating fibroblasts cultured in fibroblast medium (Figure 16 A). As an additional control and following up on our proliferation-manipulating experiments in iNSCs, one experimental condition comprised uninfected fibroblasts treated with glycerol. Unsurprisingly in light of published findings (Winiecka-Klimek *et al.*, 2015; Daekee *et al.*, 2019), 49-day-long SeV-mediated overexpression of SOX2 and/or cMYC at MOI = 5 did not suffice to convert human dermal fibroblasts into iNSCs. Yet, SeV-mediated TF overexpression also did not seem to impact the cells' DNAm ages (Figure 16 B). For all conditions except fibroblasts infected with SeV-SOX2, DNAm ages even tended to slightly but steadily increase over the cultivation period of 49 days. Notably, however, although SeV infection seemed to indeed increase the expression of the respective TFs in fibroblasts, total levels of *SOX2* and *cMYC* were still lower than those of low passage iNSCs (Figure 16 C). Although preliminary, the results of this experiment could suggest that SOX2 and/or

cMYC overexpression in fibroblasts does not induce a comparable epigenetic age reset in the absence of a transdifferentiation event, prompting the need for further studies addressing the relationship between the remodeling of cell fate and aging signatures in greater detail.

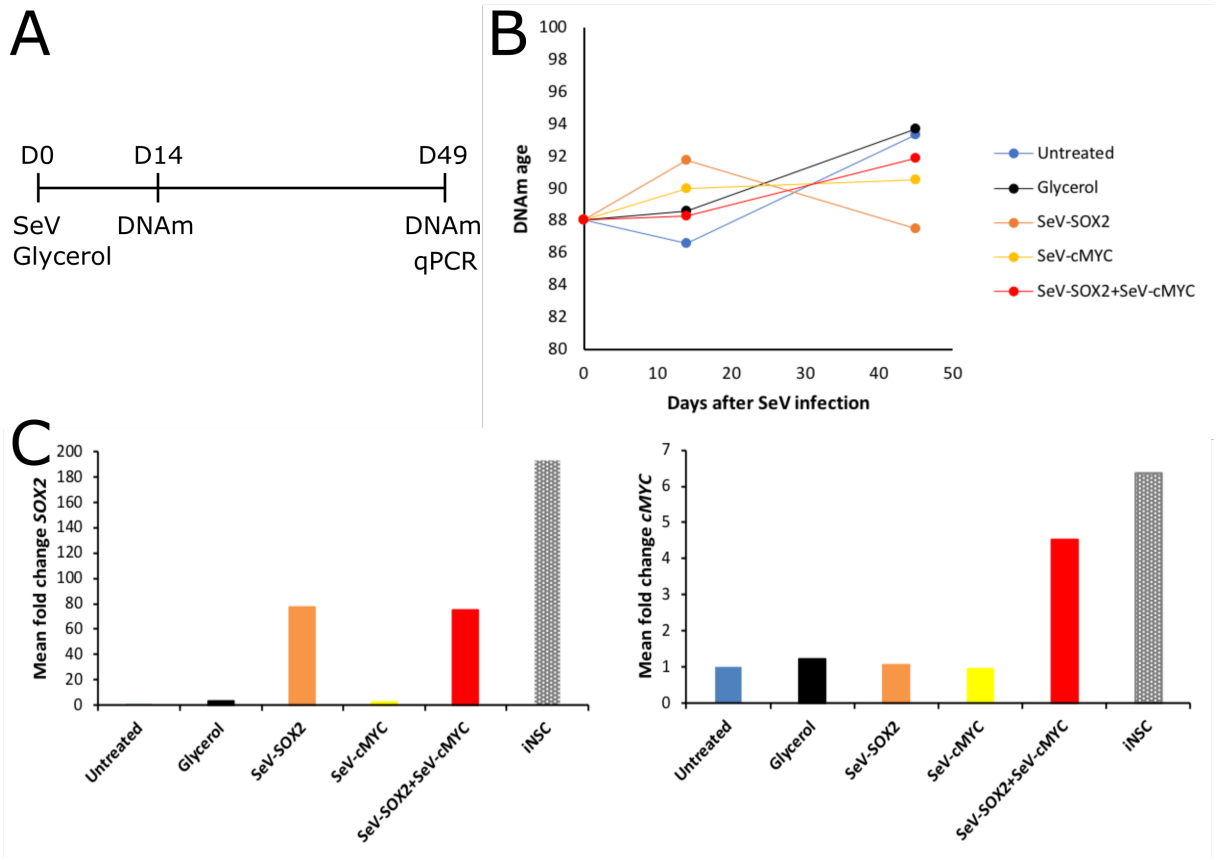

Figure 16: Impact of SeV-mediated overexpression of SOX2 and/or cMYC on DNAm age signatures in fibroblasts.
(A) Schematic representing the experimental setup of overexpressing the TFs SOX2 and/or cMYC in proliferating fibroblasts. **(B)** DNAm age prediction of untreated and glycerol-treated, as well as SeV-SOX2 and/or SeV-cMYC infected fibroblasts. N = 1. **(C)** Totals expression levels of *SOX2* and/or *cMYC* in differentially treated fibroblasts and blood-derived iNSCs as measured by qPCR. N = 1; depicted is the mean of three technical replicates.

3.2. Blood-derived iNSCs are capable of synaptic integration after transplantation into the adult mouse brain.

3.2.1. INSCs survive grafting into the CNS of adult mice and differentiate *in vivo* into neurons and glial cells.

Considering the highly rejuvenated cellular state of iNSCs, we next aimed at investigating their suitability for neuroregenerative approaches in greater depth. First, we grafted these cells into the mouse hippocampus. Immunohistochemical assessment 10 weeks post transplantation demonstrated robust cell survival after stereotaxic injection, and revealed that iNSCs-derived cells, being immunopositive for the human-specific Stem121 antibody that stains a cytoplasmic protein, readily populated the upper blade of the mouse dentate gyrus (Figure 17 A). In the hippocampus, iNSC differentiation was clearly biased toward a neuronal phenotype, as most human cells stained positive for the neuronal marker MAP2 using a human-specific antibody, while only few GFAP-positive astrocytes were double-positive for the human-specific anti-GFAP antibody Stem123 (Figure 17 B). Different

from what our lab has previously reported for striatal transplants (Sheng *et al*., 2018), we could not detect any evidence of oligodendrogenesis from iNSCs grafted into the mouse hippocampus, as judged by the absence of OLIG2- or NG2-positive human cells (data not shown). Still, these data collectively demonstrate that iNSCs not only survive transplantation into the adult mouse striatum but also the murine hippocampus, giving rise to neurons as well as glial cells upon *in vivo* maturation.

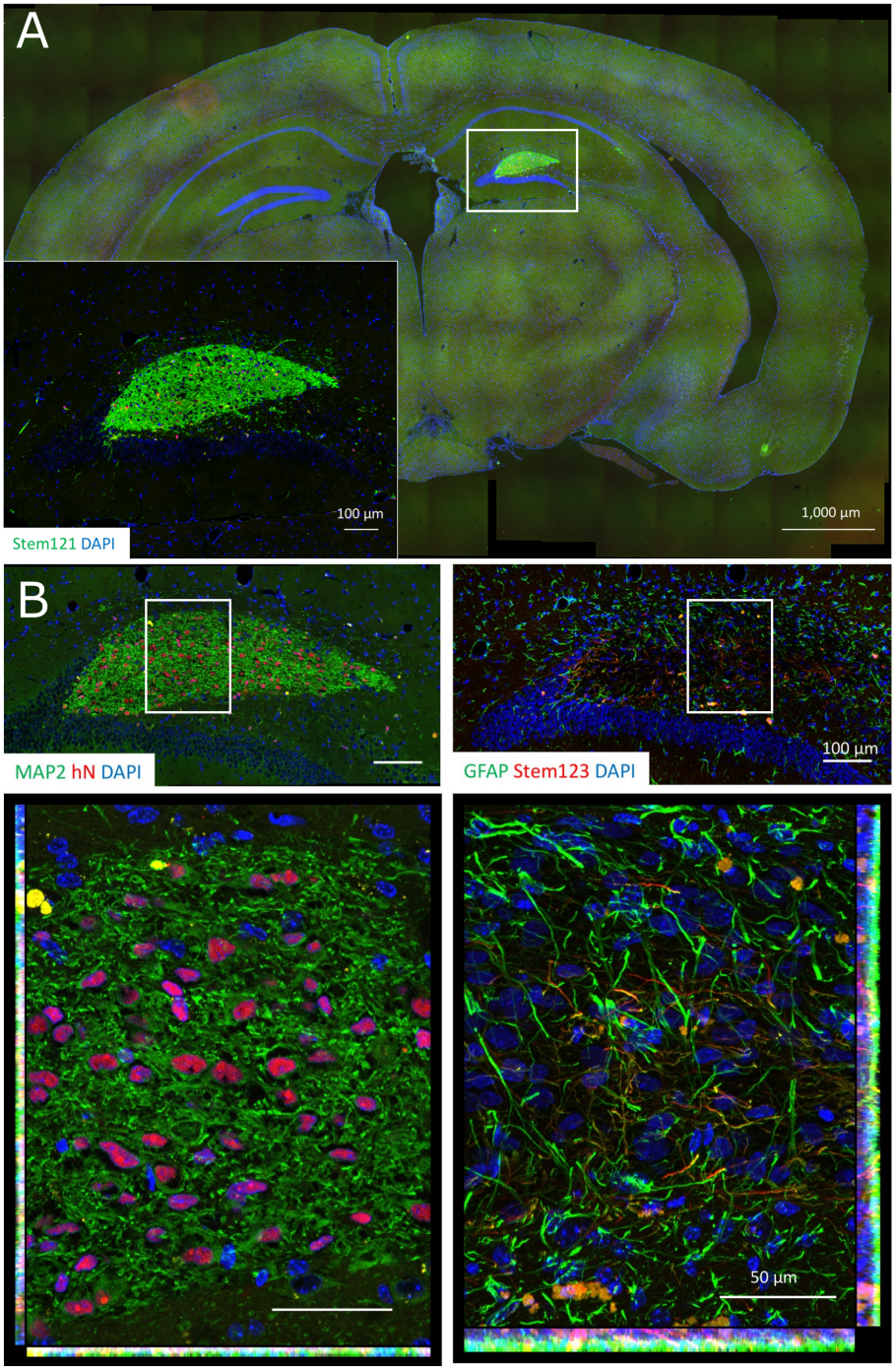

Figure 17: Immunofluorescence analysis of iNSC grafts after transplantation into the adult mouse hippocampus.
(A) Mouse brain slice stained for the human-specific cytoplasm marker Stem121 10 weeks after iNSC transplantation. Insert shows the hippocampal area (white rectangle) in greater resolution. N = 3 animals. Scale bars as indicated within the pictures. **(B)** In the mouse hippocampus, transplanted iNSCs predominantly differentiated into MAP2-positive neurons and few GFAP-positive astrocytes, staining positive for the human-specific markers hN and Stem123, respectively. Lower panels show close-ups of the central graft area (white rectangle). N = 3 animals. Scale bars as indicated: Upper panels: Scale bars = 100 μm, Lower panels: Scale bars = 50 μm.

3.2.2. Mouse neurons might synaptically connect to human iNSC xenografts.

We further aimed at assessing the capacity of blood-derived iNSCs to functionally integrate into a pre-existing host neuronal circuitry. To investigate the synaptic connectivity between the mouse brain and human iNSC-derived grafts, we employed a pRABV-based monosynaptic tracing system, which our laboratory had previously used to analyze the synaptic integration of iPSC-derived neural transplants (Doerr *et al*., 2017). In short, this system is based on the transplantation of genetically altered NSCs, which are marked by RFP expression and engineered to express a tracing cassette comprising the receptor and glycoprotein relevant for the acceptance and synaptic transmission of pRABV, respectively. After prolonged *in vivo* maturation of 10, 12, 16 or 24 weeks, human grafts were transduced by stereotaxic injection of a GFP-encoding pRABV. Mice were sacrificed by perfusion 10 days after virus injection. Brains were dehydrated and cleared before whole-brain LSFM was performed. Targeting the hippocampus as well as the striatum as transplantation sites, we assessed iNSC grafts at different time points after transplantation. Interestingly, we noticed that striatal grafts seemed to grow over time, whereas hippocampal graft volumes displayed a tendency to decrease with prolonged *in vivo* maturation (Figure 18 A). While it would be interesting to study the dynamic of graft growth in different brain regions in future experiments, we here instead focused on single GFP-positive cells outside the graft core, which were identified by LSFM in all conditions analyzed. Notably, these cells displayed highly ramified neuronal morphologies that were typically not observed in iNSC grafts, suggesting that these GFP-positive cells represented murine host neurons (Figure 18 B).

Importantly though, as a technical control for the pRABV-based monosynaptic tracing, we additionally transplanted four mice (N = 2 per transplantation site) with unlabeled wild-type iNSCs, which were not engineered to express the relevant pRABV system components. Control mice received stereotaxic injections of pRABV-GFP 16 weeks post transplantation. In three out of four of these animals, LSFM revealed the presence of GFP-positive cells (N = 6-29 cells/brain), being located within the target area as well as distant to the injection site (data not shown). The results of this control experiment, thus, indicate that some RABV particles might have escaped pseudotyping, being able to transduce cells independently of synaptic transmission.

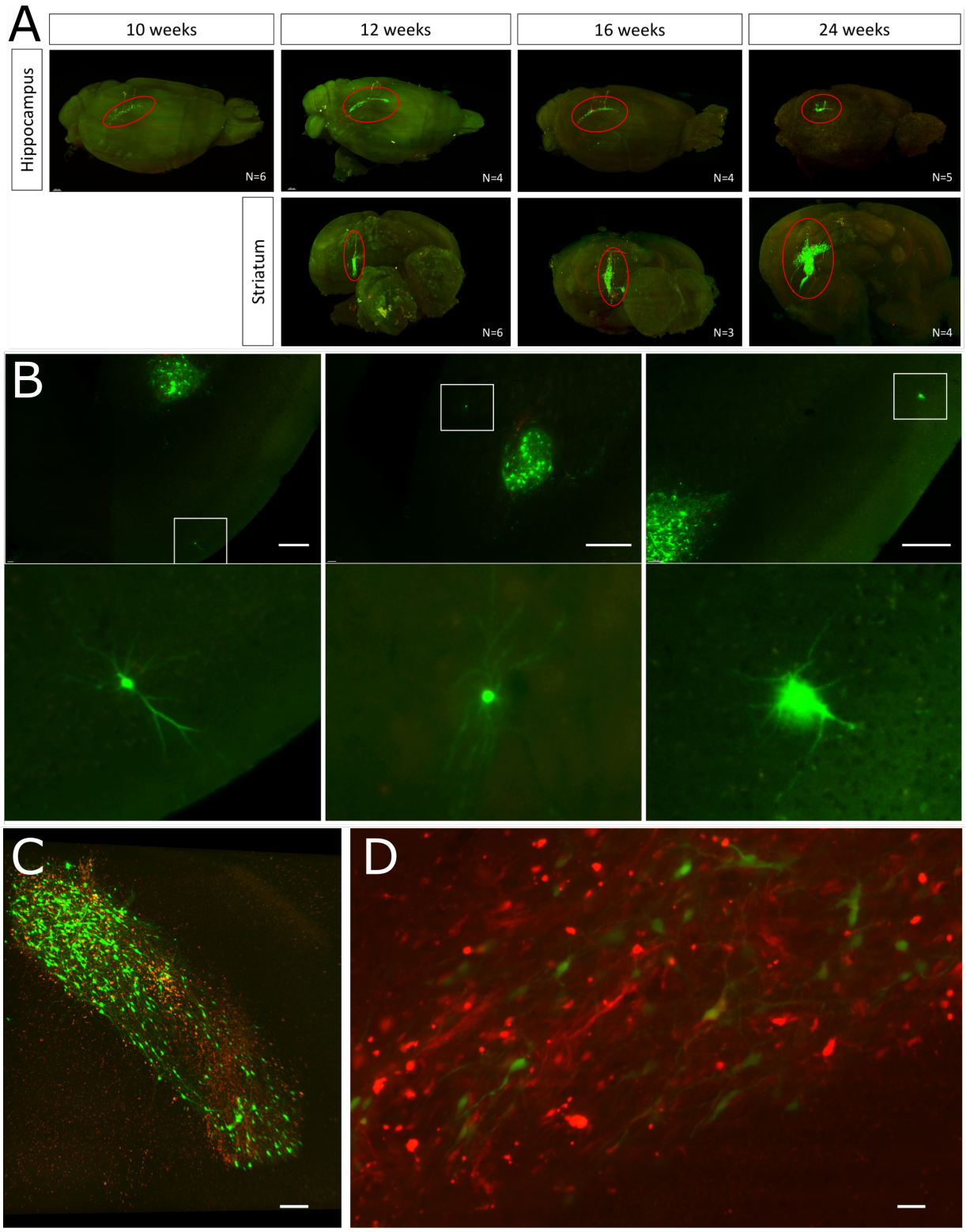

Figure 18: PRABV- and LSFM-based connectivity tracing of striatal and hippocampal iNSC grafts after up to 24 weeks of *in vivo* maturation.
(A) Time course analysis of graft growth after iNSC transplantation. Shown are representative 3D reconstructions of whole brain LSFM data. Red ovals encircle iNSC grafts. N-numbers as indicated. **(B)** Exemplary horizontal LSFM planes (upper panels) capturing GFP-positive cells with mature neuronal morphologies distant from iNSC grafts. Lower panels show close-ups of the areas indicated by white rectangles. Scale bars = 500 μm. **(C)** Representative 3D reconstruction of a hippocampal graft, which was pRABV-infected 10 weeks post transplantation, acquired via LSFM using a 12x objective. Scale bar = 100 μm. **(D)** Magnified view of one imaging plane, acquired via LSFM using a 12x objective, within the transplant region. Scale bar = 20 μm.

Despite this call for caution, we next set out to confirm the assumed mouse origin of GFP-labeled cells outside the graft core in our experimental conditions. Since RFP signal was in part diffuse in LSFM 3D reconstructions (Figure 18 C) and hard to allocate to individual cells (Figure 18 D), we decided to determine the identity of GFP-labeled cells using a species-specific antibody. To this end, we rehydrated a subset of all brains harboring engineered iNSC grafts (N = 1-2 animals per transplantation site and analysis time point) and subjected them to cryo-sectioning and subsequent immunohistochemistry using an antibody to hN. Using this method, we aimed to confirm that GFP-labelled neuronal cells outside the graft could potentially represent host neurons forming functional synapses on the transplant. Figure 19 A and Figure 19 A' display exemplary pictures of coronal sections anterior to a striatal and hippocampal graft (graft areas depicted in Figure 19 B and Figure 19 B'), respectively, which were matured for 12 weeks *in vivo* prior to pRABV injection. These representative examples demonstrate that GFP-positive cells remote from the grafts are negative for hN (Figure 19 C and Figure 19 C', with single channel images shown in D and D'), suggesting that mouse host neurons might indeed have formed functional synapses on iNSC transplants as early as 12 weeks post transplantation.

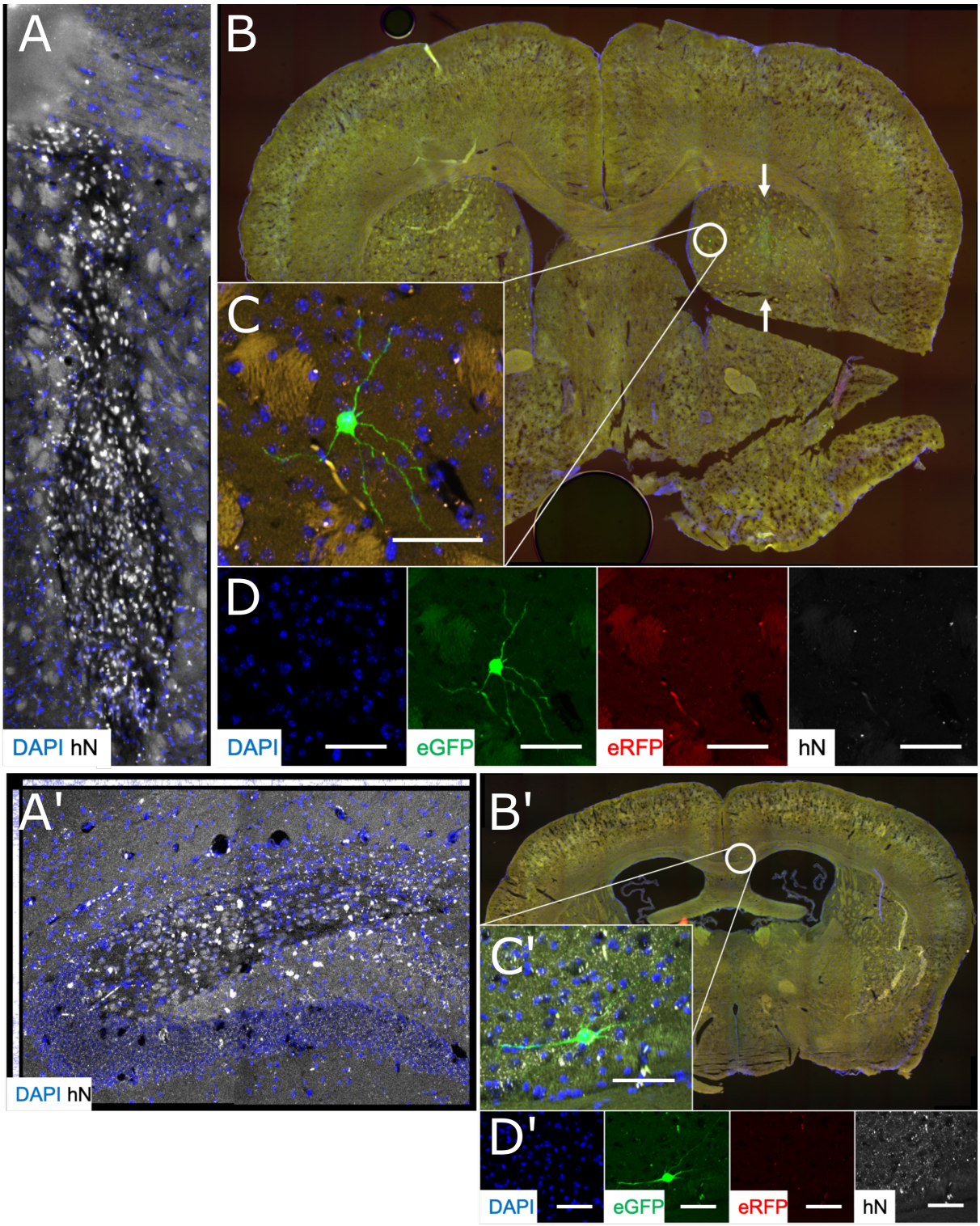

Figure 19: Detection of hN-negative, GFP-positive neurons in rehydrated mouse brain slices post LSFM.
(A) Depiction of a 12 weeks-matured striatal (A) and a hippocampal (A') graft stained against hN after LSFM and subsequent tissue rehydration. **(B)** Exemplary coronal sections anterior to the striatal (B) and hippocampal (B') iNSC grafts depicted in panels A/A'. Arrows in B indicate where first signs of the graft became apparent. Circles indicate where a cell could be identified that endogenously expressed GFP (eGFP). **(C)** Close-up of the eGFP-positive cells circled in panels B/B'. **(D)** Single channel images of the merged picture provided in panels C/C', revealing that the GFP-positive cells distant from the transplants were identified as host cells, as indicated by the absence of endogenous RFP (eRFP) and stained hN signal.

3.2.3. Human grafted iNSC-derived neurons exhibit defined neurite outgrowth patterns.

In addition to assessing graft afferents, we investigated the projection patterns of iNSC grafts in all brains that were rehydrated after LSFM by performing human NCAM-DAB visualization, following human NCAM-positive fibers across multiple coronal sections (Figure 20 A). Hippocampal grafts located in the mouse dentate gyrus projected via the fornix to septal areas and via the hippocampal CA region toward the entorhinal cortex in anterior and posterior direction, respectively (Figure 20 B). Notably, this projection pattern is concordant with the known physiological circuitry of the dentate gyrus (Patton & McNaughton, 1995). In contrast, although the neuronal outgrowth of striatal grafts seemed to overall increase over time, especially spreading along the corpus callosum, little to no projections via the globus pallidus and the subthalamic nucleus to the substantia nigra were detected (data not shown), which would resemble physiological-like striatal projection patterns (Fishell & Van Der Kooy, 1991). Altogether, these data indicate that, in addition to receiving afferent connections from the host brain, neurons derived from grafted iNSCs exhibit defined neurite projection patterns, which follow different trajectories depending on the site of neural transplantation.

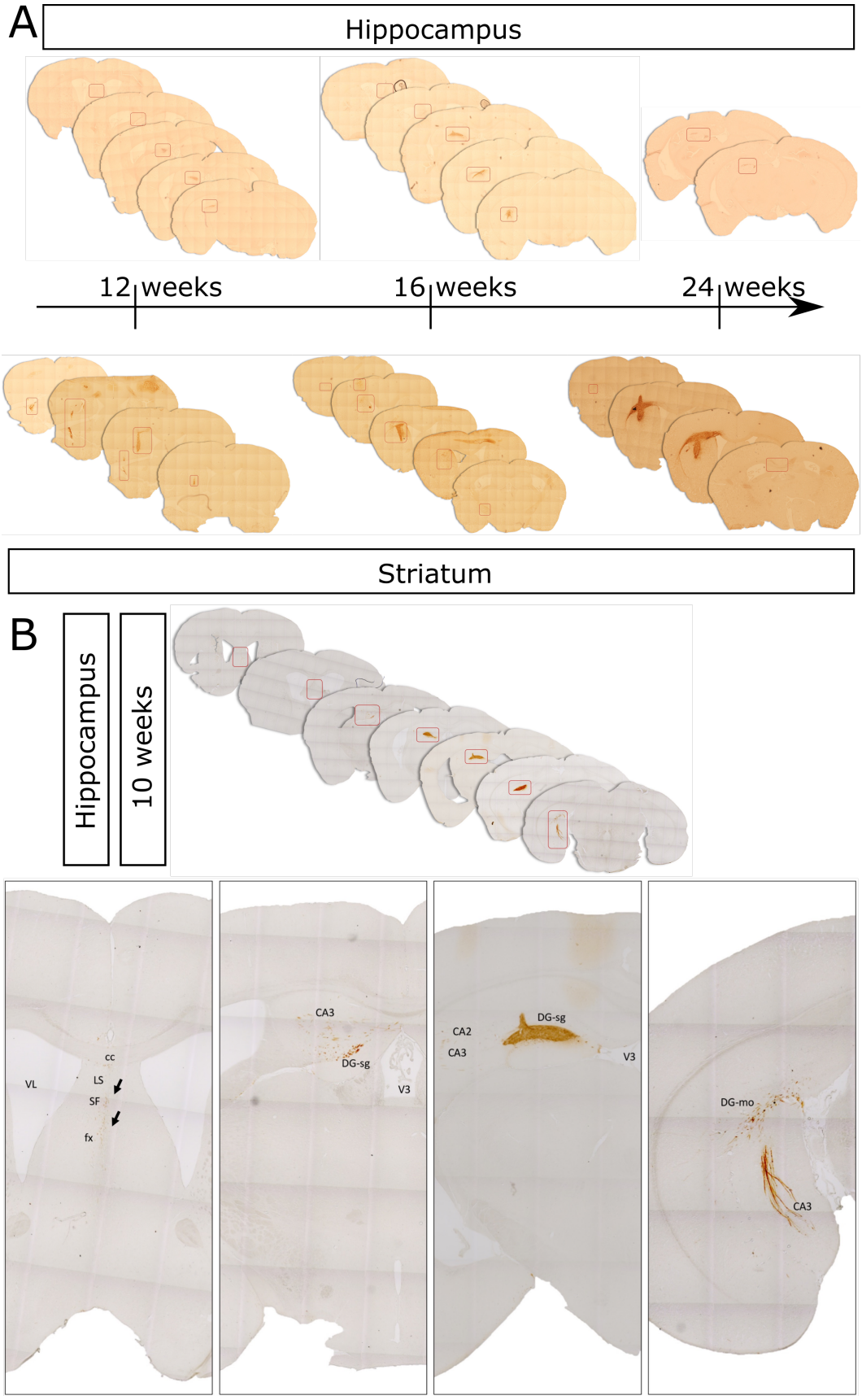

Figure 20: Human NCAM-based fiber tracking to study iNSC graft efferents.
(A) Rehydrated brains were stained against human NCAM, which was visualized by permanent DAB staining. N = 1-2 animals per group. **(B)** Exemplar of a hippocampal iNSC graft 10 weeks post transplantation, exhibiting a region-appropriate projection pattern. CA: cornu ammonis, cc: corpus callosum, DG-mo: dentate gyrus molecular layer, DG-sg: dentate gyrus granule cell layer, fx: columns of the fornix, LS: lateral septal nucleus, SF: septofimbrial nucleus, V3: third ventricle and VL: lateral ventricle. Anatomical references according to the interactive Allen brain atlas (mouse, P56, coronal).

3.2.4. Human xenografts form synapses and are electrophysiologically active.

Finally, we investigated whether transplanted human iNSCs were themselves capable of forming synapses and achieving electrophysiological functionality. To this end, we first injected $5x10^4$ human iNSCs into the cerebrum of neonatal mice. Grafted iNSCs were fluorescently labelled by lentiviral infection with an EF1α-GFP vector prior to transplantation. The intracerebral injections in neonates were performed non-stereotactically, which led to a wide-spread distribution of the grafted cells across different brain regions (Figure 21 A). In collaboration with Heinz Beck's group at the Institute of Experimental Epileptology and Cognition Research, University of Bonn, patch clamp recording of a total of 18 GFP-positive cells was performed in four animals across a time span of 4 to 6 months after grafting, revealing that while 11 out of 18 cells did not show active neuronal properties, 4 out of 18 cells exhibited immature and 3 out of 18 cells mature electrophysiological properties. More specifically, immature neurons exhibited small sodium currents but could not fire APs in response to current injection (data not shown). In contrast, mature neurons were capable of repetitive AP firing in response to current injection (Figure 21 B) and showed pronounced sodium currents (Figure 21 C). In 2 out of 3 mature iNSC-derived neurons, sPSCs were detectable, too (Figure 21 D). These data provided a first proof-of-principle that grafted iNSCs are able to develop into electrophysiologically functional neurons *in vivo*, and prompted us to investigate whether this could also be achieved by cells grafted into adult mice.

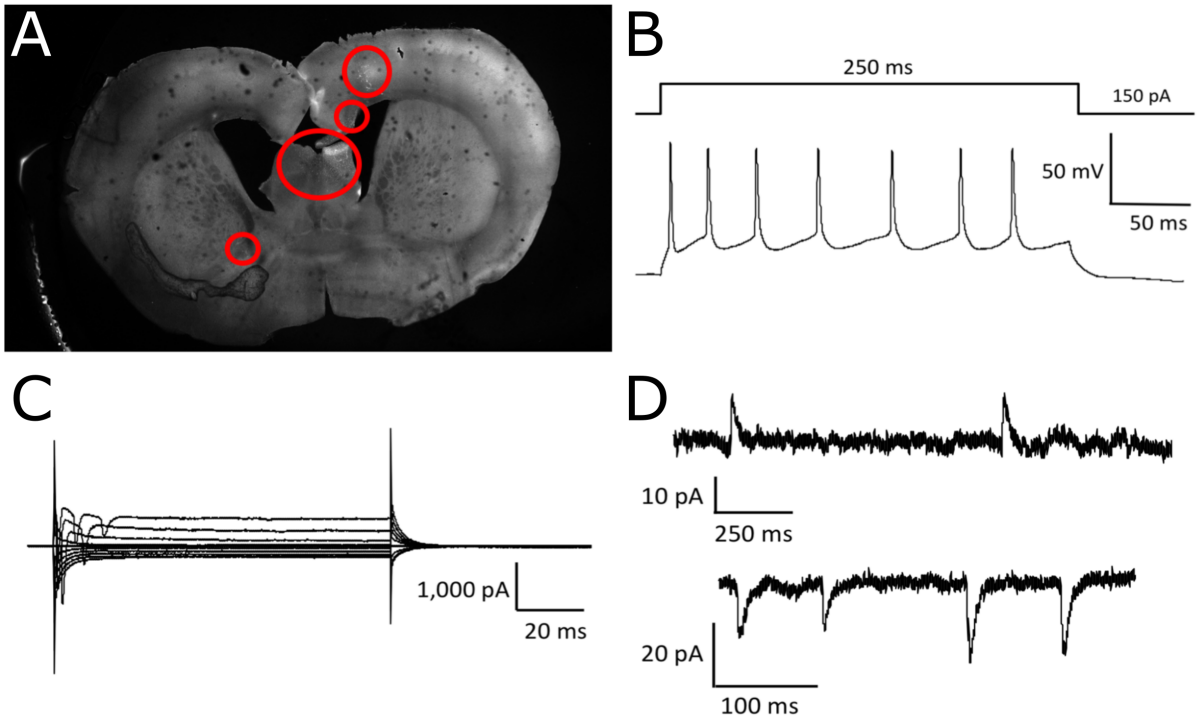

Figure 21: Electrophysiological characterization of GFP-positive cells derived from iNSCs transplanted into the neonatal mouse brain. **(A)** Overview image representing where GFP-positive iNSCs were found during patch clamping of acute brain slices (red circles). N = 4 animals in total. **(B)** Exemplary trace demonstrating that depolarizing current injection can elicit multiple APs in iNSC-derived neurons. N = 3/18 cells. **(C)** INSC-derived neurons exhibited pronounced sodium currents upon current injection. N = 3/18 cells. **(D)** Excitatory and inhibitory sPSCs were recorded in GFP-positive iNSC-derived neurons. N = 2/18 cells. Panels A-D represent exemplary images and traces provided by Pedro Royero, AG Heinz Beck, Institute of Experimental Epileptology and Cognition Research, University of Bonn.

Thus, in collaboration with Jeong Seop Rhee's group at the Max Planck Institute of Experimental Medicine in Göttingen, we next acquired preliminary data on spine formation and electrophysiological properties from three adult mice sacrificed 24 weeks and three animals sacrificed 12 weeks after transplantation of GFP-positive iNSCs, respectively. Per analysis time point, one animal received striatal and two mice hippocampal grafts. 3D reconstructions of GFP-positive dendrites, which were performed by Ali Shaib and based on MAP2 staining of mouse brain slices, demonstrated the formation of spine-like structures in transplanted iNSC-derived neurons after 24 weeks of *in vivo* maturation (Figure 22 A). A fraction of the detected spine-like structure could indeed further be classified as true spines based on co-localized expression of the pre-synaptic marker VGLUT1 and the post-synaptic marker SHANK2 (Figure 22 B). Together, the existence of spine-like structures and spines suggested that iNSC-derived neurons possess the morphological prerequisites for forming functional connections.

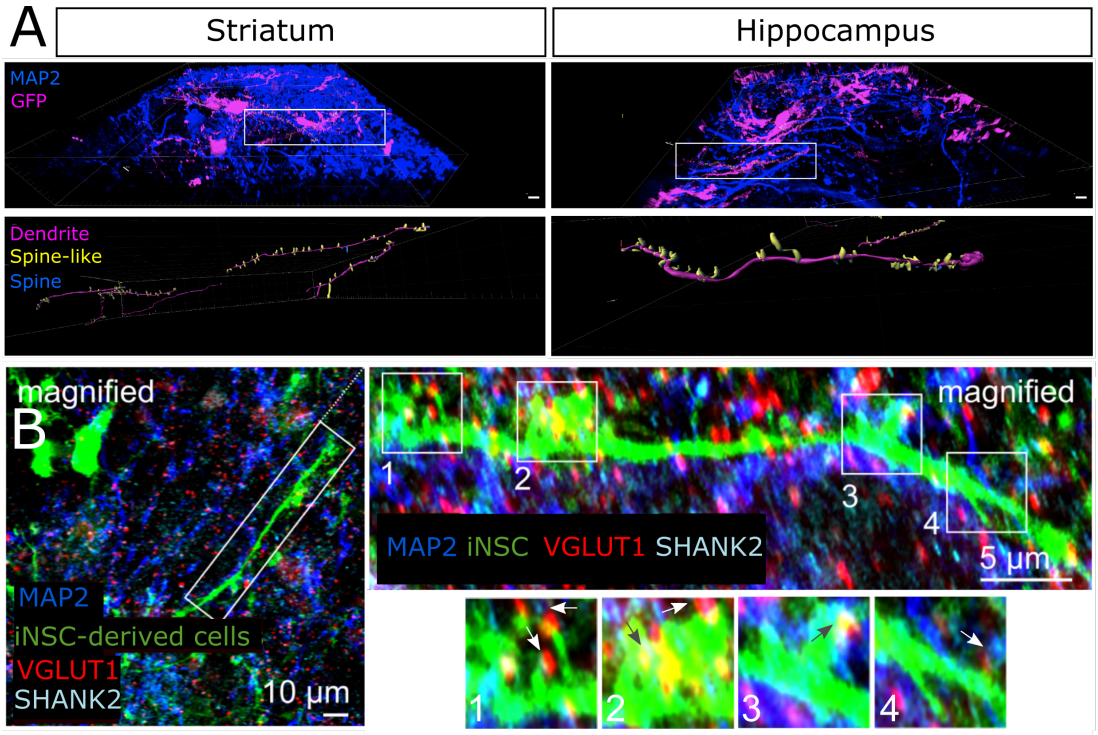

Figure 22: Visualization of spine-like structures and spines on human dendrites 24 weeks after iNSC transplantation.
(A) Representative reconstruction of MAP2-staining within 25 μm below the slice surface reveals the dendritic tree of MAP2- and GFP-co-expressing human iNSC-derived neurons. Spines were defined as spine-like dendritic structures (mushroom, stubby, thin or long structures with a length of min. 160 nm to max. 4.5 μm) with co-localized VGLUT1 and SHANK2 expression. Scale bars = 5 μm. **(B)** Representative image of a 300 μm-thick brain slice, containing a striatal iNSC transplant, stained against MAP2, the pre-synaptic marker VGLUT1 and the post-synaptic SHANK2. Scale bars as indicated in the respective excerpts. Arrows within magnified regions point toward spine-like, GFP-positive structures with co-localized VGLUT1/SHANK2 signal. Different arrow colors are used for visibility reasons only. Panels A-B were provided by Ali Shaib, AG Jeong Seop Rhee, Max-Planck Institute for Experimental Medicine, Göttingen. N = 3 animals in total.

Notably, already after 12 weeks of *in vivo* maturation, endogenous GFP (eGFP) expression seemed to be heterogenous within the graft area. Immunohistochemical staining using an antibody to hN confirmed, however, that most cells within the graft were of human origin, including a substantial number of cells, which did not express eGFP to a level that could be visualized during patch clamping (Figure 23 A). Interestingly, the vast majority of strongly eGFP-positive cells was negative for the astrocyte marker GFAP and thus presumably represented a subpopulation of iNSC-derived neurons (Figure 23 B).

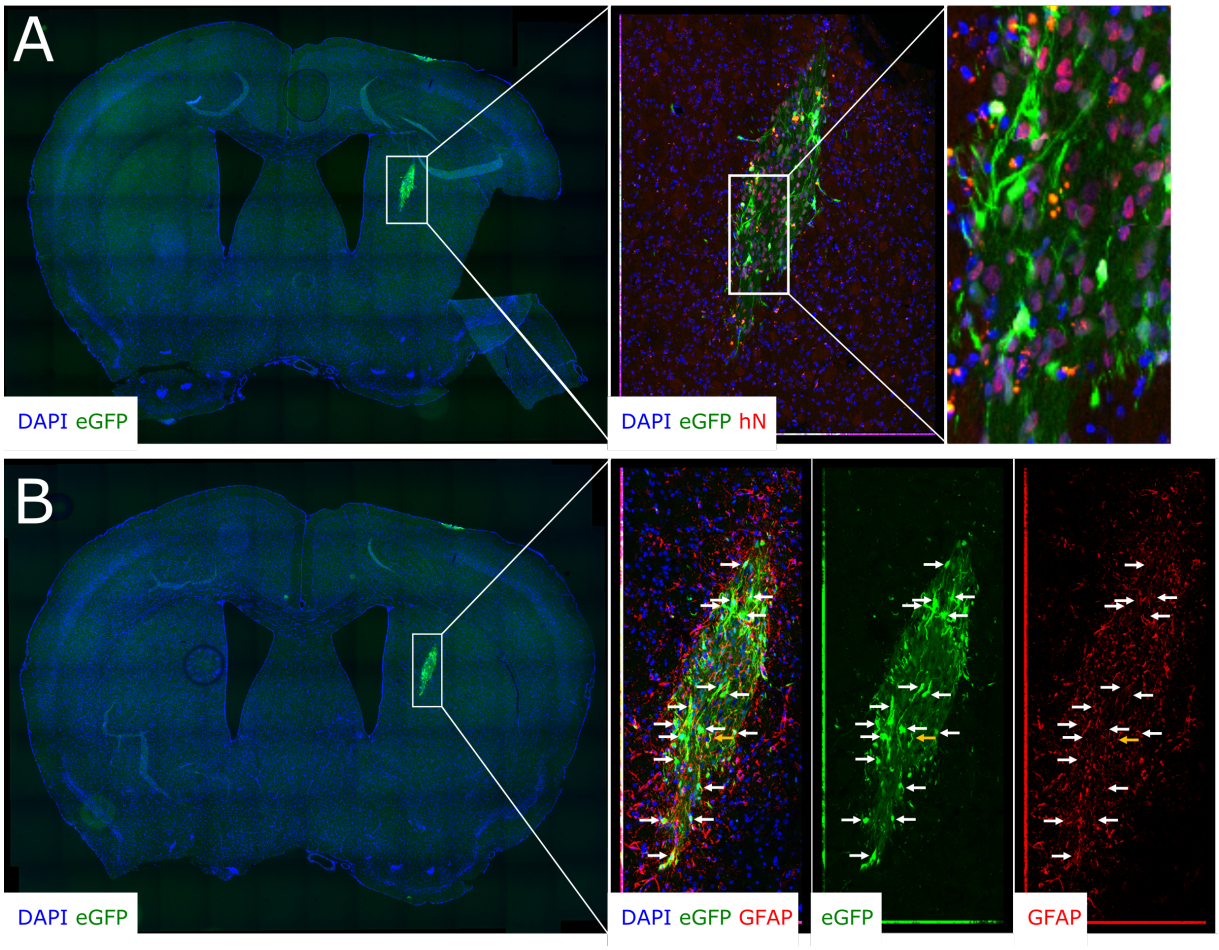

Figure 23: Characterization of an eGFP-expressing striatal iNSC graft 12 weeks post transplantation.
(A) Representative picture of a 12-weeks-matured striatal iNSC transplant section stained against DAPI and hN. Panels to the right show close-ups of the areas marked by the white rectangles. **(B)** Subsequent coronal section to slice depicted in panel A stained against DAPI and GFAP. Panels to the right show single channel and merged close-ups of the area marked by the white rectangle. White arrows mark brightly eGFP-positive cells that are negative for GFAP. The single yellow arrow points toward an eGFP- and GFAP-co-expressing fiber. Panels A-B: N = 1 animal per analysis time point (12 and 24 weeks) assessed in Bonn. More animals were sacrificed and analogously assessed by Chungku Lee, AG Jeong Seop Rhee, at the Max-Planck Institute for Experimental Medicine in Göttingen.

Electrophysiological recordings in acute slices prepared 12 weeks post grafting further revealed that EF1α-driven GFP expression seemed to be inversely correlated with the degree of neuronal maturation. Specifically, cells exhibiting high GFP expression were predominantly silent, exhibiting low sodium and potassium current densities (Figure 24 A, B), predominantly abortive AP firing patterns (Figure 24 C, D) and no detectable sPSCs (Figure 24 E). In contrast, human cells with low level GFP expression and patched cells with unresolved species identity that appeared to be GFP-negative but were found within the transplant area demonstrated increasingly more active neuronal properties. In these cells, even spontaneous AP firing (Figure 24 C, D) and sPSCs (Figure 24 E) could be measured. Altogether, these data could indicate that upon progressive neuronal maturation, transgenic GFP is silenced in iNSC-derived neurons. Albeit the need to experimentally verify this hypothesis in future experiments, our data collectively provide first evidence that iNSC-derived neurons are principally able to acquire electrophysiological functionality upon maturation in postnatal and adult murine brains.

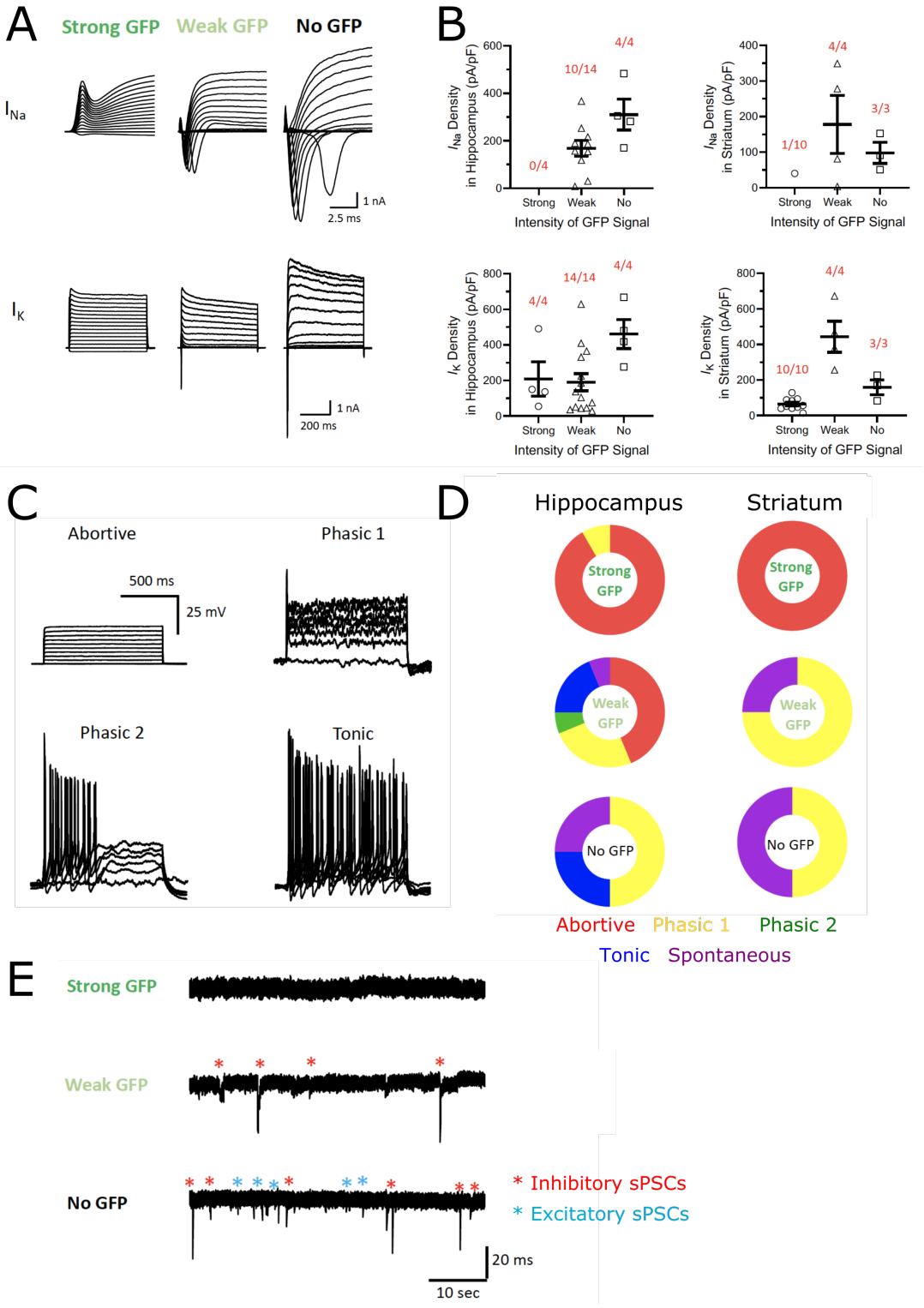

Figure 24: Electrophysiological recordings in acute brain slices prepared from adult mice carrying iNSC grafts.
(A-B) Representative electrophysiological traces (A) and quantification thereof (B) after recording sodium and potassium currents in cells, with varying GFP signal intensity, within the area of striatal and hippocampal iNSC grafts. **(C-D)** Exemplary illustration of AP classification into abortive, phasic (1+2) and tonic firing patterns (C). Whilst APs falling into these four classes were evoked by depolarizing current injection, spontaneous AP firing was further detected in weakly GFP-positive as well as GFP-negative neurons in both transplantation sites (D). **(E)** Representative traces demonstrating that no sPSCs were recorded in strongly GFP-positive cells, whereas inhibitory only and both inhibitory as well as excitatory sPSCs were detected in cells with weak and absent GFP expression, respectively. Panels A-E show exemplary traces as well as the quantification of electrophysiological properties performed and provided by Chungku Lee, AG Jeong Seop Rhee, Max-Planck Institute for Experimental Medicine, Göttingen. N = 3 animals in total.

3.3. Microglia, the immune cells of the CNS, are amenable to iNSC conversion.

3.3.1. IPSC-derived microglia convert into NSCs after overexpression of the TFs SOX2 and cMYC.

Having shown that SeV-mediated overexpression of the two TFs SOX2 and cMYC in adult peripheral blood cells yielded rejuvenated NSCs amenable to neurotransplantation, we next set out to explore whether we could alternatively also employ a brain-resident cell type of the hematopoietic lineage, namely microglia, as a starter population for iNSC conversion. This approach deemed especially attractive, since it could allow us to exploit a tissue-resident cell population, exhibiting highly versatile cellular responses to tissue injury, for neural conversion and ensuing neuroregeneration.

Due to the highly restricted access to primary human microglia, the immune cells of the CNS, we employed a protocol to differentiate human iPSCs into microglia that phenotypically, transcriptomically and functionally highly resemble primary human microglia (patent application number EP20162230; Mathews … Flitsch … *et al*.; in revision). In order to transdifferentiate iPSdMiG (provided by Mona Mathews-Ajendra) into iNSCs, we applied our original blood-to-iNSC conversion protocol with slight modifications (Figure 25 A). In essence, iPSdMiG were infected with SeV-SOX2 and SeV-cMYC as previously described, giving rise to colonies consisting of neuroepithelial-like cells within roughly 2 weeks. Distinct from EPC-to-iNSC conversion, some neuroepithelial colonies detached from the cell culture dishes during this early phase of microglia transdifferentiation. Such floating neurosphere-like structures were collected, dissociated and replated on day 13 of conversion, while still adherent single colonies were manually picked under microscopic control on day 14. On day 21, remaining colonies, which were not chosen for expansion as single colony-derived cell lines and meanwhile significantly grew in size, were dissociated, pooled and subsequently cultured as polyclonal cell lines. After establishment, all cell lines similarly grew as proliferative monolayers of cells with bipolar NSC-like morphology, regardless of their different origins (*i.e*., from neurospheres, single colonies or of polyclonal origin). At low passage, iPSdMiG-derived iNSC lines (termed ‘miciNSCs’) were first characterized, including the assessment of cellular identity and genomic integrity. After this initial QC, miciNSC lines were kept at 39 °C in order to inhibit SeV replication and thus eliminate the conversion-mediating transgenes. Afterwards, transgene-free miciNSC lines were further expanded to high passage and again subjected to final QC.

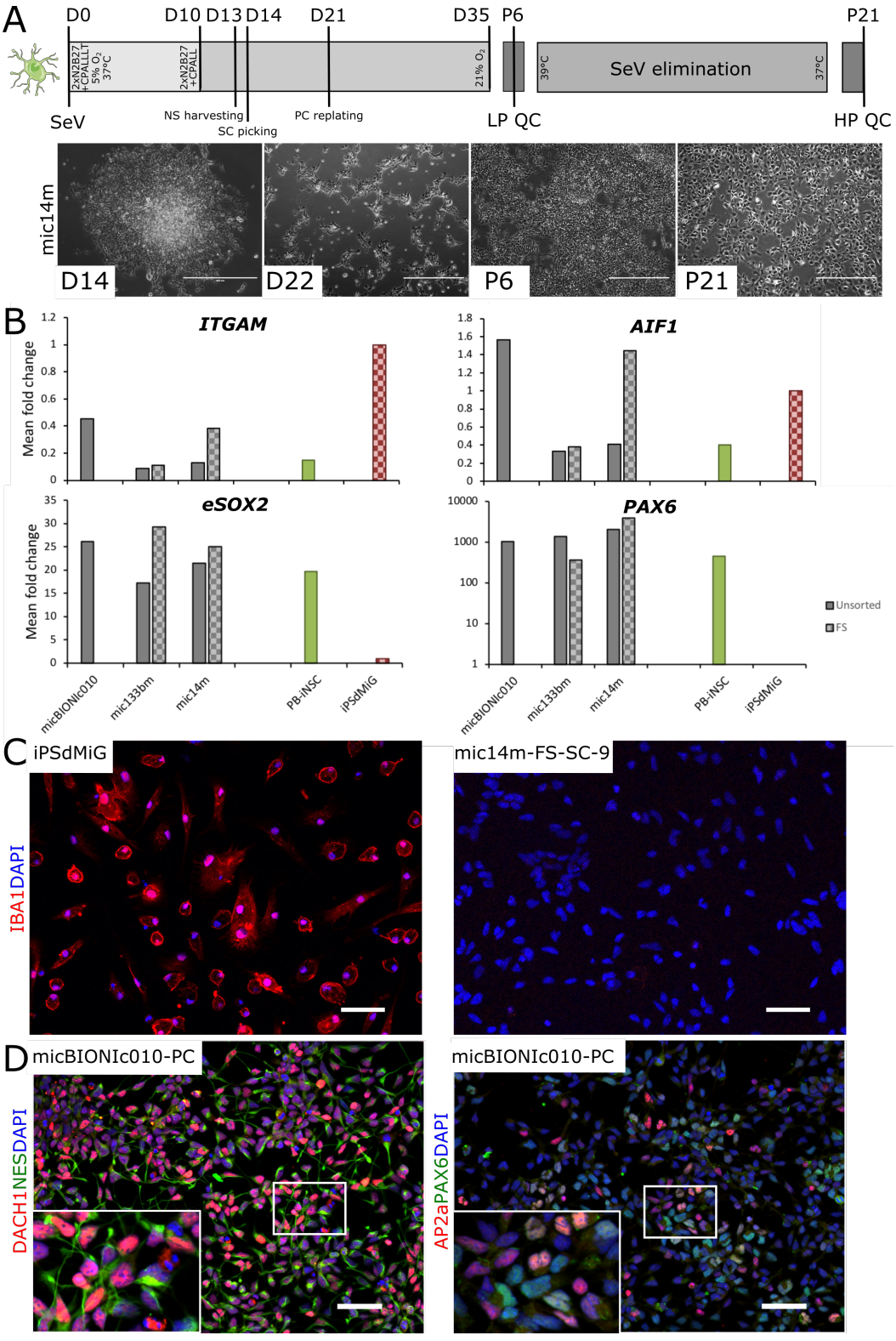

Figure 25: Characterization of iPSdMiG-derived cells after SeV-mediated overexpression of SOX2 and cMYC.
(A) Upper panel: Schematic representation of iPSdMiG-to-iNSC conversion. LP: low passage (P6), HP: high passage (P21); NS: neurosphere; SC: single colony; PC: polyclonal. The depicted microglial icon was retrieved from Servier Medical Art by Servier (SMART; https://smart.servier.com), licensed under a Creative Commons Attribution 3.0 Unported License. Lower panel: Representative phase contrast images of iNSCs at different stages within the conversion process. Scale bars = 400 μm. **(B)** QPCR-based profiling of the expression of the microglial markers *AIF1* (encoding for IBA1) and *ITGAM* (encoding for CD11b), as well as the NSC markers *SOX2* (endogenous transcript only) and *PAX6* across several miciNSC lines at low passage QC, as compared to peripheral blood-derived iNSCs (PB-iNSCs) and CD11b-purified microglial harvests (iPSdMiG). N = 1 per cell line; depicted is the mean of three technical replicates. **(C)** Representative immunostainings for the microglial marker IBA1 (red; DAPI in blue) in iPSdMiG and miciNSCs. Selection from in total N > 5 miciNSC lines stained. Scale bars = 50 μm. **(D)** Pictures representing low passage miciNSCs stained for the NSC markers DACH1, NES, AP2α and PAX6. Images are representative for in total N > 5 miciNSC lines stained. Scale bars = 50 μm. Inserts show close-ups of the areas within the white rectangles.

In total, iPSdMiG harvests from three different genotypes were successfully converted into iNSCs following the described scheme. Since iPSdMiG develop in a mixed culture with cells of neuroectodermal origin, we intended to ensure that neuroepithelial colonies emerged from true conversion events by additionally employing purified starter cultures. To this end, we repeated the conversion of two iPSdMiG lines implementing FACS for the microglial marker CD11b prior to SeV infection (denoted as miciNSC-FS-lines). Most importantly, directly harvested as well as CD11b-sorted cultures both gave rise to iNSCs. At low passage QC (P6), RNA levels of the genes encoding for the microglial markers IBA1 and CD11b, namely *AIF1* and *ITGAM*, respectively, as well as expression of the NSC markers *SOX2* and *PAX6* was comparable between unsorted and CD11b-sorted miciNSC lines (Figure 25 B). Notably though, while *SOX2* and *PAX6* expression was elevated to levels detectable in peripheral blood-derived iNSCs and *ITGAM* expression was expectedly decreased as compared to CD11b-purified iPSdMiG, expression of *AIF1* was highly heterogeneous on RNA level. Nevertheless, on protein level, IBA1 was noticeably decreased, if not completely absent, in miciNSCs (Figure 25 C). Moreover, all cell lines expressed pan-NSC markers (*i.e.*, DACH1 and NES), as well as proteins characteristic for CNS (PAX6) and PNS (AP2α) progeny (Figure 25 D).

After performing cellular characterization at passage 6, a selection of all generated miciNSC lines was subjected to transgene elimination by high temperature treatment. SeV expression levels were monitored weekly by performing RT-PCR with transgene-specific primers (Figure 26 A). After 3 to 5 weeks of cultivation at 39 °C, transgene expression levels typically decreased below the detection threshold of the employed read-out technique. One week after returning cell lines to 37 °C, the persistent absence of SeV sequences was finally re-confirmed by RT-PCR. Transgene-free miciNSC lines were then further expanded to high passage (P21) for final QC. Notably, long-term cultured iNSC lines from both conditions (± FACS) maintained genomic stability according to SNP analysis (Figure 26 B). In addition, even in the absence of the conversion-mediating transgenes, cell lines expressed early NSC markers such as NES, *SOX2*, DACH1, PAX6 and AP2α but not the microglial marker CD11b on RNA and/or protein level, as assessed by qPCR (Figure 26 C) and/or immunocytochemistry (Figure 26 D), respectively. Notably, *AIF1*/IBA1 expression exhibited a similar expression pattern in high passage miciNSCs (Figure 26 C, D) to what was previously observed in low passage miciNSCs (Figure 25 B, C).

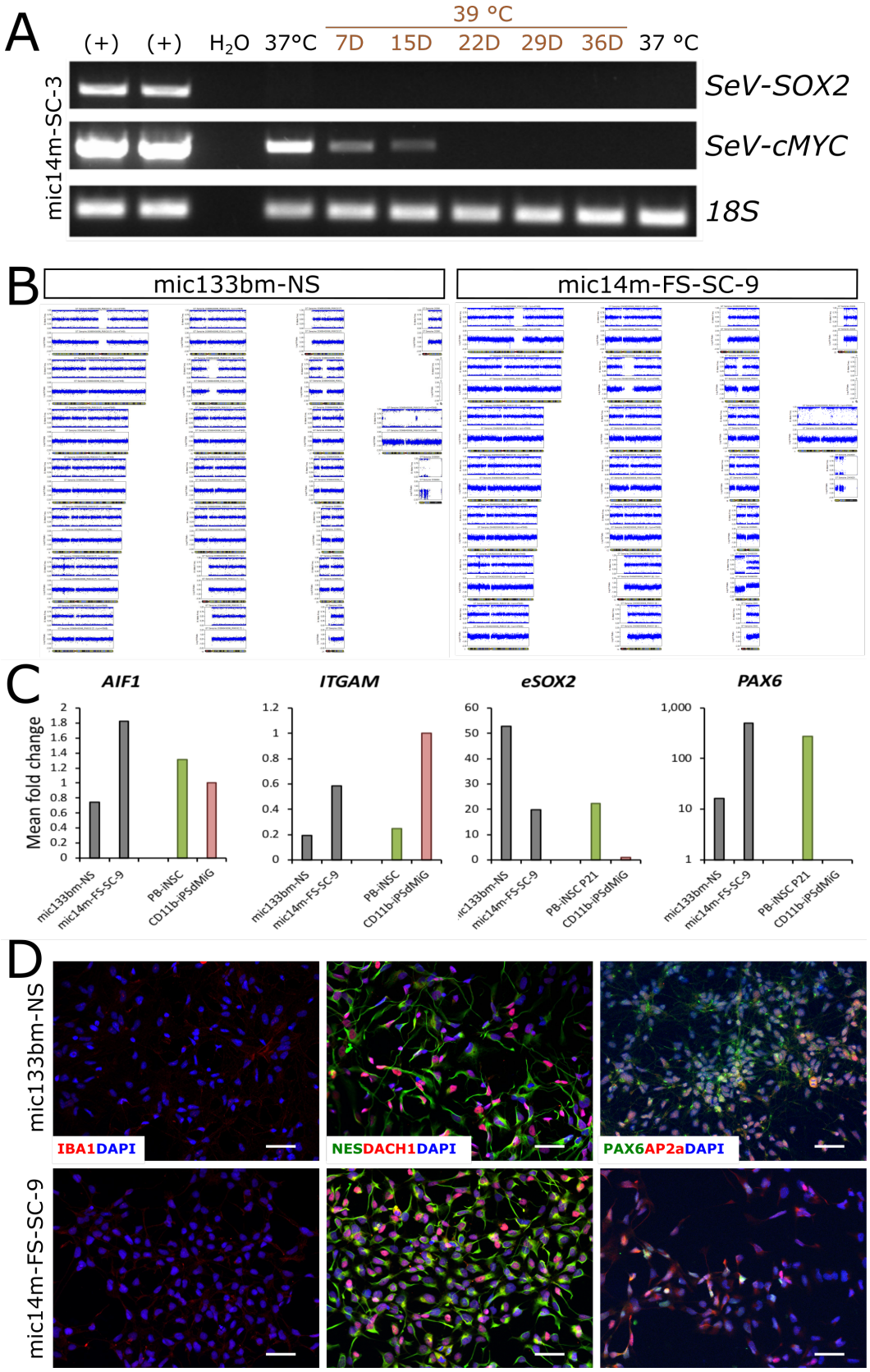

Figure 26: Genomic and phenotypic stability of miciNSCs upon transgene elimination and extended *in vitro* cultivation.
(A) RT-PCR showing progressive elimination of SeV-SOX2 and SeV-cMYC upon cultivation at 39 °C. RT-PCR results are presented for one miciNSC line only, although RT-PCRs monitoring SeV elimination were performed for all miciNSC lines cultivated beyond passage 6. (+): positive control. **(B)** SNP profiles of two miciNSC lines after transgene elimination and prolonged expansion to passage 21. **(C)** Two miciNSC lines (each one line ± CD11b-FACS) were representatively assessed for their expression of *AIF1*, *ITGAM*, endogenous *SOX2* and *PAX6* at high passage (P21) using qPCR. N = 1 per cell line; depicted is the mean of three technical replicates. **(D)** Representative images of two high passage (P21) miciNSC lines stained for IBA1, NES, DACH1, PAX6 and AP2α. Scale bars = 50 μm.

3.3.2. Microglia-derived NSCs can give rise to functional neurons, astrocytes and oligodendrocytes.

We finally investigated the ability of miciNSCs to differentiate into the three main CNS cell types of the neural lineage. When cultured in medium promoting undirected differentiation, miciNSCs readily gave rise to TUBB3-, MAP2- and NEUN-positive neurons, as well as GFAP-positive astrocytes (Figure 27 A). Patch clamp recording revealed that neurons further became electrophysiologically functional, being capable of firing single or even multiple APs in response to current injection already after 6 weeks of differentiation (Figure 27 B). Importantly, miciNSC-derived cultures even demonstrated spontaneous neuronal activity after 10 weeks of differentiation in the presence of mouse astrocytes, as neurons were capable of generating APs also in the absence of exogenous current injection (Figure 27 C). Quantification of the electrophysiological properties of miciNSC-derived neurons revealed a trend toward a lower resting membrane potential (RMP) after 10 weeks as compared to 6 weeks of undirected differentiation (Figure 27 D). In addition, although the rheobase – that is the current needed to induce AP firing – was largely unaltered at both time points, indicating similar neuronal excitability, the number of induced APs as well as the AP peak amplitude tended to increase with time. Conversely, there was a trend toward a decreased AP half-width with prolonged maturation, altogether indicating that the maturity of miciNSC-derived neurons improved with prolonged time in differentiation.

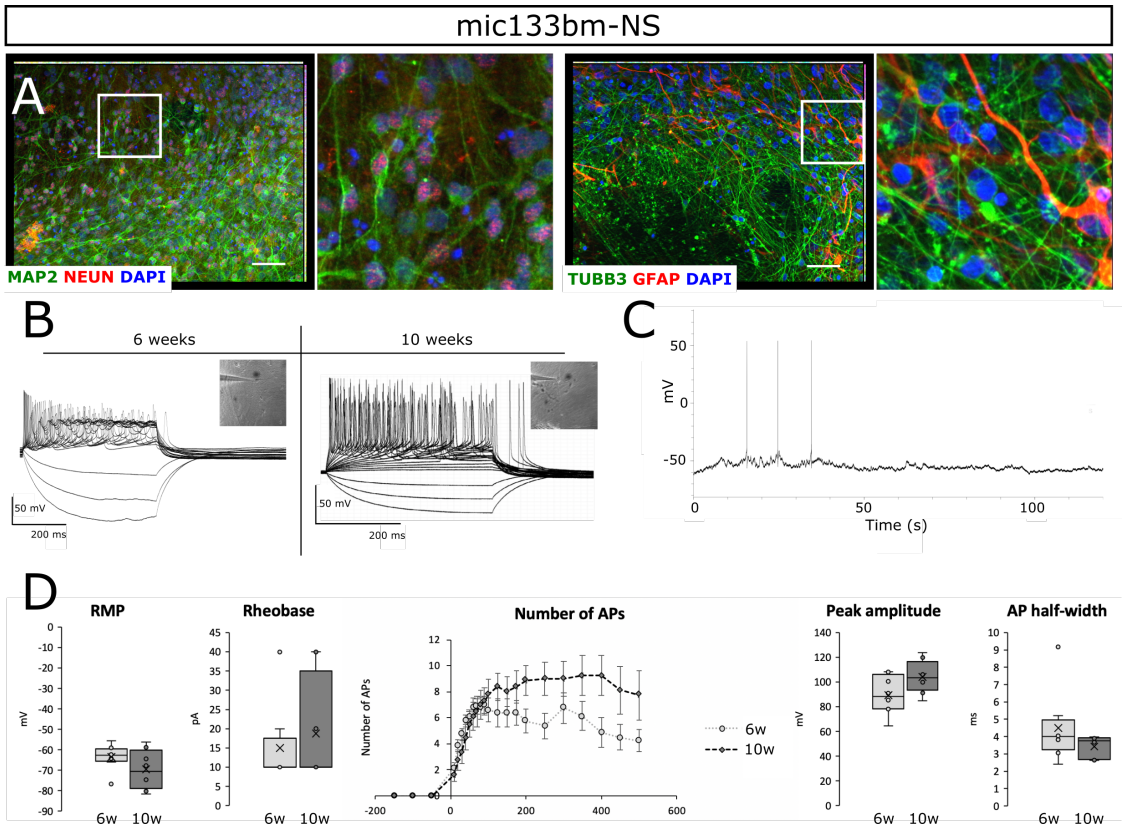

Figure 27: Characterization of miciNSC-derived cultures after 6 to 10 weeks of undirected differentiation.
(A) After 6 weeks of undirected differentiation, miciNSC-derived cultures contain TUBB3-, MAP2- and NEUN-positive neurons as well as GFAP-positive astrocytes. White rectangles indicate the position of the magnified inserts that are depicted to the right of their respective originals. Scale bars = 50 μm. **(B)** Exemplary patch clamp traces of electrophysiological recordings performed by Pascal Röderer in miciNSC-derived differentiation cultures, which were matured on mouse astrocytes for 6 or 10 weeks prior to analysis. Upper inserts show brightfield pictures of patched cells. **(C)** Exemplary trace of an electrophysiological recording demonstrating that miciNSC-derived neurons were spontaneously active after 10 weeks of differentiation. N = 2/8 cells measured after 10 weeks in astrocyte co-culture exhibited spontaneous AP firing. **(D)** Quantification of neuronal properties measured during patch clamping. N = 8 cells per time point.

When miciNSCs were subjected to a multi-stage differentiation paradigm supporting oligodendrogliogenesis (Figure 28 A), expression of the oligodendrocyte lineage- and myelin production-associated genes *OLIG2*, *NG2*, *PDGFRα* and *MBP* was induced, increasing with extended time in differentiation (Figure 28 B). Accordingly, at the end of stage III of the differentiation protocol (*i.e.*, at day 49 of oligodendrocyte differentiation), a considerable fraction of the differentiation culture expressed the oligodendrogenesis-associated TFs OLIG2 and NKX2.2 (Figure 28 C). Moreover, the detection of NG2- and O4-positive cells indicated the successful derivation of immature oligodendrocyte progenitor cells (OPCs) and oligodendrocytes, respectively.

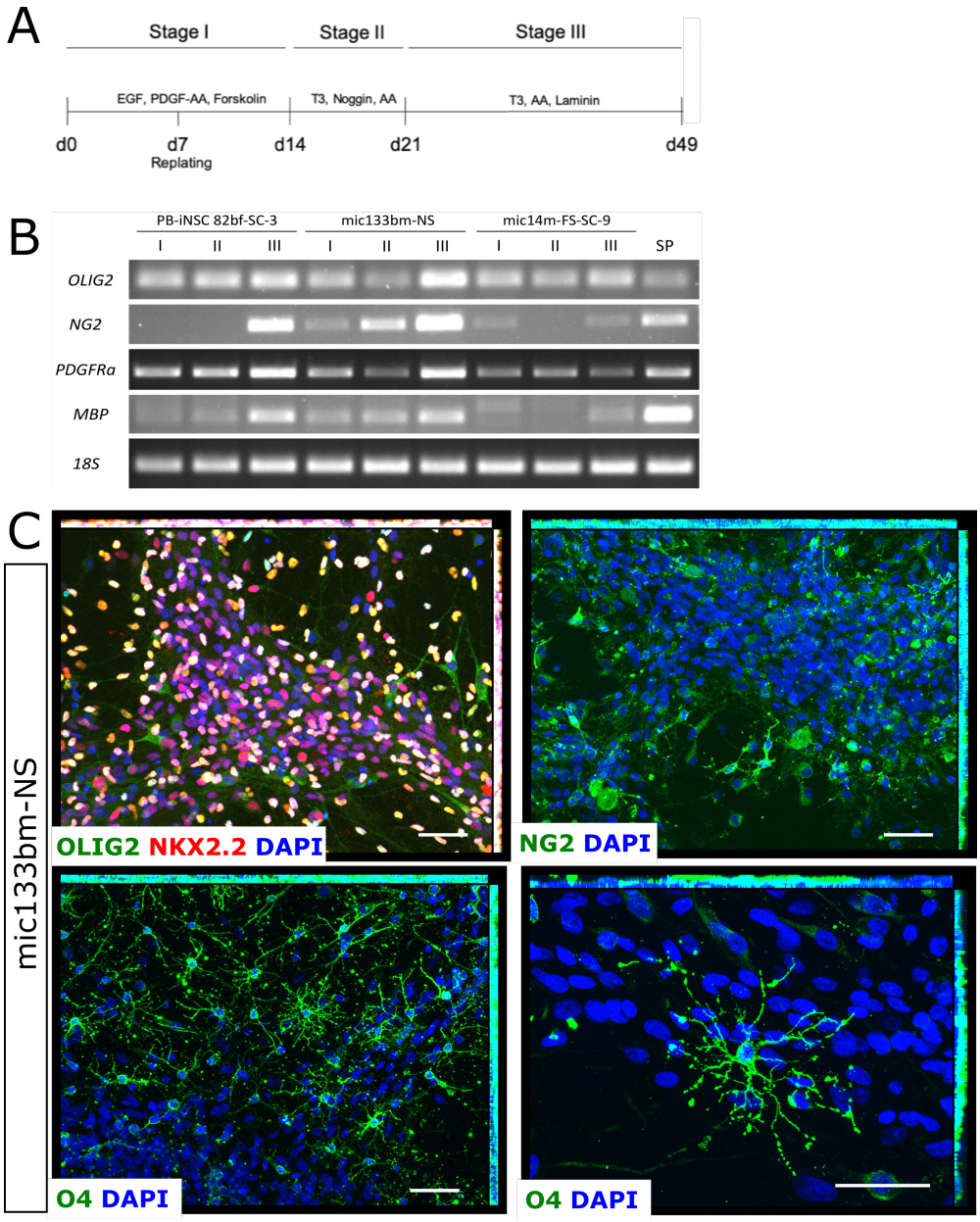

Figure 28: Assessment of the capacity of miciNSCs to give rise to oligodendrocyte lineage cells.
(A) Schematic depiction of the employed three-stage oligodendrocyte differentiation paradigm. **(B)** RT-PCR analysis of the expression of oligodendrocyte lineage- (*OLIG2*, *NG2* and *PDGFRα*) and myelin production-associated (*MBP*) genes in blood- and iPSdMiG-derived iNSCs, when subjected to oligodendrocyte differentiation-promoting culture conditions. SP = Spinal cord. **(C)** Exemplary pictures of a miciNSC-derived culture after 49 days of oligodendrocyte differentiation (*i.e.*, at the end of stage III). Immunofluorescence stainings revealing that the differentiation cultures contained OLIG2- and NKX2.2-positive oligodendrocyte lineage cells, including NG2-positive OPCs and O4-positive cells with advanced oligodendroglial morphology. Scale bars = 50 μm.

In sum, our data suggest that even CD11b-purified iPSdMiG cultures can successfully be transdifferentiated into iNSCs by overexpression of the TFs SOX2 and cMYC. Microglia-derived cell lines are genomically stable and still express typical NSC marker after long-term *in vitro* expansion and the elimination of conversion-mediating SeVs. In addition, miciNSCs demonstrate tripotent differentiation capacity, confirming their NSC-like identity after transdifferentiation.

4. Discussion

4.1. INSC conversion: A model system for investigating somatic cell rejuvenation?

4.1.1. Challenges and pitfalls associated with the quantification of biological age

In this project, we could show that transdifferentiating EPCs into iNSCs via overexpression of the two TFs SOX2 and cMYC yields cells that are highly rejuvenated on an epigenetic and cellular level. Specifically, we demonstrate that iNSCs retain less than 5 % of the DNAm age of their original blood cells, which were obtained from donors aged 0 to 101 years of age, after iNSC conversion and prolonged expansion. Comparing telomere lengths of iNSCs, smNPCs and their source blood cells, only telomeres of iPSC-derived smNPCs, but not isogenic iNSCs, are prolonged upon cell programming. On the one hand, however, telomere lengths were reported to be only modestly associated with age, being much less well correlated with cellular aging than DNAm age predictions (Lowe *et al*., 2016). On the other hand, high *TERT* expression and telomerase activity are features well described for cells acquiring a pluripotent state (Takahashi *et al*., 2007). Concordantly, others have already shown that cellular rejuvenation can indeed take place in the absence of telomere elongation (Sarkar *et al*., 2020), which is presumably a feature related to the acquisition of pluripotency rather than the reset of cellular age and, thus, not relevant to direct conversion paradigms such as ours.

In line with this assumption, iNSCs do not seem to exhibit cellular aging hallmarks: (i) Expression levels of the age-associated genes *RANBP17*, *LAMNA* and *PCDH10*, as well as the senescence-related genes *CDKN1a* and *CDKN2a* are similar in iNSCs and smNPCs. (ii) No impairments of autophagy are detectable in iNSCs. (iii) DNA damage and mitochondrial ROS production in iNSCs and smNPCs seem to be overall comparable. (vi) Expression levels of the nuclear lamina-associated *LMNB* and *LAP2α*, which are both negatively correlated with aging (Scaffidi & Misteli, 2006; Shah *et al*., 2013), are consistent in both cell types. Conversely, expression of LMNA/C is higher in iNSCs as compared to isogenic smNPCs, as well as young as compared to old donor-derived cells. Notably, although our results would be conflicting assuming that LMNA expression is positively correlated with aging (as was described for mouse fibroblasts), decreased Lmna expression was also found to be characteristic for iPSCs with higher proliferation and differentiation capacity (Zuo *et al*., 2012), which might represent a significant confounder comparing its expression in iNSCs and iPSC-derived smNPCs. Moreover, it is important to note that qualitative changes in LMNA/C expression upon aging are much better characterized than absolute differences. Specifically, aged cells exhibit LMNA/C mislocalized to the nuclear rim, revealing structural abnormalities of the nucleus such as increased folding and blebbing (Scaffidi & Misteli, 2006). These age-associated features were neither observed in iNSCs nor smNPCs derived from differentially aged donors, overall corroborating our finding that iNSC conversion yields cells devoid of cellular aging signatures.

Nevertheless, it has to be acknowledged at this point that while iPSC-derived smNPCs were chosen as reasonable negative control for cellular aging in the assays performed, no appropriate positive control could be included. Owing to the fact that cellular aging might present differently in distinct somatic cells (*e.g*., due to different developmental origins or speeds of cell cycle progression), the most proper positive control would presumably be primary NSCs from aged individuals. Ignoring the appreciable scientific debate concerning the general significance of such a population in humans for the nonce, obtaining these cells in sufficient amounts for studies such as ours seems visionary. Accordingly, to prospectively address this void, future studies might explore the

representation of cellular aging hallmarks in transformed human NSCs isolated from aged patients undergoing surgical cerebral tumor resection and/or the feasibility to account for species-specific differences in cellular aging signatures of, for instance, mouse adult NSCs. The complexity of the latter approach, however, is highlighted by a number of different examples: In human primary microglia, for instance, expression of 572 genes vary with age, but only 14 of these genes are concordantly age-associated in mouse microglia (Galatro *et al*., 2017). As for the neural system, assessing neurospheres isolated from the subventricular zone of young and aged mice identified as few as 330 regions and 254 genes that are differentially methylated and expressed upon aging, respectively (Lupo *et al*., 2018). Although Petkovich *et al*. were still able to establish a murine DNAm age predictor algorithm that accurately predicts the biological age of tissues from a number of different mouse strains and also recapitulates effects of known age-altering paradigms (Petkovich *et al*., 2017), it still seems unlikely to date that the same read-outs can be easily applied to mouse and human cells in parallel in order to assess aging in a comparative manner.

Interestingly, even within one organism, algorithms to predict DNAm ages can differ substantially. The three mouse DNAm age clocks developed by Petkovich *et al*., 2017, Tina Wang *et al*., 2017 and Stubbs *et al*., 2017, for example, do not have a single CpG in common. Although the choice of (i) the method to profile DNAm and (ii) the tissue used to train the clock algorithm might contribute to this phenomenon, this observation led to the assumption that DNAm clocks are likely to rather capture a general chronological age-associated entropic decay and smoothening of the epigenetic landscape, intriguingly indicating their serious limitation to generate biologically meaningful insights about the mechanisms driving epigenetic aging via the positioning of clock-governing CpGs (reviewed by Field *et al*., 2018). Conversely, in-depth single cell transcriptomic profiling of young and old mouse brains recently allowed the investigation of commonly regulated as well as cell type-specific age-associated transcriptomic changes within the neural system. Genes that were commonly upregulated with age across the diverse murine neural cell types were related to ribosomal proteins, long non-coding RNAs as well as immunoregulation and inflammation. Genes with decreased expression upon aging were associated with the mitochondrial respiratory chain complex, glycolysis as well as selenoproteins. Accordingly, cellular respiration, protein synthesis, inflammatory response, oxidative stress and growth factor signaling were identified as the most dominant aging-related pathways concordantly regulated within the aging mouse CNS (Ximerakis *et al*., 2019).

Thus, despite the afore-mentioned differences between rodents and humans relating to specific genes in individual cellular system, these findings indicate that fundamental concepts relating to cellular aging are most probably conserved across species. Nevertheless, the (quantitative) determination of biological age remains challenging, especially considering that for some cellular systems, appropriate positive controls might be hard to impossible to obtain.

4.1.2. The search for mechanisms contributing to the reset of aging signatures

Overall, our data indicate that blood-to-iNSC transdifferentiation yields cells that are comparable to iPSC-derived smNPCs with regard to their epigenetic and cellular aging signatures. Our conclusion that an intermediated pluripotent state might not be required for rejuvenation is supported by recent analyses of DNAm changes upon iPSC reprogramming, which show that the reset of DNAm age and the establishment of a stable, self-sustaining pluripotent state follow different time dynamics (Olova *et al*., 2019). From a conceptional point of view, these

observations support the idea that epigenetic rejuvenation might be uncoupled from cell programming itself and could thus, in principle, be achieved in somatic cells, too. Since the DNAm age reset induced by our conversion approach occurs over a prolonged period of time, this might hold great prospects for mechanistic studies, providing a blueprint for investigating potential drivers of somatic cell rejuvenation.

4.1.2.1. The relevance of stem cell proliferation

We hypothesized that stem cell proliferation, representing one of the key similarities between iPSC reprogramming and direct conversion into iNSCs, might be a main contributor to age remodeling. Conversely, we found that neither the fast conversion of proliferating iNSCs into post-mitotic neurons nor the pharmacological inhibition of proliferation by thymidine treatment significantly stalls the induced epigenetic age reset. Treating iNSCs with the proliferation inhibitor glycerol, however, tended to slightly increase DNAm ages after 5 weeks of treatment. Notably though, besides inhibiting proliferation of a number of tissues (Wiebe & Dinsdale, 1991; Dinsdale *et al*., 1992; Sugiyama *et al*., 2002; Liu & Chen, 2007; Traudt *et al*., 2014; Capiglioni *et al*., 2018) and affecting cytoskeleton and cell adhesion (Dinsdale *et al*., 1992), glycerol treatment was reported to increase the number of nucleoli per nucleus in baby hamster kidney cells (Dinsdale *et al*., 1992) and lead to the emergence of binucleated cells in Chinese hamster ovary cells (Liu & Chen, 2007). Thus, we suggest that – in light of our other proliferation-manipulating experiments, which did not yield altered DNAm age dynamics – glycerol's effect on DNAm might not reflect a genuine age-associated process. Consequently, we assume that cell division *per se* and stem cell proliferation in particular is not essential for the reset of cellular aging signatures.

4.1.2.2. Insights from transcriptomic changes during iNSC conversion: STAT3 and its potential implications in aging

In order to shed light on the mechanisms that could alternatively drive (epigenetic) rejuvenation, we next investigated global epigenetic and transcriptomic changes performing DNAm profiling and RNA sequencing at different stages of iNSC conversion. Although both analyses revealed substantial differences especially at early stages – which also entail the most substantial loss of DNAm age – the large majority of DMRs and DEGs identified seems to be attributable to continuous remodeling of cellular identity occurring at least until day 26 of conversion. In order to elucidate whether a small subset of genes altered upon the progression of iNSC conversion could still be connected to age-related processes, we compared these DEGs with genes that are differentially expressed between old and young donor-derived iNSCs at day 14 of iNSC conversion. We assumed that while different iNSC lines harvested at the same day of conversion should have underwent overall very similar degrees of cell fate remodeling irrespective of their donors' ages – despite some variability potentially arising from genotype-specific differences in the dynamics of the loss and acquisition of cell type identity – old but not young donor-derived iNSCs harvested at this early stage of conversion should still express components relevant to resetting cellular age. Following this approach, we identified *STAT3* as one of five commonly regulated DEGs. STAT3 belongs to a class of seven latent TFs and is activated upon tyrosine phosphorylation next to its carboxy-terminal region. Phosphorylated STAT3 can homo- or heterodimerize and subsequently translocate from the cytoplasm to the nucleus to induce transcription of its target genes. Due to STAT3's ability to interact with different

co-factors depending on its post-transcriptional modifications and the given microenvironmental conditions, as well as the cell type specificity of chromatin accessibility at STAT3 binding sites, the biological functions of STAT3 are impressively divers (see review by Demaria *et al*., 2014).

Interestingly, however, STAT3 is not only commonly related to a multitude of human malignancies, in which it primarily supports cell survival and proliferation via a HIF1α induction-mediated metabolic switch toward aerobic glycolysis (Demaria *et al*., 2014), STAT3 is also involved in a number of age-associated cellular processes in various different cell types. For instance, activation of STAT3 via JAK, AKT and/or mTOR downstream of insulin/IGF1 signaling is known to mediate immunosuppression, allowing the expansion of senescent cells, and induces insulin resistance via a SOCS-dependent autoregulatory feedback loop. The mechanisms by which STAT3 modulates immunological reactions are manifold and include (i) control over the growth of hematopoietic progenitor cells as well as their myeloid and lymphoid differentiation, (ii) direct regulation of immune-suppressing cell types (*e.g*., activation of regulatory T cells, polarization of macrophages toward an anti-inflammatory phenotype and alteration of the functional response of natural killer cells) inducing the secretion of anti-inflammatory cytokines, ROS and immune checkpoint proteins, and (iii) inhibition of pro-inflammatory NF-κB-dependent signaling via the induction of FOXO proteins (reviewed by Salminen *et al*., 2021). In turn, however, macrophage-secreted factors seem to stimulate NF-κB, STAT1 as well as STAT3 signaling, for instance, in the human kidney, where they corporately induce transcriptomic changes characteristic for kidney aging (O'Brown *et al*., 2015). In *Adgrg6*-mutant mice – a genetic model for endplate-oriented herniations that can lead to late-onset scoliosis – levels of phosphorylated Stat3 are elevated, too, contributing to stiffening of the intervertebral disc and the increased occurrence of herniations (Liu *et al*., 2019). Stat3 was further shown to be involved in age-associated muscle deterioration. Specifically, in the muscle of aged mice, elevation of mTOR leads to increased phosphorylation of Stat3 at serine 727. Stat3 phosphorylation subsequently upregulates Gdf15 expression, which in turn results in activation of Smad3 and Foxo1 signaling, inducing protein ubiquitination, oxidation and finally apoptosis (Tang *et al*., 2019). The aged rat tendon, on the other hand, is characterized by an increase in senescence markers $p16^{INK4A}$, SA-β-gal and SASP genes. Tendon progenitor cells undergo cell cycle arrest in G1 phase, exhibit reduced cell migration and an impaired tenogenic differentiation capacity. Although different from the phenotypes observed in aged muscle cells, also the age-associated phenotypes in tendon cells seem to be mostly dependent on phosphorylation of Stat3, since they can be significantly attenuated by treatment with short-interfering RNAs against Jak2 or Stat3 and pharmacological Jak/Stat pathway inhibition by AG490 (Chen *et al*., 2021). Similarly, in different mouse tissues and human WI38 lung fibroblasts, rapamycin treatment inhibits induction of senescence-associated p16 and p21 via Nrf2-dependent mechanisms, while reducing the number of SA-β-gal-positive cells and SASP levels by decreasing Stat3 phosphorylation (Rong Wang *et al*., 2017). Concordantly, in human endothelial cells, age-associated downregulation of the long non-coding RNA H19 leads to disinhibition of STAT3 phosphorylation, cell cycle arrest in G0/G1 phase and induction of senescence-associated markers such as p21. Functional consequences of these alterations include a reduction of the angiogenic capacity of endothelial cells, as well as their inflammatory activation, allowing tissue infiltration by leucocytes (Hofmann *et al*., 2019). Interestingly, in human colorectal cancer cells, phosphorylated STAT3 binds to the *TERT* promoter, positively regulating telomerase activity – a mechanism that can be inhibited by treatment with resveratrol (Chung *et al*., 2018), which is well known for its anti-aging effects (see review by Pyo *et al*., 2020). Finally, as in most other tissues, expression of Stat3 is up- and levels of its upstream regulator miR-125a-5p down-regulated in the mouse

liver upon aging, and caloric restriction – another potent anti-aging intervention in rodents – elicits opposite trends on miR-125a-5p and Stat3 levels (Makwana *et al*., 2017).

Notably, although these studies collectively suggest that increased Stat3 activity contributes to cell aging in different tissues, Stat3 expression was reported to decline with age in the rat brain (De-Fraja *et al*., 2000). In addition, in aged mouse brains, expression of the nuclear export protein Crm1 is increased, resulting in a redistribution of its target Stat3 to the cytoplasm (Gorostieta-Salas *et al*., 2021). In line with the decrease of Stat3 upon physiological aging in the rodent brain, phosphorylated Stat3 was shown to be reduced in the hippocampus of *klotho*-deficient mice as a consequence of decreased Bdnf levels. In this context, Stat3 reduction leads to impairments in cholinergic neurotransmission and NMDAR-dependent long-term potentiation, thereby contributing to the memory impairments exhibited by this mouse model of premature aging (Park *et al*., 2013). The observed decrease in Stat3 phosphorylation and its downstream effects on cholinergic neurotransmission and memory in *klotho*-mutant mice can be attenuated by theanine, an amino acid in green tea that was reported to exert anti-oxidant and neuroprotective anti-aging effects (Nguyen *et al*., 2019). Concordantly, in PC12 cells *in vitro* and the hippocampus of aging mice *in vivo*, expression of Bdnf, phosphorylated Jak2 and Stat3, as well as Tert are reduced in response to D-galactose-induced injury, leading to neuronal damage and behavioral impairments. These phenotypes can be reversed by treatment with cerebroprotein hydrolysate-I, representing a mixture of porcine brain peptides with anti-inflammatory and neuroprotective attributes (Zhu *et al*., 2021). Although these reports could altogether indicate that in the CNS, seemingly different from most other organ system, aging is associated with a decrease of STAT3 signaling, other studies seem to contradict this assumption. For example, during the last decade, several genomic studies and associated meta-analyses performed on blood and/or brain cells linked the upregulation of STAT3 pathway activity to aging *per se*, as well as the development of AD specifically (Xinzhong Li *et al*., 2015; Lanke *et al*., 2018; Tang & Liu, 2019). Moreover, in microglia-like mouse BV2 and neuron-like rat PC12 cells, the most abundant, blood-brain barrier-permeable cholesterol oxidation product, 27-hydrocycholesterol, increases phosphorylation as well as acetylation of Stat3 by reducing the expression of Stat3-inhibiting Sirt1, leading to a senescent-like phenotype characterized by increased expression of *Il6* and SA-β-gal. Mechanistically, Sirt1 inhibition by 27-hydrocycholesterol is attributable to increased levels of Dnmt1 and ROS, and can be attenuated by treatment with resveratrol. Importantly, also in zebrafish larvae *in vivo*, 27-hydrocycholesterol induces ROS production, downregulation of *Sirt1* and *Il6*, and an increase in SA-β-gal, resulting in the emergence of age-associated locomotor deficits that can be rescued by treatment with ROS-scavenging N-acetylcysteine or resveratrol (Jiao Liu *et al*., 2021). Lastly, in murine hippocampal NSCs, the age-associated decrease of the posttranslational modification O-linked β-N-acetylglucosamine at threonine 717 of Stat3, increasing Stat3 phosphorylation and the expression of Stat3 downstream targets like *Cdkn1a*, contributes to reduced NSC proliferation and a switch from neurogenic to gliogenic differentiation. In this model, different from what is observed in *klotho*-mutant mice, increased Stat3 phosphorylation was reported to ultimately result in altered mouse behavior associated with impaired hippocampal learning and memory (White *et al*., 2020).

In light of our experimental setup, it is important to note that studies in several different cell types, such as human normal kidney as well as breast and lung cancer cells, identified STAT3 as a potent inducer of SOX2 and/or cMYC expression (O'Brown *et al*., 2015; Zhao *et al*., 2015; Dittmer & Dittmer, 2020). Especially SOX2 seems to in turn also increase levels of phosphorylated STAT3, forming a positive regulatory feed-forward loop in cancer cells (Zhao *et al*., 2015; Dittmer & Dittmer, 2020). Although orchestrated expression of SOX2 and STAT3 is often

described in the context of cancer, it seems to be important for physiological nervous system development, too. For example, more than 10 years ago, it was already demonstrated that co-localized expression of phosphorylated Stat3 and its transcriptional downstream target Sox2 is required to induce expression of the NSC marker Nestin in mouse ESC-derived EBs *in vitro* as well as mouse embryos *in vivo* (Foshay & Gallicano, 2008). In addition, the process of differentiating human iPSCs into NSCs and finally mature neurons was recently dissected in depth using trajectory analysis of DNAm signatures and subsequent gene-gene network interaction analysis, identifying a single strongly connected network component in which *STAT3* represented the gene with the highest connectivity (Imm *et al*., 2021). This is well in line with a full body of literature describing the relevance of STAT3 signaling for the maintenance of a pluripotent state as well as neural and especially glial development. Notably, JAK-STAT signaling is potently induced by LIF, which is also a key component of our iNSC conversion and expansion medium. While STAT3 typically forms an auto-regulatory negative feedback loop via SOCS3, it at the same time promotes its own expression by the induction of *STAT3* and *JAK1*, but also the LIF signal transducer *LIFR* and its co-receptor *GP130*. This complex, partially LIF-dependent autoregulation is thought to be crucial for safeguarding the developmental timing-sensitive expression dynamics of STAT3 (reviewed by Onishi & Zandstra, 2015).

Together, these studies demonstrate that besides its implications in aging and cancer, STAT3 is also highly relevant for normal embryogenesis and neural lineage progression. Especially considering its interplay with SOX2 and LIF, future studies should attempt to shed light on the relevance of STAT3 signaling for iNSC transdifferentiation as such, as well as its specific implications for the cellular rejuvenation process elicited by this cell fate conversion paradigm. In this context, it seems interesting to investigate how total expression levels of STAT3 and STAT3 phosphorylation change depending on time in conversion and LIF exposure, and whether or not manipulation of STAT3 signaling in the course of the conversion process would have an impact on the dynamic of DNAm age changes.

4.1.2.3. SOX2 and cMYC: Inducers of transdifferentiation and/or rejuvenation?

Although the mechanism underlying the reset of biological age still remains to be unveiled, our data could potentially indicate that the observed epigenetic rejuvenation upon iNSC conversion might somehow be triggered by changes in SOX2 and/or cMYC expression and their subsequent impact on STAT3 signaling during the early phase of transdifferentiation. Since iN conversion does, in contrast, preserve aging signatures, it would thus be expected that SOX2, cMYC and/or STAT3 are not majorly altered during iN transdifferentiation. Khazaei *et al*. performed a comparative analysis of DEGs using eighteen independent microarray and RNA sequencing datasets derived from studies directly converting mouse or human fibroblasts into either iNSCs, iNs, astrocytes or OPCs, and subsequently identified TFs involved in the regulation of DEGs that were commonly altered within a given scenario. Congruent with our hypothesis, *Sox2* and *Myc* were both central TFs for the conversion of mouse fibroblasts into iNSCs, whereas they were not among the regulators of fibroblast-to-iN conversion (Khazaei *et al*., 2018). This report is in line with a previous study performed by the same lab that already identified SOX2 as a key regulatory TF and protein complex for the direct conversion of human endothelial-like cells into iNSCs (Omrani *et al*., 2018).

In light of these reports, we became interested to find out whether the TFs SOX2 and/or cMYC might also be included in alternative direct conversion paradigms yielding rejuvenated NSCs. To this end, we screened published literature on iNSC conversion for publications providing publicly available DNAm data amenable to DNAm age prediction, identifying only one data set that seemed suitable for comparison. This data set was provided by Thier *et al*., comprising DNAm data of adult human fibroblasts, neural plate border stem cells (NBSCs) transdifferentiated thereof via overexpression of the TFs BRN2, KLF4, SOX2 and ZIC3, as well as iPSC-derived NBSCs (Thier *et al*., 2019). Using two different algorithms to predict the DNAm age of these samples (Horvath, 2013; Horvath *et al*., 2018), we found that while the source fibroblasts were predicted to be mid-age (46-48 years for Horvath, 2013, and 33-38 years for Horvath *et al*., 2018), both iPSC-derived as well as directly converted iNBSCs exhibited reset DNAm ages (1-2 years for Horvath, 2013, and 0.4-0.8 years for Horvath *et al*., 2018; data not shown). This finding emphasizes that not only blood-to-iNSC but also fibroblast-to-iNBSC transdifferentiation is associated with an epigenetic rejuvenation process, as indicated by a significant decrease of the cell populations' DNAm ages. Although further studies need to thoroughly investigate whether both conversion paradigms indeed induce or converge on a shared mechanism that then causes the observed epigenetic age reset, it might be a precedent-setting fact that SOX2 is the only TF that is commonly overexpressed in both conversion paradigms.

Following up on the idea that SOX2 and/or cMYC might be capable of mediating epigenetic rejuvenation (either themselves or via STAT3), we performed preliminary experiments assessing DNAm changes upon SeV-mediated overexpression of these two TFs, alone or in combination, in human primary fibroblasts. Concordant with published data, uninfected fibroblasts showed a DNAm age increase of around 1 year per week in culture (~ 0.86 years/week in our experiment vs. ~ 1.15 years/week in Sturm *et al*., 2019). While 5-week-long overexpression of cMYC alone and SOX2 plus cMYC only marginally reduced the observed increase in DNAm age, overexpression of SOX2 alone tended to slightly reduce the DNAm age of *in vitro* proliferated fibroblasts. Notably though, expression levels induced by SeV-mediated TF overexpression were considerably lower in fibroblasts than SeV-positive iNSCs. Currently, we can thus only speculate about the relationship between the respective TF expression levels and their impact on DNAm age in different cellular systems.

Notwithstanding that these data altogether are certainly not yet solid enough to postulate that overexpression of any of these two TFs might suffice to achieve somatic cell rejuvenation – at least in neural cells – it should be mentioned that SOX2 and cMYC are not only key players in iNSC conversion as well as iPSC reprogramming, they are also themselves linked to some age-relevant pathways and convey significant epigenetic remodeling. Myc, for instance, regulates Sirt1 in a p53-dependent manner in various mouse and human cell lines (Yuan *et al*., 2017). This axis might be especially interesting given that OCT4 in turn inactivates p53 through SIRT1-mediated deacetylation in human ESCs (Zhang *et al*., 2014). Klf4 is also able to repress p53 by direct promoter interaction, but at the same time induces the p53 target p21 in immortalized mouse cells (Rowland *et al*., 2005). Additionally, KLF4 mediates p53 target specificity by increasing the DNA binding affinity of p53 (Brandt *et al*., 2012). Next to its association with Sirt1/p53 signaling, cMyc significantly regulates transcriptional expression of a large number of its target genes by various epigenetic mechanisms (reviewed by Amente *et al*., 2011), including coordinated histone acetylation and upregulation of H2A.Z on targeted promoters (Martinato *et al*., 2008). SOX2 likewise significantly mediates its regulatory effects via epigenetic mechanisms. Bertolini *et al*. profiled Sox2-bound regions in neurospheres derived from primary mouse brains on a genome-wide scale by chromatin immunoprecipitation and chromatin interaction analysis, revealing that RNA polymerase II-mediated long-range

promoter-to-enhancer interactions mainly account for Sox2's regulatory effects on transcription (Bertolini *et al*., 2019). Moreover, Sox2 was recently shown to be able to protect its target genes from methylation, and even induce passive DNA demethylation of methylated target genes in mouse ESCs. Most interestingly, Sox2 mediates its demethylating effect via counteracting DNAm maintenance during replication by inhibiting Dnmt1 activity (Vanzan *et al*., 2021). Again, STAT3 might shine up here as a potential candidate, since – although not experimentally addressed in these studies – it cannot be excluded that some of the described effects of SOX2 and/or cMYC are to some degree mediated by STAT3, considering the involvement of some shared signaling hubs such as DNMT1, SIRT1 and p53.

In this context, it seems relevant to mention that mouse cells were very recently shown to exhibit a constant decrease in DNAm age from the time of conception on up until approximately E6.5/E7.5 (*i.e*., around the time of gastrulation), only after which epigenetic aging starts. Although these epigenetic dynamics during embryogenesis are probably not comparable to postnatal aging and the somatic rejuvenation of genuinely old cells, two findings of this study are especially noteworthy: First, while epigenetic ages are comparable in wild-type embryos and Tet1/2/3 triple-knockouts at E6.5, both global DNAm and the estimated epigenetic age are increased in Tet-deficient ESC-derived EBs, equaling to E7 epiblast/E8 mesoderm stage, as compared to respective controls. Second, the epigenetic age of Dnmt1- and Dnmt3-deficient embryos was found to be higher than that of controls at E8.5. Kerepesi *et al*. proposed that these observations could be concordant with a model in which epigenetic rejuvenation occurs in two phases, namely a short induction of demethylation resulting in the removal of epigenetic damage, that is followed by *de novo* methylation (Kerepesi *et al*., 2021). As such, the exogenous overexpression of SOX2 could indeed represent a potent inducer for the initiation of epigenetic rejuvenation within our conversion system, allowing subsequent remodeling of cellular aging signatures in a SOX2-dependent or even -independent manner.

Altogether, published data as well as our own preliminary experiment addressing SOX2 and cMYC overexpression in fibroblasts could indicate that induction of SOX2 might be more likely to initiate a potential cellular rejuvenation process than ectopic expression of cMYC. This idea is supported by the observation that downregulation of Myc ameliorates aging in mice. Specifically, heterozygous deletion of Myc, leading to reduced Myc expression levels and DNA binding of Myc target genes, results in significantly increased lifespans. This is accompanied by reduced Igf1 serum levels, decreased body size as well as mass, and improved health of several tissues upon physiological aging. Mechanistically, Hofmann *et al*. could attribute the longevity-promoting effect of Myc inhibition to transcriptomic changes in the regulation of lipid metabolism and the immune system. Moreover, $Myc^{+/-}$ mice were reported to exhibit more active behavior, causing an increase in food and water consumption, as well as metabolic rates overall. On a cellular level, this altered metabolic state was shown to be reflected by a lower energy status and a decrease in protein translation. Notably, neither the amount of oxidative stress or age-associated DNA damage accumulation, nor the degree of age-induced apoptosis or tissue senescence were found to be influenced by heterozygous *Myc* deletion (Hofmann *et al*., 2015).

In light of the idea that SOX2 might be able to trigger the reset of aging signatures, at least within the context of cell programming, one key question remaining is whether cellular rejuvenation can at all be uncoupled from the process of changing cell fates. A study performed by Wolfgang Wagner and his team in 2018 initially argued against this assumption: While transfection of episomal vectors coding for OCT3/4, KLF4, SOX2, L-MYC, LIN28

and shRNA against p53 in human mesenchymal stromal cells (MSCs) under PSC culture conditions led to the derivation of iPSCs with a reset epigenetic senescence signature, epigenetic rejuvenation was not achieved when transfected cells were maintained under culture conditions that did not promote the establishment of a pluripotent state (Göbel *et al*., 2018). Yet, Sarkar *et al*. more recently investigated the consequences of interrupted reprogramming using short-term mRNA transfection of OCT4, KLF4, SOX2, cMYC, LIN28 and NANOG in human fibroblasts and endothelial cells yielding contradicting results. Although this short-term treatment did not affect cell identity and, if at all, only marginally reduced DNAm ages, it sufficed to reset a number of age-related cellular hallmarks: (i) Transcriptomic signatures of treated aged cells more closely resembled that of young cells than the transcriptome of their untreated aged counterparts. (ii) Decreased nuclear expression of H3K9me3, HP1γ and LAP2α in untreated old cells was reverted upon mRNA transfection to levels detected in young cells. (iii) Autophagosome formation and proteasomal activity were restored in old cells after treatment. (iv) An increase in mitochondrial membrane potential, decreased mitochondrial ROS production and upregulation of SIRT1 indicated that age-associated mitochondrial dysfunctions were mitigated by interrupted programming. (v) Endothelial cells but not fibroblasts further exhibited a decrease in SA-β-gal expression and SASP. Furthermore, the rejuvenating capacity of the short-term expression of iPSC reprogramming factors was demonstrated by successfully treating human chondrocytes from patients suffering from osteoarthritis, as well as conducting transplantation experiments demonstrating the improved regenerative capacity of mRNA-treated mouse and human muscle stem cells (Sarkar *et al*., 2020). These finding are thus in line with previous reports from the group of Juan Carlos Belmonte, demonstrating that short-term cyclic expression of Oct3/4, Sox2, Klf4 and cMyc *in vivo* does not lead to the establishment of a stable pluripotent fate, but can increase the regenerative capacity of multiple organs in physiologically aged mice and promote cellular rejuvenation in progeria mice suffering from premature aging (Ocampo *et al*., 2016). Accordingly, developing a better understanding of the mechanisms underlying specific conversion trajectories could be essential in order to extract and untangle what drives cell fate changes and what instructs cellular rejuvenation. This could eventually allow us to not only fully exploit this emerging technology for biomedical research and therapy, but additionally create a foundation for novel strategies seeking the fountain of youth.

4.2. The pros and cons of grafting directly converted neural cells

4.2.1. Tumorigenicity, genomic stability and immunological considerations

Clinical application of PSCs and their neural derivatives has long been compromised by safety concerns regarding their tumorigenic potential and immunogenic properties (reviewed by Tapia & Schöler, 2016 and Xin Liu *et al*., 2017). In 2009, Shinya Yamanaka's team evaluated the tumor-forming propensity of a wide variety of mouse PSC-derived secondary neurospheres (ESC- and iPSC-derived, with iPSC lines of diverse somatic origins, additionally representing different techniques used for iPSC reprogramming) upon transplantation into the murine CNS. The authors revealed that the PSC-derived neurospheres not only significantly differed in their capacity to promote tumor formation, but also in the degree of contamination with remaining undifferentiated PSCs within the neurosphere. Notably, both variables were affected by the PSC lines' somatic origin, with iPSC clones stemming from adult mouse tail tip fibroblasts exhibiting the highest amounts of undifferentiated iPSCs as well as the highest

propensity to form tumors upon transplantation (Miura *et al*., 2009). Regarding the clinical use of iPSC derivatives, these observations already argued for the necessity to (i) carefully consider the choice of the iPSC reprogramming technique and (ii) rigorously assess the purity of the differentiated cell product prior to cell transplantation. Despite this call for caution, approximately 5 % of around 250 PSC lines – some of which were indeed even produced for clinical application – were later found to carry *TP53* mutations after prolonged *in vitro* cultivation (Merkle *et al*., 2017), illustrating that additional measures such as comprehensive genome-wide sequencing are mandatory to ensure the safety of PSC lines intended for clinical application. These prerequisites might necessitate the selection of few PSC lines, which can be produced, banked and comprehensively quality controlled in big batches, and afterwards transplanted in an allogeneic rather than autologous setting. Following such an approach, banking iPSC lines of different major histocompatibility complex (MHC) haplotypes might be endorsed, since grafting of MHC-matched cell products was shown to dampen the immune response and increase the survival of iPSC-derived dopaminergic neurons after neurotransplantation in a non-human primate model (Morizane *et al*., 2017).

Importantly, the concerns of tumorigenicity and immunogenicity seem to be much less relevant for the transplantation of directly converted cells. Since iNs are probably not well suited for neuroregenerative approaches due to limitations associated to scalable production as well as the significant degree of cellular age preservation and, thus, increased susceptibility to disease-causing signals, iNSCs are more of interest to this biomedical application. Indeed, iNSC transplants do not seem to exhibit considerable overgrowth or tumor-forming capacities, most likely because direct conversion-derived cell products lack contaminating, undifferentiated PSCs. In 2012, Ring *et al*. transplanted both, iPSC-derived and directly converted NSCs into the CNS of mice. While the latter population did not form tumors at all, more than 60 % of all mice developed tumors after grafting iPSC-derived NSCs (Ring *et al*., 2012). In our own experiments, we also did not observe tumors in any animal receiving iNSC transplants. Interestingly, we further noticed that the grafts of our previous studies using PSC-derived NSCs (Doerr *et al*., 2017) were considerably larger than those generated by iNSC transplantation, despite stereotactically injecting approximately the same number of neural progenitors. This indicates that iNSCs might exit the cell cycle much faster post grafting than PSC-derivatives. This assumption is supported by the observation that proliferative Ki67-positive cells can be detected up to 12 weeks after transplantation of ESC-derived NSCs (Steinbeck *et al*., 2012), whereas we could not detect any Ki67-positive cells as early as 2 weeks after iNSC transplantation (data not shown). Considering that it is preferable to graft cells close to the timepoint of cell cycle exit (see review by Thompson & Björklund, 2015), this feature could make transplantation of iNSCs superior to the transplantation of PSC derivatives, including PSC-derived NSCs as well as more mature neurons (*e.g*., derived via forward programming). Nevertheless, also transdifferentiated cells would need to undergo rigorous QC prior to application, including the assessment of genomic integrity. Accordingly, iNSCs destined for clinical application should be transgene-free upon transplantation, which precludes the use of conversion factor delivery systems that are stably integrating into the host genome. To this end, it is worth mentioning that other experimental tools than classical retroviral or lentiviral systems have already been employed for the delivery of TFs or activation of endogenous reprogramming-inducing genes. These include non-integrating viruses (Meng *et al*., 2012; Lu *et al*., 2013; Tongguang Wang *et al*., 2013; Castaño *et al*., 2014; Lau *et al*., 2014; Sheng *et al*., 2018), plasmids and episomal vectors (Adler *et al*., 2012; Lihui Wang *et al*., 2013; Xu *et al*., 2014; Zhu *et al*., 2014; Liao *et al*., 2015; Capetian *et al*., 2016; Kim *et al*., 2016; Tang *et al*., 2016), pro-neural exosomes released upon ultrasound stimulation (Lee *et al*., 2018), mRNAs (Bo Eun Kim *et al*., 2018; Connor *et al*., 2018; Kang *et al*., 2019; Monk *et al*., 2021) and

microRNAs (Yoo *et al*., 2011), proteins (Maucksch *et al*., 2012; Mirakhori *et al*., 2015) or even transdifferentiation paradigms based solely on chemical cocktails (Cheng *et al*., 2014; Feng *et al*., 2014; Hu *et al*., 2015; Xiang Li *et al*., 2015; Zhang *et al*., 2016; Zheng *et al*., 2016; Han *et al*., 2016; Kim *et al*., 2016; Park *et al*., 2017; Tang *et al*., 2018; Yang *et al*., 2019; Xu *et al*., 2019; Qin *et al*., 2020). Lastly, it is important to point out that due to the comparably short time frames required for transdifferentiation, it is conceivable that directly converted cells are much better suited for autologous transplantation, eliminating the need for generating large MHC haplotype banks and/or long-term administration of immunosuppressants after cell therapy.

4.2.2. Graft functionality and its capability to integrate into pre-established neuronal networks

Despite these advantages, our study is the first to our knowledge attempting to show that human iNSCs can not only survive and differentiate into electrophysiologically functional neurons *in vivo*, but might potentially even be able to establish synaptic connections to the adult mouse brain after transplantation. Specifically, we observed robust survival of striatal iNSC grafts after 24 weeks post transplantation, which even tended to increase in size over time, whereas graft volumes of hippocampal transplants seemed to decrease after prolonged time *in vivo*. This observation is in line with previous reports published by our lab and others about (i) increasing graft areas of striatal human ESC-derived dopaminergic neuron transplants due to progressive dispersion of grafted neurons into the host tissue, reaching a steady-state only after 180 days of *in vivo* maturation (Piao *et al*., 2021), and (ii) steadily declining hippocampal graft volumes after transplantation of ESC-derived NSCs from 3 to 48 weeks post transplantation (Steinbeck *et al*., 2012). Furthermore, also our finding that NSC differentiation is highly biased toward a neuronal phenotype at the hippocampal transplantation site, giving rise to mostly neurons, very few astrocytes but no oligodendrocytes, is concordant with a previous report of our lab on the differentiation capacity of transplanted iPSC-derived lt-NES cells (Steinbeck *et al*., 2012).

Using pRABV-based monosynaptic tracing, we next identified single GFP-positive mouse neurons distant from the graft core, which could represent host neurons synaptically connected to the human iNSC graft. Notably, however, since some GFP-positive cells were also found in control experiments, injecting pRABV-GFP after transplantation of wild-type iNSCs (*i.e*., iNSCs lacking relevant pRABV system components), we cannot rule out that at least a fraction of these GFP-labelled mouse neurons were actually not synaptically connected to graft-derived neurons but rather illustrate off-target effects of the pRABV virus. Yet, we would expect that in the presence of cells harboring receptors for the pRABV, off-target infections are less frequent than under conditions in which no cell population in the xenogeneic brain is readily susceptible to the pRABV. In order to verify this assumption, additional control experiments employing transplantation of iNSCs that are equipped with the pRABV receptor but not the for the synaptic transmission of pRABV critical glycoprotein should be performed next. Assuming we would be able to corroborate our hypothesis that off-target viral infections are prevented – or at least reduced – in the presence of pRABV receptor-expressing cells, our data could suggest that murine host neurons are indeed capable of forming functional synapses onto grafted iNSC-derived cells. Although we have not yet performed experiments addressing the possibility that these GFP-positive cells might then derive from host-graft cell fusion events (see review by Thompson & Björklund, 2015), the facts that cell fusion was not observed after grafting lt-NES cells (Steinbeck *et al*., 2012) and that the more comprehensively characterized GFP-positive cells

in the present study were not only hN- but also RFP-negative and not bi-nucleated, argue against this option. Sticking with our current assumption that the detected GFP-positive cells outside the graft indeed represent connected host neurons, it appears, on the first sight, as if the afferent innervation of human transplants is increased for ESC-derived cells (Doerr *et al*., 2017) as compared to grafted iNSCs. A simple comparison of the number of connected host neurons could be invalid though, since the number of available human input neurons for pRABV-based tracing, as well as the coverage of the transplant with pRABV, seems to differ substantially between both setups. One reason for the increased graft volume in Doerr *et al*., 2017, albeit transplanting approximately the same amount of cells (40,000 or 60,000 cells in Doerr *et al*., 2017 vs. 50,000 cells in the present study), could be the potential existence of proliferative, differentiation-resistant NSCs and/or neuronal precursors *in vivo* after transplantation of PSC-derived NSCs, which – in the absence of histological tumor formation – has already been described for other human iPSC-derived cell preparations (Tanimoto *et al*., 2020). Thus, highly elaborate stereological quantification methods should prospectively be implemented for calculating the ratio of input-to-output neurons across the whole xenografted mouse brain, shedding light on the degree of network integration that is actually achieved by iPSC-derived and directly converted NSC transplants.

In this study, we further investigated the axonal projection patterns of human iNSC transplant-derived neurons. While striatal neurons in the rodent brain physiologically project via the globus pallidus and the subthalamic nucleus to the substantia nigra (Fishell & Van Der Kooy, 1991), human NCAM-based tracing of striatal iNSC-derived graft efferents revealed only very little innervation of the globus pallidus and no fibers were detected in the latter two structures. Notably though, also transplants composed of fetal rat striatal tissue placed into the striatum of ibotenic acid-lesioned adult rats do not extend fibers to the substantia nigra even 3.5 to 20 months post transplantation. In addition, after injecting Fluoro-Gold into the ipsilateral pallidus, the number of retrogradely labelled neurons in these fetal tissue grafts was found to only account for 12 % of the number of neurons that innervate the pallidus in the intact rat caudate-putamen (Wictorin *et al*., 1989). Similar innervation patterns were obtained after grafting striatal tissue extracted from embryonic mice into the striatum of ibotenic acid-lesioned rats. In these experiments, fibers were additionally found to project through the corpus callosum, particularly if striatal grafts extended through the corpus callosum into the overlying cortex (Wictorin *et al*., 1991) – an observation that was also made in the course of this study. Altogether, these findings indicate that the rather limited recapitulation of physiological-like striatal projection patterns might not be exclusive for iNSC-derived grafts, but could be generally attributable to this specific transplantation site. Accordingly, in contrast to our observations in the striatum, after transplantation of iNSCs into the hippocampal dentate gyrus, graft-derived efferents seemed to be largely region-appropriate, albeit the extent and speed of host brain innervation might lack behind that of lt-NES cell grafts. Specifically, Steinbeck *et al*., 2012 detected some human axons projecting to the hippocampal pyramidal cell layer of the contralateral hippocampus via the fimbria already 3 months after transplantation. Although we could similarly observe projections to the CA3 region within the ipsilateral hemisphere as early as 10 weeks after iNSC transplantation, fibers did not reach the contralateral hemisphere within our 24 week-long observation period.

Lastly, performing electrophysiological characterization of graft-derived neurons, we revealed that transplanted iNSCs can give rise to neurons capable of firing APs and receiving synaptic input as evidenced by the recording of sPSCs. Importantly, the extent of electrophysiological maturity needs to be further investigated though, since our experiments also revealed downregulation of GFP, which was used to identify human neurons during patch

clamping of acute brain slices, upon *in vivo* maturation – a phenomenon known from former studies using GFP-expressing transgenic reporter mice (see review by Thompson & Björklund, 2015). For future experiments, we therefore suggest to engineer iNSCs to express GFP from the neuronal synapsin instead of the ubiquitous EF1α promoter, in order to be able to deeply characterize mature neuronal properties after transplantation of iNSCs into the murine CNS.

Finally, it has to be noted that we cannot exclude that the integrative capacity of iNSCs after transplantation into the adult mouse striatum and hippocampus might have been hampered by their non-orthotopical, posteriorized regional and/or subtype identity. Ai *et al*., who transplanted differently patterned monkey fibroblast-derived iNSCs into the adult monkey striatum or prefrontal cortex, reported that robust graft survival could only be achieved, if the regional phenotype of iNSCs matched the respective transplantation site (Ai *et al*., 2016). This is in line with the most prevalent view to date that brain region-specific neural connectivity requires a matched neuronal subtype identity (compare, for instance, Espuny-Camacho *et al*., 2013 and others). However, the fine-tuning of NSC identity is much less advanced for direct conversion approaches than for differentiation paradigms starting from PSCs. Although the generation of region-defined NSC subtypes via transdifferentiation might prospectively be achieved by additionally employing region-specific TFs for direct conversion – to some degree paralleling developments in the field of iPSC forward programming – this aspect represents a hurdle that still needs to be overcome on the route to clinical translation.

In sum, while we believe that our study provides exciting first evidence for the general capacity of human iNSCs to functionally mature and establish synaptic connections within the murine host brain, it is hard to conclude at this point already whether or not the extend of innervation achieved by iNSC transplantation is comparable to what PSC-derived grafts can yield. In this context, it is also relevant to remember that our study was performed using unlesioned mice as graft recipients. However, it seems that the lesioned CNS possesses an increased regenerative capacity (compare, for example, Buffo *et al*., 2005; Grande *et al*., 2013), which could facilitate the integration of *in situ* converted as well as transplanted cells after depletion of host equivalents. Performing transplantation experiments in a disease or CNS lesion context, further offers the possibility to implement sophisticated read-out methods for assessing the capacity of grafted cells to restore neuronal circuitry and contribute to behavioral recovery, as was impressively demonstrated by the groups of Malin Parmar and Lorenz Studer in the context of PD. For example, pRABV-based monosynaptic tracing was implemented to characterize afferent and efferent graft innervation patterns after transplanting human ESC-derived dopaminergic precursors into the striatum of 6-OHDA-lesioned rats, revealing that established local as well as long-range projection circuitries resemble endogenous patterns (Grealish *et al*., 2015). Likewise, human NCAM fiber tracking and pRABV-based transsynaptic tracing demonstrated that human ESC-derived dopaminergic precursors, grafted to the midbrain of parkinsonian rats, progressively innervate appropriate forebrain target structures and receive nigral afferents resembling the physiological circuitry, respectively. Most interestingly, the time dynamic of graft-derived efferents reaching the dorsolateral striatum matched behavioral improvements in amphetamine-induced rotations, suggesting a causal relation of both observations (Cardoso *et al*., 2018). This notion is further supported by the finding that optogenetic silencing of graft-derived dopamine-releasing neurons – originating from human ESC-derived dopaminergic neuronal progenitors transplanted into the striatum of adult 6-OHDA-lesioned mice, which progressively innervate the dorsolateral host striatum after grafting – completely abrogates the behavioral recovery otherwise observed in freely-moving animals (Steinbeck *et al*., 2015). Accordingly, future studies should continue

addressing the therapeutic potential of iNSCs within CNS lesion and/or disease models, simultaneously providing mechanistic insights into how these cells contribute to neuroregeneration. A better understanding of these complex processes is certainly needed before directly converted NSCs could eventually replace PSC-derived cell products for clinical use.

4.3. Microglia-derived NSCs: Prospects for neuroregeneration

Microglia – the immune cells of the CNS – plastically and efficiently respond to cerebral injury by inducing proliferation and exerting pro- or anti-inflammatory effects, depending on the cellular context. Next to their immunomodulatory function, brain-resident microglia help maintaining CNS tissue homeostasis by several mechanisms, including the clearance of cellular debris by phagocytosis, the modulation of neurotransmission by synaptic pruning as well as controlling the turnover of neuromodulators and myelination, and the influencing of cell fate decisions (reviewed, for example, by Wright-Jin & Gutmann, 2019). Notably, however, inappropriate immune responses conveyed by dysfunctional and/or aged microglia were shown to be detrimental to tissue recovery and are thought to significantly contribute to various neurological and neurodegenerative diseases (see also reviews by Mecca *et al.*, 2018 and Tan *et al.*, 2020). Our data indicate that human iPSdMiG can be converted into tripotent iNSCs *in vitro* using the SeV-SOX2- and SeV-cMYC-based conversion system we originally developed for blood-to-iNSC conversion with slight modifications. Importantly, we obtained similar data using unsorted and CD11b-purified iPSdMiG as starter populations. This finding strongly suggests that CD11b-positive microglia, but not co-developing neural cells, are the source of neuroepithelial colonies arising within 2 weeks after SeV infection, and we are currently working on prospectively reinforcing this conclusion by the implementation of a genetic construct allowing microglial lineage tracing.

4.3.1. Using transgenic iPSC-derived microglia as a Trojan horse for wide-spread delivery of neural conversion-prone cells to the brain

To our knowledge, we are the first to report about transdifferentiating human microglia into neural cells *in vitro* – a strategy that might have the makings to become a reasonable alternative for biomedical application, being exploitable in at least two distinct ways: On the one hand, we expect that one could make use of the significant migratory potential microglia are endowed with. Over the years, several models have been developed exhibiting a significant degree of chimerism after localized intracerebral transplantation of human PSC-derived primitive macrophage/microglia precursors into neonatal mice. In these models, transplanted precursors consistently and predominantly mature into homeostatic microglia that (i) transcriptionally highly resemble adult human microglia, (ii) widely distribute throughout the host brain by migration, and (iii) functionally engage in, for example, synaptic pruning and the immune response to lipopolysaccharide challenge (mimicking bacterial infection), cuprizone-induced demyelination (being a mouse model of multiple sclerosis) as well as injected oligomeric amyloid-β (as a mouse model for AD; Mancuso *et al*., 2019; Svoboda *et al*., 2019; Ranjie Xu *et al*., 2020). As an alternative to invasive intracerebral transplantation or the targeted destruction of the blood-brain barrier, which would allow blood-derived macrophages to invade the brain, the group of Alexandra Stolzing explored intranasal as well as intravenous application of *in vitro*-derived microglia-like cells as delivery routes to the CNS. Specifically,

microglia-like cells derived from the bone marrow of young (3 months old) or aged (> 12 months old) mice were nasally or systemically applied to differentially aged recipient animals, and their biodistribution was assessed 10 and 28 days after administration. After 10 days, microglia were detected in the cortex, cerebellum and hippocampus, but also in the blood and in submandibular as well as axillary lymph nodes of mice receiving either intranasal or intravenous microglia transplantation. The latter application route also distributed microglia to the mouse lung and kidney. After 28 days, old donor-derived microglia were neither detectable in young nor aged recipients. Conversely, young donor-derived microglia applied to aged recipients were still persistent in the cortex, olfactory bulb or brain stem, as well as peripheral organs (Leovsky *et al*., 2015). Notably, the bone marrow origin of the microglia-like cells transplanted by Stolzing and colleagues might have contributed to their distribution into peripheral organs. It was previously shown that while intravenously injected spleen-derived primary mouse macrophages populate peripheral tissues and lymph nodes but not the brain within 6 days after application, mouse ESC-derived microglia transplanted via the same route are primarily found in the corpus callosum and hippocampus of mice but very rarely in the periphery (Tsuchiya *et al*., 2005). Very recently, Parajuli *et al*. reported that also human IBA1- and Stem121-positive iPSdMiG are able to invade the cortex, hippocampus and cerebellum of adult immunocompetent mice after transnasal transplantation, but only survive for longer periods of time within the latter two brain regions (Parajuli *et al*., 2021).

Nevertheless, these and other reports addressing the migratory potential of exogenously applied (human) microglia, for instance after stroke (Narantuya *et al*., 2010), strongly encourage us to next explore whether rejuvenated iPSdMiG are able to home the CNS of adult mice after stereotaxic intracerebral transplantation and/or peripheral application. If so, engineering patient-derived iPSCs to harbor inducible transgene cassettes instructing iNSC conversion before clinical application of the migratory iPSdMiG derived thereof, could represent an attractive alternative to conventional cell transplantation – especially considering their potential for treating non-localized lesions affecting various parts of the brain. In preparation for such experiments, we have meanwhile equipped human iPSCs with a DOX-inducible expression cassette encoding the two TFs SOX2 and cMYC (data not shown), and are currently in the process of generating larger quantities of SOX2-cMYC-equipped iPSdMiG, presumably representing conversion-amenable cells (*i.e*., 'convertibles'). We aim to use these cells for firstly demonstrating the principal feasibility to transdifferentiate convertibles via DOX application *in vitro*, and then secondly translating this system to the *in situ* iNSC conversion of transplanted human iPSdMiG-convertibles in the adult mouse brain. Notably, in the tissue context, it could become critical that the efficacy of brain chimerization after intravenous and intracerebral application of bone marrow- or blood-derived precursor cells and microglia, respectively, has been shown to depend on the availability of a microglia-free niche, for instance, by ablation of endogenous, brain-resident microglia (Zhen Xu *et al*., 2020). Nonetheless, we propose that this approach represents a promising strategy for autologous clinical application of miciNSCs for treating non-localized cell loss, as is encountered in neurodegenerative diseases such as AD.

4.3.2. Targeting endogenous microglia for *in vivo* neural conversion

Experiments addressing the *in situ* convertibility of transplanted iPSdMiG could provide valuable insights into the general feasibility to transdifferentiate human microglia into neural cells in a native brain environment. Along this line, yet as an alternative to this specific route, endogenous microglia could prospectively be directly targeted to

convert into iNSCs *in vivo*. The general feasibility of transdifferentiating brain-resident microglia was already suggested by Matsuda *et al*. in 2019, who reported the Neurod1-mediated conversion of adult striatal mouse microglia into neurons. Specifically, the authors described that lentiviral infection using a CD68 promoter-driven construct, targeting around 60 % of Iba1- and Tmem119-co-expressing microglia in control experiments, converts around 75 % of all Neurod1-transduced cells into Darpp32-positive MSNs. These microglia-derived neurons were even reported to generate APs and sPSCs 4 weeks post transduction (Matsuda *et al*., 2019). Notwithstanding the fact that, as discussed earlier, the results of this study have recently been challenged (Rao *et al*., 2021), several biological as well as methodological aspects would first need to be addressed before our own microglia-to-iNSC approach could eventually be translated to a clinically applicable *in vivo* scenario.

First, it still has to be demonstrated that not only iPSdMiG, but also primary human microglia are amenable to transdifferentiation. To this end, we are currently preparing *ex vivo* experiments converting primary microglia, which are isolated from surgical specimens retrieved from patients undergoing tumor resection or hippocampectomies, into iNSCs *in vitro*. Interestingly, human adult astrocytes isolated from various brain regions were shown to be differentially prone to NGN2- as well as ASCL1-mediated neuronal conversion (Hu *et al*., 2019), and microglia are likewise known to exhibit regional heterogeneity (reviewed by Tan *et al*., 2020). Therefore, experiments with freshly isolated primary cells should, if possible, simultaneously address the questions whether microglia from different brain regions are equally amenable to iNSC conversion and, if so, whether the resulting iNSC populations show differences with regard to their differentiation propensity. Second, adaptations of the delivery system for conversion-mediating factors might need to be employed, since this should optimally be good manufacturing practice compliant and applicable in living humans. Here, established viral vector systems successfully applied in gene therapy approaches such as AAVs (Liu *et al*., 2015; Torper *et al*., 2015; Pereira *et al*., 2017) might represent an attractive solution. Notably, although we recently screened various capsid-modified AAV serotype variants in human cell programming-derived cell types, yielding a number of lead candidates capable of modulating gene expression in, for instance, blood-derived iNSCs and iPSC-derived astrocytes, we did not yet succeed in identifying AAVs that efficiently transduce iPSdMiG *in vitro* (Flitsch *et al*., in revision). Thus, non-viral approaches such as transducible proteins, mRNAs, or small molecules might alternatively qualify for delivering the required cell programming cues to microglia *in vivo* (for a review on recent technologies facilitating *in vivo* reprogramming, see Larouche & Aguilar, 2019). Whatever delivery system is chosen, it has to enable factor distribution to the lesion site. For focal lesions, stereotaxic delivery can be considered, but more global cell loss might require modes of systemic administration that are not impeded by the blood-brain barrier. Moreover, multiple rounds of factor administration or delivery of depots such as scaffold-bound conversion factors and/or enhancers might be necessary (reviewed by Larouche & Aguilar, 2019 and Bruggeman *et al*., 2019), as the local microenvironment *in vivo* was shown to significantly affect conversion efficiency. For example, Wang *et al*. found that decreasing p53-p21 signaling increases the yield of astrocyte-derived neuroblasts by preventing p53-induced cell cycle exit, while locally secreted neurotrophins can support their maturation (Niu *et al*., 2015; Wang *et al*., 2016). Magdalena Götz and her team reported that counteracting oxidative stress and ferroptosis can significantly increase neuron derivation from glial cells *in vivo* (Gascón *et al*., 2016). To this end, preliminary data on the efficiency to convert mouse microglia into iNSCs *in vivo* could be useful to predict which measures would need to be taken to ensure clinical efficacy.

Such pre-experiments in mice could further serve to evaluate the clinical safety of the suggested approach. A risk factor to be considered in the context of *in vivo* conversion is the emergence of partially programmed cells, the potential tumorigenicity of such cells – especially considering the use of cMYC in our conversion paradigm – and their potential impact on tissue homeostasis. Finally, as *in vivo* conversion efficiencies increase, depletion of the target cell population can become a serious issue. This might, however, be less relevant for proliferative populations such as astrocytes (Chen *et al*., 2019; Wu *et al*., 2020) and potentially also microglia. Moreover, although full depletion of brain-resident microglia can be foreseen to have negative consequences for tissue homeostasis, reducing the number of insult-activated microglia, and thus dampening an exaggerated immune response, by direct cell fate conversion might actually represent a therapeutic strategy on its own – next to the neuroregenerative effect microglia-derived NSCs could eventually exert via cell replacement.

5. Concluding remarks and perspectives

In sum, we could show that blood-to-iNSC conversion yields cells that are epigenetically rejuvenated and overall display a lack of cellular aging hallmarks comparable to isogenic iPSC-derived NSCs. These rejuvenated, blood-derived iNSCs can further mature into functional neurons upon intracerebral transplantation, which might potentially even be capable of integrating into the host neuronal circuitry *in vivo*. Moreover, we were able to translate our conversion system, which is based on the SeV-mediated overexpression of the TFs SOX2 and cMYC, to iPSdMiG. Although these cells represent a good proxy for hardly accessible primary human microglia, our future work will necessarily extend to the isolation of human microglia from primary brain tissue and their subsequent conversion into iNSCs *ex vivo*. We will then re-evaluate the capability of our conversion system to also erase age-associated microglial signatures, and continue to explore mechanisms that might eventually enable us to rejuvenate somatic cells in the presence or absence of a cell fate shift. In addition, we will attempt to appreciate the prospects of our approach to convert microglia *in vivo* by investigating the amenability of xenografted human TF-equipped iPSdMiG to convert into iNSCs *in situ* after cerebral or peripheral transplantation in adult mice (Figure 29). We propose that neural conversion of microglia, representing a brain-resident cell population that is dynamically reacting to and attracted by various types of cerebral injury, will prospectively enable us to treat focal as well as non-localized cell loss across the brain, and hope that the results of both suggested experimental streams will in the future allow us to evaluate the principal feasibility to implement this paradigm as a clinically relevant and viable strategy for treating human neurological and neurodegenerative diseases.

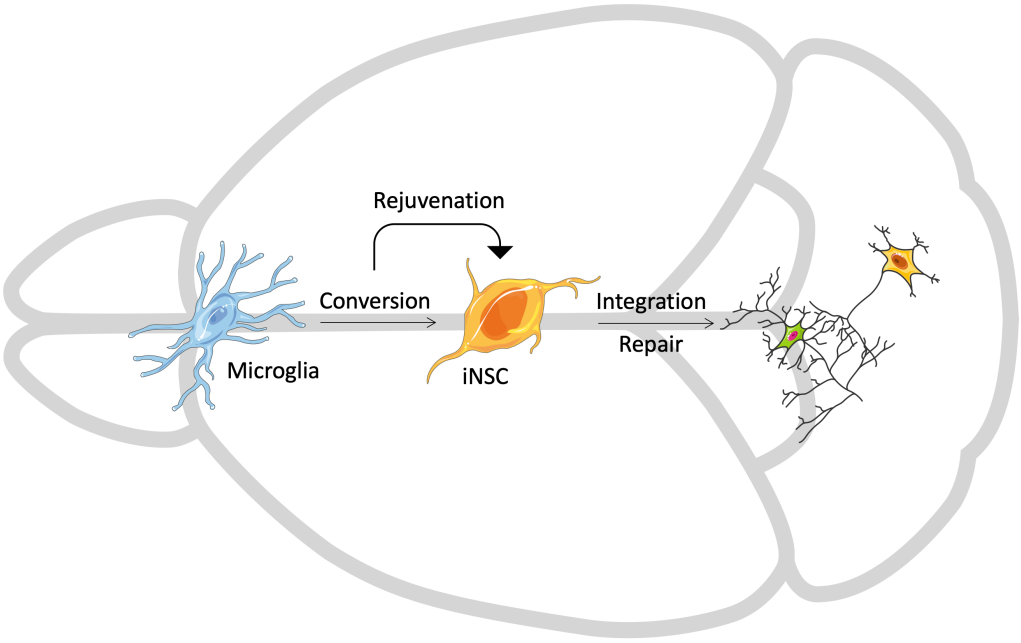

Figure 29: Schematic representation of the vision to use *in situ*/*in vivo* converted iNSCs for neuroregeneration.
Based on this project's findings, we are next aiming for translating our microglia-to-iNSC conversion paradigm to an *in situ* and/or *in vivo* context. Based on our recent findings, we assume that even within a native brain environment, microglia-derived iNSCs will undergo epigenetic and cellular rejuvenation upon transdifferentiation. Furthermore, we suggest that microglia-derived iNSCs might possess the capacity to functionally integrate into existing neuronal circuits, thereby being capable to contribute to neuronal repair after various types of brain injury. Figure elements for brain cells were retrieved from Servier Medical Art by Servier (SMART; https://smart.servier.com), licensed under a Creative Commons Attribution 3.0 Unported License. Figure element representing mouse brain was modified from Luigi Petrucco, © 2020, 'Mouse head schema', Zenodo (https://doi.org/10.5281/zenodo.3925903), licensed under a Creative Commons Attribution 4.0 International License.

References

Abernathy, D.G., Kim, W.K., McCoy, M.J., Lake, A.M., Ouwenga, R., Lee, S.W., Xing, X., Li, D., Lee, H.J., Heuckeroth, R.O., *et al*. (2017) 'MicroRNAs induce a permissive chromatin environment that enables neuronal subtype-specific reprogramming of adult human fibroblasts', *Cell Stem Cell*, 21(3), pp. 332–348. doi:10.1016/j.stem.2017.08.002.

Adler, A.F., Grigsby, C.L., Kulangara, K., Wang, H., Yasuda, R. & Leong, K.W. (2012) 'Nonviral direct conversion of primary mouse embryonic fibroblasts to neuronal cells', *Molecular Therapy Nucleic Acids*, 1(7), p. e32. doi:10.1038/mtna.2012.25.

Ai, Z., Xiang, Z., Li, Yuemin, Liu, G., Wang, H., Zheng, Y., Qiu, X., Zhao, S., Zhu, X., Li, Yanhua, *et al*. (2016) 'Conversion of monkey fibroblasts to transplantable telencephalic neuroepithelial stem cells', *Biomaterials*, 77, pp. 53–65. doi:10.1016/j.biomaterials.2015.10.079.

van den Akker, E., Satchwell, T.J., Pellegrin, S., Daniels, G. & Toye, A.M. (2010) 'The majority of the in vitro erythroid expansion potential resides in CD34 - cells, outweighing the contribution of CD34 + cells and significantly increasing the erythroblast yield from peripheral blood samples', *Haematologica*, 95(9), pp. 1594–1598. doi:10.3324/haematol.2009.019828.

Alexa, A., Rahnenführer, J. & Lengauer, T. (2006) 'Improved scoring of functional groups from gene expression data by decorrelating GO graph structure', *Bioinformatics*, 22(13), pp. 1600–1607. doi:10.1093/bioinformatics/btl140.

Ambasudhan, R., Talantova, M., Coleman, R., Yuan, X., Zhu, S., Lipton, S.A. & Ding, S. (2011) 'Direct reprogramming of adult human fibroblasts to functional neurons under defined conditions', *Cell Stem Cell*, 9(2), pp. 113–118. doi:10.1016/j.stem.2011.07.002.

Amente, S., Lania, L. & Majello, B. (2011) 'Epigenetic reprogramming of Myc target genes', *American journal of cancer research*, 1(3), pp. 413–418. doi:Not available.

Arvidsson, A., Collin, T., Kirik, D., Kokaia, Z. & Lindvall, O. (2002) 'Neuronal replacement from endogenous precursors in the adult brain after stroke', *Nature Medicine*, 8(9), pp. 963–970. doi:10.1038/nm747.

Aryee, M.J., Jaffe, A.E., Corrada-Bravo, H., Ladd-Acosta, C., Feinberg, A.P., Hansen, K.D. & Irizarry, R.A. (2014) 'Minfi: A flexible and comprehensive Bioconductor package for the analysis of Infinium DNA methylation microarrays', *Bioinformatics*, 30(10), pp. 1363–1369. doi:10.1093/bioinformatics/btu049.

Aydin, B., Kakumanu, A., Rossillo, M., Moreno-Estellés, M., Garipler, G., Ringstad, N., Flames, N., Mahony, S. & Mazzoni, E.O. (2019) 'Proneural factors Ascl1 and Neurog2 contribute to neuronal subtype identities by establishing distinct chromatin landscapes', *Nature Neuroscience*, 22(6), pp. 897–908. doi:10.1038/s41593-019-0399-y.

Baek, J.H., Son, H., Jeong, Y.H., Park, S.W. & Kim, H.J. (2019) 'Chronological aging standard curves of telomere length and mitochondrial DNA copy number in twelve tissues of C57BL/6 male mouse', *Cells*, 8(3), p. E247. doi:10.3390/cells8030247.

Bar-Nur, O., Verheul, C., Sommer, A.G., Brumbaugh, J., Schwarz, B.A., Lipchina, I., Huebner, A.J., Mostoslavsky, G. & Hochedlinger, K. (2015) 'Lineage conversion induced by pluripotency factors involves transient passage through an iPSC stage', *Nature Biotechnology*, 33(7), pp. 761–768. doi:10.1038/nbt.3247.

Barker, R.A., Götz, M. & Parmar, M. (2018) 'New approaches for brain repair - from rescue to reprogramming', *Nature*, 557(7705), pp. 329–334. doi:10.1038/s41586-018-0087-1.

Barretto, N., Zhang, H., Powell, S.K., Fernando, M.B., Zhang, S., Flaherty, E.K., Ho, S.M., Slesinger, P.A., Duan, J. & Brennand, K.J. (2020) 'ASCL1- and DLX2-induced GABAergic neurons from hiPSC-derived NPCs', *Journal of Neuroscience Methods*, 334(February), p. 108548. doi:10.1016/j.jneumeth.2019.108548.

Behr, B., Ko, S.H., Wong, V.W., Gurtner, G.C. & Longaker, M.T. (2010) 'Stem cells', *Plastic and Reconstructive Surgery*, 126(4), pp. 1163–1171. doi:10.1097/PRS.0b013e3181ea42bb.

Bekaert, S., De Meyer, T. & Van Oostveldt, P. (2005) 'Telomere attrition as ageing biomarker', *Anticancer Research*, 25(4), pp. 3011–3022. doi:Not available.

Berninger, B., Costa, M.R., Koch, U., Schroeder, T., Sutor, B., Grothe, B. & Götz, M. (2007) 'Functional properties of neurons derived from in vitro reprogrammed postnatal astroglia', *Journal of Neuroscience*, 27(32), pp. 8654–8664. doi:10.1523/JNEUROSCI.1615-07.2007.

Bernstein, B.E., Meissner, A. & Lander, E.S. (2007) 'The mammalian epigenome', *Cell*, 128(4), pp. 669–681. doi:10.1016/j.cell.2007.01.033.

Bertolini, J.A., Favaro, R., Zhu, Y., Pagin, M., Ngan, C.Y., Wong, C.H., Tjong, H., Vermunt, M.W., Martynoga, B., Barone, C., *et al*. (2019) 'Mapping the global chromatin connectivity network for Sox2 function in neural stem cell maintenance', *Cell Stem Cell*, 24(3), pp. 462-476.e6. doi:10.1016/j.stem.2019.02.004.

Biswas, D. & Jiang, P. (2016) 'Chemically induced reprogramming of somatic cells to pluripotent stem cells and neural cells', *International Journal of Molecular Sciences*, 17(2), p. 226. doi:10.3390/ijms17020226.

Blanchard, J.W., Eade, K.T., Szücs, A., Lo Sardo, V., Tsunemoto, R.K., Williams, D., Sanna, P.P. & Baldwin, K.K. (2015) 'Selective conversion of fibroblasts into peripheral sensory neurons', *Nature Neuroscience*, 18(1), pp. 25–35. doi:10.1038/nn.3887.

Bolós, M., Hu, Y., Young, K.M., Foa, L. & Small, D.H. (2014) 'Neurogenin 2 mediates amyloid-β precursor protein-stimulated neurogenesis', *Journal of Biological Chemistry*, 289(45), pp. 31253–31261. doi:10.1074/jbc.M114.581918.

Boyer, L.A., Tong, I.L., Cole, M.F., Johnstone, S.E., Levine, S.S., Zucker, J.P., Guenther, M.G., Kumar, R.M., Murray, H.L., Jenner, R.G., *et al*. (2005) 'Core transcriptional regulatory circuitry in human embryonic stem cells', *Cell*, 122(6), pp. 947–956. doi:10.1016/j.cell.2005.08.020.

Bracken, A.P., Kleine-Kohlbrecher, D., Dietrich, N., Pasini, D., Gargiulo, G., Beekman, C., Theilgaard-Mönch, K., Minucci, S., Porse, B.T., Marine, J.C., *et al*. (2007) 'The Polycomb group proteins bind throughout the INK4A-ARF locus and are disassociated in senescent cells', *Genes and Development*, 21(5), pp. 525–530.

doi:10.1101/gad.415507.

Brandt, T., Townsley, F.M., Teufel, D.P., Freund, S.M.V. & Veprintsev, D.B. (2012) 'Molecular basis for modulation of the p53 target selectivity by KLF4', *PLoS ONE*, 7(10), p. e48252. doi:10.1371/journal.pone.0048252.

Brennand, K.J., Marchetto, M.C., Benvenisty, N., Brüstle, O., Ebert, A., Izpisua Belmonte, J.C., Kaykas, A., Lancaster, M.A., Livesey, F.J., McConnell, M.J., *et al*. (2015) 'Creating patient-specific neural cells for the in vitro study of brain disorders', *Stem Cell Reports*, 5(6), pp. 933–945. doi:10.1016/j.stemcr.2015.10.011.

Bruggeman, K.F., Moriarty, N., Dowd, E., Nisbet, D.R. & Parish, C.L. (2019) 'Harnessing stem cells and biomaterials to promote neural repair', *British Journal of Pharmacology*, 176(3), pp. 355–368. doi:10.1111/bph.14545.

Buffo, A., Vosko, M.R., Ertürk, D., Hamann, G.F., Jucker, M., Rowitch, D. & Götz, M. (2005) 'Expression pattern of the transcription factor Olig2 in response to brain injuries: implications for neuronal repair', *Proceedings of the National Academy of Sciences of the United States of America*, 102(50), pp. 18183–18188. doi:10.1073/pnas.0506535102.

Buganim, Y., Faddah, D.A. & Jaenisch, R. (2013) 'Mechanisms and models of somatic cell reprogramming', *Nature Reviews Genetics*, 14(6), pp. 427–439. doi:10.1038/nrg3473.

Byers, B., Cord, B., Nguyen, H.N., Schüle, B., Fenno, L., Lee, P.C., Deisseroth, K., Langston, J.W., Pera, R.R. & Palmer, T.D. (2011) 'SNCA triplication Parkinson's patient's iPSC-derived DA neurons accumulate α-synuclein and are susceptible to oxidative stress', *PLoS ONE*, 6(11), p. e26159. doi:10.1371/journal.pone.0026159.

Caiazzo, M., Dell'Anno, M.T., Dvoretskova, E., Lazarevic, D., Taverna, S., Leo, D., Sotnikova, T.D., Menegon, A., Roncaglia, P., Colciago, G., *et al*. (2011) 'Direct generation of functional dopaminergic neurons from mouse and human fibroblasts', *Nature*, 476(7359), pp. 224–227. doi:10.1038/nature10284.

Capetian, P., Azmitia, L., Pauly, M.G., Krajka, V., Stengel, F., Bernhardi, E.-M., Klett, M., Meier, B., Seibler, P., Stanslowsky, N., *et al*. (2016) 'Plasmid-based generation of induced neural stem cells from adult human fibroblasts', *Frontiers in Cellular Neuroscience*, 10, p. 245. doi:10.3389/fncel.2016.00245.

Capiglioni, A.M., Lorenzetti, F., Quiroga, A.D., Parody, J.P., Ronco, M.T., Pisani, G.B., Carrillo, M.C., Ceballos, M.P. & Alvarez, M. de L. (2018) 'Attenuation of liver cancer development by oral glycerol supplementation in the rat', *European Journal of Nutrition*, 57(3), pp. 1215–1224. doi:10.1007/s00394-017-1404-4.

Cardoso, T., Adler, A.F., Mattsson, B., Hoban, D.B., Nolbrant, S., Wahlestedt, J.N., Kirkeby, A., Grealish, S., Björklund, A. & Parmar, M. (2018) 'Target-specific forebrain projections and appropriate synaptic inputs of hESC-derived dopamine neurons grafted to the midbrain of parkinsonian rats', *Journal of Comparative Neurology*, 526(13), pp. 2133–2146. doi:10.1002/cne.24500.

Castaño, J., Menendez, P., Bruzos-Cidon, C., Straccia, M., Sousa, A., Zabaleta, L., Vazquez, N., Zubiarrain, A., Sonntag, K.C., Ugedo, L., *et al*. (2014) 'Fast and efficient neural conversion of human hematopoietic cells', *Stem Cell Reports*, 3(6), pp. 1118–1131. doi:10.1002/cpsc.16.

Cawthon, R.M. (2009) 'Telomere length measurement by a novel monochrome multiplex quantitative PCR method', *Nucleic Acids Research*, 37(3), p. e21. doi:10.1093/nar/gkn1027.

Cenini, G., Hebisch, M., Iefremova, V., Flitsch, L.J., Breitkreuz, Y., Tanzi, R.E., Kim, D.Y., Peitz, M. & Brüstle, O. (2021) 'Dissecting Alzheimer's disease pathogenesis in human 2D and 3D models', *Molecular and Cellular Neuroscience*, 110, p. 103568. doi:10.1016/j.mcn.2020.103568.

Chanda, S., Marro, S., Wernig, M. & Südhof, T.C. (2013) 'Neurons generated by direct conversion of fibroblasts reproduce synaptic phenotype caused by autism-associated neuroligin-3 mutation', *Proceedings of the National Academy of Sciences of the United States of America*, 110(41), pp. 16622–16627. doi:10.1073/pnas.1316240110.

Chanda, S., Ang, C.E., Davila, J., Pak, C., Mall, M., Lee, Q.Y., Ahlenius, H., Jung, S.W., Südhof, T.C. & Wernig, M. (2014) 'Generation of induced neuronal cells by the single reprogramming factor ASCL1', *Stem Cell Reports*, 3(2), pp. 282–296. doi:10.1016/j.stemcr.2014.05.020.

Chandel, N.S., Jasper, H., Ho, T.T. & Passegué, E. (2016) 'Metabolic regulation of stem cell function in tissue homeostasis and organismal ageing', *Nature Cell Biology*, 18(8), pp. 823–832. doi:10.1038/ncb3385.

Cheffer, A., Flitsch, L.J., Krutenko, T., Röderer, P., Sokhranyaeva, L., Iefremova, V., Hajo, M., Peitz, M., Schwarz, M.K. & Brüstle, O. (2020) 'Human stem cell-based models for studying autism spectrum disorder-related neuronal dysfunction', *Molecular Autism*, 11(1), p. 99. doi:10.1186/s13229-020-00383-w.

Chen, H., Zheng, X. & Zheng, Y. (2015) 'Lamin-B in systemic inflammation, tissue homeostasis, and aging', *Nucleus*, 6(3), pp. 183–186. doi:10.1080/19491034.2015.1040212.

Chen, M., Xiao, L., Dai, G., Lu, P., Zhang, Y., Li, Y., Ni, M. & Rui, Y. (2021) 'Inhibition of JAK-STAT signaling pathway alleviates age-related phenotypes in tendon stem/progenitor cells', *Frontiers in Cell and Developmental Biology*, 9, p. 650250. doi:10.3389/fcell.2021.650250.

Chen, Y.C., Ma, N.X., Pei, Z.F., Wu, Z., Do-Monte, F.H., Keefe, S., Yellin, E., Chen, M.S., Yin, J.C., Lee, G., *et al*. (2019) 'A NeuroD1 AAV-based gene therapy for functional brain repair after ischemic injury through in vivo astrocyte-to-neuron conversion', *Molecular Therapy*, 28(1), pp. 217–234. doi:10.1016/j.ymthe.2019.09.003.

Cheng, L., Hu, W., Qiu, B., Zhao, J., Yu, Y., Guan, W., Wang, M., Yang, W. & Pei, G. (2014) 'Generation of neural progenitor cells by chemical cocktails and hypoxia', *Cell Research*, 24(6), pp. 665–679. doi:10.1038/cr.2014.32.

Chuang, C.Y., Yang, C.C., Soong, B.W., Yu, C.Y., Chen, S.H., Huang, H.P. & Kuo, H.C. (2019) 'Modeling spinocerebellar ataxias 2 and 3 with iPSCs reveals a role for glutamate in disease pathology', *Scientific Reports*, 9(1), p. 1166. doi:10.1038/s41598-018-37774-2.

Chung, S.S., Dutta, P., Austin, D., Wang, P., Awad, A. & Vadgama, J. V. (2018) 'Combination of resveratrol and 5-flurouracil enhanced antitelomerase activity and apoptosis by inhibiting STAT3 and Akt signaling pathways in human colorectal cancer cells', *Oncotarget*, 9(68), pp. 32943–32957. doi:10.18632/oncotarget.25993.

Chung, S.Y., Kishinevsky, S., Mazzulli, J.R., Graziotto, J., Mrejeru, A., Mosharov, E. V., Puspita, L., Valiulahi,

P., Sulzer, D., Milner, T.A., *et al*. (2016) 'Parkin and PINK1 patient iPSC-derived midbrain dopamine neurons exhibit mitochondrial dysfunction and α-synuclein accumulation', *Stem Cell Reports*, 7(4), pp. 664–677. doi:10.1016/j.stemcr.2016.08.012.

Conforti, P., Besusso, D., Bocchi, V.D., Faedo, A., Cesana, E., Rossetti, G., Ranzani, V., Svendsen, C.N., Thompson, L.M., Toselli, M., *et al*. (2018) 'Faulty neuronal determination and cell polarization are reverted by modulating HD early phenotypes', *Proceedings of the National Academy of Sciences of the United States of America*, 115(4), pp. E762–E771. doi:10.1073/pnas.1715865115.

Connor, B., Firmin, E., McCaughey-Chapman, A., Monk, R., Lee, K., Liot, S., Geiger, J., Rudolph, C. & Jones, K. (2018) 'Conversion of adult human fibroblasts into neural precursor cells using chemically modified mRNA', *Heliyon*, 4(11), p. e00918. doi:10.1016/j.heliyon.2018.e00918.

Cooper, O., Seo, H., Andrabi, S., Guardia-Laguarta, C., Graziotto, J., Sundberg, M., McLean, J.R., Carrillo-Reid, L., Xie, Z., Osborn, T., *et al*. (2012) 'Pharmacological rescue of mitochondrial deficits in iPSC-derived neural cells from patients with familial Parkinson's disease', *Science Translational Medicine*, 4(141), p. 141ra90. doi:10.1126/scitranslmed.3003985.

Correa-Cerro, L.S., Piao, Y., Sharov, A.A., Nishiyama, A., Cadet, J.S., Yu, H., Sharova, L. V., Xin, L., Hoang, H.G., Thomas, M., *et al*. (2011) 'Generation of mouse ES cell lines engineered for the forced induction of transcription factors', *Scientific Reports*, 1, p. 167. doi:10.1038/srep00167.

Corti, S., Nizzardo, M., Simone, C., Falcone, M., Donadoni, C., Salani, S., Rizzo, F., Nardini, M., Riboldi, G., Magri, F., *et al*. (2012) 'Direct reprogramming of human astrocytes into neural stem cells and neurons', *Experimental Cell Research*, 318(13), pp. 1528–1541. doi:10.1016/j.yexcr.2012.02.040.

Csete, M. (2010) 'Translational prospects for human induced pluripotent stem cells', *Regenerative Medicine*, 5(4), pp. 509–519. doi:10.2217/rme.10.39.

Daekee, K., Mi-Jung, H., Minjun, J., Hee-Jin, A., Kwang-Won, S. & Kyung-Sun, K. (2019) 'Generation of genetically stable human direct conversion-derived neural stem cells using quantity control of proto-oncogene expression', *Molecular Therapy - Nucleic Acids*, 14, pp. 388–397. doi:10.1016/j.omtn.2018.12.009.

Davis, R.L., Weintraub, H. & Lassar, A.B. (1987) 'Expression of a single transfected cDNA converts fibroblasts to myoblasts', *Cell*, 51(6), pp. 987–1000. doi:10.1016/0092-8674(87)90585-X.

De-Fraja, C., Conti, L., Govoni, S., Battaini, F. & Cattaneo, E. (2000) 'STAT signalling in the mature and aging brain', *International Journal of Developmental Neuroscience*, 18(4–5), pp. 439–446. doi:10.1016/S0736-5748(00)00007-1.

Demaria, M., Camporeale, A. & Poli, V. (2014) 'STAT3 and metabolism: How many ways to use a single molecule?', *International Journal of Cancer*, 135(9), pp. 1997–2003. doi:10.1002/ijc.28767.

Dinsdale, C.J., Mirza, F.M. & Wiebe, J.P. (1992) 'Glycerol alters cytoskeleton and cell adhesion while inhibiting cell proliferation', *Cell Biology International Reports*, 16(7), pp. 591–602. doi:10.1016/s0309-1651(06)80001-9.

Dittmer, A. & Dittmer, J. (2020) 'Carcinoma-associated fibroblasts promote growth of Sox2-expressing breast cancer cells', *Cancers*, 12(11), p. 3435. doi:10.3390/cancers12113435.

Doerr, J., Schwarz, M.K., Wiedermann, D., Leinhaas, A., Jakobs, A., Schloen, F., Schwarz, I., Diedenhofen, M., Braun, N.C., Koch, P., *et al*. (2017) 'Whole-brain 3D mapping of human neural transplant innervation', *Nature Communications*, 8, p. 14162. doi:10.1038/ncomms14162.

Dorst, M.C., Díaz-Moreno, M., Dias, D.O., Guimarães, E.L., Holl, D., Kalkitsas, J., Silberberg, G. & Göritz, C. (2021) 'Astrocyte-derived neurons provide excitatory input to the adult striatal circuitry', *Proceedings of the National Academy of Sciences of the United States of America*, 118(33), p. e2104119118. doi:10.1073/pnas.2104119118.

Drouin-Ouellet, J., Pircs, K., Barker, R.A., Jakobsson, J. & Parmar, M. (2017) 'Direct neuronal reprogramming for disease modeling studies using patient-derived neurons: what have we learned?', *Frontiers in Neuroscience*, 11, p. 530. doi:10.3389/fnins.2017.00530.

Drouin-Ouellet, J., Lau, S., Brattås, P.L., Rylander Ottosson, D., Pircs, K., Grassi, D.A., Collins, L.M., Vuono, R., Andersson Sjöland, A., Westergren-Thorsson, G., *et al*. (2017) 'REST suppression mediates neural conversion of adult human fibroblasts via microRNA-dependent and -independent pathways', *EMBO Molecular Medicine*, 9(8), pp. 1117–1131. doi:10.15252/emmm.201607471.

Eisenberg, T., Knauer, H., Schauer, A., Büttner, S., Ruckenstuhl, C., Carmona-Gutierrez, D., Ring, J., Schroeder, S., Magnes, C., Antonacci, L., *et al*. (2009) 'Induction of autophagy by spermidine promotes longevity', *Nature Cell Biology*, 11(11), pp. 1305–1314. doi:10.1038/ncb1975.

Ermolaeva, M., Neri, F., Ori, A. & Rudolph, K.L. (2018) 'Cellular and epigenetic drivers of stem cell ageing', *Nature Reviews Molecular Cell Biology*, 19(9), pp. 594–610. doi:10.1038/s41580-018-0020-3.

Espuny-Camacho, I., Michelsen, K.A., Gall, D., Linaro, D., Hasche, A., Bonnefont, J., Bali, C., Orduz, D., Bilheu, A., Herpoel, A., *et al*. (2013) 'Pyramidal neurons derived from human pluripotent stem cells integrate efficiently into mouse brain circuits in vivo', *Neuron*, 77(3), pp. 440–456. doi:10.1016/j.neuron.2012.12.011.

Fahy, G.M., Brooke, R.T., Watson, J.P., Good, Z., Vasanawala, S.S., Maecker, H., Leipold, M.D., Lin, D.T.S., Kobor, M.S. & Horvath, S. (2019) 'Reversal of epigenetic aging and immunosenescent trends in humans', *Aging Cell*, 18(6), p. e13028. doi:10.1111/acel.13028.

Faiz, M., Sachewsky, N., Gascón, S., Bang, K.W.A., Morshead, C.M. & Nagy, A. (2015) 'Adult neural stem cells from the subventricular zone give rise to reactive astrocytes in the cortex after stroke', *Cell Stem Cell*, 17(5), pp. 624–634. doi:10.1016/j.stem.2015.08.002.

Falk, S. & Götz, M. (2017) 'Glial control of neurogenesis', *Current Opinion in Neurobiology*, 47, pp. 188–195. doi:10.1016/j.conb.2017.10.025.

Feng, N., Han, Q., Li, J., Wang, S., Li, H., Yao, X. & Zhao, R.C. (2014) 'Generation of highly purified neural stem cells from human adipose-derived mesenchymal stem cells by Sox1 activation', *Stem Cells and Development*, 23(5), pp. 515–529. doi:10.1089/scd.2013.0263.

Field, A.E., Robertson, N.A., Wang, T., Havas, A., Ideker, T. & Adams, P.D. (2018) 'DNA methylation clocks in aging: Categories, causes, and consequences', *Molecular Cell*, 71(6), pp. 882–895. doi:10.1016/j.molcel.2018.08.008.

Fishell, G. & Van Der Kooy, D. (1991) 'Pattern formation in the striatum: Neurons with early projections to the substantia nigra survive the cell death period', *Journal of Comparative Neurology*, 312(1), pp. 33–42. doi:10.1002/cne.903120104.

Flitsch, L.J., Börner, K., Stüllein, C., Ziegler, S., Sonntag-Buck, V., Semkova, V., Au Yeung, S.W.C., Schlee, J., Hajo, M., Mathews, M., *et al*. (In revision) 'Identification of Adeno-associated virus variants for gene transfer into human neural cell types by parallel capsid screening', Preprint available. doi:10.21203/rs.3.rs-861785/v1.

Flitsch, L.J. & Brüstle, O. (2019) 'Evolving principles underlying neural lineage conversion and their relevance for biomedical translation', *F1000Research*, 8, p. F1000 Faculty Rev-1548. doi:10.12688/f1000research.18926.1.

Flitsch, L.J., Laupman, K.E. & Brüstle, O. (2020) 'Transcription factor-based fate specification and forward programming for neural regeneration', *Frontiers in Cellular Neuroscience*, 14, p. 121. doi:10.3389/fncel.2020.00121.

Florian, M.C., Leins, H., Gobs, M., Han, Y., Marka, G., Soller, K., Vollmer, A., Sakk, V., Nattamai, K.J., Rayes, A., *et al*. (2020) 'Inhibition of Cdc42 activity extends lifespan and decreases circulating inflammatory cytokines in aged female C57BL/6 mice', *Aging Cell*, 19(9), p. e13208. doi:10.1111/acel.13208.

Foshay, K.M. & Gallicano, G.I. (2008) 'Regulation of Sox2 by STAT3 initiates commitment to the neural precursor cell fate', *Stem Cells and Development*, 17(2), pp. 269–278. doi:10.1089/scd.2007.0098.

Friling, S., Andersson, E., Thompson, L.H., Jonsson, M.E., Hebsgaard, J.B., Nanou, E., Alekseenko, Z., Marklund, U., Kjellander, S., Volakakis, N., *et al*. (2009) 'Efficient production of mesencephalic dopamine neurons by Lmxla expression in embryonic stem cells', *Proceedings of the National Academy of Sciences of the United States of America*, 106(18), pp. 7613–7618. doi:10.1073/pnas.0902396106.

Galatro, T.F., Holtman, I.R., Lerario, A.M., Vainchtein, I.D., Brouwer, N., Sola, P.R., Veras, M.M., Pereira, T.F., Leite, R.E.P., Möller, T., *et al*. (2017) 'Transcriptomic analysis of purified human cortical microglia reveals age-associated changes', *Nature Neuroscience*, 20(8), pp. 1162–1171. doi:10.1038/nn.4597.

Galkin, F., Zhang, B., Dmitriev, S.E. & Gladyshev, V.N. (2019) 'Reversibility of irreversible aging', *Ageing Research Reviews*, 49, pp. 104–114. doi:10.1016/j.arr.2018.11.008.

Gao, L., Guan, W., Wang, M., Wang, H., Yu, J., Liu, Q., Qiu, B., Yu, Y., Ping, Y., Bian, X., *et al*. (2017) 'Direct generation of human neuronal cells from adult astrocytes by small molecules', *Stem Cell Reports*, 8(3), pp. 538–547. doi:10.1016/j.stemcr.2017.01.014.

García-Prat, L., Martínez-Vicente, M., Perdiguero, E., Ortet, L., Rodríguez-Ubreva, J., Rebollo, E., Ruiz-Bonilla, V., Gutarra, S., Ballestar, E., Serrano, A.L., *et al*. (2016) 'Autophagy maintains stemness by preventing senescence', *Nature*, 529(7584), pp. 37–42. doi:10.1038/nature16187.

Gascón, S., Murenu, E., Masserdotti, G., Ortega, F., Russo, G.L., Petrik, D., Deshpande, A., Heinrich, C., Karow, M., Robertson, S.P., *et al*. (2016) 'Identification and successful negotiation of a metabolic checkpoint in direct neuronal reprogramming', *Cell Stem Cell*, 18(3), pp. 396–409. doi:10.1016/j.stem.2015.12.003.

Geoffroy, C.G., Critchley, J.A., Castro, D.S., Ramelli, S., Barraclough, C., Descombes, P., Guillemot, F. & Raineteau, O. (2009) 'Engineering of dominant active basic helix-loop-helix proteins that are resistant to negative regulation by postnatal central nervous system antineurogenic cues', *Stem Cells*, 27(4), pp. 847–856. doi:10.1002/stem.17.

Ghasemi-Kasman, M., Hajikaram, M., Baharvand, H. & Javan, M. (2015) 'MicroRNA-mediated in vitro and in vivo direct conversion of astrocytes to neuroblasts', *PLoS ONE*, 10(6), p. e0127878. doi:10.1371/journal.pone.0127878.

Giorgetti, A., Marchetto, M.C.N., Li, M., Yu, D., Fazzina, R., Mu, Y., Adamo, A., Paramonov, I., Cardoso, J.C., Monasterio, M.B., *et al*. (2012) 'Cord blood-derived neuronal cells by ectopic expression of Sox2 and c-Myc', *Proceedings of the National Academy of Sciences of the United States of America*, 109(31), pp. 12556–12561. doi:10.1073/pnas.1209523109.

Göbel, C., Goetzke, R., Eggermann, T. & Wagner, W. (2018) 'Interrupted reprogramming into induced pluripotent stem cells does not rejuvenate human mesenchymal stromal cells', *Scientific Reports*, 8(1), p. 11676. doi:10.1038/s41598-018-30069-6.

Gorostieta-Salas, E., Moreno-Blas, D., Geronimo-Olvera, C., Cisneros, B., Court, F.A. & Castro-Obregon, S. (2021) 'Enhanced activity of exportin-1/CRM1 in neurons contributes to autophagy dysfunction and senescent features in old mouse brain', *Oxidative Medicine and Cellular Longevity*, 2021, p. 6682336. doi:10.1155/2021/6682336.

Gorris, R., Fischer, J., Erwes, K.L., Kesavan, J., Peterson, D.A., Alexander, M., Nöthen, M.M., Peitz, M., Quandel, T., Karus, M., *et al*. (2015) 'Pluripotent stem cell-derived radial glia-like cells as stable intermediate for efficient generation of human oligodendrocytes', *Glia*, 63(12), pp. 2152–2167. doi:10.1002/glia.22882.

Graf, T. & Enver, T. (2009) 'Forcing cells to change lineages', *Nature*, 462(7273), pp. 587–594. doi:10.1038/nature08533.

Grande, A., Sumiyoshi, K., López-Juárez, A., Howard, J., Sakthivel, B., Aronow, B., Campbell, K. & Nakafuku, M. (2013) 'Environmental impact on direct neuronal reprogramming in vivo in the adult brain', *Nature Communications*, 4, p. 2373. doi:10.1038/ncomms3373.

Grealish, S., Heuer, A., Cardoso, T., Kirkeby, A., Jönsson, M., Johansson, J., Björklund, A., Jakobsson, J. & Parmar, M. (2015) 'Monosynaptic tracing using modified rabies virus reveals early and extensive circuit integration of human embryonic stem cell-derived neurons', *Stem Cell Reports*, 4(6), pp. 975–983. doi:10.1016/j.stemcr.2015.04.011.

Grealish, S., Drouin-Ouellet, J. & Parmar, M. (2016) 'Brain repair and reprogramming: the route to clinical translation', *Journal of Internal Medicine*, 280(3), pp. 265–275. doi:10.1111/joim.12475.

Guilbert, S.M., Cardoso, D., Lévy, N., Muchir, A. & Nissan, X. (2021) 'Hutchinson-Gilford progeria syndrome: Rejuvenating old drugs to fight accelerated ageing', *Methods*, 190, pp. 3–12. doi:10.1016/j.ymeth.2020.04.005.

Guo, Z., Zhang, L., Wu, Z., Chen, Y., Wang, F. & Chen, G. (2014) 'In vivo direct reprogramming of reactive glial cells into functional neurons after brain injury and in an Alzheimer's disease model', *Cell Stem Cell*, 14(2), pp. 188–202. doi:10.1016/j.stem.2013.12.001.

Han, D.W., Tapia, N., Hermann, A., Hemmer, K., Höing, S., Araúzo-Bravo, M.J., Zaehres, H., Wu, G., Frank, S., Moritz, S., *et al*. (2012) 'Direct reprogramming of fibroblasts into neural stem cells by defined factors', *Cell Stem Cell*, 10(4), pp. 465–472. doi:10.1016/j.stem.2012.02.021.

Han, Y.C., Lim, Y., Duffieldl, M.D., Li, H., Liu, J., Abdul Manaph, N.P., Yang, M., Keating, D.J. & Zhou, X.F. (2016) 'Direct reprogramming of mouse fibroblasts to neural stem cells by small molecules', *Stem cells international*, 2016, p. 4304916. doi:10.1155/2016/4304916.

Hanna, J., Saha, K., Pando, B., Van Zon, J., Lengner, C.J., Creyghton, M.P., Van Oudenaarden, A. & Jaenisch, R. (2009) 'Direct cell reprogramming is a stochastic process amenable to acceleration', *Nature*, 462(7273), pp. 595–601. doi:10.1038/nature08592.

Hanna, J.H., Saha, K. & Jaenisch, R. (2010) 'Pluripotency and cellular reprogramming: facts, hypotheses, unresolved issues', *Cell*, 143(4), pp. 508–525. doi:10.1016/j.cell.2010.10.008.

Hansen, S.K., Stummann, T.C., Borland, H., Hasholt, L.F., Tümer, Z., Nielsen, J.E., Rasmussen, M.A., Nielsen, T.T., Daechsel, J.C.A., Fog, K., *et al*. (2016) 'Induced pluripotent stem cell - derived neurons for the study of spinocerebellar ataxia type 3', *Stem Cell Research*, 17(2), pp. 306–317. doi:10.1016/j.scr.2016.07.004.

Heinrich, C., Blum, R., Gascón, S., Masserdotti, G., Tripathi, P., Sánchez, R., Tiedt, S., Schroeder, T., Götz, M. & Berninger, B. (2010) 'Directing astroglia from the cerebral cortex into subtype specific functional neurons', *PLoS Biology*, 8(5), p. e1000373. doi:10.1371/journal.pbio.1000373.

Heinrich, C., Gascón, S., Masserdotti, G., Lepier, A., Sanchez, R., Simon-Ebert, T., Schroeder, T., G¨otz, M. & Berninger, B. (2011) 'Generation of subtype-specific neurons from postnatal astroglia of the mouse cerebral cortex', *Nature Protocols*, 6(2), pp. 214–228. doi:10.1038/nprot.2010.188.

Heinrich, C., Bergami, M., Gascón, S., Lepier, A., Viganò, F., Dimou, L., Sutor, B., Berninger, B. & Götz, M. (2014) 'Sox2-mediated conversion of NG2 glia into induced neurons in the injured adult cerebral cortex', *Stem Cell Reports*, 3(6), pp. 1000–1014. doi:10.1016/j.stemcr.2014.10.007.

Hemmer, K., Zhang, M., Van Wüllen, T., Sakalem, M., Tapia, N., Baumuratov, A., Kaltschmidt, C., Kaltschmidt, B., Schöler, H.R., Zhang, W., *et al*. (2014) 'Induced neural stem cells achieve long-term survival and functional integration in the adult mouse brain', *Stem Cell Reports*, 3(3), pp. 423–431. doi:10.1016/j.stemcr.2014.06.017.

Hennekam, R.C.M. (2006) 'Hutchinson-Gilford progeria syndrome: Review of the phenotype', *American Journal of Medical Genetics Part A*, 140(23), pp. 2603–2624. doi:10.1002/ajmg.a.31346.

Herdy, J., Schafer, S., Kim, Y., Ansari, Z., Zangwill, D., Ku, M., Paquola, A., Lee, H., Mertens, J. & Gage, F.H.

(2019) ‘Chemical modulation of transcriptionally enriched signaling pathways to optimize the conversion of fibroblasts into neurons’, *eLife*, 8, p. e41356. doi:10.7554/elife.41356.

Herrero-Navarro, Á., Puche-Aroca, L., Moreno-Juan, V., Sempere-Ferràndez, A., Espinosa, A., Susín, R., Torres-Masjoan, L., Leyva-Díaz, E., Karow, M., Figueres-Oñate, M., *et al*. (2021) ‘Astrocytes and neurons share region-specific transcriptional signatures that confer regional identity to neuronal reprogramming’, *Science Advances*, 7(15), p. eabe8978. doi:10.1126/SCIADV.ABE8978.

Ho, S.M., Hartley, B.J., TCW, J., Beaumont, M., Stafford, K., Slesinger, P.A. & Brennand, K.J. (2016) ‘Rapid Ngn2-induction of excitatory neurons from hiPSC-derived neural progenitor cells’, *Methods*, 101, pp. 113–124. doi:10.1016/j.ymeth.2015.11.019.

Hofmann, J.W., Zhao, X., De Cecco, M., Peterson, A.L., Pagliaroli, L., Manivannan, J., Hubbard, G.B., Ikeno, Y., Zhang, Y., Feng, B., *et al*. (2015) ‘Reduced expression of MYC increases longevity and enhances healthspan’, *Cell*, 160(3), pp. 477–488. doi:10.1016/j.cell.2014.12.016.

Hofmann, P., Sommer, J., Theodorou, K., Kirchhof, L., Fischer, A., Li, Y., Perisic, L., Hedin, U., Maegdefessel, L., Dimmeler, S., *et al*. (2019) ‘Long non-coding RNA H19 regulates endothelial cell aging via inhibition of STAT3 signalling’, *Cardiovascular Research*, 115(1), pp. 230–242. doi:10.1093/cvr/cvy206.

Hong, J.Y., Lee, S.H., Lee, S.C., Kim, J.W., Kim, K.P., Kim, S.M., Tapia, N., Lim, K.T., Kim, J., Ahn, H.S., *et al*. (2014) ‘Therapeutic potential of induced neural stem cells for spinal cord injury’, *Journal of Biological Chemistry*, 289(47), pp. 32512–32525. doi:10.1074/jbc.M114.588871.

Horvath, S. (2013) ‘DNA methylation age of human tissues and cell types.’, *Genome Biology*, 14(10), p. R115. doi:10.1186/gb-2013-14-10-r115.

Horvath, S., Oshima, J., Martin, G.M., Lu, A.T., Quach, A., Cohen, H., Felton, S., Matsuyama, M., Lowe, D., Kabacik, S., *et al*. (2018) ‘Epigenetic clock for skin and blood cells applied to Hutchinson Gilford progeria syndrome and ex vivo studies’, *Aging*, 10(7), pp. 1758–1775. doi:10.18632/aging.101508.

Hou, P.S., Chuang, C.Y., Yeh, C.H., Chiang, W., Liu, H.J., Lin, T.N. & Kuo, H.C. (2017) ‘Direct conversion of human fibroblasts into neural progenitors using transcription factors enriched in human ESC-derived neural progenitors’, *Stem Cell Reports*, 8(1), pp. 54–68. doi:10.1016/j.stemcr.2016.11.006.

Hsieh, J., Nakashima, K., Kuwabara, T., Mejia, E. & Gage, F.H. (2004) ‘Histone deacetylase inhibition-mediated neuronal differentiation of multipotent adult neural progenitor cells’, *Proceedings of the National Academy of Sciences of the United States of America*, 101(47), pp. 16659–16664. doi:10.1073/pnas.0407643101.

Hu, W., Qiu, B., Guan, W., Wang, Q., Wang, M., Li, W., Gao, L., Shen, L., Huang, Y., Xie, G., *et al*. (2015) ‘Direct conversion of normal and Alzheimer’s disease human fibroblasts into neuronal cells by small molecules’, *Cell Stem Cell*, 17(2), pp. 204–212. doi:10.1016/j.stem.2015.07.006.

Hu, X., Qin, S., Huang, X., Yuan, Y., Tan, Z., Gu, Y., Cheng, X., Wang, D., Lian, X.F., He, C., *et al*. (2019) ‘Region-restrict astrocytes exhibit heterogeneous susceptibility to neuronal reprogramming’, *Stem Cell Reports*, 12(2), pp. 290–304. doi:10.1016/j.stemcr.2018.12.017.

Huh, C.J., Zhang, B., Victor, M.B., Dahiya, S., Batista, L.F.Z., Horvath, S. & Yoo, A.S. (2016) 'Maintenance of age in human neurons generated by microRNA-based neuronal conversion of fibroblasts', *Elife*, 5, p. e18648. doi:10.7554/eLife.18648.

Ichida, J.K., Staats, K.A., Davis-Dusenbery, B.N., Clement, K., Galloway, K.E., Babos, K.N., Shi, Y., Son, E.Y., Kiskinis, E., Atwater, N., *et al*. (2018) 'Comparative genomic analysis of embryonic, lineage-converted, and stem cell-derived motor neurons', *Development*, 145(22), p. dev.168617. doi:10.1242/dev.168617.

Iefremova, V., Manikakis, G., Krefft, O., Jabali, A., Weynans, K., Wilkens, R., Marsoner, F., Brändl, B., Müller, F.J., Koch, P., *et al*. (2017) 'An organoid-based model of cortical development identifies non-cell-autonomous defects in Wnt signaling contributing to Miller-Dieker syndrome', *Cell Reports*, 19(1), pp. 50–59. doi:10.1016/j.celrep.2017.03.047.

Imm, J., Pishva, E., Ali, M., Kerrigan, T.L., Jeffries, A., Burrage, J., Glaab, E., Cope, E.L., Jones, K.M., Allen, N.D., *et al*. (2021) 'Characterization of DNA methylomic signatures in induced pluripotent stem cells during neuronal differentiation', *Frontiers in Cell and Developmental Biology*, 9, p. 647981. doi:10.3389/fcell.2021.647981.

Jaenisch, R. & Young, R. (2008) 'Stem cells, the molecular circuitry of pluripotency and nuclear reprogramming', *Cell*, 132(4), pp. 567–582. doi:10.1016/j.cell.2008.01.015.

Jiang, H., Xu, Z., Zhong, P., Ren, Y., Liang, G., Schilling, H.A., Hu, Z., Zhang, Y., Wang, X., Chen, S., *et al*. (2015) 'Cell cycle and p53 gate the direct conversion of human fibroblasts to dopaminergic neurons', *Nature Communications*, 6, p. 10100. doi:10.1038/ncomms10100.

Kamentsky, L., Jones, T.R., Fraser, A., Bray, M.A., Logan, D.J., Madden, K.L., Ljosa, V., Rueden, C., Eliceiri, K.W. & Carpenter, A.E. (2011) 'Improved structure, function and compatibility for CellProfiler: Modular high-throughput image analysis software', *Bioinformatics*, 27(8), pp. 1179–1180. doi:10.1093/bioinformatics/btr095.

Kang, P.J., Son, D., Ko, T.H., Hong, W., Yun, W., Jang, J., Choi, J. Il, Song, G., Lee, J., Kim, I.Y., *et al*. (2019) 'mRNA-driven generation of transgene-free neural stem cells from human urine-derived cells', *Cells*, 8(9), p. 1043. doi:10.3390/cells8091043.

Karow, M., Sánchez, R., Schichor, C., Masserdotti, G., Ortega, F., Heinrich, C., Gascón, S., Khan, M.A., Lie, D.C., Dellavalle, A., *et al*. (2012) 'Reprogramming of pericyte-derived cells of the adult human brain into induced neuronal cells', *Cell Stem Cell*, 11(4), pp. 471–476. doi:10.1016/j.stem.2012.07.007.

Karow, M., Camp, J.G., Falk, S., Gerber, T., Pataskar, A., Gac-Santel, M., Kageyama, J., Brazovskaja, A., Garding, A., Fan, W., *et al*. (2018) 'Direct pericyte-to-neuron reprogramming via unfolding of a neural stem cell-like program', *Nature Neuroscience*, 21(7), pp. 932–940. doi:10.1038/s41593-018-0168-3.

Kerepesi, C., Zhang, B., Lee, S.G., Trapp, A. & Gladyshev, V.N. (2021) 'Epigenetic clocks reveal a rejuvenation event during embryogenesis followed by aging', *Science Advances*, 7(26), p. eabg6082. doi:10.1126/sciadv.abg6082.

Khazaei, N., Rastegar-Pouyani, S., O'Toole, N., Wee, P., Mohammadnia, A. & Yaqubi, M. (2018) 'Regulating

the transcriptomes that mediate the conversion of fibroblasts to various nervous system neural cell types', *Journal of Cellular Physiology*, 233(4), pp. 3603–3614. doi:10.1002/jcp.26221.

Kikuchi, T., Morizane, A., Doi, D., Magotani, H., Onoe, H., Hayashi, T., Mizuma, H., Takara, S., Takahashi, R., Inoue, H., *et al*. (2017) 'Human iPS cell-derived dopaminergic neurons function in a primate Parkinson's disease model', *Nature*, 548(7669), pp. 592–596. doi:10.1038/nature23664.

Kim, B.E., Choi, S.W., Shin, J.H., Kim, J.J., Kang, I., Lee, B.C., Lee, J.Y., Kook, M.G. & Kang, K.S. (2018) 'Single-factor SOX2 mediates direct neural reprogramming of human mesenchymal stem cells via transfection of in vitro transcribed mRNA', *Cell Transplantation*, 27(7), pp. 1154–1167. doi:10.1177/0963689718771885.

Kim, H.-J., McMillan, E., Han, F. & Svendsen, C.N. (2009) 'Regionally specified human neural progenitor cells derived from the mesencephalon and forebrain undergo increased neurogenesis following overexpression of ASCL1', *Stem Cells*, 27(2), pp. 390–398. doi:10.1634/stemcells.2007-1047.

Kim, J., Efe, J.A., Zhu, S., Talantova, M., Yuan, X., Wang, S., Lipton, S.A., Zhang, K. & Ding, S. (2011) 'Direct reprogramming of mouse fibroblasts to neural progenitors', *Proceedings of the National Academy of Sciences of the United States of America*, 108(19), pp. 7838–7843. doi:10.1073/pnas.1103113108/-/DCSupplemental.www.pnas.org/cgi/doi/10.1073/pnas.1103113108.

Kim, J., Su, S.C., Wang, H., Cheng, A.W., Cassady, J.P., Lodato, M.A., Lengner, C.J., Chung, C.Y., Dawlaty, M.M., Tsai, L.H., *et al*. (2011) 'Functional integration of dopaminergic neurons directly converted from mouse fibroblasts', *Cell Stem Cell*, 9(5), pp. 413–419. doi:10.1016/j.stem.2011.09.011.

Kim, J.H., Auerbach, J.M., Rodríguez-Gómez, J.A., Velasco, I., Gavin, D., Lumelsky, N., Lee, S.H., Nguyen, J., Sánchez-Pernaute, R., Bankiewicz, K., *et al*. (2002) 'Dopamine neurons derived from embryonic stem cells function in an animal model of Parkinson's disease', *Nature*, 418(6893), pp. 50–56. doi:10.1038/nature00900.

Kim, J.Y., Koh, H.C., Lee, J.Y., Chang, M.Y., Kim, Y.C., Chung, H.Y., Son, H., Lee, Y.S., Studer, L., McKay, R., *et al*. (2003) 'Dopaminergic neuronal differentiation from rat embryonic neural precursors by Nurr1 overexpression', *Journal of Neurochemistry*, 85(6), pp. 1443–1454. doi:10.1046/j.1471-4159.2003.01780.x.

Kim, Jongpil, Kim, H., Yoo, J., Shin, J., Chang, Y., Jung, J., Jo, D.G., Kim, Janghwan, Jang, W., Lengner, C.J., *et al*. (2017) 'Modelling APOE ϵ3/4 allele-associated sporadic Alzheimer's disease in an induced neuron', *Brain*, 140(8), pp. 2193–2209. doi:10.1093/brain/awx144.

Kim, K., Doi, A., Wen, B., Ng, K., Zhao, R., Cahan, P., Kim, J., Aryee, M.J., Ji, H., Ehrlich, L.I.R., *et al*. (2010) 'Epigenetic memory in induced pluripotent stem cells', *Nature*, 467(7313), pp. 285–290. doi:10.1038/nature09342.

Kim, S.M., Kim, J.W., Kwak, T.H., Park, S.W., Kim, K.P., Park, H., Lim, K.T., Kang, K., Kim, J., Yang, J.H., *et al*. (2016) 'Generation of integration-free induced neural stem cells from mouse fibroblasts', *Journal of Biological Chemistry*, 291(27), pp. 14199–14212. doi:10.1074/jbc.M115.713578.

Kim, Y., Zheng, X., Ansari, Z., Bunnell, M.C., Herdy, J.R., Traxler, L., Lee, H., Paquola, A.C.M., Blithikioti, C., Ku, M., *et al*. (2018) 'Mitochondrial aging defects emerge in directly reprogrammed human neurons due to their

metabolic profile', *Cell Reports*, 23(9), pp. 2550–2558. doi:10.1016/j.celrep.2018.04.105.

Kirkeby, A., Grealish, S., Wolf, D.A., Nelander, J., Wood, J., Lundblad, M., Lindvall, O. & Parmar, M. (2012) 'Generation of regionally specified neural progenitors and functional neurons from human embryonic stem cells under defined conditions', *Cell Reports*, 1(6), pp. 703–714. doi:10.1016/j.celrep.2012.04.009.

Kirkeby, A., Nolbrant, S., Tiklova, K., Heuer, A., Kee, N., Cardoso, T., Rylander Ottosson, D., Lelos, M.J., Rifes, P., Dunnett, S.B., *et al*. (2017) 'Predictive markers guide differentiation to improve graft outcome in clinical translation of hESC-based therapy for Parkinson's disease', *Cell Stem Cell*, 20, pp. 135–148. doi:10.1016/j.stem.2016.09.004.

Koch, P., Breuer, P., Peitz, M., Jungverdorben, J., Kesavan, J., Poppe, D., Doerr, J., Ladewig, J., Mertens, J., Tüting, T., *et al*. (2011) 'Excitation-induced ataxin-3 aggregation in neurons from patients with Machado-Joseph disease', *Nature*, 480(7378), pp. 543–546. doi:10.1038/nature10671.

Komatsu, M. & Ichimura, Y. (2010) 'Physiological significance of selective degradation of p62 by autophagy', *FEBS Letters*, 584(7), pp. 1374–1378. doi:10.1016/j.febslet.2010.02.017.

Kriks, S., Shim, J.W., Piao, J., Ganat, Y.M., Wakeman, D.R., Xie, Z., Carrillo-Reid, L., Auyeung, G., Antonacci, C., Buch, A., *et al*. (2011) 'Dopamine neurons derived from human ES cells efficiently engraft in animal models of Parkinson's disease', *Nature*, 480(7378), pp. 547–551. doi:10.1038/nature10648.

Kronenberg, G., Gertz, K., Cheung, G., Buffo, A., Kettenmann, H., Götz, M. & Endres, M. (2010) 'Modulation of fate determinants Olig2 and Pax6 in resident glia evokes spiking neuroblasts in a model of mild brain ischemia', *Stroke*, 41(12), pp. 2944–2949. doi:10.1161/STROKEAHA.110.583039.

De la Rossa, A., Bellone, C., Golding, B., Vitali, I., Moss, J., Toni, N., Lüscher, C. & Jabaudon, D. (2013) 'In vivo reprogramming of circuit connectivity in postmitotic neocortical neurons', *Nature Neuroscience*, 16(2), pp. 193–200. doi:10.1038/nn.3299.

Ladewig, J., Mertens, J., Kesavan, J., Doerr, J., Poppe, D., Glaue, F., Herms, S., Wernet, P., Kögler, G., Müller, F.J., *et al*. (2012) 'Small molecules enable highly efficient neuronal conversion of human fibroblasts', *Nature Methods*, 9(6), pp. 575–578. doi:10.1038/nmeth.1972.

Lancaster, M.A. & Knoblich, J.A. (2014) 'Organogenesisin a dish: Modeling development and disease using organoid technologies', *Science*, 345(6194), p. 1247125. doi:10.1126/science.1247125.

Lanke, V., Moolamalla, S.T.R., Roy, D. & Vinod, P.K. (2018) 'Integrative analysis of hippocampus gene expression profiles identifies network alterations in aging and Alzheimer's disease', *Frontiers in Aging Neuroscience*, 10, p. 153. doi:10.3389/fnagi.2018.00153.

Lapasset, L., Milhavet, O., Prieur, A., Besnard, E., Babled, A., Ait-Hamou, N., Leschik, J., Pellestor, F., Ramirez, J.-M., De Vos, J., *et al*. (2011) 'Rejuvenating senescent and centenarian human cells by reprogramming through the pluripotent state', *Genes and Development*, 25(21), pp. 2248–2253. doi:10.1101/gad.173922.111.2248.

Larouche, J. & Aguilar, C.A. (2019) 'New technologies to enhance in vivo reprogramming for regenerative

medicine', *Trends in Biotechnology*, 37(6), pp. 604–617. doi:10.1016/j.tibtech.2018.11.003.

Lau, S., Ottosson, D.R., Jakobsson, J. & Parmar, M. (2014) 'Direct neural conversion from human fibroblasts using self-regulating and nonintegrating viral vectors', *Cell Reports*, 9(5), pp. 1673–1680. doi:10.1016/j.celrep.2014.11.017.

Lee, H., Lee, H.Y., Lee, B.E., Gerovska, D., Park, S.Y., Zaehres, H., Araúzo-Bravo, M.J., Kim, J.I., Ha, Y., Schöler, H.R., *et al*. (2020) 'Sequentially induced motor neurons from human fibroblasts facilitate locomotor recovery in a rodent spinal cord injury model', *eLife*, 9, p. e52069. doi:10.7554/eLife.52069.

Lee, Y.S., Jung, W.Y., Heo, H., Park, M.G., Oh, S.H., Park, B.G. & Kim, S. (2018) 'Exosome-mediated ultra-effective direct conversion of human fibroblasts into neural progenitor-like cells', *ACS Nano*, 12(3), pp. 2531–2538. doi:10.1021/acsnano.7b08297.

Leovsky, C., Fabian, C., Naaldijk, Y., Jäger, C., Jang, H.J., Böhme, J., Rudolph, L. & Stolzing, A. (2015) 'Biodistribution of in vitro-derived microglia applied intranasally and intravenously to mice: Effects of aging', *Cytotherapy*, 17(11), pp. 1617–1626. doi:10.1016/j.jcyt.2015.07.019.

Lessel, D., Wu, D., Trujillo, C., Ramezani, T., Lessel, I., Alwasiyah, M.K., Saha, B., Hisama, F.M., Rading, K., Goebel, I., *et al*. (2017) 'Dysfunction of the MDM2/p53 axis is linked to premature aging', *Journal of Clinical Investigation*, 127(10), pp. 3598–3608. doi:10.1172/JCI92171.

Li, M. & Izpisua Belmonte, J.C. (2018) 'Deconstructing the pluripotency gene regulatory network', *Nature Cell Biology*, 20(4), pp. 382–392. doi:10.1038/s41556-018-0067-6.

Li, S., Shi, Y., Yao, X., Wang, X., Shen, L., Rao, Z., Yuan, J., Liu, Y., Zhou, Z., Zhang, Z., *et al*. (2019) 'Conversion of astrocytes and fibroblasts into functional noradrenergic neurons', *Cell Reports*, 28(3), pp. 682-697.e7. doi:10.1016/j.celrep.2019.06.042.

Li, W., Li, K., Wei, W. & Ding, S. (2013) 'Chemical approaches to stem cell biology and therapeutics', *Cell Stem Cell*, 13(3), pp. 270–283. doi:10.1016/j.stem.2013.08.002.

Li, X., Long, J., He, T., Belshaw, R. & Scott, J. (2015) 'Integrated genomic approaches identify major pathways and upstream regulators in late onset Alzheimer's disease', *Scientific Reports*, 5, p. 12393. doi:10.1038/srep12393.

Li, X., Zuo, X., Jing, J., Ma, Y., Wang, Jiaming, Liu, D., Zhu, J., Du, X., Xiong, L., Du, Y., *et al*. (2015) 'Small-molecule-driven direct reprogramming of mouse fibroblasts into functional neurons', *Cell Stem Cell*, 17(2), pp. 195–203. doi:10.1016/j.stem.2015.06.003.

Li, X., Tzeng, S.Y., Liu, X., Tammia, M., Cheng, Y.-H., Rolfe, A., Sun, D., Zhang, N., Green, J.J., Wen, X., *et al*. (2016) 'Nanoparticle-mediated transcriptional modifications enhances neuronal differentiation of human neural stem cells following transplantation in rat brain', *Biomaterials*, 84, pp. 157–166. doi:10.1016/j.physbeh.2017.03.040.

Liao, W., Huang, N., Yu, J., Jares, A., Yang, J., Zieve, G., Avila, C., Jiang, X., Zhang, X.B. & Ma, Y. (2015) 'Direct conversion of cord blood CD34+ cells into neural stem cells by OCT4', *Stem Cells Translational Medicine*,

4(7), pp. 755–763.

Lim, S.M., Choi, W.J., Oh, K.W., Xue, Y., Choi, J.Y., Kim, Sung Hoon, Nahm, M., Kim, Y.E., Lee, J., Noh, M.Y., *et al*. (2016) 'Directly converted patient-specific induced neurons mirror the neuropathology of FUS with disrupted nuclear localization in amyotrophic lateral sclerosis', *Molecular Neurodegeneration*, 11, p. 8. doi:10.1186/s13024-016-0075-6.

Lim, S.M., Choi, B.-O., Oh, S., Choi, W.J., Oh, K.-W., Nahm, M., Xue, Y., Choi, J.H., Choi, J.Y., Kim, Y.-E., *et al*. (2016) 'Patient fibroblasts-derived induced neurons demonstrate autonomous neuronal defects in adult-onset Krabbe disease', *Oncotarget*, 7(46), pp. 74496–74509. doi:10.18632/oncotarget.12812.

Lin, H.-C., He, Z., Ebert, S., Schörnig, M., Santel, M., Nikolova, M.T., Weigert, A., Hevers, W., Kasri, N.N., Taverna, E., *et al*. (2021) 'NGN2 induces diverse neuron types from human pluripotency', *Stem Cell Reports*, 16(9), pp. 2118–2127. doi:10.1016/j.stemcr.2021.07.006.

Lipinski, M.M., Zheng, B., Lu, T., Yan, Z., Py, B.F., Ng, A., Xavier, R.J., Li, C., Yankner, B.A., Scherzer, C.R., *et al*. (2010) 'Genome-wide analysis reveals mechanisms modulating autophagy in normal brain aging and in Alzheimer's disease', *Proceedings of the National Academy of Sciences of the United States of America*, 107(32), pp. 14164–14169. doi:10.1073/pnas.1009485107.

Liu, C.H. & Chen, L.H. (2007) 'Enhanced recombinant M-CSF production in CHO cells by glycerol addition: Model and validation', *Cytotechnology*, 54(2), pp. 89–96. doi:10.1007/s10616-007-9078-z.

Liu, F., Zhang, Y., Chen, F., Yuan, J., Li, S., Han, S., Lu, D., Geng, J., Rao, Z., Sun, L., *et al*. (2021) 'Neurog2 directly converts astrocytes into functional neurons in midbrain and spinal cord', *Cell death & disease*, 12(3), p. 225. doi:10.1038/s41419-021-03498-x.

Liu, G.H., Qu, J., Suzuki, K., Nivet, E., Li, M., Montserrat, N., Yi, F., Xu, X., Ruiz, S., Zhang, W., *et al*. (2012) 'Progressive degeneration of human neural stem cells caused by pathogenic LRRK2', *Nature*, 491(7425), pp. 603–607. doi:10.1038/nature11557.

Liu, J., Jiao, K., Zhou, Q., Yang, J., Yang, K., Hu, C., Zhou, M. & Li, Z. (2021) 'Resveratrol alleviates 27-hydroxycholesterol-induced senescence in nerve cells and affects zebrafish locomotor behavior via activation of SIRT1-mediated STAT3 signaling', *Oxidative Medicine and Cellular Longevity*, 2021, p. 6673343. doi:10.1155/2021/6673343.

Liu, M.L., Zang, T. & Zhang, C.L. (2016) 'Direct lineage reprogramming reveals disease-specific phenotypes of motor neurons from human ALS patients', *Cell Reports*, 14(1), pp. 115–128. doi:10.1016/j.celrep.2015.12.018.

Liu, X., Li, W., Fu, X. & Xu, Y. (2017) 'The immunogenicity and immune tolerance of pluripotent stem cell derivatives', *Frontiers in Immunology*, 8, p. 645. doi:10.3389/fimmu.2017.00645.

Liu, Y., Xue, Y., Ridley, S., Zhang, D., Rezvani, K., Fu, X.D. & Wang, H. (2014) 'Direct reprogramming of Huntington's disease patient fibroblasts into neuron-like cells leads to abnormal neurite outgrowth, increased cell death, and aggregate formation', *PLoS ONE*, 9(10), p. e109621. doi:10.1371/journal.pone.0109621.

Liu, Y., Miao, Q., Yuan, J., Han, S., Zhang, P., Li, S., Rao, Z., Zhao, W., Ye, Q., Geng, J., *et al*. (2015) 'Ascl1 converts dorsal midbrain astrocytes into functional neurons in vivo', *Journal of Neuroscience*, 35(25), pp. 9336–9355. doi:10.1523/JNEUROSCI.3975-14.2015.

Liu, Y., Qiao, F., Leiferman, P.C., Ross, A., Schlenker, E.H. & Wang, H. (2017) 'FOXOs modulate proteasome activity in human-induced pluripotent stem cells of Huntington's disease and their derived neural cells', *Human Molecular Genetics*, 26(22), pp. 4416–4428. doi:10.1093/hmg/ddx327.

Liu, Y., Yu, C., Daley, T.P., Wang, F., Cao, W.S., Bhate, S., Lin, X., Still II, C., Liu, H., Zhao, D., *et al*. (2018) 'CRISPR activation screens systematically identify factors that drive neuronal fate and reprogramming', *Cell Stem Cell*, 23(5), pp. 758–771. doi:10.1016/j.stem.2018.09.003.

Liu, Z., Easson, G.W.D., Zhao, J., Makki, N., Ahituv, N., Hilton, M.J., Tang, S.Y. & Gray, R.S. (2019) 'Dysregulation of STAT3 signaling is associated with endplate-oriented herniations of the intervertebral disc in Adgrg6 mutant mice', *PLoS Genetics*, 15(10), p. e1008096. doi:10.1371/journal.pgen.1008096.

Livak, K.J. & Schmittgen, T.D. (2001) 'Analysis of relative gene expression data using real-time quantitative PCR and the 2-ΔΔCT method', *Methods*, 25(4), pp. 402–408. doi:10.1006/meth.2001.1262.

Lodato, M.A., Rodin, R.E., Bohrson, C.L., Coulter, M.E., Barton, A.R., Kwon, M., Sherman, M.A., Vitzthum, C.M., Luquette, L.J., Yandava, C., *et al*. (2018) 'Aging and neurodegeneration are associated with increased mutations in single human neurons', *Science*, 359(6375), pp. 555–559. doi:10.1126/science.aao4426.

Loeb, L.A., Wallace, D.C. & Martin, G.M. (2005) 'The mitochondrial theory of aging and its relationship to reactive oxygen species damage and somatic mtDNA mutations', *Proceedings of the National Academy of Sciences of the United States of America*, 102(50), pp. 18769–18770. doi:10.1073/pnas.0509776102.

Love, M.I., Huber, W. & Anders, S. (2014) 'Moderated estimation of fold change and dispersion for RNA-seq data with DESeq2', *Genome Biology*, 15(12), p. 550. doi:10.1186/s13059-014-0550-8.

Lowe, D., Horvath, S. & Raj, K. (2016) 'Epigenetic clock analyses of cellular senescence and ageing', *Oncotarget*, 7(8), pp. 8524–8531. doi:10.18632/oncotarget.7383.

Lu, J., Liu, H., Huang, C.T.L., Chen, H., Du, Z., Liu, Y., Sherafat, M.A. & Zhang, S.C. (2013) 'Generation of integration-free and region-specific neural progenitors from primate fibroblasts', *Cell Reports*, 3(5), pp. 1580–1591. doi:10.1016/j.celrep.2013.04.004.

Lujan, E., Chanda, S., Ahlenius, H., Südhof, T.C. & Wernig, M. (2012) 'Direct conversion of mouse fibroblasts to self-renewing, tripotent neural precursor cells', *Proceedings of the National Academy of Sciences of the United States of America*, 109(7), pp. 2527–2532. doi:10.1073/pnas.1121003109.

Lujan, E., Zunder, E.R., Ng, Y.H., Goronzy, I.N., Nolan, G.P. & Wernig, M. (2015) 'Early reprogramming regulators identified by prospective isolation and mass cytometry', *Nature*, 521(7552), pp. 352–356. doi:10.1038/nature14274.

Luo, C., Lee, Q.Y., Wapinski, O., Castanon, R., Nery, J.R., Mall, M., Kareta, M.S., Cullen, S.M., Goodell, M.A.,

Chang, H.Y., *et al*. (2019) 'Global DNA methylation remodeling during direct reprogramming of fibroblasts to neurons', *Elife*, 8, p. e40197. doi:10.7554/eLife.40197.

Lupo, G., Nisi, P.S., Esteve, P., Paul, Y.L., Novo, C.L., Sidders, B., Khan, M.A., Biagioni, S., Liu, H.K., Bovolenta, P., *et al*. (2018) 'Molecular profiling of aged neural progenitors identifies Dbx2 as a candidate regulator of age-associated neurogenic decline', *Aging Cell*, 17(3), p. e12745. doi:10.1111/acel.12745.

Ly, H. (2011) 'Telomere dynamics in induced pluripotent stem cells: Potentials for human disease modeling', *World Journal of Stem Cells*, 3(10), p. 89. doi:10.4252/wjsc.v3.i10.89.

Ma, L., Hu, B., Liu, Y., Vermilyea, S.C., Liu, H., Gao, L., Sun, Y., Zhang, X. & Zhang, S.-C. (2012) 'Human embryonic stem cell-derived GABA neurons correct locomotion deficits in quinolinic acid-lesioned mice', *Cell Stem Cell*, 10(4), pp. 455–464. doi:10.1016/j.stem.2012.01.021.

Makwana, K., Patel, S.A., Velingkaar, N., Ebron, J.S., Shukla, G.C. & Kondratov, R. V. (2017) 'Aging and calorie restriction regulate the expression of miR-125a-5p and its target genes Stat3, Casp2 and Stard13', *Aging*, 9(7), pp. 1825–1843. doi:10.18632/aging.101270.

Mall, M., Kareta, M.S., Chanda, S., Ahlenius, H., Perotti, N., Zhou, B., Grieder, S.D., Ge, X., Drake, S., Euong Ang, C., *et al*. (2017) 'Myt1l safeguards neuronal identity by actively repressing many non-neuronal fates', *Nature*, 544(7649), pp. 245–249. doi:10.1038/nature21722.

Mancuso, R., Van Den Daele, J., Fattorelli, N., Wolfs, L., Balusu, S., Burton, O., Liston, A., Sierksma, A., Fourne, Y., Poovathingal, S., *et al*. (2019) 'Stem-cell-derived human microglia transplanted in mouse brain to study human disease', *Nature Neuroscience*, 22(12), pp. 2111–2116. doi:10.1038/s41593-019-0525-x.

Marro, S., Pang, Z.P., Yang, N., Tsai, M.C., Qu, K., Chang, H.Y., Südhof, T.C. & Wernig, M. (2011) 'Direct lineage conversion of terminally differentiated hepatocytes to functional neurons', *Cell Stem Cell*, 9(11), pp. 374–382. doi:10.1016/j.stem.2011.09.002.

Martinat, C., Bacci, J.J., Leete, T., Kim, J., Vanti, W.B., Newman, A.H., Cha, J.H., Gether, U., Wang, H. & Abeliovich, A. (2006) 'Cooperative transcription activation by Nurr1 and Pitx3 induces embryonic stem cell maturation to the midbrain dopamine neuron phenotype', *Proceedings of the National Academy of Sciences of the United States of America*, 103(8), pp. 2874–2879. doi:10.1073/pnas.0511153103.

Martinato, F., Cesaroni, M., Amati, B. & Guccione, E. (2008) 'Analysis of Myc-induced histone modifications on target chromatin', *PLoS ONE*, 3(11), p. e3650. doi:10.1371/journal.pone.0003650.

Masserdotti, G., Gillotin, S., Sutor, B., Drechsel, D., Irmler, M., Jørgensen, H.F., Sass, S., Theis, F.J., Beckers, J., Berninger, B., *et al*. (2015) 'Transcriptional mechanisms of proneural factors and REST in regulating neuronal reprogramming of astrocytes', *Cell Stem Cell*, 17(1), pp. 74–88. doi:10.1016/j.stem.2015.05.014.

Mata-Garrido, J., Casafont, I., Tapia, O., Berciano, M.T. & Lafarga, M. (2016) 'Neuronal accumulation of unrepaired DNA in a novel specific chromatin domain: structural, molecular and transcriptional characterization', *Acta Neuropathologica Communications*, 4, p. 41. doi:10.1186/s40478-016-0312-9.

Mathews, M., Wißfeld, J., Flitsch, L.J., Shahraz, A., Semkova, V., Breitkreuz, Y., Neumann, H. & Brüstle, O. (In revision) 'Developmentally informed large-scale production and cryopreservation of human induced pluripotent stem cell-derived microglia', No preprint available.

Matsuda, T., Irie, T., Katsurabayashi, S., Hayashi, Y., Nagai, T., Hamazaki, N., Adefuin, A.M.D., Miura, F., Ito, T., Kimura, H., *et al*. (2019) 'Pioneer factor NeuroD1 rearranges transcriptional and epigenetic profiles to execute microglia-neuron conversion', *Neuron*, 101(3), pp. 472–485. doi:10.1016/j.neuron.2018.12.010.

Matsui, T., Takano, M., Yoshida, K., Ono, S., Fujisaki, C., Matsuzaki, Y., Toyama, Y., Nakamura, M., Okano, H. & Akamatsu, W. (2012) 'Neural stem cells directly differentiated from partially reprogrammed fibroblasts rapidly acquire gliogenic competency', *Stem Cells*, 30(6), pp. 1109–1119. doi:10.1002/stem.1091.

Mattugini, N., Bocchi, R., Scheuss, V., Russo, G.L., Torper, O., Lao, C.L. & Götz, M. (2019) 'Inducing different neuronal subtypes from astrocytes in the injured mouse cerebral cortex', *Neuron*, 103(6), pp. 1086-1095.e5. doi:10.1016/j.neuron.2019.08.009.

Maucksch, C., Firmin, E., Butler-Munro, C., Montgomery, J.M., Dottori, M. & Connor, B. (2012) 'Non-viral generation of neural precursor-like cells from adult human fibroblasts', *Journal of Stem Cells and Regenerative Medicine*, 8(3), pp. 162–170. doi:http://dx.doi.org/10.1126/science.1093155.

Mayran, A. & Drouin, J. (2018) 'Pioneer transcription factors shape the epigenetic landscape', *Journal of Biological Chemistry*, 293(36), pp. 13795–13804. doi:10.1074/jbc.R117.001232.

Maza, I., Caspi, I., Zviran, A., Chomsky, E., Rais, Y., Viukov, S., Geula, S., Buenrostro, J.D., Weinberger, L., Krupalnik, V., *et al*. (2015) 'Transient acquisition of pluripotency during somatic cell transdifferentiation with iPSC reprogramming factors', *Nature Biotechnology*, 33(7), pp. 769–774. doi:10.1038/nbt.3270.

Mazzoni, E.O., Mahony, S., Closser, M., Morrison, C.A., Nedelec, S., Williams, D.J., An, D., Gifford, D.K. & Wichterle, H. (2013) 'Synergistic binding of transcription factors to cell-specific enhancers programs motor neuron identity', *Nature Neuroscience*, 16(9), pp. 1219–1227. doi:10.1038/nn.3467.

Mecca, C., Giambanco, I., Donato, R. & Arcuri, C. (2018) 'Microglia and aging: The role of the TREM2–DAP12 and CX3CL1-CX3CR1 axes', *International Journal of Molecular Sciences*, 19(1), p. 318. doi:10.3390/ijms19010318.

Meijer, M., Rehbach, K., Brunner, J.W., Classen, J.A., Lammertse, H.C.A., van Linge, L.A., Schut, D., Krutenko, T., Hebisch, M., Cornelisse, L.N., *et al*. (2019) 'A single-cell model for synaptic transmission and plasticity in human iPSC-derived neurons', *Cell Reports*, 27, pp. 2199–2211. doi:10.1016/j.celrep.2019.04.058.

Mendelsohn, A.R. & Larrick, J.W. (2015) 'Aging stem cells lose the capability to distribute damaged proteins asymmetrically', *Rejuvenation Research*, 18(6), pp. 581–584. doi:10.1089/rej.2015.1800.

Meng, F., Chen, S., Miao, Q., Zhou, K., Lao, Q., Zhang, X., Guo, W. & Jiao, J. (2012) 'Induction of fibroblasts to neurons through adenoviral gene delivery', *Cell Research*, 22(2), pp. 436–440. doi:10.1038/cr.2011.185.

Merkle, F.T., Ghosh, S., Kamitaki, N., Mitchell, J., Avior, Y., Mello, C., Kashin, S., Mekhoubad, S., Ilic, D.,

Charlton, M., *et al*. (2017) 'Human pluripotent stem cells recurrently acquire and expand dominant negative P53 mutations', *Nature*, 545(7653), pp. 229–233. doi:10.1038/nature22312.

Mertens, J., Stüber, K., Wunderlich, P., Ladewig, J., Kesavan, J.C., Vandenberghe, R., Vandenbulcke, M., Van Damme, P., Walter, J., Brüstle, O., *et al*. (2013) 'APP processing in human pluripotent stem cell-derived neurons is resistant to NSAID-based γ-secretase modulation', *Stem Cell Reports*, 1(6), pp. 491–498. doi:10.1016/j.stemcr.2013.10.011.

Mertens, J., Paquola, A.C.M., Ku, M., Hatch, E., Böhnke, L., Ladjevardi, S., McGrath, S., Campbell, B., Lee, H., Herdy, J.R., *et al*. (2015) 'Directly reprogrammed human neurons retain aging-associated transcriptomic signatures and reveal age-related nucleocytoplasmic defects', *Cell Stem Cell*, 17(6), pp. 705–718. doi:10.1016/j.stem.2015.09.001.

Mertens, J., Marchetto, M.C., Bardy, C. & Gage, F.H. (2016) 'Evaluating cell reprogramming, differentiation and conversion technologies in neuroscience', *Nature Reviews Neuroscience*, 17(7), pp. 424–437. doi:10.1038/nrn.2016.46.

Mertens, J., Herdy, J.R., Traxler, L., Schafer, S.T., Schlachetzki, J.C.M., Böhnke, L., Reid, D.A., Lee, H., Zangwill, D., Fernandes, D.P., *et al*. (2021) 'Age-dependent instability of mature neuronal fate in induced neurons from Alzheimer's patients', *Cell Stem Cell*, 28(9), pp. 1533-1548.e6. doi:10.1016/j.stem.2021.04.004.

Meyer, K., Ferraiuolo, L., Miranda, C.J., Likhite, S., McElroy, S., Renusch, S., Ditsworth, D., Lagier-Tourenne, C., Smith, R.A., Ravits, J., *et al*. (2014) 'Direct conversion of patient fibroblasts demonstrates non-cell autonomous toxicity of astrocytes to motor neurons in familial and sporadic ALS', *Proceedings of the National Academy of Sciences of the United States of America*, 111(2), pp. 829–832. doi:10.1073/pnas.1314085111.

Miller, J.D., Ganat, Y.M., Kishinevsky, S., Bowman, R.L., Liu, B., Tu, E.Y., Mandal, P.K., Vera, E., Shim, J.W., Kriks, S., *et al*. (2013) 'Human iPSC-based modeling of late-onset disease via progerin-induced aging', *Cell Stem Cell*, 13(6), pp. 691–705. doi:10.1016/j.stem.2013.11.006.

Mirakhori, F., Zeynali, B., Rassouli, H., Shahbazi, E., Hashemizadeh, S., Kiani, S., Salekdeh, G.H. & Baharvand, H. (2015) 'Induction of neural progenitor-like cells from human fibroblasts via a genetic material-free approach', *PLoS ONE*, 10(8), p. e0135479. doi:10.1371/journal.pone.0135479.

Miskinyte, G., Devaraju, K., Grønning Hansen, M., Monni, E., Tornero, D., Woods, N.B., Bengzon, J., Ahlenius, H., Lindvall, O. & Kokaia, Z. (2017) 'Direct conversion of human fibroblasts to functional excitatory cortical neurons integrating into human neural networks', *Stem Cell Research and Therapy*, 8(1), p. 207. doi:10.1186/s13287-017-0658-3.

Mitchell, S.J., Scheibye-Knudsen, M., Longo, D.L. & De Cabo, R. (2015) 'Animal models of aging research: Implications for human aging and age-related diseases', *Annual Review of Animal Biosciences*, 3, pp. 283–303. doi:10.1146/annurev-animal-022114-110829.

Miura, K., Okada, Y., Aoi, T., Okada, A., Takahashi, K., Okita, K., Nakagawa, M., Koyanagi, M., Tanabe, K., Ohnuki, M., *et al*. (2009) 'Variation in the safety of induced pluripotent stem cell lines', *Nature Biotechnology*,

27(8), pp. 743–745. doi:10.1038/nbt.1554.

Mizushima, N., Ohsumi, Y. & Yoshimori, T. (2002) 'Autophagosome formation in mammalian cells', *Cell Structure and Function*, 27(6), pp. 421–429. doi:10.1247/csf.27.421.

Mizushima, N. & Yoshimori, T. (2007) 'How to interpret LC3 immunoblotting', *Autophagy*, 3(6), pp. 542–545. doi:10.4161/auto.4600.

Monk, R., Lee, K., Jones, K.S. & Connor, B. (2021) 'Directly reprogrammed Huntington's disease neural precursor cells generate striatal neurons exhibiting aggregates and impaired neuronal maturation', *Stem Cells*, 39(10), pp. 1410–1422. doi:10.1002/stem.3420.

Montecucco, A., Zanetta, F. & Biamonti, G. (2015) 'Molecular mechanisms of etoposide', *EXCLI Journal*, 14, pp. 95–108. doi:10.17179/excli2014-561.

Moore, D.L., Pilz, G.A., Araúzo-Bravo, M.J., Barral, Y. & Jessberger, S. (2015) 'A mechanism for the segregation of age in mammalian neural stem cells', *Science*, 349(6254), pp. 1334–1338. doi:10.1126/science.aac9868.

Morizane, A., Kikuchi, T., Hayashi, T., Mizuma, H., Takara, S., Doi, H., Mawatari, A., Glasser, M.F., Shiina, T., Ishigaki, H., *et al*. (2017) 'MHC matching improves engraftment of iPSC-derived neurons in non-human primates', *Nature Communications*, 8(1), p. 385. doi:10.1038/s41467-017-00926-5.

Morris, T.J., Butcher, L.M., Feber, A., Teschendorff, A.E., Chakravarthy, A.R., Wojdacz, T.K. & Beck, S. (2014) 'ChAMP: 450k chip analysis methylation pipeline', *Bioinformatics*, 30(3), pp. 428–430. doi:10.1093/bioinformatics/btt684.

Nakatomi, H., Kuriu, T., Okabe, S., Yamamoto, S., Hatano, O., Kawahara, N., Tamura, A., Kirino, T. & Nakafuku, M. (2002) 'Regeneration of hippocampal pyramidal neurons after ischemic brain injury by recruitment of endogenous neural progenitors', *Cell*, 110(4), pp. 429–441. doi:10.1016/S0092-8674(02)00862-0.

Narantuya, D., Nagai, A., Abdullah, M., Masuda, J., Kobayashi, S., Yamaguchi, S. & Kim, S.U. (2010) 'Human microglia transplanted in rat focal ischemia brain induce neuroprotection and behavioral improvement', *PLoS ONE*, 5(7), p. e11746. doi:10.1371/journal.pone.0011746.

Nefzger, C.M., Rossello, F.J., Chen, J., Liu, X., Knaupp, A.S., Firas, J., Paynter, J.M., Pflueger, J., Buckberry, S., Lim, S.M., *et al*. (2017) 'Cell type of origin dictates the route to pluripotency', *Cell Reports*, 21(10), pp. 2649–2660. doi:10.1016/j.celrep.2017.11.029.

Nehme, R., Zuccaro, E., Ghosh, S.D., Li, C., Sherwood, J.L., Pietilainen, O., Barrett, L.E., Limone, F., Worringer, K.A., Kommineni, S., *et al*. (2018) 'Combining NGN2 programming with developmental patterning generates human excitatory neurons with NMDAR-mediated synaptic transmission', *Cell Reports*, 23(8), pp. 2509–2523. doi:10.1016/j.celrep.2018.04.066.

Ng, A.H.M., Khoshakhlagh, P., Rojo Arias, J.E., Pasquini, G., Wang, K., Swiersy, A., Shipman, S.L., Appleton, E., Kiaee, K., Kohman, R.E., *et al*. (2021) 'A comprehensive library of human transcription factors for cell fate engineering', *Nature Biotechnology*, 39(4), pp. 510–519. doi:10.1038/s41587-020-0742-6.

Ng, Y.H., Chanda, S., Janas, J.A., Yang, N., Kokubu, Y., Südhof, T.C. & Wernig, M. (2021) 'Efficient generation of dopaminergic induced neuronal cells with midbrain characteristics', *Stem Cell Reports*, 16(7), pp. 1763–1776. doi:10.1016/j.stemcr.2021.05.017.

Nguyen, B.T., Sharma, N., Shin, E.J., Jeong, J.H., Lee, S.H., Jang, C.G., Nah, S.Y., Nabeshima, T., Yoneda, Y. & Kim, H.C. (2019) 'Theanine attenuates memory impairments induced by klotho gene depletion in mice', *Food and Function*, 10(1), pp. 325–332. doi:10.1039/c8fo01577e.

Nguyen, H.N., Byers, B., Cord, B., Shcheglovitov, A., Byrne, J., Gujar, P., Kee, K., Schüle, B., Dolmetsch, R.E., Langston, W., *et al*. (2011) 'LRRK2 mutant iPSC-derived DA neurons demonstrate increased susceptibility to oxidative stress', *Cell Stem Cell*, 8(3), pp. 267–280. doi:10.1016/j.stem.2011.01.013.

Nickolls, A.R., Lee, M.M., Espinoza, D.F., Szczot, M., Lam, R.M., Wang, Q., Beers, J., Zou, J., Nguyen, M.Q., Solinski, H.J., *et al*. (2020) 'Transcriptional programming of human mechanosensory neuron subtypes from pluripotent stem cells', *Cell Reports*, 30(3), pp. 932-946.e7. doi:10.1016/j.celrep.2019.12.062.

Nishiyama, A., Xin, L., Sharov, A.A., Thomas, M., Mowrer, G., Meyers, E., Piao, Y., Mehta, S., Yee, S., Nakatake, Y., *et al*. (2009) 'Uncovering early response of gene regulatory networks in ESCs by systematic induction of transcription factors', *Cell Stem Cell*, 5(4), pp. 420–433. doi:10.1016/j.stem.2009.07.012.

Niu, W., Zang, T., Zou, Y., Fang, S., Smith, D.K., Bachoo, R. & Zhang, C.L. (2013) 'In vivo reprogramming of astrocytes to neuroblasts in the adult brain', *Nature Cell Biology*, 15(10), pp. 1164–1175. doi:10.1038/ncb2843.

Niu, W., Zang, T., Smith, D.K., Vue, T.Y., Zou, Y., Bachoo, R., Johnson, J.E. & Zhang, C.L. (2015) 'SOX2 reprograms resident astrocytes into neural progenitors in the adult brain', *Stem Cell Reports*, 4(5), pp. 780–794. doi:10.1016/j.stemcr.2015.03.006.

O'Brown, Z.K., Van Nostrand, E.L., Higgins, J.P. & Kim, S.K. (2015) 'The inflammatory transcription factors NFκB, STAT1 and STAT3 drive age-associated transcriptional changes in the human kidney', *PLoS Genetics*, 11(12), p. e1005734. doi:10.1371/journal.pgen.1005734.

O'Shea, K.S. (2001) 'Neuronal differentiation of mouse embryonic stem cells: Lineage selection and forced differentiation paradigms', *Blood Cells, Molecules, and Diseases*, 27(3), pp. 705–712. doi:10.1006/bcmd.2001.0435.

Ocampo, A., Reddy, P., Martinez-Redondo, P., Platero-Luengo, A., Hatanaka, F., Hishida, T., Li, M., Lam, D., Kurita, M., Beyret, E., *et al*. (2016) 'In vivo amelioration of age-associated hallmarks by partial reprogramming', *Cell*, 167(7), pp. 1719–1733. doi:10.1016/j.cell.2016.11.052.

Ohori, Y., Yamamoto, S. -i., Nagao, M., Sugimori, M., Yamamoto, N., Nakamura, K. & Nakafuku, M. (2006) 'Growth factor treatment and genetic manipulation stimulate neurogenesis and oligodendrogenesis by endogenous neural progenitors in the injured adult spinal cord', *Journal of Neuroscience*, 26(46), pp. 11948–11960. doi:10.1523/JNEUROSCI.3127-06.2006.

Olova, N., Simpson, D.J., Marioni, R.E. & Chandra, T. (2019) 'Partial reprogramming induces a steady decline in epigenetic age before loss of somatic identity', *Aging Cell*, 18(1), p. e12877. doi:10.1111/acel.12877.

Omrani, M.R., Yaqubi, M. & Mohammadnia, A. (2018) 'Transcription factors in regulatory and protein subnetworks during generation of neural stem cells and neurons from direct reprogramming of non-fibroblastic cell sources', *Neuroscience*, 380, pp. 63–77. doi:10.1016/j.neuroscience.2018.03.033.

Onishi, K. & Zandstra, P.W. (2015) 'LIF signaling in stem cells and development', *Development*, 142(13), pp. 2230–2236. doi:10.1242/dev.117598.

Pang, Z.P., Yang, N., Vierbuchen, T., Ostermeier, A., Fuentes, D.R., Yang, T.Q., Citri, A., Sebastiano, V., Marro, S., Südhof, T.C., *et al*. (2011) 'Induction of human neuronal cells by defined transcription factors', *Nature*, 476(7359), pp. 220–223. doi:10.1038/nature10202.

Parajuli, B., Saito, H., Shinozaki, Y., Shigetomi, E., Miwa, H., Yoneda, S., Tanimura, M., Omachi, S., Asaki, T., Takahashi, K., *et al*. (2021) 'Transnasal transplantation of human induced pluripotent stem cell-derived microglia to the brain of immunocompetent mice', *Glia*, 69(10), pp. 2332–2348. doi:10.1002/glia.23985.

Park, C.-H., Kang, J.S., Shin, Y.H., Chang, M.Y., Chung, S., Koh, H.-C., Zhu, M.H., Oh, S.B., Lee, Y.-S., Panagiotakos, G., *et al*. (2006) 'Acquisition of in vitro and in vivo functionality of Nurr1-induced dopamine neurons', *FASEB Journal*, 20(14), pp. 2553–2555. doi:10.1096/fj.06-6159fje.

Park, J., Lee, N., Lee, Jaekwang, Choe, E.K., Kim, M.K., Lee, Jeonghoon, Byun, M.S., Chon, M.W., Kim, S.W., Lee, C.J., *et al*. (2017) 'Small molecule-based lineage switch of human adipose-derived stem cells into neural stem cells and functional GABAergic neurons', *Scientific Reports*, 7(1), p. 10166. doi:10.1038/s41598-017-10394-y.

Park, S.J., Shin, E.J., Min, S.S., An, J., Li, Z., Hee Chung, Y., Hoon Jeong, J., Bach, J.H., Nah, S.Y., Kim, W.K., *et al*. (2013) 'Inactivation of JAK2/STAT3 signaling axis and downregulation of M1 mAChR cause cognitive impairment in klotho mutant mice, a genetic model of aging', *Neuropsychopharmacology*, 38(8), pp. 1426–1437. doi:10.1038/npp.2013.39.

Patro, R., Duggal, G., Love, M.I., Irizarry, R.A. & Kingsford, C. (2017) 'Salmon provides fast and bias-aware quantification of transcript expression', *Nature Methods*, 14(4), pp. 417–419. doi:10.1038/nmeth.4197.

Patton, P.E. & McNaughton, B. (1995) 'Connection matrix of the hippocampal formation: I. The dentate gyrus', *Hippocampus*, 5(4), pp. 245–286. doi:10.1002/hipo.450050402.

Payne, N.L., Sylvain, A., O'Brien, C., Herszfeld, D., Sun, G. & Bernard, C.C.A. (2015) 'Application of human induced pluripotent stem cells for modeling and treating neurodegenerative diseases', *New Biotechnology*, 32(1), pp. 212–228. doi:10.1016/j.nbt.2014.05.001.

Pereira, M., Pfisterer, U., Rylander, D., Torper, O., Lau, S., Lundblad, M., Grealish, S. & Parmar, M. (2014) 'Highly efficient generation of induced neurons from human fibroblasts that survive transplantation into the adult rat brain', *Scientific Reports*, 4, p. 6330. doi:10.1038/srep06330.

Pereira, M., Birtele, M., Shrigley, S., Benitez, J.A., Hedlund, E., Parmar, M. & Ottosson, D.R. (2017) 'Direct reprogramming of resident NG2 glia into neurons with properties of fast-spiking parvalbumin-containing interneurons', *Stem Cell Reports*, 9(3), pp. 742–751. doi:10.1016/j.stemcr.2017.07.023.

Petkovich, D.A., Podolskiy, D.I., Lobanov, A. V., Lee, S.G., Miller, R.A. & Gladyshev, V.N. (2017) 'Using DNA methylation profiling to evaluate biological age and longevity interventions', *Cell Metabolism*, 25(4), pp. 954-960.e6. doi:10.1016/j.cmet.2017.03.016.

Pfisterer, U., Kirkeby, A., Torper, O., Wood, J., Nelander, J., Dufour, A., Björklund, A., Lindvall, O., Jakobsson, J. & Parmar, M. (2011) 'Direct conversion of human fibroblasts to dopaminergic neurons', *Proceedings of the National Academy of Sciences of the United States of America*, 108(25), pp. 10343–10348. doi:10.1073/pnas.1105135108.

Pfisterer, U., Wood, J., Nihlberg, K., Hallgren, O., Bjermer, L., Westergren-Thorsson, G., Lindvall, O. & Parmar, M. (2011) 'Efficient induction of functional neurons from adult human fibroblasts', *Cell Cycle*, 10(19), pp. 3311–3316. doi:10.4161/cc.10.19.17584.

Pfisterer, U., Ek, F., Lang, S., Soneji, S., Olsson, R. & Parmar, M. (2016) 'Small molecules increase direct neural conversion of human fibroblasts', *Scientific Reports*, 6, p. 38290. doi:10.1038/srep38290.

Piao, J., Zabierowski, S., Dubose, B.N., Hill, E.J., Navare, M., Claros, N., Rosen, S., Ramnarine, K., Horn, C., Fredrickson, C., *et al*. (2021) 'Preclinical efficacy and safety of a human embryonic stem cell-derived midbrain dopamine progenitor product, MSK-DA01', *Cell Stem Cell*, 28(2), pp. 217-229.e7. doi:10.1016/j.stem.2021.01.004.

Polo, J.M., Liu, S., Figueroa, M.E., Kulalert, W., Eminli, S., Tan, K.Y., Apostolou, E., Stadtfeld, M., Li, Y., Shioda, T., *et al*. (2010) 'Cell type of origin influences the molecular and functional properties of mouse induced pluripotent stem cells', *Nature Biotechnology*, 28(8), pp. 848–855. doi:10.1038/nbt.1667.

Prasad, A., Teh, D.B.L., Shah Jahan, F.R., Manivannan, J., Chua, S.M. & All, A.H. (2017) 'Direct conversion through transdifferentiation: Efficacy and safety', *Stem Cells and Development*, 26(3), pp. 154–165. doi:10.1089/scd.2016.0174.

Prigione, A., Hossini, A.M., Lichtner, B., Serin, A., Fauler, B., Megges, M., Lurz, R., Lehrach, H., Makrantonaki, E., Zouboulis, C.C., *et al*. (2011) 'Mitochondrial-associated cell death mechanisms are reset to an embryonic-like state in aged donor-derived iPS cells harboring chromosomal aberrations', *PLoS ONE*, 6(11), p. e27352. doi:10.1371/journal.pone.0027352.

Pyo, I.S., Yun, S., Yoon, Y.E., Choi, J.W. & Lee, S.J. (2020) 'Mechanisms of aging and the preventive effects of resveratrol on age-related diseases', *Molecules*, 25(20), p. 4649. doi:10.3390/molecules25204649.

Pyo, J.O., Yoo, S.M., Ahn, H.H., Nah, J., Hong, S.H., Kam, T.I., Jung, S. & Jung, Y.K. (2013) 'Overexpression of Atg5 in mice activates autophagy and extends lifespan', *Nature Communications*, 4, p. 2300. doi:10.1038/ncomms3300.

Qin, H., Zhao, A.D., Sun, M.L., Ma, K. & Fu, X.B. (2020) 'Direct conversion of human fibroblasts into dopaminergic neuron-like cells using small molecules and protein factors', *Military Medical Research*, 7(1), p. 52. doi:10.1186/s40779-020-00284-2.

Rao, Y., Du, S., Yang, B., Wang, Yuqing, Li, Y., Li, R., Zhou, T., Du, X., He, Y., Wang, Yafei, *et al*. (2021)

'NeuroD1 induces microglial apoptosis and cannot induce microglia-to-neuron cross-lineage reprogramming', *Neuron*, 109(24), pp. 4094-4108.e5. doi:10.1016/j.neuron.2021.11.008.

Reinhardt, P., Glatza, M., Hemmer, K., Tsytsyura, Y., Thiel, C.S., Höing, S., Moritz, S., Parga, J.A., Wagner, L., Bruder, J.M., *et al*. (2013) 'Derivation and expansion using only small molecules of human neural progenitors for neurodegenerative disease modeling', *PLoS ONE*, 8(3), p. e59252. doi:10.1371/journal.pone.0059252.

Reinhardt, P., Schmid, B., Burbulla, L.F., Schöndorf, D.C., Wagner, L., Glatza, M., Höing, S., Hargus, G., Heck, S.A., Dhingra, A., *et al*. (2013) 'Genetic correction of a Lrrk2 mutation in human iPSCs links parkinsonian neurodegeneration to ERK-dependent changes in gene expression', *Cell Stem Cell*, 12(3), pp. 354–367. doi:10.1016/j.stem.2013.01.008.

Rhee, H.J., Shaib, A.H., Rehbach, K., Lee, C., Seif, P., Thomas, C., Gideons, E., Guenther, A., Krutenko, T., Hebisch, M., *et al*. (2019) 'An autaptic culture system for standardized analyses of iPSC-derived human neurons', *Cell Reports*, 27(7), pp. 2212-2228.e7. doi:10.1016/j.celrep.2019.04.059.

Riera, C.E., Merkwirth, C., De Magalhaes Filho, C.D. & Dillin, A. (2016) 'Signaling networks determining life span', *Annual Review of Biochemistry*, 85, pp. 35–64. doi:10.1146/annurev-biochem-060815-014451.

Ring, K.L., Tong, L.M., Balestra, M.E., Javier, R., Andrews-Zwilling, Y., Li, G., Walker, D., Zhang, W.R., Kreitzer, A.C. & Huang, Y. (2012) 'Direct reprogramming of mouse and human fibroblasts into multipotent neural stem cells with a single factor', *Cell Stem Cell*, 11(1), pp. 100–109. doi:10.1016/j.stem.2012.05.018.

Rivetti Di Val Cervo, P., Romanov, R.A., Spigolon, G., Masini, D., Martín-Montañez, E., Toledo, E.M., La Manno, G., Feyder, M., Pifl, C., Ng, Y.H., *et al*. (2017) 'Induction of functional dopamine neurons from human astrocytes in vitro and mouse astrocytes in a Parkinson's disease model', *Nature Biotechnology*, 35(5), pp. 444–452. doi:10.1038/nbt.3835.

Robinson, M., Chapani, P., Styan, T., Vaidyanathan, R. & Willerth, S.M. (2016) 'Functionalizing Ascl1 with novel intracellular protein delivery technology for promoting neuronal differentiation of human induced pluripotent stem cells', *Stem Cell Reviews and Reports*, 12(4), pp. 476–483. doi:10.1007/s12015-016-9655-7.

Rouaux, C. & Arlotta, P. (2013) 'Direct lineage reprogramming of post-mitotic callosal neurons into corticofugal neurons in vivo', *Nature Cell Biology*, 15(2), pp. 214–221. doi:10.1038/ncb2660.

Rowland, B.D., Bernards, R. & Peeper, D.S. (2005) 'The KLF4 tumour suppressor is a transcriptional repressor of p53 that acts as a context-dependent oncogene', *Nature Cell Biology*, 7(11), pp. 1074–1082. doi:10.1038/ncb1314.

Sahin, E., Colla, S., Liesa, M., Moslehi, J., Müller, F.L., Guo, M., Cooper, M., Kotton, D., Fabian, A.J., Walkey, C., *et al*. (2011) 'Telomere dysfunction induces metabolic and mitochondrial compromise', *Nature*, 470(7334), pp. 359–365. doi:10.1038/nature09787.

Salminen, A., Kaarniranta, K. & Kauppinen, A. (2021) 'Insulin/IGF-1 signaling promotes immunosuppression via the STAT3 pathway: impact on the aging process and age-related diseases', *Inflammation Research*, 70(10–12), pp. 1043–1061. doi:10.1007/s00011-021-01498-3.

Sánchez-Danés, A., Consiglio, A., Richaud, Y., Rodríguez-Pizà, I., Dehay, B., Edel, M., Bové, J., Memo, M., Vila, M., Raya, A., *et al*. (2012) 'Efficient generation of A9 midbrain dopaminergic neurons by lentiviral delivery of LMX1A in human embryonic stem cells and induced pluripotent stem cells', *Human Gene Therapy*, 23(1), pp. 56–69. doi:10.1089/hum.2011.054.

Lo Sardo, V., Ferguson, W., Erikson, G.A., Topol, E.J., Baldwin, K.K. & Torkamani, A. (2017) 'Influence of donor age on induced pluripotent stem cells', *Nature Biotechnology*, 35(1), pp. 69–74. doi:10.1038/nbt.3749.

Sarkar, T.J., Quarta, M., Mukherjee, S., Colville, A., Paine, P., Doan, L., Tran, C.M., Chu, C.R., Horvath, S., Qi, L.S., *et al*. (2020) 'Transient non-integrative expression of nuclear reprogramming factors promotes multifaceted amelioration of aging in human cells', *Nature Communications*, 11(1), p. 1545. doi:10.1038/s41467-020-15174-3.

Sayols, S. (2020) 'rrvgo: A Bioconductor package to reduce and visualize gene ontology terms'. doi:https://ssayols.github.io/rrvgo.

Scaffidi, P. & Misteli, T. (2006) 'Lamin A-dependent nuclear defects in human aging', *Science*, 312(5776), pp. 1059–1063. doi:10.1126/science.1127168.

Schörnig, M., Ju, X., Fast, L., Ebert, S., Weigert, A., Kanton, S., Schaffer, T., Kasri, N.N., Treutlein, B., Peter, B., *et al*. (2021) 'Comparison of induced neurons reveals slower structural and functional maturation in humans than in apes', *eLife*, 10, p. e59323. doi:10.7554/eLife.59323.

Schriner, S.E., Linford, N.J., Martin, G.M., Treuting, P., Ogburn, C.E., Emond, M., Coskun, P.E., Ladiges, W., Wolf, N., Van Remmen, H., *et al*. (2005) 'Extension of murine life span by overexpression of catalase targeted to mitochondria', *Science*, 308(5730), pp. 1909–1911. doi:10.1126/science.1106653.

Seibler, P., Graziotto, J., Jeong, H., Simunovic, F., Klein, C. & Krainc, D. (2011) 'Mitochondrial parkin recruitment is impaired in neurons derived from mutant PINK1 induced pluripotent stem cells', *Journal of Neuroscience*, 31(16), pp. 5970–5976. doi:10.1523/JNEUROSCI.4441-10.2011.

Sen, P., Shah, P.P., Nativio, R. & Berger, S.L. (2016) 'Epigenetic mechanisms of longevity and aging', *Cell*, 166(4), pp. 822–839. doi:10.1016/j.cell.2016.07.050.

Serre, A., Snyder, E.Y., Mallet, J. & Buchet, D. (2012) 'Overexpression of basic helix-loop-helix transcription factors enhances neuronal differentiation of fetal human neural progenitor cells in various ways', *Stem Cells and Development*, 21(4), pp. 539–553. doi:10.1089/scd.2011.0079.

Shah, P.P., Donahue, G., Otte, G.L., Capell, B.C., Nelson, D.M., Cao, K., Aggarwala, V., Cruickshanks, H.A., Rai, T.S., McBryan, T., *et al*. (2013) 'Lamin B1 depletion in senescent cells triggers large-scale changes in gene expression and the chromatin landscape', *Genes and Development*, 27(16), pp. 1787–1799. doi:10.1101/gad.223834.113.

Shahbazi, E., Moradi, S., Nemati, S., Satarian, L., Basiri, M., Gourabi, H., Zare Mehrjardi, N., Günther, P., Lampert, A., Händler, K., *et al*. (2016) 'Conversion of human fibroblasts to stably self-renewing neural stem cells with a single zinc-finger transcription factor', *Stem Cell Reports*, 6(4), pp. 539–551.

doi:10.1016/j.stemcr.2016.02.013.

Shannon, P., Markiel, A., Ozier, O., Baliga, N.S., Wang, J.T., Ramage, D., Amin, N., Schwikowski, B. & Ideker, T. (2003) 'Cytoscape: A software environment for integrated models of biomolecular interaction networks', *Genome Research*, 13, pp. 2489–2504. doi:10.1101/gr.1239303.metabolite.

Sheng, C., Zheng, Q., Wu, J., Xu, Z., Wang, Libin, Li, W., Zhang, H., Zhao, X.Y., Liu, L., Wang, Z., *et al*. (2012) 'Direct reprogramming of Sertoli cells into multipotent neural stem cells by defined factors', *Cell Research*, 22(1), pp. 208–218. doi:10.1038/cr.2011.175.

Sheng, C., Zheng, Q., Wu, J., Xu, Z., Sang, L., Wang, Libin, Guo, C., Zhu, W., Tong, M., Liu, L., *et al*. (2012) 'Generation of dopaminergic neurons directly from mouse fibroblasts and fibroblast-derived neural progenitors', *Cell Research*, 22(4), pp. 769–772. doi:10.1038/cr.2012.32.

Sheng, C., Jungverdorben, J., Wiethoff, H., Lin, Q., Flitsch, L.J., Eckert, D., Hebisch, M., Fischer, J., Kesavan, J., Weykopf, B., *et al*. (2018) 'A stably self-renewing adult blood-derived induced neural stem cell exhibiting patternability and epigenetic rejuvenation', *Nature Communications*, 9(1), p. 4047. doi:10.1038/s41467-018-06398-5.

Shi, D., Murty, V. V. & Gu, W. (2015) 'PCDH10, a novel p53 transcriptional target in regulating cell migration', *Cell Cycle*, 14(6), pp. 857–866. doi:10.1080/15384101.2015.1004935.

Shi, Z., Zhang, J., Chen, S., Li, Y., Lei, X., Qiao, H., Zhu, Q., Hu, B., Zhou, Q. & Jiao, J. (2016) 'Conversion of fibroblasts to parvalbumin neurons by one transcription factor, Ascl1, and the chemical compound forskolin', *Journal of Biological Chemistry*, 291(26), pp. 13560–13570. doi:10.1074/jbc.M115.709808.

Silva, J. & Smith, A. (2008) 'Capturing pluripotency', *Cell*, 132(4), pp. 532–536. doi:10.1016/j.cell.2008.02.006.

Sirko, S., Behrendt, G., Johansson, P.A., Tripathi, P., Costa, M., Bek, S., Heinrich, C., Tiedt, S., Colak, D., Dichgans, M., *et al*. (2013) 'Reactive glia in the injured brain acquire stem cell properties in response to sonic hedgehog', *Cell Stem Cell*, 12(4), pp. 426–439. doi:10.1016/j.stem.2013.01.019.

Smith, D.K., Yang, J., Liu, M.L. & Zhang, C.L. (2016) 'Small molecules modulate chromatin accessibility to promote NEUROG2-mediated fibroblast-to-neuron reprogramming', *Stem Cell Reports*, 7(5), pp. 955–969. doi:10.1016/j.stemcr.2016.09.013.

Son, E.Y., Ichida, J.K., Wainger, B.J., Toma, J.S., Rafuse, V.F., Woolf, C.J. & Eggan, K. (2011) 'Conversion of mouse and human fibroblasts into functional spinal motor neurons', *Cell Stem Cell*, 9(3), pp. 205–218. doi:10.1016/j.stem.2011.07.014.

Soneson, C., Love, M.I. & Robinson, M.D. (2016) 'Differential analyses for RNA-seq: Transcript-level estimates improve gene-level inferences', *F1000Research*, 4, p. 1521. doi:10.12688/F1000RESEARCH.7563.2.

Song, Z., Jadali, A., Fritzsch, B. & Kwan, K.Y. (2017) 'NEUROG1 regulates CDK2 to promote proliferation in otic progenitors', *Stem Cell Reports*, 9(5), pp. 1516–1529. doi:10.1016/j.stemcr.2017.09.011.

Steinbeck, J.A., Koch, P., Derouiche, A. & Brüstle, O. (2012) 'Human embryonic stem cell-derived neurons

establish region-specific, long-range projections in the adult brain', *Cellular and Molecular Life Sciences*, 69(3), pp. 461–470. doi:10.1007/s00018-011-0759-6.

Steinbeck, J.A., Choi, S.J., Mrejeru, A., Ganat, Y., Deisseroth, K., Sulzer, D., Mosharov, E. V. & Studer, L. (2015) 'Optogenetics enables functional analysis of human embryonic stem cell-derived grafts in a Parkinson's disease model', *Nature Biotechnology*, 33(2), pp. 204–209. doi:10.1038/nbt.3124.

Stubbs, T.M., Bonder, M.J., Stark, A.K., Krueger, F., von Meyenn, F., Stegle, O., Reik, W., Bolland, D., Butcher, G., Chandra, T., *et al*. (2017) 'Multi-tissue DNA methylation age predictor in mouse', *Genome Biology*, 18(1), p. 68. doi:10.1186/s13059-017-1203-5.

Studer, L., Vera, E. & Cornacchia, D. (2015) 'Programming and reprogramming cellular age in the era of induced pluripotency', *Cell Stem Cell*, 16(6), pp. 591–600. doi:10.1016/j.stem.2015.05.004.

Sturm, G., Cardenas, A., Bind, M.A., Horvath, S., Wang, S., Wang, Y., Hägg, S., Hirano, M. & Picard, M. (2019) 'Human aging DNA methylation signatures are conserved but accelerated in cultured fibroblasts', *Epigenetics*, 14(10), pp. 961–976. doi:10.1080/15592294.2019.1626651.

Su, Z., Niu, W., Liu, M.L., Zou, Y. & Zhang, C.L. (2014) 'In vivo conversion of astrocytes to neurons in the injured adult spinal cord', *Nature Communications*, 5, p. 3338. doi:10.1038/ncomms4338.

Sugiyama, N., Mizuguchi, T., Aoki, T., Hui, T., Inderbitzin, D., Demetriou, A.A. & Rozga, J. (2002) 'Glycerol suppresses proliferation of rat hepatocytes and human HepG2 cells', *Journal of Surgical Research*, 103(2), pp. 236–242. doi:10.1006/jsre.2002.6367.

Sun, A.X., Yuan, Q., Tan, S., Xiao, Y., Wang, D., Khoo, A.T.T., Sani, L., Tran, H.D., Kim, P., Chiew, Y.S., *et al*. (2016) 'Direct induction and functional maturation of forebrain GABAergic neurons from human pluripotent stem cells', *Cell Reports*, 16(7), pp. 1942–1953. doi:10.1016/j.celrep.2016.07.035.

Sun, C.K., Zhou, D., Zhang, Z., He, L., Zhang, F., Wang, X., Yuan, J., Chen, Q., Wu, L.G. & Yang, Q. (2014) 'Senescence impairs direct conversion of human somatic cells to neurons', *Nature Communications*, 5, p. 4112. doi:10.1038/ncomms5112.

Sun, Y., Nadal-Vicens, M., Misono, S., Lin, M.Z., Zubiaga, A., Hua, X., Fan, G. & Greenberg, M.E. (2001) 'Neurogenin promotes neurogenesis and inhibits glial differentiation by independent mechanisms', *Cell*, 104(3), pp. 365–376. doi:10.1016/S0092-8674(01)00224-0.

Svendsen, C.N., Caldwell, M.A. & Ostenfeld, T. (1999) 'Human neural stem cells: Isolation, expansion and transplantation', *Brain Pathology*, 9(3), pp. 499–513. doi:10.1111/j.1750-3639.1999.tb00538.x.

Svoboda, D.S., Barrasa, M.I., Shu, J., Rietjens, R., Zhang, S., Mitalipova, M., Berube, P., Fu, D., Shultz, L.D., Bell, G.W., *et al*. (2019) 'Human iPSC-derived microglia assume a primary microglia-like state after transplantation into the neonatal mouse brain', *Proceedings of the National Academy of Sciences of the United States of America*, 116(50), pp. 25293–25303. doi:10.1073/pnas.1913541116.

Szlachcic, W.J., Switonski, P.M., Krzyzosiak, W.J., Figlerowicz, M. & Figiel, M. (2015) 'Huntington disease

iPSCs show early molecular changes in intracellular signaling, the expression of oxidative stress proteins and the p53 pathway', *DMM Disease Models and Mechanisms*, 8(9), pp. 1047–1057. doi:10.1242/dmm.019406.

Tabansky, I. & Stern, J.N.H. (2016) 'Basics of stem cell biology as applied to the brain', in *Stem Cells in Neuroendocrinology*. Springer, pp. 11–24. doi:10.1007/978-3-319-41603-8_2.

Takahashi, K., Tanabe, K., Ohnuki, M., Narita, M., Ichisaka, T., Tomoda, K. & Yamanaka, S. (2007) 'Induction of pluripotent stem cells from adult human fibroblasts by defined factors', *Cell*, 131(5), pp. 861–872. doi:10.1016/j.cell.2007.11.019.

Takahashi, K. & Yamanaka, S. (2006) 'Induction of pluripotent stem cells from mouse embryonic and adult fibroblast cultures by defined factors', *Cell*, 126(4), pp. 663–676. doi:10.1016/j.cell.2006.07.024.

Tan, Y.L., Yuan, Y. & Tian, L. (2020) 'Microglial regional heterogeneity and its role in the brain', *Molecular Psychiatry*, 25(2), pp. 351–367. doi:10.1038/s41380-019-0609-8.

Tang, H., Inoki, K., Brooks, S. V., Okazawa, H., Lee, M., Wang, J., Kim, M., Kennedy, C.L., Macpherson, P.C.D., Ji, X., *et al*. (2019) 'mTORC1 underlies age-related muscle fiber damage and loss by inducing oxidative stress and catabolism', *Aging Cell*, 18(3), p. e12943. doi:10.1111/acel.12943.

Tang, R. & Liu, H. (2019) 'Identification of temporal characteristic networks of peripheral blood changes in Alzheimer's disease based on weighted gene co-expression network analysis', *Frontiers in Aging Neuroscience*, 11, p. 83. doi:10.3389/fnagi.2019.00083.

Tang, X., Wang, S., Bai, Y., Wu, J., Fu, L., Li, M., Xu, Q., Xu, Z.Q.D., Alex Zhang, Y. & Chen, Z. (2016) 'Conversion of adult human peripheral blood mononuclear cells into induced neural stem cell by using episomal vectors', *Stem Cell Research*, 16(2), pp. 236–242. doi:10.1016/j.scr.2016.01.016.

Tang, Y., Liu, M.L., Zang, T. & Zhang, C.L. (2017) 'Direct reprogramming rather than iPSC-based reprogramming maintains aging hallmarks in human motor neurons', *Frontiers in Molecular Neuroscience*, 10, p. 359. doi:10.3389/fnmol.2017.00359.

Tang, Y., Xiong, S., Yu, P., Liu, F. & Cheng, L. (2018) 'Direct conversion of mouse fibroblasts into neural stem cells by chemical cocktail requires stepwise activation of growth factors and Nup210', *Cell Reports*, 24(5), pp. 1355-1362.e3. doi:10.1016/j.celrep.2018.06.116.

Tanimoto, Y., Yamasaki, T., Nagoshi, N., Nishiyama, Y., Nori, S., Nishimura, S., Iida, T., Ozaki, M., Tsuji, O., Ji, B., *et al*. (2020) 'In vivo monitoring of remnant undifferentiated neural cells following human induced pluripotent stem cell-derived neural stem/progenitor cells transplantation', *Stem Cells Translational Medicine*, 9(4), pp. 465–477. doi:10.1002/sctm.19-0150.

Tao, Y. & Zhang, S.C. (2016) 'Neural subtype specification from human pluripotent stem cells', *Cell Stem Cell*, 19(5), pp. 573–586. doi:10.1016/j.stem.2016.10.015.

Tapia, N. & Schöler, H.R. (2016) 'Molecular obstacles to clinical translation of iPSCs', *Cell Stem Cell*, 19(3), pp. 298–309. doi:10.1016/j.stem.2016.06.017.

Teratani-Ota, Y., Yamamizu, K., Piao, Y., Sharova, L., Amano, M., Yu, H., Schlessinger, D., Ko, M.S.H. & Sharov, A.A. (2016) 'Induction of specific neuron types by overexpression of single transcription factors', *In Vitro Cellular and Developmental Biology - Animal*, 52(9), pp. 961–973. doi:10.1007/s11626-016-0056-7.

Theka, I., Caiazzo, M., Dvoretskova, E., Leo, D., Ungaro, F., Curreli, S., Managò, F., Dell'Anno, M.T., Pezzoli, G., Gainetdinov, R.R., *et al*. (2013) 'Rapid generation of functional dopaminergic neurons from human induced pluripotent stem cells through a single-step procedure using cell lineage transcription factors', *Stem Cells Translational Medicine*, 2(6), pp. 473–479. doi:10.5966/sctm.2012-0133.

Thier, M., Wörsdörfer, P., Lakes, Y.B., Gorris, R., Herms, S., Opitz, T., Seiferling, D., Quandel, T., Hoffmann, P., Nöthen, M.M., *et al*. (2012) 'Direct conversion of fibroblasts into stably expandable neural stem cells', *Cell Stem Cell*, 10(4), pp. 473–479. doi:10.1016/j.stem.2012.03.003.

Thier, M.C., Hommerding, O., Panten, J., Pinna, R., García-González, D., Berger, T., Wörsdörfer, P., Assenov, Y., Scognamiglio, R., Przybylla, A., *et al*. (2019) 'Identification of embryonic neural plate border stem cells and their generation by direct reprogramming from adult human blood cells', *Cell Stem Cell*, 24(1), pp. 166–182. doi:10.1016/j.stem.2018.11.015.

Thoma, E.C., Wischmeyer, E., Offen, N., Maurus, K., Sirén, A.L., Schartl, M. & Wagner, T.U. (2012) 'Ectopic expression of neurogenin 2 alone is sufficient to induce differentiation of embryonic stem cells into mature neurons', *PLoS ONE*, 7(6), p. e38651. doi:10.1371/journal.pone.0038651.

Thompson, L.H. & Björklund, A. (2015) 'Reconstruction of brain circuitry by neural transplants generated from pluripotent stem cells', *Neurobiology of Disease*, 79, pp. 28–40. doi:10.1016/j.nbd.2015.04.003.

Tian, C., Ambroz, R.J., Sun, L., Wang, Y., Ma, K., Chen, Q., Zhu, B. & Zheng, J.C. (2012) 'Direct conversion of dermal fibroblasts into neural progenitor cells by a novel cocktail of defined factors', *Current Molecular Medicine*, 12(2), pp. 126–137. doi:10.2174/156652412798889018.

Tian, C., Li, Yuju, Huang, Y., Wang, Y., Chen, D., Liu, J., Deng, X., Sun, L., Anderson, K., Qi, X., *et al*. (2015) 'Selective generation of dopaminergic precursors from mouse fibroblasts by direct lineage conversion', *Scientific Reports*, 5, p. 12622. doi:10.1038/srep12622.

Tian, Y., Morris, T.J., Webster, A.P., Yang, Z., Beck, S., Feber, A. & Teschendorff, A.E. (2017) 'ChAMP: Updated methylation analysis pipeline for Illumina BeadChips', *Bioinformatics*, 33(24), pp. 3982–3984. doi:10.1093/bioinformatics/btx513.

Tian, Z., Guo, F., Biswas, S. & Deng, W. (2016) 'Rationale and methodology of reprogramming for generation of induced pluripotent stem cells and induced neural progenitor cells', *International Journal of Molecular Sciences*, 17(4), p. 594. doi:10.3390/ijms17040594.

Tian, Z., Zhao, Q., Biswas, S. & Deng, W. (2018) 'Methods of reactivation and reprogramming of neural stem cells for neural repair', *Methods*, 133, pp. 3–20. doi:10.1016/j.ymeth.2017.08.014.

Tong, M., Hernandez, J.L., Purcell, E.K., Altschuler, R.A. & Duncan, R.K. (2010) 'The intrinsic electrophysiological properties of neurons derived from mouse embryonic stem cells overexpressing neurogenin-

1', *American Journal of Physiology-Cell Physiology*, 299(6), pp. C1335–C1344. doi:10.1152/ajpcell.00207.2010.

Torper, O., Pfisterer, U., Wolf, D.A., Pereira, M., Lau, S., Jakobsson, J., Björklund, A., Grealish, S. & Parmar, M. (2013) 'Generation of induced neurons via direct conversion in vivo', *Proceedings of the National Academy of Sciences*, 110(17), pp. 7038–7043. doi:10.1073/pnas.1303829110.

Torper, O., Ottosson, D.R., Pereira, M., Lau, S., Cardoso, T., Grealish, S. & Parmar, M. (2015) 'In vivo reprogramming of striatal NG2 glia into functional neurons that integrate into local host circuitry', *Cell Reports*, 12(3), pp. 474–481. doi:10.1016/j.celrep.2015.06.040.

Traudt, C.M., McPherson, R.J., Studholme, C., Millen, K.J. & Juul, S.E. (2014) 'Systemic glycerol decreases neonatal rabbit brain and cerebellar growth independent of intraventricular hemorrhage', *Pediatric Research*, 75(3), pp. 389–394. doi:10.1038/pr.2013.236.

Treutlein, B., Lee, Q.Y., Camp, J.G., Mall, M., Koh, W., Shariati, S.A.M., Sim, S., Neff, N.F., Skotheim, J.M., Wernig, M., *et al*. (2016) 'Dissecting direct reprogramming from fibroblast to neuron using single-cell RNA-seq', *Nature*, 534(7607), pp. 391–395. doi:10.1038/nature18323.

Tsuchiya, T., Park, K.C., Toyonaga, S., Yamada, S.M., Nakabayashi, H., Nakai, E., Ikawa, N., Furuya, M., Tominaga, A. & Shimizu, K. (2005) 'Characterization of microglia induced from mouse embryonic stem cells and their migration into the brain parenchyma', *Journal of Neuroimmunology*, 160(1–2), pp. 210–218. doi:10.1016/j.jneuroim.2004.10.025.

Tsunemoto, R., Lee, S., Szücs, A., Chubukov, P., Sokolova, I., Blanchard, J.W., Eade, K.T., Bruggemann, J., Wu, C., Torkamani, A., *et al*. (2018) 'Diverse reprogramming codes for neuronal identity', *Nature*, 557(7705), pp. 375–380. doi:10.1038/s41586-018-0103-5.

Turrens, J.F. (2003) 'Mitochondrial formation of reactive oxygen species', *Journal of Physiology*, 552(2), pp. 335–344. doi:10.1113/jphysiol.2003.049478.

Vadodaria, K.C., Mertens, J., Paquola, A., Bardy, C., Li, X., Jappelli, R., Fung, L., Marchetto, M.C., Hamm, M., Gorris, M., *et al*. (2016) 'Generation of functional human serotonergic neurons from fibroblasts', *Molecular Psychiatry*, 21(1), pp. 49–61. doi:10.1038/mp.2015.161.

Vanzan, L., Soldati, H., Ythier, V., Anand, S., Francis, N., Murr, R., Braun, S.M.G., Francis, N. & Murr, R. (2021) 'High throughput screening identifies SOX2 as a super pioneer factor that inhibits DNA methylation maintenance at its binding sites', *Nature Communications*, 12(1), p. 3337. doi:10.1038/s41467-021-23630-x.

Velychko, S., Kang, K., Kim, S.M., Kwak, T.H., Kim, K.P., Park, C., Hong, K., Chung, C.H., Hyun, J.K., MacCarthy, C.M., *et al*. (2019) 'Fusion of reprogramming factors alters the trajectory of somatic lineage conversion', *Cell Reports*, 27(1), pp. 30-39.e4. doi:10.1016/j.celrep.2019.03.023.

Vera, E., Bosco, N. & Studer, L. (2016) 'Generating late-onset human iPSC-based disease models by inducing neuronal age-related phenotypes through telomerase manipulation', *Cell Reports*, 17(4), pp. 1184–1192. doi:10.1016/j.celrep.2016.09.062.

Victor, M.B., Richner, M., Hermanstyne, T.O., Ransdell, J.L., Sobieski, C., Deng, P.Y., Klyachko, V.A., Nerbonne, J.M. & Yoo, A.S. (2014) 'Generation of human striatal neurons by microRNA-dependent direct conversion of fibroblasts', *Neuron*, 84(2), pp. 311–323. doi:10.1016/j.neuron.2014.10.016.

Victor, M.B., Richner, M., Olsen, H.E., Lee, S.W., Monteys, A.M., Ma, C., Huh, C.J., Zhang, B., Davidson, B.L., Yang, X.W., *et al*. (2018) 'Striatal neurons directly converted from Huntington's disease patient fibroblasts recapitulate age-associated disease phenotypes', *Nature Neuroscience*, 21(3), pp. 341–352. doi:10.1038/s41593-018-0075-7.

Vierbuchen, T., Ostermeier, A., Pang, Z.P., Kokubu, Y., Südhof, T.C. & Wernig, M. (2010) 'Direct conversion of fibroblasts to functional neurons by defined factors', *Nature*, 463(7284), pp. 1035–1041. doi:10.1038/nature08797.

Waddington, C.H. (1957) 'The cybernetics of development', in *The strategy of the genes*. George Allen & Unwin LTD, London, pp. 26–38. doi:Not available.

Wainger, B.J., Buttermore, E.D., Oliveira, J.T., Mellin, C., Lee, S., Saber, W.A., Wang, A.J., Ichida, J.K., Chiu, I.M., Barrett, L., *et al*. (2015) 'Modeling pain in vitro using nociceptor neurons reprogrammed from fibroblasts', *Nature Neuroscience*, 18(1), pp. 17–24. doi:10.1038/nn.3886.

Wang, L.-L., Serrano, C., Zhong, X., Ma, S., Zou, Y. & Zhang, C.-L. (2021) 'Revisiting astrocyte to neuron conversion with lineage tracing in vivo', *Cell*, 184(21), pp. 5465-5481.e16. doi:10.1016/j.cell.2021.09.005.

Wang, L.L., Su, Z., Tai, W., Zou, Y., Xu, X.M. & Zhang, C.L. (2016) 'The p53 pathway controls SOX2-mediated reprogramming in the adult mouse spinal cord', *Cell Reports*, 17(3), pp. 891–903. doi:10.1016/j.celrep.2016.09.038.

Wang, L., Wang, Linli, Huang, W., Su, H., Xue, Y., Su, Z., Liao, B., Wang, H., Bao, X., Qin, D., *et al*. (2013) 'Generation of integration-free neural progenitor cells from cells in human urine', *Nature Methods*, 10(1), pp. 84–89. doi:10.1038/nmeth.2283.

Wang, R., Yu, Z., Sunchu, B., Shoaf, J., Dang, I., Zhao, S., Caples, K., Bradley, L., Beaver, L.M., Ho, E., *et al*. (2017) 'Rapamycin inhibits the secretory phenotype of senescent cells by a Nrf2-independent mechanism', *Aging Cell*, 16(3), pp. 564–574. doi:10.1111/acel.12587.

Wang, T., Choi, E., Monaco, M.C.G., Campanac, E., Medynets, M., Do, T., Rao, P., Johnson, K.R., Elkahloun, A.G., Von Geldern, G., *et al*. (2013) 'Derivation of neural stem cells from human adult peripheral CD34+ cells for an autologous model of neuroinflammation', *PLoS ONE*, 8(11), p. e81720. doi:10.1371/journal.pone.0081720.

Wang, T., Tsui, B., Kreisberg, J.F., Robertson, N.A., Gross, A.M., Yu, M.K., Carter, H., Brown-Borg, H.M., Adams, P.D. & Ideker, T. (2017) 'Epigenetic aging signatures in mice livers are slowed by dwarfism, calorie restriction and rapamycin treatment', *Genome Biology*, 18(1), p. 57. doi:10.1186/s13059-017-1186-2.

Wapinski, O.L., Vierbuchen, T., Qu, K., Lee, Q.Y., Chanda, S., Fuentes, D.R., Giresi, P.G., Ng, Y.H., Marro, S., Neff, N.F., *et al*. (2013) 'Hierarchical mechanisms for direct reprogramming of fibroblasts to neurons', *Cell*, 155(3), pp. 621–635. doi:10.1016/j.cell.2013.09.028.

Weykopf, B., Haupt, S., Jungverdorben, J., Flitsch, L.J., Hebisch, M., Liu, G.H., Suzuki, K., Belmonte, J.C.I., Peitz, M., Blaess, S., *et al*. (2019) 'Induced pluripotent stem cell-based modeling of mutant LRRK2-associated Parkinson's disease', *European Journal of Neuroscience*, 49(4), pp. 561–589. doi:10.1111/ejn.14345.

White, C.W., Fan, X., Maynard, J.C., Wheatley, E.G., Bieri, G., Couthouis, J., Burlingame, A.L. & Villeda, S.A. (2020) 'Age-related loss of neural stem cell O-GlcNAc promotes a glial fate switch through STAT3 activation', *Proceedings of the National Academy of Sciences of the United States of America*, 117(36), pp. 22214–22224. doi:10.1073/pnas.2007439117.

White, M.D. & Plachta, N. (2020) 'Specification of the first mammalian cell lineages in vivo and in vitro', *Cold Spring Harbor Perspectives in Biology*, 12(4), p. a035634. doi:10.1101/cshperspect.a035634.

Wictorin, K., Simerly, R.B., Isacson, O., Swanson, L.W. & Björklund, A. (1989) 'Connectivity of striatal grafts implanted into the ibotenic acid-lesioned striatum - III. Efferent projecting graft neurons and their relation to host afferents within the grafts', *Neuroscience*, 30(2), pp. 313–330. doi:10.1016/0306-4522(89)90256-X.

Wictorin, K., Lagenaur, C.F., Lund, R.D. & Björklund, A. (1991) 'Efferent projections to the host brain from intrastriatal striatal mouse-to-rat grafts: Time course and tissue-type specificity as revealed by a mouse specific neuronal marker', *European Journal of Neuroscience*, 3(1), pp. 86–101. doi:10.1111/j.1460-9568.1991.tb00814.x.

Wiebe, J.P. & Dinsdale, C.J. (1991) 'Inhibition of cell proliferation by glycerol', *Life Sciences*, 48(16), pp. 1511–1517. doi:10.1016/0024-3205(91)90275-g.

Wilkinson, A.C., Nakauchi, H. & Göttgens, B. (2017) 'Mammalian transcription factor networks: Recent advances in interrogating biological complexity', *Cell Systems*, 5(4), pp. 319–331. doi:10.1016/j.cels.2017.07.004.

Winiecka-Klimek, M., Smolarz, M., Walczak, M.P., Zieba, J., Hulas-Bigoszewska, K., Kmieciak, B., Piaskowski, S., Rieske, P., Grzela, D.P. & Stoczynska-Fidelus, E. (2015) 'SOX2 and SOX2-MYC reprogramming process of fibroblasts to the neural stem cells compromised by senescence', *Plos One*, 10(11), p. e0141688. doi:10.1371/journal.pone.0141688.

Wright-Jin, E.C. & Gutmann, D.H. (2019) 'Microglia as dynamic cellular mediators of brain function', *Trends in Molecular Medicine*, 25(11), pp. 967–979. doi:10.1016/j.molmed.2019.08.013.

Wu, J., Sheng, C., Liu, Z., Jia, W., Wang, B., Li, M., Fu, L., Ren, Z., An, J., Sang, L., *et al*. (2015) 'Lmx1a enhances the effect of iNSCs in a PD model', *Stem Cell Research*, 14(1), pp. 1–9. doi:10.1016/j.scr.2014.10.004.

Wu, Z., Parry, M., Hou, X.Y., Liu, M.H., Wang, H., Cain, R., Pei, Z.F., Chen, Y.C., Guo, Z.Y., Abhijeet, S., *et al*. (2020) 'Gene therapy conversion of striatal astrocytes into GABAergic neurons in mouse models of Huntington's disease', *Nature Communications*, 11(1), p. 1105. doi:10.1038/s41467-020-14855-3.

Xiao, D., Liu, X., Zhang, M., Zou, M., Deng, Q., Sun, D., Bian, X., Cai, Y., Guo, Y., Liu, S., *et al*. (2018) 'Direct reprogramming of fibroblasts into neural stem cells by single non-neural progenitor transcription factor Ptf1a', *Nature Communications*, 9(1), p. 2865. doi:10.1038/s41467-018-05209-1.

Ximerakis, M., Lipnick, S.L., Innes, B.T., Simmons, S.K., Adiconis, X., Dionne, D., Mayweather, B.A., Nguyen,

L., Niziolek, Z., Ozek, C., *et al*. (2019) 'Single-cell transcriptomic profiling of the aging mouse brain', *Nature Neuroscience*, 22(10), pp. 1696–1708. doi:10.1038/s41593-019-0491-3.

Xu, G., Wu, F., Gu, X., Zhang, J., You, K., Chen, Y., Getachew, A., Zhuang, Y., Zhong, X., Lin, Z., *et al*. (2019) 'Direct conversion of human urine cells to neurons by small molecules', *Scientific Reports*, 9(1), p. 16707. doi:10.1038/s41598-019-53007-6.

Xu, R., Li, X., Boreland, A.J., Posyton, A., Kwan, K., Hart, R.P. & Jiang, P. (2020) 'Human iPSC-derived mature microglia retain their identity and functionally integrate in the chimeric mouse brain', *Nature Communications*, 11(1), p. 1577. doi:10.1038/s41467-020-15411-9.

Xu, X.L., Yang, J.P., Fu, L.N., Ren, R.T., Yi, F., Suzuki, K., Liu, K., Ding, Z.C., Qu, J., Zhang, W.Q., *et al*. (2014) 'Direct reprogramming of porcine fibroblasts to neural progenitor cells', *Protein and Cell*, 5(1), pp. 4–7. doi:10.1007/s13238-013-0015-y.

Xu, Z., Jiang, H., Zhong, P., Yan, Z., Chen, S. & Feng, J. (2016) 'Direct conversion of human fibroblasts to induced serotonergic neurons', *Molecular Psychiatry*, 21(1), pp. 62–70. doi:10.1038/mp.2015.101.

Xu, Z., Rao, Y., Huang, Y., Zhou, T., Feng, R., Xiong, S., Yuan, T.F., Qin, S., Lu, Y., Zhou, X., *et al*. (2020) 'Efficient strategies for microglia replacement in the central nervous system', *Cell Reports*, 33(8), p. 108443. doi:10.1016/j.celrep.2020.108443.

Yadav, T., Quivy, J.P. & Almouzni, G. (2018) 'Chromatin plasticity: A versatile landscape that underlies cell fate and identity', *Science*, 361(6409), pp. 1332–1336. doi:10.1126/science.aat8950.

Yamamizu, K., Piao, Y., Sharov, A.A., Zsiros, V., Yu, H., Nakazawa, K., Schlessinger, D. & Ko, M.S.H. (2013) 'Identification of transcription factors for lineage-specific ESC differentiation', *Stem Cell Reports*, 1(6), pp. 545–559. doi:10.1016/j.stemcr.2013.10.006.

Yamamizu, K., Sharov, A.A., Piao, Y., Amano, M., Yu, H., Nishiyama, A., Dudekula, D.B., Schlessinger, D. & Ko, M.S.H. (2016) 'Generation and gene expression profiling of 48 transcription-factor-inducible mouse embryonic stem cell lines', *Scientific Reports*, 6, p. 25667. doi:10.1038/srep25667.

Yang, N., Chanda, S., Marro, S., Ng, Y.H., Janas, J.A., Haag, D., Ang, C.E., Tang, Y., Flores, Q., Mall, M., *et al*. (2017) 'Generation of pure GABAergic neurons by transcription factor programming', *Nature Methods*, 14(6), pp. 621–628. doi:10.1038/nmeth.4291.

Yang, Y., Jiao, J., Gao, R., Le, R., Kou, X., Zhao, Y., Wang, H., Gao, S. & Wang, Y. (2015) 'Enhanced rejuvenation in induced pluripotent stem cell-derived neurons compared with directly converted neurons from an aged mouse', *Stem Cells and Development*, 24(23), pp. 2767–2777. doi:10.1089/scd.2015.0137.

Yang, Y., Chen, R., Wu, X., Zhao, Y., Fan, Y., Xiao, Z., Han, J., Sun, L., Wang, X. & Dai, J. (2019) 'Rapid and efficient conversion of human fibroblasts into functional neurons by small molecules', *Stem Cell Reports*, 13(5), pp. 862–876. doi:10.1016/j.stemcr.2019.09.007.

Yi, F., Danko, T., Botelho, S.C., Patzke, C., Pak, C., Wernig, M. & Südhof, T.C. (2016) 'Autism-associated

SHANK3 haploinsufficiency causes Ih channelopathy in human neurons', *Science*, 352(6286), p. aaf2669. doi:10.1016/0390-6035(79)90080-4.

Yiangou, L., Grandy, R.A., Morell, C.M., Tomaz, R.A., Osnato, A., Kadiwala, J., Muraro, D., Garcia-Bernardo, J., Nakanoh, S., Bernard, W.G., *et al*. (2019) 'Method to synchronize cell cycle of human pluripotent stem cells without affecting their fundamental characteristics', *Stem Cell Reports*, 12(1), pp. 165–179. doi:10.1016/j.stemcr.2018.11.020.

Yin, J.C., Zhang, L., Ma, N.X., Wang, Y., Lee, G., Hou, X.Y., Lei, Z.F., Zhang, F.Y., Dong, F.P., Wu, G.Y., *et al*. (2019) 'Chemical conversion of human fetal astrocytes into neurons through modulation of multiple signaling pathways', *Stem Cell Reports*, 12(3), pp. 488–501. doi:10.1016/j.stemcr.2019.01.003.

Yoo, A.S., Sun, A.X., Li, L., Shcheglovitov, A., Portmann, T., Li, Y., Lee-Messer, C., Dolmetsch, R.E., Tsien, R.W. & Crabtree, G.R. (2011) 'MicroRNA-mediated conversion of human fibroblasts to neurons', *Nature*, 476(7359), pp. 228–231. doi:10.1038/nature10323.

Yu, C., Liu, K., Tang, S. & Ding, S. (2014) 'Chemical approaches to cell reprogramming', *Current Opinion in Genetics and Development*, 28, pp. 50–56. doi:10.1016/j.gde.2014.09.006.

Yu, K.R., Shin, J.H., Kim, J.J., Koog, M.G., Lee, J.Y., Choi, S.W., Kim, H.S., Seo, Y., Lee, S.H., Shin, T.H., *et al*. (2015) 'Rapid and efficient direct conversion of human adult somatic cells into neural stem cells by HMGA2/let-7b', *Cell Reports*, 10(3), pp. 441–452. doi:10.1016/j.celrep.2014.12.038.

Yuan, F., Liu, L., Lei, Y. & Tang, P. (2017) 'P53 inhibits the upregulation of sirtuin 1 expression induced by c-Myc', *Oncology Letters*, 14(4), pp. 4396–4402. doi:10.3892/ol.2017.6661.

Zarei-Kheirabadi, M., Hesaraki, M., Kiani, S. & Baharvand, H. (2019) 'In vivo conversion of rat astrocytes into neuronal cells through neural stem cells in injured spinal cord with a single zinc-finger transcription factor', *Stem Cell Research and Therapy*, 10(1), p. 380. doi:10.1186/s13287-019-1448-x.

Zhang, L., Yin, J.C., Yeh, H., Ma, N.X., Lee, G., Chen, X.A., Wang, Y., Lin, L., Chen, L., Jin, P., *et al*. (2015) 'Small molecules efficiently reprogram human astroglial cells into functional neurons', *Cell Stem Cell*, 17(6), pp. 735–747. doi:10.1016/j.stem.2015.09.012.

Zhang, M., Lin, Y.H., Sun, Y.J., Zhu, S., Zheng, J., Liu, K., Cao, N., Li, K., Huang, Y. & Ding, S. (2016) 'Pharmacological reprogramming of fibroblasts into neural stem cells by signaling-directed transcriptional activation', *Cell Stem Cell*, 18(5), pp. 653–667. doi:10.1016/j.stem.2016.03.020.

Zhang, Q.-J., Li, J.-J., Lin, X., Lu, Y.-Q., Guo, X.-X., Dong, E.-L., Zhao, M., He, J., Wang, N. & Chen, W.-J. (2017) 'Modeling the phenotype of spinal muscular atrophy by the direct conversion of human fibroblasts to motor neurons', *Oncotarget*, 8(7), pp. 10945–10953. doi:10.18632/oncotarget.14641.

Zhang, W., Qu, J., Liu, G.H. & Belmonte, J.C.I. (2020) 'The ageing epigenome and its rejuvenation', *Nature Reviews Molecular Cell Biology*, 21(3), pp. 137–150. doi:10.1038/s41580-019-0204-5.

Zhang, Y., Pak, C., Han, Y., Ahlenius, H., Zhang, Z., Chanda, S., Marro, S., Patzke, C., Acuna, C., Covy, J., *et al*.

(2013) ‘Rapid single-step induction of functional neurons from human pluripotent stem cells’, *Neuron*, 78(5), pp. 785–798. doi:10.1016/j.neuron.2013.05.029.

Zhang, Z.-N., Chung, S.-K., Xu, Z. & Xu, Y. (2014) ‘Oct4 maintains the pluripotency of human embryonic stem cells by inactivating p53 through Sirt1-mediated deacyetylation’, *Stem Cells*, 32(1), pp. 157–165. doi:10.1002/stem.1532.

Zhao, D., Pan, C., Sun, J., Gilbert, C., Drews-Elger, K., Azzam, D.J., Picon-Ruiz, M., Kim, M., Ullmer, W., El-Ashry, D., *et al*. (2015) ‘VEGF drives cancer-initiating stem cells through VEGFR-2/Stat3 signaling to upregulate Myc and Sox2’, *Oncogene*, 34(24), pp. 3107–3119. doi:10.1038/onc.2014.257.

Zheng, J., Choi, K.A., Kang, P.J., Hyeon, S., Kwon, S., Moon, J.H., Hwang, I., Kim, Y.I., Kim, Y.S., Yoon, B.S., *et al*. (2016) ‘A combination of small molecules directly reprograms mouse fibroblasts into neural stem cells’, *Biochemical and Biophysical Research Communications*, 476(1), pp. 42–48. doi:10.1016/j.bbrc.2016.05.080.

Zhou, H., Su, J., Hu, X., Zhou, C., Li, H., Chen, Z., Xiao, Q., Wang, B., Wu, W., Sun, Y., *et al*. (2020) ‘Glia-to-neuron conversion by CRISPR-CasRx alleviates symptoms of neurological disease in mice’, *Cell*, 181(3), pp. 590-603.e16. doi:10.1016/j.cell.2020.03.024.

Zhou, L.N., Hua, X., Deng, W.Q., Wu, Q.N., Mei, H. & Chen, B. (2015) ‘PCDH10 interacts with hTERT and negatively regulates telomerase activity’, *Medicine (United States)*, 94(50), p. e2230. doi:10.1097/MD.0000000000002230.

Zhou, Q. & Melton, D.A. (2008) ‘Extreme makeover: Converting one cell into another’, *Cell Stem Cell*, 3(4), pp. 382–388. doi:10.1016/j.stem.2008.09.015.

Zhu, L., Liu, Y., Wu, X., Ren, Y., Zhang, Q., Ren, L. & Guo, Y. (2021) ‘Cerebroprotein hydrolysate-I protects senescence-induced by D-galactose in PC12 cells and mice’, *Food Science and Nutrition*, 9(7), pp. 3722–3731. doi:10.1002/fsn3.2333.

Zhu, S., Ambasudhan, R., Sun, W., Kim, H.J., Talantova, M., Wang, X., Zhang, M., Zhang, Y., Laurent, T., Parker, J., *et al*. (2014) ‘Small molecules enable OCT4-mediated direct reprogramming into expandable human neural stem cells’, *Cell Research*, 24(1), pp. 126–129. doi:10.1038/cr.2013.156.

Zou, Q., Yan, Q., Zhong, J., Wang, K., Sun, H., Yi, X. & Lai, L. (2014) ‘Direct conversion of human fibroblasts into neuronal restricted progenitors’, *Journal of Biological Chemistry*, 289(8), pp. 5250–5260. doi:10.1074/jbc.M113.516112.

Zuo, B., Yang, J., Wang, F., Wang, L., Yin, Y., Dan, J., Liu, N. & Liu, L. (2012) ‘Influences of lamin A levels on induction of pluripotent stem cells’, *Biology Open*, 1(11), pp. 1118–1127. doi:10.1242/bio.20121586.

Supplemental Information

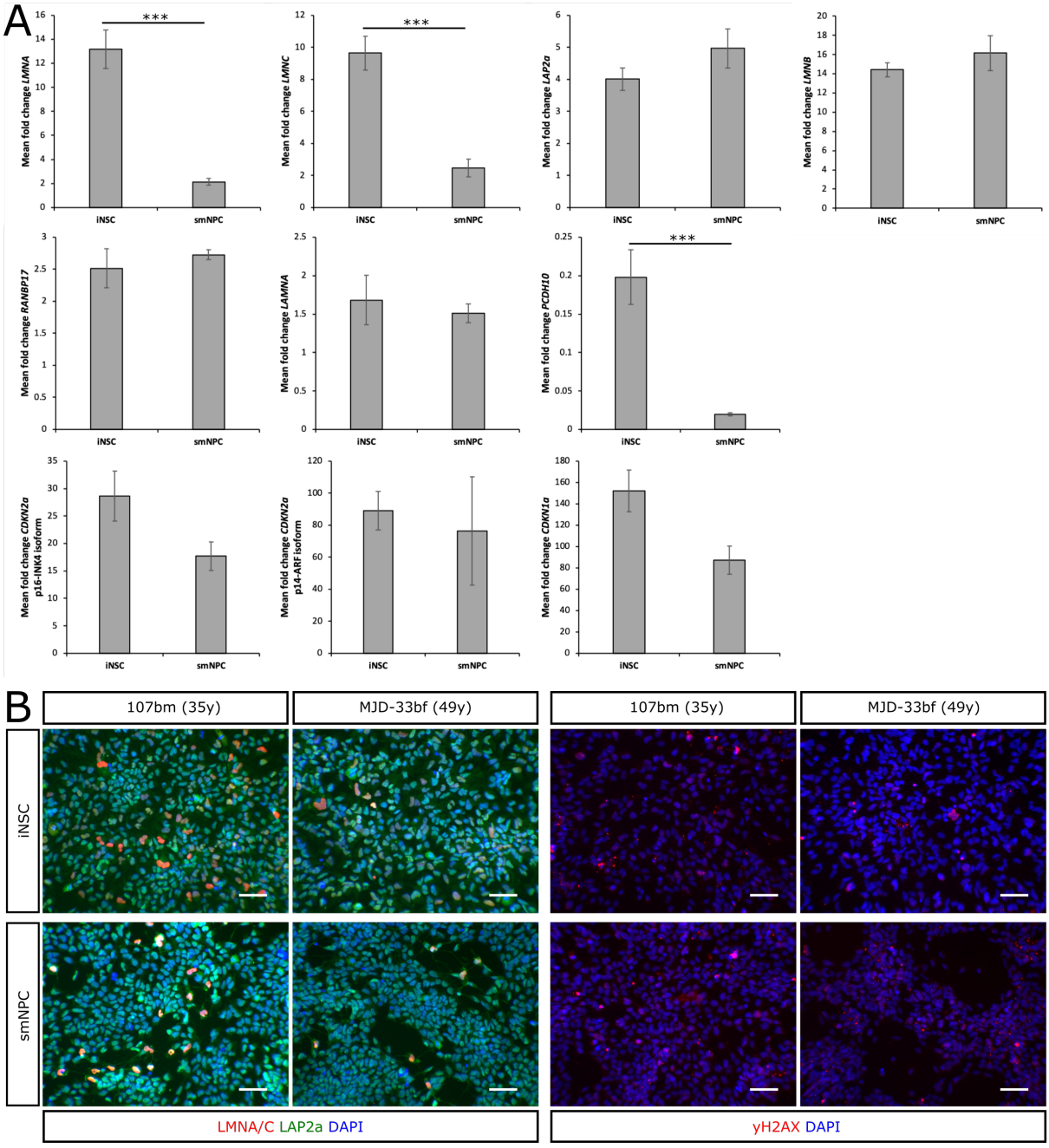

Supplementary Figure 1: Expression of genes and proteins related to diverse age-associated pathways in mid-age donor-derived iNSCs and smNPCs.
(A) QPCR-based expression profiling of the nuclear lamina-associated genes *LMNA*, *LMNC*, *LAP2a* and *LMNB*, the age-related genes *RANBP17*, *LAMNA* and *PCDH10*, as well as the senescence-mediating genes *CDKN2a* (isoforms p16-INK4 and p14-ARF) and *CDKN1a*. N = 6 with three independent replicates of two genotypes. Results of the Wilcoxon tests: *LMNA*: $p = 0.0004$; *LMNC*: $p = 0.0004$; *PCDH10*: $p = 0.0004$. **(B)** Representative stainings for LMNA/C and LAP2a, as well as the DNA DSB marker γH2AX in isogenic iNSCs and smNPCs. Scale bars = 50 μm. N = 3 independent replicates per genotype. Parts of these data were published as Supplementary Figure 13 of Sheng *et al.*, 2018.

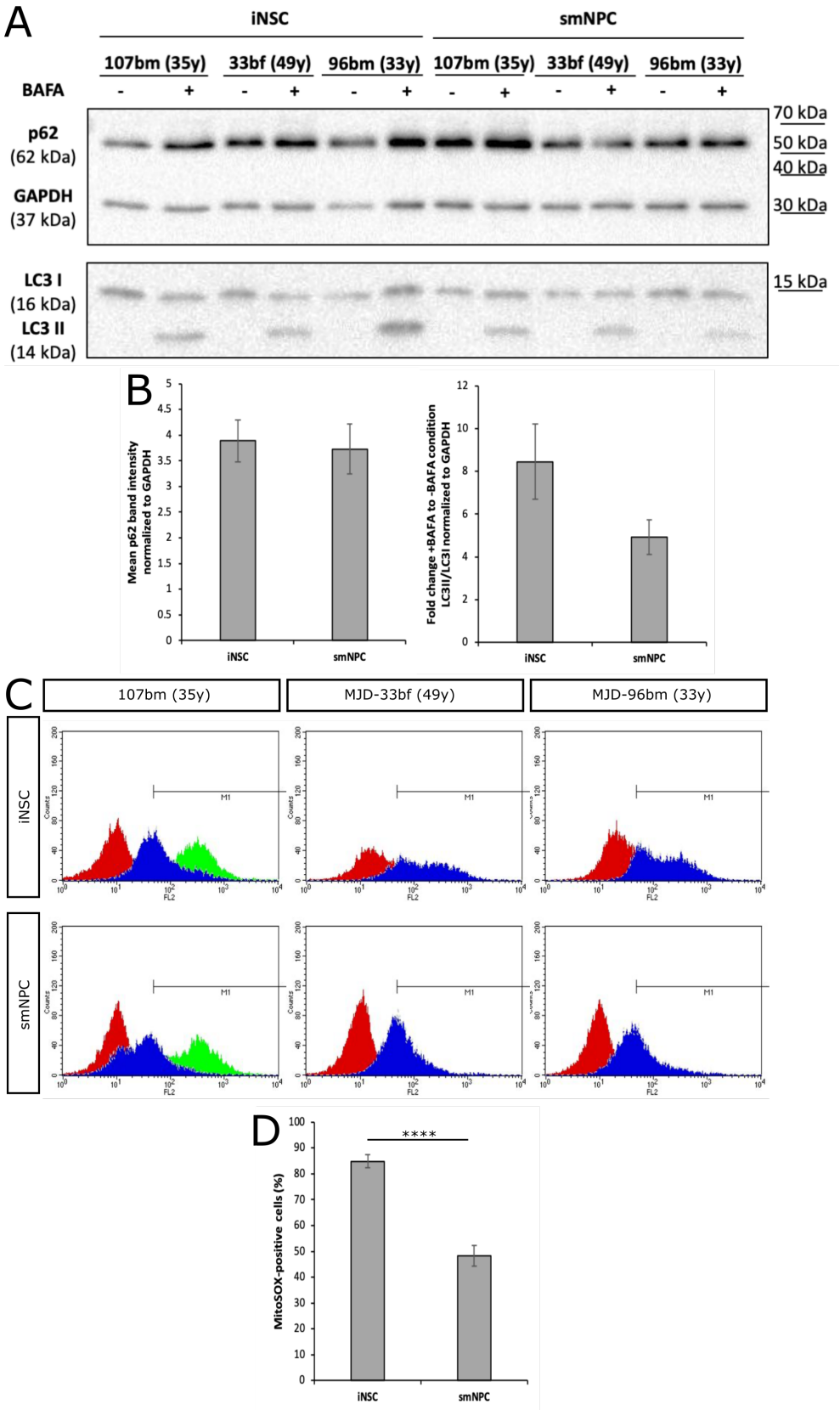

Supplementary Figure 2: Autophagy and mitochondrial ROS production in mid-age donor-derived directly converted and iPSC-derived NSCs.
(A) Representative Western blot detecting p62, the LC3 isoforms I and II as well as the house-keeping protein GAPDH in mid-age donor-derived iNSCs and smNPCs under ± BAFA treatment conditions. **(B)** Results of Western blot quantification. N = 9 with three independent replicates of three genotypes. **(C)** Representative flow cytometry raw data (acquired using FACSCalibur flow cytometer) depicting unstained control (red), MitoSOX-stained sample (blue) and FCCP-treated positive control (green). **(D)** Quantification of flow cytometry data revealing the percentage of MitoSOX-positive iNSCs and smNPCs. N = 9 with three independent replicates of three genotypes. Result of the Wilcoxon test: $p < 3x10^{-9}$.

Acknowledgements

Before acknowledging all persons, who have escorted me on my way to finalizing this PhD thesis, I would like to express my sincere gratitude to all of my PhD thesis committee members for their willingness to evaluate it. In this context, special thanks go to my two reviewers, namely Prof. Dr. Oliver Brüstle and Prof. Dr. Waldemar Kolanus, as well as PD Dr. Gerhild van Echten-Deckert and Prof. Dr. Ulrich Kubitscheck.

Now, although this might not be common practice, the first persons I would very much like to thank here for their contribution to my academic path so far are Sabine Vay and Adele Rüger. Working in Adele's lab during my Master thesis under Sabine's and her supervision made me fell in love with neural stem cells and their great potential, and thereby laid out the most important basis for my PhD thesis – passion for the research field I chose to continue working in. Moreover, both are simply amazing persons and great role models for women in science, which are only few of a lot more reasons why I am glad to have had the chance to work with both.

Naturally, however, the person who has so far most significantly impacted my scientific and professional development is my dear mentor Oliver Brüstle. I am incredibly thankful that, back in 2011, he picked me to work on this terrifically interesting research project, and continued to support me in any possible way up until now. Next to being of utmost help for developing this research project, I am thankful that he allowed me to get involved in writing primary articles, literature reviews and grant applications, as well as trusting in me to be able to adequately represent our work at international conferences. I sincerely hope that I will be allowed to benefit from his tremendous amount of experience also in future, and hereby promise to do my best to not let him down.

Next, I would like to express my thanks to my early stage supervisors Chao Sheng and Michael Peitz for introducing me to the research field and the great plethora of methods we currently have at hands to address biomedical questions. In this context, also big thanks to Cornelia Thiele and especially Anke Leinhaas for practically teaching me relevant methods in cell culture and animal experimentation, respectively.

When it comes to supervising and teaching, one person I would like to especially highlight is Andy Till, whom I owe a lot. Being my later stage supervisor, he truly widened my horizon, helping me to critically look at my project from a different angle than the stem cell perspective. Additionally, with his infectious positive and motivating attitude, he will always act as a model to me of how to shape lab life and communication.

Moreover, I would like to thank my current team members Hideaki Matsumura, Luzia Heidrich and Rachel Konang for their constant support – be it practically in the lab or by challenging my views on, amongst others, scientific topics. Likewise, thanks to all students, whom I had the honor to directly or indirectly supervise over the last years: Linda Schneider, Karen Laupman, Janina Kaspar, Christiane Antosik, Smit Mahajani, Elena Costantini, Anastasia Cakmak, Marie Schöneich, Miguel Pereira, Laura Schmitz-Gielsdorf and Natalia Garcia Perez. They were all of great help, either to the project specifically and/or by helping me to shape my idea of how to become a (better) supervisor – and I promise to never stop to continue improving.

Lastly, I would like to thank all my external collaborators for their hands-on support as well as great scientific discussions, especially Ullrich Wüllner, Anja Schneider, Waltraut Merz, Michael Ziller, Chungku Lee, Ali Shaib, Jeong Seop Rhee, Nils Brose, Pedro Royero, Heinz Beck, Martin Schwarz, Julia Franzen and Wolfgang Wagner. Importantly, here, I would also like to acknowledge the great input of all my internal collaborators and colleagues

from the Institute of Reconstructive Neurobiology. Irrespective of whether I needed scientific advice, organizational help, emotional support or simply some relaxed time with joy and laughter, you were always there for me. Although this thank-you applies to everyone who is or has been working with me during the last couple of years, I would like to specifically mention our Institute's fairies Bärbel Wagner and Alexandra Rabe, as well as my dear former and current colleagues Christina Au Yeung, Nils Braun, Yannik Breitkreuz, Andreas Elanzew, Vanessa Frickel, Jasmin Jatho-Gröger, Frederike Klaus, Mona Mathews-Ajendra, Pascal Röderer, Julia Schlee and Jannis Wißfeld.

Having that said, I would now like to continue thanking my family and friends. To do so, I will switch to my/our mother tongue to make sure that they understand every single word I am writing: Meiner Familie und Freunden möchte ich insbesondere aufgrund der Bedingungslosigkeit danken, mit der sie mich über die Jahre unterstützt haben. Die meisten von ihnen haben wahrscheinlich bis heute nicht verstanden, woran ich eigentlich arbeite – und das ist absolut in Ordnung. Für sie war immer ausreichend, dass ich von meiner Arbeit fasziniert bin. Ich finde es absolut fesselnd, dass Bienenköniginnen mehrere Jahre leben können, obwohl Arbeiterbienen normalerweise nur Wochen bis Monate überleben und das, obwohl sie die gleichen Gene haben wie ihre Königinnen. Ebenso spannend finde ich, dass sich Anfang des 19ten Jahrhunderts reiche Menschen der Transplantation von Schimpansenhoden unterzogen haben, weil sie dachten dies könne ihr zu erwartendes Lebensalter erhöhen. Und auch, wenn ihnen dies alles vollkommen zusammenhanglos erscheinen muss, sind sie es über die vielen Jahre nicht müde geworden, sich solche Anekdoten anzuhören und mich darin zu unterstützen meinen Weg zu gehen. Sie haben zurückgesteckt und akzeptiert, dass ich häufig nicht so viel Zeit für sie aufbringen konnte, wie ich es mir eigentlich gewünscht hätte. Tatsächlich haben sie sich (fast) nie darüber beklagt und mir immer das Gefühl gegeben, dass es okay ist für den Moment meiner Arbeit den Vorrang zu geben.

Die letzten Sätze möchte ich aber einzig meinem Partner Matthias widmen. Er hat mir, wie alle anderen in meinem privaten Umfeld, Räume gelassen mich meiner Arbeit zu widmen und mich darin, soweit es ihm möglich war, zudem aktiv unterstützt. Nicht nur durch seine allgemeine Fähigkeit auch mal auf mich zu verzichten, die mich insbesondere unter diesen besonderen Umständen durchaus sehr glücklich gestimmt hat, sondern ebenso durch unzählige Kleinigkeiten, wie den nicht abbrechenden Zulauf an leckerem Kaffee. Auch wenn dies im ersten Moment paradox erscheinen mag, möchte ich ihm aber ganz besonders für die Momente danken, in denen er mich eben nicht unterstützt, sondern mich und meinen Arbeitswahn in die nötigen Schranken gewiesen hat. Wie eigentlich immer, wusste er in diesen Momenten besser als ich, dass eine Pause nötig war, und hat mit dieser beneidenswerten Einsicht wohl viele Male meine körperliche und seelische Gesundheit bewahrt. Ich kann mich sehr glücklich schätzen voller Überzeugung sagen zu können, dass ich in ihm einen starken Partner gefunden habe, auf den ich in allen Lebenslagen vertrauen kann. Für dieses Grundvertrauen und so ziemlich alles andere danke ich dir von Herzen.